Springer Series in Solid and Structural Mechanics 6

Michel Frémond

Collisions Engineering: Theory and Applications

EXTRAS ONLINE

Springer

Springer Series in Solid and Structural Mechanics

Volume 6

More information about this series at http://www.springer.com/series/10616

Michel Frémond

Collisions Engineering: Theory and Applications

Springer

Michel Frémond
Department of Civil Engineering
and Computer Science
Universita of Rome “Tor Vergata”
Rome
Italy

Additional material to this book can be downloaded from http://extras.springer.com.
Additional content of this book can be viewed and downloaded from http://dicii.uniroma2.it/?PG=25.26.73, https://ifsttar.libcast.com/mast-sdoa

ISSN 2195-3511 ISSN 2195-352X (electronic)
Springer Series in Solid and Structural Mechanics
ISBN 978-3-662-52694-1 ISBN 978-3-662-52696-5 (eBook)
DOI 10.1007/978-3-662-52696-5

Library of Congress Control Number: 2016940331

Printed on acid-free paper

This Springer imprint is published by Springer Nature
The registered company is Springer-Verlag GmbH Berlin Heidelberg

Preface

Predictive theories of collisions occurring in solid and fluid mechanics are investigated in this book. It is devoted to collisions which may be assumed instantaneous: collisions of rigid solids, collisions of deformable solids and collisions of solids and fluids. Collisions being dissipative, the coupled thermal and mechanical phenomena are considered in the predictive theories. Applications to collision engineering are presented, crowd motions, debris flow motions, shape memory alloys motions.

These problems have been investigated in the framework of the Laboratorio Lagrange, bringing together Italian and French scientists. In particular scientists from l'Università di Roma "Tor Vergata" and from l'École nationale des ponts et chaussés: Professors Federica Caselli, Francesco Federico, Michel Frémond, Directeur de Recherche Pierre Argoul, Doctors Michele Marino and Bachar Kabalan.

Some of the computations which illustrate the presentation are due to Doctors Stella Brach and Alberto Frau, they are warmly thanked.

Parts of this book are based on lectures given at the Scuola di Ingegneria of the Università di Roma "Tor Vergata".

November 2015 Michel Frémond

Contents

Chapter 1
Introduction

The investigation of collisions occurring in the motion of solids has captured the attention of scientists from the beginning of the establishment of the mechanical sciences. Today the topic is still active. That just shows how many aspects it has. It is even related to the very bases of mechanics. In this book, we consider collisions which may be assumed *instantaneous*. This subjective choice leaves numerous openings for science and engineering. As we are going to see, it is not very restrictive.

We develop the idea that a system of solids is *deformable*. Indeed, moving solids form a *mechanical system*. And the form of this system changes because the solids move one's with respect to the others. The first element of the theory is to identify and quantify the deformation of the system. When this is achieved, we define *internal generalized forces* with either a power or a work as in mechanical parlance or with a duality product in mathematical parlance. This point of view gives the *equations of motion* derived from the *principle of virtual work*.

To complete the theory, we need constitutive laws for the internal generalized forces. Once the expression of the work of the internal generalized forces is chosen, the constitutive laws are obtained with *experiments* which are guided by the laws of thermodynamics. These relationships exhibit the quantities which have to be related and measured. As the constitutive laws are infinitely numerous, we facilitate their derivation by using *pseudo-potentials of dissipation* introduced by Jean Jacques Moreau. Many phenomena are described by pseudo-potentials of dissipation. These behaviours have a physical feature: the effect, for instance the percussion in two solids colliding is roughly proportional to the cause, here the deformation velocity of the system made of the two solids. A phenomenon which has such a property may fall in the formalism of pseudo-potentials of dissipation. In this case, a linear constitutive law complemented with the reactions to the internal constraints, mainly the impenetrability conditions, is sufficient to capture the core of the physical properties. This is only in the enhancement of the modelling that non linear constitutive laws may by introduced.

From our point of view, the essence of physics has to appear in the combination of the equations of motion and of linear constitutive laws with the mandatory non linear reactions to the internal constraints.

M. Frémond, *Collisions Engineering: Theory and Applications*,
Springer Series in Solid and Structural Mechanics 6,
DOI 10.1007/978-3-662-52696-5_1

Of course, all the phenomena do not fall within the scope of pseudo-potential of dissipation. There are situations where the effect is not clearly proportional to the cause. This is the case of the Coulomb's friction law which is in someway related to collisions as we will see in Chap. 2. The friction phenomena are not progressive. A small action does not produce a small sliding velocity and a large actions does not produce a large sliding velocity. There is a threshold depending on the pressure which is applied. In this situation, pseudo-potentials of dissipation are unsuitable. To keep the versatility of pseudo-potentials, we may use *dissipation functions* which are no longer convex functions. These functions keep a part of the good properties of pseudo-potentials, for instance the second law is still satisfied, but the equations are no longer monotone. unicity of possible solutions is problematic. But this not always a drawback.

The mathematical aspect of the predictive theories is not addressed. Each time it is possible, we mention experimental and numerical results to illustrate the presentation.

After the bases of the theory are presented in the first Chapter after this introduction, Chap. 2, developments and applications are described in the following Chaps. 3–10.

In Chap. 2, we present the basic ides predicting the motion of a point above an immobile plane. The concepts, the velocity of deformation, and the internal percussion are introduced. In Chap. 3 we use the adaptability of the basic ideas to develop the theory for the motion of two points moving on an axis. The thermal effect of collisions is investigated. Because we assume the collision is instantaneous, we are induced to assume the temperatures are discontinuous with respect to time. The collisions being dissipative, it results the temperatures tend to increase. And diffusion tends to equalize the temperatures. Those two effects intervene in the theory. Chapters 4 and 5 are devoted to enhancements of the results to the motions of disks in a plane and the motion of balls above a plane and in a box. The numerical results show the variety of the possible motions in a box. We see in these Chapters that the attractive notion of coefficient of restitution well fitted for collision of two balls is ill-suited to different systems. Chapter 6 is devoted to the motions of crowds: pedestrians are assumed to be either points or disks with or without interactions at a distance to modelize children holding hands of their parents. The pedestrians may collide or avoid to collide. The examples, people getting out of a theater, getting off a train, pedestrians walking on a bridge... illustrate the possibilities and the versatility of this theory. Chapter 7 investigate the collisions of deformable solids with obstacle, with and without thermal phenomena. The theory predicts the micro-rebounds of a steel bar which vibrates after colliding an obstacle. Chapter 8 describes collisions of solids and fluids. the theory predicts the large painful percussion pressure a diver experiments in a belly flop. It predicts also that the behaviour of a flat stone colliding the surface of a lake depends on the relative importance of the horizontal velocity and of the falling velocity. When the horizontal velocity is larger than the falling velocity, the stone ricochets, when it is not, it does bounce. This is what we experiment when skipping stone on a lake. Chapter 9 investigate the collision of debris flows with structures. It is shown that a smooth damping protection may be used to protect

buildings. In Chap. 10, we investigate collision of a solid made of shape memory alloy with an obstacle. The thermal effects produce both and increase of temperature and possibly an austenite-martensite phase change. In the following motion, the solid may recover its initial position.

Chapter 2
The Theory: Mechanics. An Example: Collision of a Point and a Plane

Michel Frémond

2.1 A System Made of a Point and a Plane

The system we consider is made of a point and an obstacle, for instance a plane. The point moves above the plane, can collide it, can slide on it. But it cannot interpenetrate it. Indeed, the two elements of the system, the point and the plane are not deformable. And it is not possible to speak of deformation when each of them is considered by itself. But when we consider the system made of the point and the plane, this system is deformable because the distance of the point to the plane changes, [14]. The development of this idea in the sequel gives a productive and elegant theory.

We assume also that the duration of the collisions of the point with the plane, i.e., the time for the point to adapt to the kinematic incompatibility, is negligible with respect to the time scale of the theory. For instance, with respect to the time flight. Thus we assume, the collisions are instantaneous. As for an example of such a motion, one may think of the motion of a soccer ball over a soccer field. The system is made of the soccer ball and the field. Collisions result from external actions due to the players and from internal actions due to the kinematic constraint which is that the soccer ball call cannot interpenetrate the field.

Remark 2.1 The collision theory has mainly been developed for solids. The traditional approach (see for example, [4, 36–38]) is based on the coefficients of restitution which is appropriated in simple situations but may be in contradiction with the basic principles of mechanics in more complex setups [3, 4, 7, 25, 37, 38].

2.2 The Velocities

The velocity of the point is a smooth function of time t when the flight is smooth. When it is not, for instance when colliding the plane or when hitted by some external percussion. At such a time, the velocity is discontinuous. There is velocity

M. Frémond, *Collisions Engineering: Theory and Applications*,
Springer Series in Solid and Structural Mechanics 6,
DOI 10.1007/978-3-662-52696-5_2

$$\mathbf{U}^{-}(t) = \lim_{\Delta t \to 0, \Delta t > 0} \mathbf{U}(t - \Delta t), \tag{2.1}$$

before the collision and velocity

$$\mathbf{U}^{+}(t) = \lim_{\Delta t \to 0, \Delta t > 0} \mathbf{U}(t + \Delta t), \tag{2.2}$$

after the collision. The virtual velocities $\mathbf{V}$ are possible velocities of the point or possible velocities of the point we may think of. In terms of mechanics and mathematics, the virtual velocities are elements of the linear space which is induced by the formula giving the actual velocity. In this example, we choose the space of bounded variation 3-D vectors denoted $\mathcal{V}$, [1, 2, 31]. For the sake of simplicity, we assume the plane is fixed in a Galilean reference frame and remains immobile even when collided by the point. This is the case if the plane, the obstacle, is very massive compared to the point. Note that this is the case of the soccer field.

The discontinuity of velocity is denoted

$$[\mathbf{U}(t)] = \mathbf{U}^{+}(t) - \mathbf{U}^{-}(t). \tag{2.3}$$

More generally discontinuity of quantity A is denoted

$$[A(t)] = A^{+}(t) - A^{-}(t), \tag{2.4}$$

with

$$A^{+}(t) = \lim_{\Delta t \to 0, \Delta t > 0} A(t + \Delta t), \; A^{-}(t) = \lim_{\Delta t \to 0, \Delta t > 0} A(t - \Delta t) \tag{2.5}$$

2.3 The Velocity of Deformation

The choice of the velocity of deformation of the system has to be in agreement with observations. It is reasonable to choose as velocity of deformation of the system, the velocity of the point with respect to the plane obstacle which is assumed to be immobile, for instance assuming it is very massive. It is obvious that if the velocity of the point with respect to the plane is null, the shape of the system does not change. To be precise, if the velocity of the point is parallel to the plane, the form of the system changes. In particular, if the point slides on the plane, the shape changes because the distance of a reference point of the plane to the point changes.

2.4 The Principle of Virtual Work

A productive way to derive the equations of motion in mechanics is to use the Principle of Virtual Work, [16–19]. We think it may be founded on experimental observations. Let us consider a system and apply actions. We see that the work we provide to the system between times t_1 and t_2, $t_1 \leq t_2$ is used to modify its velocity and to modify its shape. We assume that this work, the work of the external forces, $\mathcal{W}_{ext}(t_1, t_2)$, is the sum of two works:

- the work to modify the velocity which is the actual work of the acceleration forces, $\mathcal{W}_{acc}(t_1, t_2)$;
- the work to modify the shape or the form which is the opposite of the classical actual work of the internal forces, $-\mathcal{W}_{int}(t_1, t_2)$.

$$\mathcal{W}_{ext}(t_1, t_2) = \mathcal{W}_{acc}(t_1, t_2) - \mathcal{W}_{int}(t_1, t_2)), \tag{2.6}$$

Experiments lead also to assume the works are additive functions of time t and linear functions of the velocities. Thus we have

$$\mathcal{W}_{ext}(\mathbf{V}, t_1, t_2) = \int_{t_1}^{t_2} \mathcal{P}_{ext}(\mathbf{V}(\boldsymbol{\tau}))d\tau + \sum_t \mathcal{T}_{ext}(\mathbf{V}, t), \tag{2.7}$$

$$\mathcal{W}_{acc}(\mathbf{V}, t_1, t_2) = \int_{t_1}^{t_2} \mathcal{P}_{acc}(\mathbf{V}(\boldsymbol{\tau}))d\tau + \sum_t \mathcal{T}_{acc}(\mathbf{V}, t), \tag{2.8}$$

$$\mathcal{W}_{int}(\mathbf{V}, t_1, t_2) = \int_{t_1}^{t_2} \mathcal{P}_{int}(\mathbf{V}(\boldsymbol{\tau}))d\tau + \sum_t \mathcal{T}_{int}(\mathbf{V}, t). \tag{2.9}$$

The works have a density with respect to the Lebesgue measure, the power $\mathcal{P}_{ext}(\mathbf{V}(\boldsymbol{\tau}))$ and a density with respect to the atomic measure, the work $\mathcal{T}_{ext}(\mathbf{V}, t)$. Experimental result (2.6) becomes

$$\mathcal{W}_{ext}(\mathbf{U}, t_1, t_2) = \mathcal{W}_{acc}(\mathbf{U}, t_1, t_2) - \mathcal{W}_{int}(\mathbf{U}, t_1, t_2), \tag{2.10}$$

The principle of virtual works extends this relationship to virtual velocities $\mathbf{V}$ and to any times t_1 and t_2, $t_1 \leq t_2$,

$$\forall \mathbf{V} \in \mathcal{V},\ \forall t_1,\ \forall t_2,\ t_1 \leq t_2, \tag{2.11}$$

$$\mathcal{W}_{ext}(\mathbf{V}, t_1, t_2) = \mathcal{W}_{acc}(\mathbf{V}, t_1, t_2) - \mathcal{W}_{int}(\mathbf{V}, t_1, t_2), \tag{2.12}$$

or in its classical formulation,

$$\forall \mathbf{V} \in \mathcal{V},\ \forall t_1,\ \forall t_2,\ t_1 \leq t_2, \tag{2.13}$$

$$\mathcal{W}_{acc}(\mathbf{V}, t_1, t_2) = \mathcal{W}_{int}(\mathbf{V}, t_1, t_2) + \mathcal{W}_{ext}(\mathbf{V}, t_1, t_2). \tag{2.14}$$

Let us investigate the principle of virtual work and define the different works. To be didactic, we assume only one time t between times t_1 and t_2 where there is an atomic part in the works. The work of the acceleration forces is

2.4.1 The Work of the Acceleration Forces

In the smooth evolution, the work of the acceleration force is the sum of the classical power

$$\mathcal{P}_{acc}(\mathbf{V}(\tau)) = m\frac{\mathrm{d}\mathbf{U}}{\mathrm{d}t}(\tau)\cdot\mathbf{V}(\boldsymbol{\tau}), \tag{2.15}$$

where m is the mass of the point. Let us note that we have

Theorem 2.1 *In a smooth evolution, the variation of the kinetic energy is equal to the actual work of the acceleration*

$$\mathcal{W}_{acc}(\mathbf{U}, t_1, t_2) = \int_{t_1}^{t_2} \mathcal{P}_{acc}(\mathbf{U}(\boldsymbol{\tau}))d\tau = \frac{m}{2}(\mathbf{U}(t_2))^2 - \frac{m}{2}(\mathbf{U}(t_1))^2. \tag{2.16}$$

In the non smooth evolution, the work $\mathcal{T}_{acc}(\mathbf{V}, t)$ of the non smooth acceleration force, the discontinuity of the velocity $(\mathbf{U}^+(t) - \mathbf{U}^-(t))$ is

$$\mathcal{T}_{acc}(\mathbf{V}, t) = m(\mathbf{U}^+(t) - \mathbf{U}^-(t))\cdot L(\mathbf{V}), \tag{2.17}$$

where $L(\mathbf{V})$ is a linear function of velocity $\mathbf{V} \in \mathcal{V}$. Because we want to keep Theorem 2.1, we choose

$$L(\mathbf{V}) = \frac{\mathbf{V}^+(t) + \mathbf{V}^-(t)}{2}, \tag{2.18}$$

and have

$$\mathcal{T}_{acc}(\mathbf{V}, t) = m(\mathbf{U}^+(t) - \mathbf{U}^-(t))\cdot\frac{\mathbf{V}^+(t) + \mathbf{V}^-(t)}{2}, \tag{2.19}$$

with theorem

Theorem 2.2 *In a non smooth evolution, the variation of the kinetic energy is equal to the actual work of the acceleration*

$$\mathcal{T}_{acc}(\mathbf{U}, t) = \frac{m}{2}(\mathbf{U}^+(t))^2 - \frac{m}{2}(\mathbf{U}^-(t))^2. \tag{2.20}$$

The work of the acceleration with an atomic part at time t is

$$\mathcal{W}_{acc}(\mathbf{V}, t_1, t_2) = \int_{t_1}^{t_2} \mathcal{P}_{acc}(\mathbf{V}(\boldsymbol{\tau}))d\tau + \mathcal{T}_{acc}(\mathbf{V}, t) \tag{2.21}$$

$$= \int_{t_1}^{t_2} m\frac{\mathrm{d}\mathbf{U}}{\mathrm{d}t} \cdot \mathbf{V} d\tau + m(\mathbf{U}^+(t) - \mathbf{U}^-(t)) \cdot \frac{\mathbf{V}^+(t) + \mathbf{V}^-(t)}{2}. \tag{2.22}$$

The choice of the non smooth part of the virtual work of the acceleration forces is based on the wish to have its actual value to be equal to the variation of the kinetic energy.

2.4.1.1 The Theorem of the Kinetic Energy

The actual work of the acceleration forces, $\mathcal{W}_{acc}(\mathbf{U}, t_1, t_2)$ satisfies the theorem of kinetic energy, the théorème de l'énergie cinétique in French and il teorema dell'energia cinetica in Italian.

Theorem 2.3 *In an evolution, the variation of the kinetic energy is equal to the sum of the actual, internal and external works*

$$\frac{m}{2}(\mathbf{U}^+(t))^2 - \frac{m}{2}(\mathbf{U}^-(t))^2 = \mathcal{W}_{int}(\mathbf{U}, t_1, t_2) + \mathcal{W}_{ext}(\mathbf{U}, t_1, t_2). \tag{2.23}$$

Proof It is a direct application of Theorems 2.1 and 2.2. □

2.4.2 The Work of the External Forces

To define this work let us go back to the soccer field where a player kicks the ball which is flying. The external action of the player modifies instantaneously the ball velocity. The player has applied an instantaneous work. An other interesting observation is to look at a ball of a pin-ball machine hitting a bumper and getting an impulse from an electrical device which modifies instantaneously its velocity. Considering the system to be the ball. The system has received an external work which can be measured (at least we may think of such a measure) through the electrical energy consumption. We conclude that the work of the external forces we consider has jumps: it is a bounded variation function of time. Its time derivative has a density with respect to the Lebesgue measure and a density with respect to the atomic measure. The density with respect to the Lebesgue measure is the classical power we have defined in the previous section. Based on this idea, we choose the work of the external forces to be

$$\mathcal{W}_{ext}(\mathbf{V}, t_1, t_2) = \int_{t_1}^{t_2} \mathcal{P}_{ext}(\mathbf{V}(\boldsymbol{\tau}))d\tau + \mathcal{T}_{ext}(\mathbf{V}, t) \tag{2.24}$$

$$= \int_{t_1}^{t_2} \mathbf{f}^{ext}(\tau) \cdot \mathbf{V}(\boldsymbol{\tau})d\tau + \mathbf{P}^{ext}(t) \cdot \frac{\mathbf{V}^+(t) + \mathbf{V}^-(t)}{2}, \tag{2.25}$$

with

$$\mathcal{P}_{ext}(\mathbf{V}(\boldsymbol{\tau})) = \mathbf{f}^{ext}(\tau) \cdot \mathbf{V}(\tau)), \tag{2.26}$$

$$\mathcal{T}_{ext}(\mathbf{V}, t) = \mathbf{P}^{ext}(t) \cdot \frac{\mathbf{V}^{+}(t) + \mathbf{V}^{-}(t)}{2}, \tag{2.27}$$

where $\mathbf{f}^{ext}$ is the external force, for instance the gravity, and $\mathbf{P}^{ext}(t)$ the external percussion, the kick of the soccer player in the example, applied to the point.

Remark 2.2 The work of the external percussion may be

$$\mathcal{T}_{ext}(\mathbf{V}, t) = \mathbf{P}^{ext+}(t) \cdot \mathbf{V}^{+}(t) + \mathbf{P}^{ext-}(t) \cdot \mathbf{V}^{-}(t). \tag{2.28}$$

In fact, our choice is not restrictive, [18–20]. It has the advantage of being simple.

2.4.3 The Work of the Internal Forces

The virtual work of the internal force is a linear function of the virtual velocities of deformation which is null for any rigid system velocities. Because the plane is immobile, the rigid system velocities are $\mathbf{V}^{+} = \mathbf{V}^{-} = 0$. The work of the internal forces has to satisfy the Galilean relativity: the work of the internal force has to be null for any constant translation velocity of the system. Let us note that this property is equivalent to the internal work is null in any rigid body motion. A rigid body motion is such that the distance of the material points remains constant, thus in this situation the position of the points remain constant (remember the plane is immobile). The quantity which measures the evolution has to be null in such a motion. The distance of the material points of the system does not change. Because, the plane is immobile the only rigid body motion has a null velocity. Because the work of the internal forces is a linear function of the velocity, it is null for any rigid body motion. The work of the internal forces is a linear function of the velocity of deformation. Our choice is

$$\mathcal{W}_{int}(\mathbf{V}, t_1, t_2) = \int_{t_1}^{t_2} \mathcal{P}_{int}(\mathbf{V}(\boldsymbol{\tau}))d\tau + \mathcal{T}_{int}(\mathbf{V}, t) \tag{2.29}$$

$$= -\int_{t_1}^{t_2} \mathbf{R}^{int}(\tau) \cdot \mathbf{V}(\boldsymbol{\tau})d\tau - \mathbf{P}^{int}(t) \cdot \frac{\mathbf{V}^{+}(t) + \mathbf{V}^{-}(t)}{2}, \tag{2.30}$$

with

$$\mathcal{P}_{int}(\mathbf{V}(\boldsymbol{\tau})) = -\mathbf{R}^{int}(\tau) \cdot \mathbf{V}(\boldsymbol{\tau}), \tag{2.31}$$

$$\mathcal{T}_{int}(\mathbf{V}, t) = -\mathbf{P}^{int}(t) \cdot \frac{\mathbf{V}^{+}(t) + \mathbf{V}^{-}(t)}{2}, \tag{2.32}$$

Internal force $\mathbf{R}^{int}$ is a classical force which intervenes in smooth evolution, when the point is sliding on the plane or if there are at a distance interactions between the plane and the point, for instance if the point is tight to the plane by a long elastic string. Internal percussion $\mathbf{P}^{int}$ intervenes when the point collides with the plane.

Remark 2.3 The work of the internal percussion may be

$$\mathcal{T}_{int}(\mathbf{V}, t) = -\mathbf{P}^{int+}(t) \cdot \mathbf{V}^{+}(t) - \mathbf{P}^{int-}(t) \cdot \mathbf{V}^{-}(t). \tag{2.33}$$

In fact, this choice does not provide new opportunities, [18–20]. As said in Remark 2.2, it has the advantage of being simple. In case no external percussion is applied, the equation of motion, (2.41) down below, gives

$$\mathbf{P}^{int}(t) = \frac{\mathbf{P}^{int+}(t) + \mathbf{P}^{int-}(t)}{2}. \tag{2.34}$$

It is the choice of the works of the acceleration forces which is the important and leading choice.

2.5 The Equations of Motion

We derive the equations of motion using the assumption that time interval $]t_1, t[$ contains only one time t, $t_1 < t < t_2$, where two of the densities, i.e., the works, of the atomic measure are not null. By choosing virtual velocity with compact support in interval $]t_1, t[$, we get

$$\forall \mathbf{V} \in \mathcal{V}, \tag{2.35}$$

$$\int_{t_1}^{t} m \frac{\mathrm{d}\mathbf{U}}{\mathrm{d}t}(\tau) \cdot \mathbf{V}(\tau) d\tau = -\int_{t_1}^{t} \mathbf{R}^{int}(\tau) \cdot \mathbf{V}(\tau) d\tau + \int_{t_1}^{t} \mathbf{f}^{ext}(\tau) \cdot \mathbf{V}(\tau) d\tau. \tag{2.36}$$

The fondamental lemma of the variation calculus gives

$$m \frac{\mathrm{d}\mathbf{U}}{\mathrm{d}t} = -\mathbf{R}^{int} + \mathbf{f}^{ext}, \ a.e.\ in\ ]t_1, t[\,. \tag{2.37}$$

Remark 2.4 *a.e.* means almost everywhere or almost always in this context.

This relationship is also valid almost everywhere in interval $]t, t_2[$. It results it is valid almost everywhere in whole interval $]t_1, t_2[$.

Then the principle becomes

$$\forall \mathbf{V} \in \mathcal{V}, \tag{2.38}$$

$$m\,[\mathbf{U}(t)] \cdot \frac{\mathbf{V}^+(t) + \mathbf{V}^-(t)}{2} \tag{2.39}$$

$$= -\mathbf{P}^{int}(t) \cdot \frac{\mathbf{V}^+(t) + \mathbf{V}^-(t)}{2} + \mathbf{P}^{ext}(t) \cdot \frac{\mathbf{V}^+(t) + \mathbf{V}^-(t)}{2}. \tag{2.40}$$

It gives immediately

$$m\,[\mathbf{U}(t)] = -\mathbf{P}^{int}(t) + \mathbf{P}^{ext}(t). \tag{2.41}$$

Previous relationship shows that at time t at least two of its quantities are non null Because at times different from t, its three quantities are null, relationship (2.41) is satisfied at any time

$$\forall t \in]t_1, t_2[\,,\ m\,[\mathbf{U}(t)] = -\mathbf{P}^{int}(t) + \mathbf{P}^{ext}(t). \tag{2.42}$$

Remark 2.5 For a soccer ball, previous relationship is

1. when $m\,[\mathbf{U}(t)]$ and $\mathbf{P}^{int}(t)$ are non null with $\mathbf{P}^{ext}(t) = 0$, there is a collision: soccer ball hits the field;
2. when $m\,[\mathbf{U}(t)]$ and $\mathbf{P}^{ext}(t)$ are non null with $\mathbf{P}^{int}(t) = 0$, a player kicks the ball which is flying;
3. when $\mathbf{P}^{int}(t)$ and $\mathbf{P}^{ext}(t)$ are non null with $m\,[\mathbf{U}(t)] = 0$, a player kicks the ball vertically downward. Nothing occurs, the percussion applied by the foot of the player is equilibrated by the reaction of the field. Note that because it is impossible that the ball surges from the field, we have $\mathbf{U}^-(t) \cdot \mathbf{N} \leq 0$, where $\mathbf{N}$ is the upward normal vector to the field. Because the ball cannot interpenetrate the field, we have $\mathbf{U}^+(t) \cdot \mathbf{N} \geq 0$. Because the discontinuity of velocity is null, we get $\mathbf{U}^-(t) \cdot \mathbf{N} = \mathbf{U}^+(t) \cdot \mathbf{N} = 0$. Thus the ball is either at rest or sliding on the field;
4. when the three quantities of relationship (2.37) are non null there is a concomitant collision with the field and a kick by a player.

The other example of external percussion concomitant to a collision has been mentioned by Jean Jacques Moreau: in an electrical pin ball machine an impulse due to an electrical device is applied to a steel ball whenever it collides some obstacle called bumper.

A more general derivation of the equation of motion from the principle of virtual power is given in the book [19].

2.5.1 Properties of the Equations of Motion

The two Eqs. (2.37) and (2.42) describe:

- the smooth evolution, the free flight and the sliding of the point on the plane with Eq. (2.37) where the Lebesgue measure intervenes;
- the non smooth evolution or the collisions, with Eq. (2.41) where the atomic Dirac measure intervenes. This equation may be read two way: if there is a discontinuity of velocity, there is either an internal or an external percussion and if there is a percussion either external or internal, there is a discontinuity of velocity.

When Eq. (2.37) is no longer valid, quantities of Eq. (2.41) are non null. This is the case either if there is a kinematic constraint: the point hits the plane, or if there is a constraint related to the force, a sthenic constraint. This unexpected and not very common cause of discontinuity of velocity, an example of which is known as the Painlevé's paradox, [24, 26, 33–35], is not a paradox and it is taken into account by our theory, [19, 22].

Remark 2.6 Equations of motion (2.37) and (2.42) may be understood as a unique equality of measures

$$m d\mathbf{U} = -\mathbf{Z}^{int} + \mathbf{Z}^{ext}. \tag{2.43}$$

Differential measure $d\mathbf{U}$ is defined by

$$\langle d\mathbf{U}, \boldsymbol{\varphi} \rangle = \mathcal{T}_{acc}(t_1, t_2, \boldsymbol{\varphi}), \tag{2.44}$$

where $\boldsymbol{\varphi}$ is a continuous virtual velocity with compact support. This measure satisfies

$$\langle d\mathbf{U}, \boldsymbol{\varphi} \rangle = -\int_{t_1}^{t_2} \mathbf{U} \frac{d\boldsymbol{\varphi}}{dt} d\tau, \tag{2.45}$$

if $\boldsymbol{\varphi}$ is smooth enough. Measures $\mathbf{Z}^{int}$, the internal forces, and $\mathbf{Z}^{ext}$, the externals forces, are defined by

$$\left\langle \mathbf{Z}^{int}, \boldsymbol{\varphi} \right\rangle = \int_{t_1}^{t_2} \mathbf{R}^{int} \boldsymbol{\varphi} d\tau + \mathbf{P}^{int}(t) \boldsymbol{\varphi}(t), \tag{2.46}$$

$$\left\langle \mathbf{Z}^{ext}, \boldsymbol{\varphi} \right\rangle = \int_{t_1}^{t_2} \mathbf{f} \boldsymbol{\varphi} d\tau + \mathbf{P}^{ext}(t) \boldsymbol{\varphi}(t), \tag{2.47}$$

[29, 31]. In [31], Jean Jacques Moreau describe these equations with differential inclusions. Relationship (2.43) is an equality in the dual space of the space of bounded variations functions. An existence mathematical result of solutions of (2.43) is given in [9].

2.6 The Laws of Thermodynamics

For the sake of simplicity, we assume the point and plane have the same constant temperature T. Thus any heat which is produced is expelled toward the exterior. The case where the temperatures of the colliding solids evolve is investigated in Chap. 3 and in [6, 15, 19, 28].

2.6.1 The First Law

The energy balance is

$$\mathcal{E}^-(t_2) - \mathcal{E}^+(t_1) + \mathcal{K}^-(t_2) - \mathcal{K}^+(t_1) = \mathcal{T}_{ext}(t_1, t_2, \mathbf{U}) + \mathcal{C}(t_1, t_2), \tag{2.48}$$

where $\mathcal{E}$ is the internal energy of the system and $\mathcal{C}(t_1, t_2)$ is the amount of heat received by the system between times t_1 and t_2

$$\mathcal{C}(t_1, t_2) = \int_{t_1}^{t_2} TQ(\tau)d\tau + TB(t), \tag{2.49}$$

where $TQ(\tau)$ is the Lebesgue density of heat received at temperature T and $TB(t)$ is the heat received instantaneously at temperature T at collision time t. It is possible to measure those heat quantities, (see Chap. 3). If internal energy depends only on temperature, $-TQ(\tau)$ is the heat resulting from friction and $-TB(t)$ is the heat burst resulting from the collision. We have

$$\mathcal{E}^-(t_2) - \mathcal{E}^+(t_1) = \int_{t_1}^{t_2} \frac{d\mathcal{E}}{dt} d\tau + [\mathcal{E}(t)]\,, \tag{2.50}$$

Theorem of kinetic energy 2.3

$$\mathcal{T}_{acc}(t_1, t_2, \mathbf{U}) = \mathcal{T}_{int}(t_1, t_2, \mathbf{U}) + \mathcal{T}_{ext}(t_1, t_2, \mathbf{U}), \tag{2.51}$$

gives with the energy balance

$$\mathcal{E}^-(t_2) - \mathcal{E}^+(t_1) = -\mathcal{T}_{int}(t_1, t_2, \mathbf{U}) + \mathcal{C}(t_1, t_2). \tag{2.52}$$

This relationship satisfied for any times t_1 and t_2, gives

$$\frac{d\mathcal{E}}{dt} = \mathbf{R}^{int} \cdot \mathbf{U} + TQ, \ a.e.\ in\ ]t_1, t_2[\,, \tag{2.53}$$

and

$$[\mathcal{E}(t)] = \mathbf{P}^{int}(t) \cdot \frac{\mathbf{U}^+(t) + \mathbf{U}^-(t)}{2} + TB(t), \ \forall t \in]t_1, t_2[\,. \tag{2.54}$$

The last relationship describes the effects of the internal mechanical heat burst and of a possible external heat burst. Its quantities are null when there is neither collision, i.e., neither internal heat burst, nor external heat burst. If the internal energy depends only on temperature T, heat produced by a collision is expelled toward the external without modifying the temperature in agreement with our assumption. In a smooth evolution, the heat produced by friction is also immediately expelled toward the exterior. The case where the temperatures are no longer constant is investigated in [19].

2.6.2 The Second Law

The second law is

$$\mathcal{S}^-(t_2) - \mathcal{S}^+(t_1) \geq \int_{t_1}^{t_2} Q(\tau)d\tau + B(t), \tag{2.55}$$

where $\mathcal{S}$ is the entropy of the system and t is the collision time. We have

$$\mathcal{S}^-(t_2) - \mathcal{S}^+(t_1) = \int_{t_1}^{t_2} \frac{d\mathcal{S}}{dt} d\tau + [\mathcal{S}(t)]\,, \tag{2.56}$$

The law which is satisfied for any times t_1 and t_2 gives

$$\frac{d\mathcal{S}}{dt} \geq Q, \ a.e.\ in\ ]t_1, t_2[\,, \tag{2.57}$$

and

$$[\mathcal{S}(t)] \geq B(t), \quad \forall t \in]t_1, t_2[\,. \tag{2.58}$$

If the entropy depends only on temperature T and if there is no external burst of heat at times different from time t, the elements of this relationship are null at times different from time t.

2.6.2.1 A Useful Inequality

Let us recall that the free energy is $\Psi = \mathcal{E} - T\mathcal{S}$. Combining relationships (2.53) and (2.57), we get

$$\frac{d\Psi}{dt} \leq \mathbf{R}^{int} \cdot \mathbf{U}, \ a.e.\ in\ ]t_1, t_2[\,, \tag{2.59}$$

and combining relationships (2.54) and (2.58)

$$[\Psi(t)] \leq \mathbf{P}^{int}(t) \cdot \frac{\mathbf{U}^{+}(t) + \mathbf{U}^{-}(t)}{2}, \quad \forall t \in]t_1, t_2[\,. \tag{2.60}$$

If the free energy depends only on temperature T and if there is no external burst of heat at times different from time t, the elements of this relationship are null at times different from time t.

2.7 The Constitutive Laws

The two internal forces $\mathbf{R}^{int}$ and $\mathbf{P}^{int}(t)$ result from theoretical choices and experiments. Theoretical choices are controlled by relationships (2.59) and (2.60). They are a guide for the general expression of the internal forces which depend on some parameters. Experiments can be used to quantify them. In any case it is always possible to have an idea of their value. The theoretical results given by the predictive theory is compared to practical results. If we do not get what is expected and useful for the engineering project, adaptation are to be made. The simplest is to change the expression of the internal forces. The more sophisticated is to change some of the assumptions of the predictive theory. For instance to assume the solid, the soccer ball, is no longer represented by a point but it is represented either by a rigid solid or by a deformable solid and use the theories given either in Chaps. 4, 5, 6 or in 7. Let us recall a predictive theory is subjective: it is the engineer who chooses the sophistication of the theory he needs. In this book, we keep the instantaneity assumption for the different collisions but the other assumptions may be changed.

Internal forces are split into non dissipative or elastic forces and dissipative forces

$$\mathbf{R}^{int} = \mathbf{R}^{inte} + \mathbf{R}^{intd}, \ \mathbf{P}^{int} = \mathbf{P}^{inte} + \mathbf{P}^{intd}. \tag{2.61}$$

The definition of the internal forces is based on this splitting and on the structure of relationships (2.59) and (2.60): non dissipative forces are defined with the system free energy and the dissipative forces are defined either with a pseudo-potential of dissipation or with a dissipation function as for the Coulomb's friction law. This method described further down is not very demanding and offers innumerable openings with the advantage of satisfying automatically the mechanical laws (2.59) and (2.60). Of course, it is possible to follow another way but there are risks and verifications are to be performed. An example of such a situation is the restitution coefficient which is perfect for the collision of two spheres but is misleading in case of collisions of two or many solids (see [5, 7, 19]).

In this chapter, we want to give the basic elements of the collision theory and to show its large scope. For this purpose, we focus on simple constitutive laws, in fact in many cases on linear constitutive laws besides the non interpenetration conditions and thresholds we cannot avoid. We are convince that with those simple laws we

may capture the main physical properties. The fine and sophisticated constitutive laws will be easily integrated and adapted to each particular system.

2.7.1 The Free Energy and the Non Dissipative Forces

The free energy depends on the system state variables and defines the non dissipative or elastic forces. In the present situation, we may choose the position of the point with respect to the plane $\mathbf{x}(t)$ as state variable. It intervenes when there are at a distance interactions between the point and the plane, for instance when the ball is connected to a point of the plane by a long elastic wire. In this case the free energy depends on $\mathbf{x}(t) - \mathbf{x}_o$ where $\mathbf{x}_o$ is the elastic wire fixation point we choose as origin, [21]. Because the free energy accounts for the static properties, it has to take into account that the point is above the plane:

$$d(\mathbf{x}(t)) = \mathbf{x}(t) \cdot \mathbf{N} \geq 0, \tag{2.62}$$

where $\mathbf{N}$ is the upward normal vector to the plane. We forget the at a distance interactions and choose simple free energy Ψ

$$\Psi(\mathbf{x}) = I_+(d(\mathbf{x})), \tag{2.63}$$

where I_+ is the indicator function of $\mathbb{R}^+$ (see [12, 13, 32] or the appendix). Non dissipative forces are the generalized derivatives of the free energy

$$\mathbf{R}^{inte} \in \partial I_+(d(\mathbf{x}))\mathbf{N} = \partial\Psi(\mathbf{x}), \tag{2.64}$$

$$\mathbf{P}^{inte} = 0, \tag{2.65}$$

where ∂I_+ is the subdifferential set of function I_+, (see [12, 13, 32] or Sect. A.2.1 and A.4 of the appendix). Non dissipative force $-\mathbf{R}^{inte}$ is the non interpenetration reaction force of the plane: the action of the plane on the point. It is null if the point is not in contact with the plane. It is directed upward when the point slides on the plane. The non dissipative percussion $\mathbf{P}^{inte}$ is null because $[\Psi(t)] = 0$. In a collision, the non interpenetration is not ensured by a non dissipative percussion. It is to be ensured by a dissipative percussion. This means that the non interpenetration reaction works. This reaction cannot be workless or perfect (liaison parfaite in French, vincolo perfetto in Italian). The dissipative character of collisions appears. Some properties we are accustomed to disappear. We mention them in the sequel.

Remark 2.7 Adjective elastic is used with its abstract meaning equivalent to non dissipative.

2.7.2 The Dissipative Forces

Relationships (2.59) and (2.60) show that it is wise to assume that the internal forces depend not only on d, as we already know, but also on $\mathbf{U}$ and $\left(\mathbf{U}^+(t)+\mathbf{U}^-(t)\right)/2$ which describe how the form of the system evolves.

2.7.2.1 The Dissipative Forces Defined with a Pseudo-potential of Dissipation

A pseudo-potential of dissipation $\Phi(X,\chi)$, introduced by Jean Jacques Moreau, is a convex function of X, with value in $\bar{\mathbb{R}}=\mathbb{R}\cup\{\infty\}$, positive and null at the origin, $\Phi(0,\chi)=0$, [23, 27, 30]. At any time $\chi(t)$ depends on the past but not on X. Internal dissipative forces are given by the subdifferential set with respect to X of $\Phi(X,\chi)$ (see [12, 13, 32] or Sect. A.4 of the appendix).

In the present situation, X is either $\mathbf{U}$ or $\left(\mathbf{U}^+(t)+\mathbf{U}^-(t)\right)/2$. The internal dissipative forces are either $\mathbf{R}^{intd}$ or $\mathbf{P}^{intd}$

$$\mathbf{R}^{intd}\in\partial\tilde{\varphi}(\mathbf{U},\chi),\ \mathbf{P}^{intd}\in\partial\tilde{\Phi}(\frac{\mathbf{U}^+ +\mathbf{U}^-}{2},\chi). \tag{2.66}$$

Assuming there is no at a distance actions, the dissipative forces are null when the point is not in contact with the plane. Thus we let d be a χ quantity and choose pseudo-potentials of dissipation null for $d>0$

$$\tilde{\varphi}(\mathbf{U},d)=\begin{cases}0,\ \textit{if}\ d>0,\\ \varphi(\mathbf{U}),\ \textit{if}\ d=0,\end{cases} \tag{2.67}$$

for smooth evolution, and

$$\tilde{\Phi}(\frac{\mathbf{U}^+ +\mathbf{U}^-}{2},d,\mathbf{U}^-\cdot\mathbf{N})=\begin{cases}0,\ \text{if}\ d>0,\\ \Phi(\frac{\mathbf{U}^+ +\mathbf{U}^-}{2})+I_+(\mathbf{U}^+\cdot\mathbf{N}),\ \text{if}\ d=0,\end{cases} \tag{2.68}$$

for the collisions; i.e., for the non smooth evolutions. We have added $\mathbf{U}^-\cdot\mathbf{N}$ in quantities χ for the non interpenetration condition. Because when $d=0$, non interpenetration is insured if normal velocity after collision is directed upward, $\mathbf{U}^+\cdot\mathbf{N}\geq 0$. This is why indicator function

$$I_+(\mathbf{U}^+\cdot\mathbf{N})=I_+(\frac{\mathbf{U}^+ +\mathbf{U}^-}{2}\cdot\mathbf{N}-\frac{\mathbf{U}^-}{2}\cdot\mathbf{N}), \tag{2.69}$$

intervenes. Clearly it is a function of $(\mathbf{U}^+ +\mathbf{U}^-)/2$ and $\chi=(d,\mathbf{U}^-\cdot\mathbf{N})$. For $X=0$, $X=(\mathbf{U}^+ +\mathbf{U}^-)/2=0$, indicator function

$$I_+(0 - \frac{\mathbf{U}^-}{2} \cdot \mathbf{N}), \tag{2.70}$$

is actually null because normal velocity before collision, $\mathbf{U}^- \cdot \mathbf{N} \leq 0$, is non positive.

Remark 2.8 Situation where $\mathbf{U}^- \cdot \mathbf{N} > 0$, is physically impossible because the point cannot surge from the plane Moreover $\tilde{\Phi}$ is no longer a pseudo-potential of dissipation because $\tilde{\Phi}(0, d, \mathbf{U}^- \cdot \mathbf{N}) = +\infty$ for $d = 0$.

Dissipative forces are defined by

$$\mathbf{R}^{intd} \in \partial\tilde{\varphi}(\mathbf{U}, d) = \begin{cases} 0, \ \textit{if } d > 0, \\ \partial\varphi(\mathbf{U}), \ \text{if } d = 0, \end{cases} \tag{2.71}$$

$$\mathbf{P}^{intd} = \mathbf{P}^{int} \in \partial\tilde{\Phi}(\frac{\mathbf{U}^+ + \mathbf{U}^-}{2}, d, \mathbf{U}^- \cdot \mathbf{N}) \tag{2.72}$$

$$= \begin{cases} 0, \ \textit{if } d > 0, \\ \partial\Phi(\frac{\mathbf{U}^+ + \mathbf{U}^-}{2}) + \partial I_+(\frac{\mathbf{U}^+ + \mathbf{U}^-}{2} \cdot \mathbf{N} - \frac{\mathbf{U}^-}{2} \cdot \mathbf{N})\mathbf{N}, \ \textit{if } d = 0. \end{cases} \tag{2.73}$$

Remark 2.9 Subdifferential set $\partial\tilde{\Phi}(X, \chi)$ is computed with respect to $X \in \mathbb{R}^3$ with the usual scalar product in $\mathbb{R}^3$.

These forces are actually null when there is no contact. Non interpenetration percussion

$$P^{reac}\mathbf{N} \in \partial I_+(\frac{\mathbf{U}^+ + \mathbf{U}^-}{2} \cdot \mathbf{N} - \frac{\mathbf{U}^-}{2} \cdot \mathbf{N})\mathbf{N} = \partial I_+(\mathbf{U}^+ \cdot \mathbf{N})\mathbf{N}, \tag{2.74}$$

is normal to the plane. It is active only if $\mathbf{U}^+ \cdot \mathbf{N} = 0$, i.e., if the future normal velocity is null meaning that there is a risk of interpenetration. We remark that the non interpenetration reaction appears when the other mechanical effects are not sufficient to prevent interpenetration. This percussion works with work

$$P^{reac}\mathbf{N} \cdot \frac{\mathbf{U}^+ + \mathbf{U}^-}{2} = P^{reac}\frac{\mathbf{U}^- \cdot \mathbf{N}}{2} \geq 0. \tag{2.75}$$

We denote in the sequel

$$\mathbf{P}^{int} = \mathbf{P}^d + P^{reac}\mathbf{N} = \mathbf{P}^d + \mathbf{P}^{reac}. \tag{2.76}$$

2.7.2.2 Internal Forces Defined with a Dissipation Function

A dissipation function is a real function $\Phi(X, \chi)$ where at any time $\chi(t)$ depends on the past and possibly on X. This function is differentiable or has a generalized derivative with respect to X, in a domain which contains at least the origin, $X = 0$. It satisfies

$$\forall Y,\ grad_X \Phi(Y, \chi) \cdot Y \geq 0. \tag{2.77}$$

The dissipative forces are given by the derivative of $\Phi(X, \chi)$ with respect to X.

2.7.2.3 A Property of Dissipative Internal Forces Defined Either with a Pseudo-potential of Dissipation or with a Dissipation Function

An advantage of defining the dissipative forces either with a pseudo-potential of dissipation or with a function of dissipation is that relationships (2.59) and (2.60) are satisfied. Moreover experimental results fit very often with pseudo-potential of dissipation. There are some cases but important cases where experimental results are more easily taken into account by a dissipation function.

Theorem 2.4 *If dissipative internal forces are defined either by a pseudo-potential of dissipation or by a dissipation function, relationships (2.59) et (2.60) are satisfied.*

Proof In case of a pseudo-potential, the proof is classical [18, 27]. In case of a dissipation function, the proof relies on relationship (2.77).

Examples are given in following section. Let us note that a pseudo-potential of dissipation is a dissipation function but the converse is not true.

The presentation of the predictive theory of the motion of a point above a plane is achieved. It remains to identify the constitutive laws with experiments giving hints to choose either a pseudo-potential of dissipation or a function of dissipations.

2.8 Examples of Collisions with Internal Forces Defined with a Pseudo-potential of Dissipation

In these examples, we decouple the collision normal to the plane phenomena from the tangential phenomena.

We define the normal and tangential percussions

$$\mathbf{P}^{int} = P_N \mathbf{N} + \mathbf{P}_T,\ P_N = \mathbf{P}^{int} \cdot \mathbf{N}, \tag{2.78}$$

with the normal and tangential velocities

$$\mathbf{U} = U_N \mathbf{N} + \mathbf{U}_T,\ U_N = \mathbf{U} \cdot \mathbf{N}. \tag{2.79}$$

We split the pseudo-potential into a part giving the normal percussion depending on the normal velocity and a part giving the tangential percussion depending on the tangential velocity

$$\Phi(\frac{\mathbf{U}^+ + \mathbf{U}^-}{2}) + I_+(\mathbf{U}^+ \cdot \mathbf{N}) = \Phi_T(\frac{\mathbf{U}_T^+ + \mathbf{U}_T^-}{2}) + I_+(\mathbf{U}^+ \cdot \mathbf{N}) + \Phi_N(\frac{U_N^+ + U_N^-}{2}). \tag{2.80}$$

2.8.1 First Example

The normal and tangential evolutions are decoupled. And we choose $\Phi_T = 0$ and $\Phi_N(X) = kX^2$ quadratic functions giving linear internal forces (besides the non interpenetration reaction). Moreover $\Phi_T = 0$, gives a tangential percussion null We have

$$P_N \in \frac{\partial \Phi_N}{\partial X}(\frac{U_N^+ + U_N^-}{2}) + \partial I_+(\frac{U_N^+ + U_N^-}{2} - \frac{U_N^-}{2}) \tag{2.81}$$

$$= k(U_N^+ + U_N^-) + \partial I_+(U_N^+), \tag{2.82}$$

$$P_N^d = k(U_N^+ + U_N^-),\ P_N^{reacd} \in \partial I_+(U_N^+), \tag{2.83}$$

$$\mathbf{P}_T = 0. \tag{2.84}$$

2.8.1.1 A Collision

Let us consider le point falling on the plane. Equations of motion and constitutive laws give

$$m\,[\mathbf{U}_T] = -\mathbf{P}_T = 0, \tag{2.85}$$

$$m\,[U_N] = -P_N \in -k(U_N^+ + U_N^-) - \partial I_+(U_N^+). \tag{2.86}$$

First equation proves that the tangential velocity is continuous: it is not modified by the collision. Second equation is easy to solve

- if $m < k$, i.e., if the solid is light or the dissipation is important in collisions, the point bounces with velocity

$$U_N^+ = \frac{m-k}{m+k} U_N^-, \tag{2.87}$$

and non interpenetration reaction percussion is null

$$P_N^{reacd} = 0\,; \tag{2.88}$$

- if $m > k$, if the solid is heavy or if the dissipation is not important in collisions, the point does not bounce. It remains in contact with the plane and slides

$$U_N^+ = 0, \tag{2.89}$$

and non interpenetration reaction percussion is

$$P_N^{reacd} = (m-k)U_N^- \leq 0, \tag{2.90}$$

the dissipative percussion being

$$P_N^d = kU_N^-. \tag{2.91}$$

Dissipated energy is

$$\mathbf{P}^{int} \cdot \frac{\mathbf{U}^+ + \mathbf{U}^-}{2} = (P_N^d + P_N^{reacd})\frac{U_N^+ + U_N^-}{2} = \tag{2.92}$$

$$= \frac{k}{2}(\frac{2m}{m+k})^2 \left(U_N^-\right)^2, \text{ if } m < k, \tag{2.93}$$

$$= \frac{k}{2}\left(U_N^-\right)^2 + \frac{m-k}{2}\left(U_N^-\right)^2 = \frac{m}{2}\left(U_N^-\right)^2, \text{ if } m > k. \tag{2.94}$$

We remark again that the non interpenetration reaction percussion is dissipative and it intervenes only if interpenetration is at risk, i.e., if the point does not bounce. The energy dissipated by this reaction is maximal for $k = 0$. It decreases to 0 when k increases up to m. We may note that if k is small, dissipation is mostly due to the reaction percussion and that if k is large the whole dissipation is due to the dissipative percussion. This is in agreement with our vocabulary. Let us also note another property which may be surprising, when dissipative parameter k is infinite, dissipation is null. But when k tends toward infinity, deformation velocity $U_N^+ + U_N^-$ tends to 0. The system tends to become rigid! Thus it is correct that the dissipation tends to 0, the dissipation in a rigid or undeformable system. The pseudo-potential tends to $I_0(U_N^+ + U_N^-)$ where I_0 is the indicator function of the origin. If we assume the same type of constitutive law for the smooth evolution pseudo-potential $I_0(U_N)$ implies rigidity for the vertical displacement. As soon as the point gets into contact with the plane, it is irremediably fixed to it. It remains free to slide on the plane without dissipation with the tangential constitutive law we have chosen. Thus it is good that the dissipated energy tends to 0 when k tends to ∞.

2.8.2 Second Example

We may choose sophisticated pseudo-potentials. For instance

$$\Phi_N\left(\frac{U_N^+ + U_N^-}{2}\right) = k_0 np\left(\frac{U_N^+ + U_N^- + 2U_{\lim}}{2}\right) \tag{2.95}$$

$$+k\left(np\left(\frac{U_N^+ + U_N^- + 2U_{\lim}}{2}\right)\right)^2, \tag{2.96}$$

where we assume $(k_0/m) \geq U_{\lim} \geq 0$ and $np(x)$ denotes the negative part function see (A.2.1)

$$np(x) = \begin{cases} -x, \ if \ x \leq 0, \\ 0, \ if \ x \geq 0. \end{cases} \tag{2.97}$$

Remark 2.10 We have

$$\left| \left(np(\frac{U_N^+ + U_N^- + 2U_{\lim}}{2}) \right) \right| = np\left(\frac{U_N^+ + U_N^- + 2U_{\lim}}{2} \right). \tag{2.98}$$

The subdifferential set of $np(x)$ is

$$G(x) = \begin{cases} 0, \ if \ x > 0, \\ [-1, 0], \ sii f \ x = 0, \\ -1, \ if \ x < 0. \end{cases} \tag{2.99}$$

Graph $G(x) = -H(-x)$ where graph $H(x)$ is the subdifferential set of the positive part function defined by formula (A.2.1). Constitutive law is

$$P_N \in k_0 G(U_N^+ + U_N^- + 2U_{\lim}) - k\left(np(U_N^+ + U_N^- + 2U_{\lim})\right) + \partial I_+(U_N^+). \tag{2.100}$$

We let $X = U_N^+ + U_N^- + 2U_{\lim}$

$$mX + k_0 G(X) - knp(X) + \partial I_+(X - U_N^- - 2U_{\lim}) \ni 2m\left(U_N^- + U_{\lim}\right). \tag{2.101}$$

In the case $m - k \geq 0$, i.e., if the point is heavy or the dissipation is not important in collisions we have, (remember we have assumed $U_{\lim} \leq k_0/(2m)$)

$$U_N^+ = 0, \ \text{if} \ 0 \leq -U_N^- \leq 2U_{\lim} \tag{2.102}$$

$$U_N^+ = -U_N^- - 2U_{\lim}, \ if \ 2U_{\lim} \leq -U_N^- \leq U_{\lim} + \frac{k_0}{2m}, \tag{2.103}$$

$$U_N^+ = \frac{k_0}{m+k} + \frac{m-k}{m+k} U_N^- - \frac{2k}{m+k} U_{\lim}, \tag{2.104}$$

$$if \ U_{\lim} + \frac{k_0}{2m} \leq -U_N^- \leq \frac{k_0}{m-k} - \frac{2k}{m-k} U_{\lim}, \tag{2.105}$$

$$U_N^+ = 0, \ \text{if} \ -U_N^- \geq \frac{k_0}{m-k} - \frac{2k}{m-k} U_{\lim}. \tag{2.106}$$

Function $-U_N^- \to U_N^+$ shown on Fig. 2.1, illustrates what happened when a gangsters' car, pursued by a police one, drives on speed bumps (the car is shown by a point):

- when the car travels at low speed, it takes off on the first speed bump and falls back at low vertical speed. $0 \leq -U_N^- \leq 2U_{\text{lim}}$. The car does not bounce back, $U_N^+ = 0$, the gangsters haven't found out that the police follows them;
- on the next speed bump, the gangsters understand the police is after them. They try to escape and increase their speed. The car takes off and falls back at a vertical speed $-U_N^-$ satisfying

$$2U_{\text{lim}} \leq -U_N^- \leq \frac{k_0}{m-k} - \frac{2k}{m-k}U_{\text{lim}}. \tag{2.107}$$

  The car bounces as it falls back, it keeps travelling, potentially bouncing back several times while accelerating more and more;
- on the following speed bump, the gangsters' car is at a breakneck speed, it flies off and falls back at a high vertical speed,

$$-U_N^- \geq \frac{k_0}{m-k} - \frac{2k}{m-k}U_{\text{lim}}. \tag{2.108}$$

  As it falls back, the springs and shock absorbers are not sufficient to withstand the impact. They break and thus unable the car to bounce. As such, the car does not bounce, $U_N^+ = 0$ and is not in a state to travel as it is not suspended anymore. The police can now stops the gangsters.

Function U_N^+ versus $-U_N^-$ plotted on Fig. 2.1 shows that the physical behaviours may be non monotonous and sophisticated whereas the constitutive laws are rather simple.

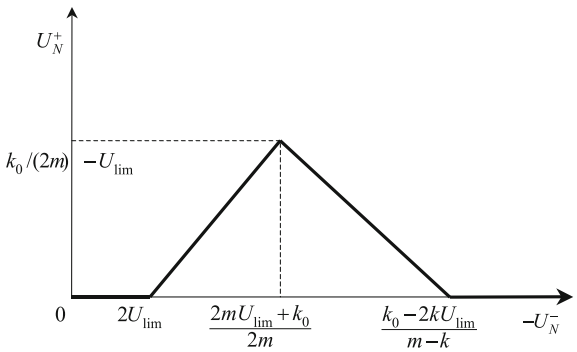

Fig. 2.1 The vertical velocity U_N^+ of a solid after collision versus its velocity $-U_N^-$ before collision. The solid shown by a point, bounces only at medium vertical velocity. At low or high velocity, it does not bounce. This is what happens when a car drives on speed bumps. After taking off on the bump, when falling down with a low vertical velocity, it does not bounce, it bounces when falling down at medium velocity due to its springs and shock absorbers and does not bounce when falling at high velocity, breaking its springs and shock absorbers

2.8.3 Third Example. Interpenetration Is Possible

Let us consider a steel ball falling on a tightened sheet of paper. Depending on its velocity and mass, it can get through the sheet of paper. We choose the following pseudo-potential of dissipation no longer involving the non interpenetration condition (2.68).

$$\tilde{\Phi}(\frac{\mathbf{U}^+ + \mathbf{U}^-}{2}, \frac{\mathbf{U}^-}{2}) = k_0 np\left(\frac{U_N^+ + U_N^-}{2} - \frac{U_N^-}{2}\right) \tag{2.109}$$

$$+k\left(\frac{U_N^+ + U_N^-}{2}\right)^2, \tag{2.110}$$

It satisfies $\tilde{\Phi}(0, \mathbf{U}^-/2) = 0$ because $\mathbf{U}^- \cdot \mathbf{N} < 0$. Internal percussion is

$$P_N = \frac{\partial \tilde{\Phi}}{\partial((\mathbf{U}^+ + \mathbf{U}^-)/2)} \in k\left(U_N^+ + U_N^-\right) + k_0 G\left(U_N^+\right), \tag{2.111}$$

where graph G, subdifferential set of negative part function np, is defined by (2.99). Equation giving normal velocity

$$m(U_N^+ - U_N^-) = -P_N \in -k_0 G\left(U_N^+\right) - k(U_N^+ + U_N^-), \tag{2.112}$$

is solved by letting $X = U_N^+ + U_N^-$. It becomes

$$mX + k_0 G(X - U_N^-) + kX \ni 2mU_N^-. \tag{2.113}$$

Because graph $Y \to mY + k_0 G(Y - U_N^-) + kY$ is monotone, maximal and surjective, Previous equation has one and only one solution which is

1. si $m - k \leq 0$, i.e., either the ball is light or the system is very dissipative, the ball bounces with velocity

$$U_N^+ = \frac{m-k}{m+k} U_N^- \; ; \tag{2.114}$$

2. if $m - k \geq 0$, i.e., if the ball is heavy or the system is weakly dissipative,

   a. if falling velocity is low,

$$-U_N^- \leq \frac{k_0}{m-k}, \tag{2.115}$$

   the ball does not bounce. It is stopped by the sheet of paper

$$U_N^+ = 0 \; ; \tag{2.116}$$

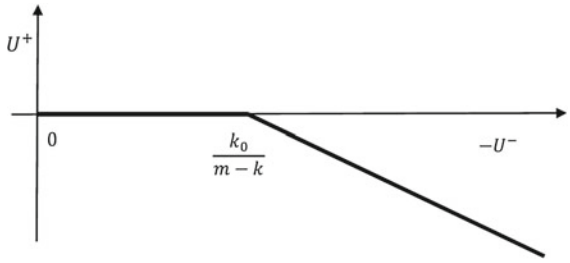

Fig. 2.2 The velocity U^+ of the steel ball versus its velocity $-U^-$ before colliding the sheet of paper. When the falling velocity is low, $-U^- \leq k_0/(m-k)$, the ball is stopped by the sheet of paper. When it is high, $-U^- \geq k_0/(m-k)$, the steel ball transfixes the sheet of paper

b. if falling velocity is large

$$-U_N^- \geq \frac{k_0}{m-k}, \tag{2.117}$$

the ball transfixes the sheet of paper with velocity

$$U_N^+ = \frac{k_0}{m+k} + \frac{m-k}{m+k}U_N^-, \tag{2.118}$$

$$U_N^- < U_N^+ \leq 0. \tag{2.119}$$

The ball is still falling but it is slowed down when getting through the sheet of paper, (Fig. 2.2).

This idea has been used by to predict avalanches of rocks in mountain forests. The trees can be broken by the falling rocks, [11].

Remark 2.11 Quasi-static collision. If we neglect the inertia effects. Collision equation of motion becomes

$$0 = m\,[\mathbf{U}] = -\mathbf{P}^{int} + \mathbf{P}^{ext}. \tag{2.120}$$

When there is no external percussion and the constitutive law is given by pseudo-potential of dissipation

$$I_+(U_N^+) + \Phi_N\left(\frac{U_N^+ + U_N^-}{2}\right), \tag{2.121}$$

we have

$$0 \in \partial I_+(U_N^+) + \partial\Phi_N\left(\frac{U_N^+ + U_N^-}{2}\right). \tag{2.122}$$

This equation has always solution $U_N^+ + U_N^- = 0$. The point rebounces. No information is given on the tangential motion. We may choose the continuity of the tangential velocity.

2.9 Examples of Dissipative Forces Defined with a Function of Dissipation

The important behaviour described by a function of dissipation is the Coulomb behaviour which intervenes in the smooth motion but also in the collisions. Moreover the two constitutive laws are related, [19].

2.9.1 The Coulomb's Friction Law

The normal and tangential forces are

$$\mathbf{R}^{int} = R_N\mathbf{N} + \mathbf{R}_T,\ R_N = \mathbf{R}^{int}\cdot\mathbf{N}. \tag{2.123}$$

The normal and tangential velocities are

$$\mathbf{U} = U_N\mathbf{N} + \mathbf{U}_T,\ U_N = \mathbf{U}\cdot\mathbf{N}. \tag{2.124}$$

We choose

$$X = \begin{pmatrix} U_N \\ \mathbf{U}_T \end{pmatrix},\ \chi = -R_N, \tag{2.125}$$

and

$$\Phi(X,\chi) = \begin{pmatrix} 0 \\ -R_N\phi(\mathbf{U}_T) \end{pmatrix}, \tag{2.126}$$

where ϕ is a pseudo-potential of dissipation.

Pseudo-potential $\phi(\mathbf{U}_T) = \mu\,\|\mathbf{U}_T\|$ where $\mathbf{U}_T$ is the tangential velocity, is often chosen. Function $\Phi(X,\chi)$ is not a pseudo-potential of dissipation because normal reaction $\chi = -R_N$ is not a function of the state quantities, i.e., position or distance d. It can depend on $\mathbf{U}_T$. Coulomb's friction law is defined by

$$\mathbf{R}^{inte} = \begin{pmatrix} R_N^e \\ \mathbf{R}_T^e \end{pmatrix} \in \begin{pmatrix} \partial I_+(d) \\ 0 \end{pmatrix}, \tag{2.127}$$

$$\mathbf{R}^{intd} = \begin{pmatrix} R_N^d \\ \mathbf{R}_T^d \end{pmatrix} \in \begin{pmatrix} 0 \\ -R_N\partial\phi(\mathbf{U}_T) \end{pmatrix}, \tag{2.128}$$

$$\mathbf{R}^{int} = \mathbf{R}^{inte} + \mathbf{R}^{intd} = \begin{pmatrix} R_N \\ \mathbf{R}_T \end{pmatrix} \in \begin{pmatrix} \partial I_+(d) \\ 0 \end{pmatrix} + \begin{pmatrix} 0 \\ -R_N\partial\phi(\mathbf{U}_T) \end{pmatrix}. \tag{2.129}$$

Tangential force is given by relationships

$$\mathbf{R}_T = -R_N\mu\frac{\mathbf{U}_T}{\|\mathbf{U}_T\|},\ \text{if } \mathbf{U}_T \neq 0, \tag{2.130}$$

$$\|\mathbf{R}_T\| \leq -R_N\mu,\ \text{if } \mathbf{U}_T = 0. \tag{2.131}$$

2.9.2 The Coulomb's Collision Law

For collisions, internal percussion is split in the same way

$$\mathbf{P}^{int} = P_N \mathbf{N} + \mathbf{P}_T,\ P_N = \mathbf{P}^{int} \cdot \mathbf{N}. \tag{2.132}$$

Coulomb collision dissipation function is

$$X = \begin{pmatrix} \frac{U_N^+ + U_N^-}{2} \\ \frac{\mathbf{U}_T^+ + \mathbf{U}_T^-}{2} \end{pmatrix},\ \chi = \left(-P_N,\ \frac{U_N^-}{2},\ d \right), \tag{2.133}$$

and

$$\Phi(X, \chi) = 0,\ \textit{if}\ d > 0, \tag{2.134}$$

$$\Phi(X, \chi) = \begin{pmatrix} \Phi_N(\frac{U_N^+ + U_N^-}{2}) + I_+(\frac{U_N^+ + U_N^-}{2} - \frac{U_N^-}{2}) \\ -P_N \phi(\frac{\mathbf{U}_T^+ + \mathbf{U}_T^-}{2}) \end{pmatrix},\ \textit{if}\ d = 0. \tag{2.135}$$

Collision Coulomb constitutive law is

$$\mathbf{P}^{int} = \begin{pmatrix} P_N \\ \mathbf{P}_T \end{pmatrix} = \mathbf{P}^d + \mathbf{P}^{reac}, \tag{2.136}$$

$$\mathbf{P}^{int} = 0,\ \textit{if}\ d > 0, \tag{2.137}$$

$$\mathbf{P}^{int} \in \begin{pmatrix} \partial \Phi_N(\frac{U_N^+ + U_N^-}{2}) + \partial I_+(\frac{U_N^+ + U_N^-}{2} - \frac{U_N^-}{2}) \\ -P_N \partial \phi(\frac{\mathbf{U}_T^+ + \mathbf{U}_T^-}{2}) \end{pmatrix},\ \textit{if}\ d = 0, \tag{2.138}$$

$$\mathbf{P}^d \in \begin{pmatrix} \partial \Phi_N(\frac{U_N^+ + U_N^-}{2}) \\ -P_N \partial \phi(\frac{\mathbf{U}_T^+ + \mathbf{U}_T^-}{2}) \end{pmatrix},\ \mathbf{P}^{reac} \in \begin{pmatrix} \partial I_+(\frac{U_N^+ + U_N^-}{2} - \frac{U_N^-}{2}) \\ 0 \end{pmatrix},\ \textit{if}\ d = 0, \tag{2.139}$$

where Φ_N and ϕ are pseudo-potentials of dissipation. Function $\Phi(X, \chi)$ is not a pseudo-potential of dissipation because P_N depends on $U_N^+ + U_N^-$. We see again that collisions are uniquely dissipative phenomenons.

2.9.3 Experimental Results

Experimental results, [7, 8, 10] show that $\phi(\mathbf{U}_T) = \mu \left\| \frac{\mathbf{U}_T^+ + \mathbf{U}_T^-}{2} \right\|$ may be chosen for collisions of small steel squares with a marble table (see Figs. 2.3 and 2.4). Then tangential percussion is

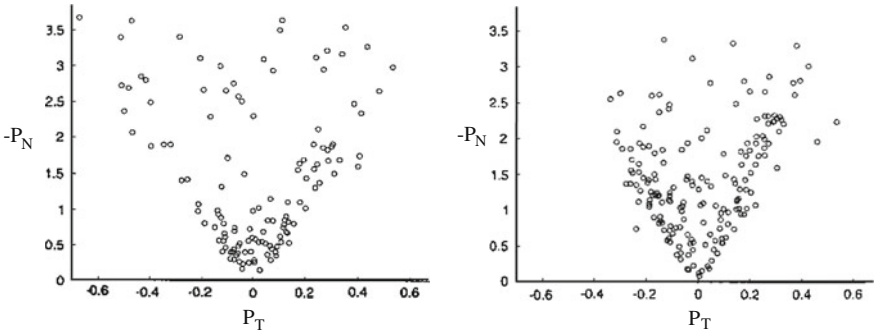

Fig. 2.3 Normal percussion $-P_N$ versus tangential percussion P_T for two small solids colliding a marble table. Coulomb cone with collision coefficient of friction $\mu = 0.22$ is conspicuous. *Left* figure is for small steel triangles and *right* figure for small steel rectangles, [7]

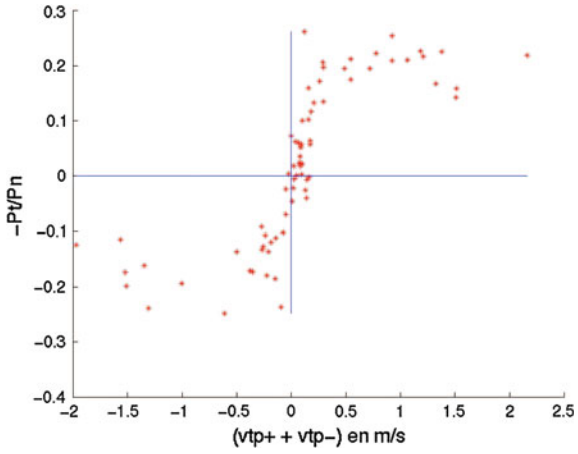

Fig. 2.4 Quotient $-P_T/P_N$ versus $U_T^+ + U_T^-$ in m/s for small steel triangles colliding a marble table. Collision coefficient of friction is 0.22 equal to the smooth motion coefficient of friction Coulomb's law appears clearly even if the experimental results are scattered, [7]. One may compare with Fig. 2.5 where no functional relationship appears

$$\mathbf{P}_T = -P_N \mu \frac{\mathbf{U}_T^+ + \mathbf{U}_T^-}{\left\| \mathbf{U}_T^+ + \mathbf{U}_T^- \right\|}, \text{ if } \mathbf{U}_T^+ + \mathbf{U}_T^- \neq 0, \tag{2.140}$$

$$\|\mathbf{P}_T\| \leq -P_N \mu, \text{ if } \mathbf{U}_T^+ + \mathbf{U}_T^- = 0. \tag{2.141}$$

These experimental results show that there are good functional relationships between percussions and velocity of deformation $\mathbf{U}^+ + \mathbf{U}^-$ whereas nothing pertinent appears when investigating the percussions versus either the deformation velocity before collision, $\mathbf{U}^-$ or the deformation velocity after collision, $\mathbf{U}^+$, [7, 17]. This is in agreement with theoretical inequality (2.60) which suggests that to relate $\mathbf{P}^{int}$ and $\mathbf{U}^+ + \mathbf{U}^-$ may be productive. Let us note that there is a priori no hint to look for relationships between these quantities. As already said the important interest of relationship (2.60) is to guide experimental work and theoretical choices.

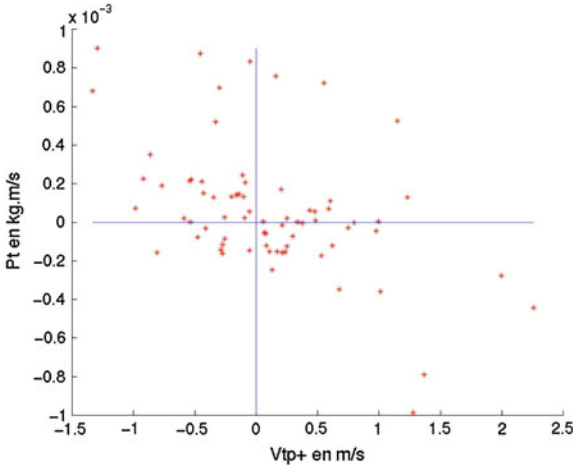

Fig. 2.5 Tangential internal percussion versus tangential velocity U_T^+ after collision. No functional relationship may be founded. We have the same result for the tangential percussion versus tangential velocity U_T^- before collision

2.9.4 Relationships Between Smooth Friction and Collision Constitutive Laws

The experimental results for collisions between steel small solids and a marble table, in fact a massive polished stone table, give a Coulomb's collision coefficient 0.17 approximatively. The dry coefficient of friction for steel-stone is of this order, around 0.2. Moreover it appears a relationship between collisions with the Coulomb law and smooth sliding on the plane with Coulomb friction law. It may be proved that smooth sliding is the limit of periodic small jumps (Coulomb collisions with rebounds) when the amplitude of the jumps tends to zero, [19]. Thus experimental and theoretical results suggest to have for both smooth friction and non smooth collisions, the Coulomb's law with the same coefficient. Of course this choice is not compulsory but without more experimental information, it is reasonable.

References

1. Ambrosio, L., Fusco, N., Pallara, D.: Special Functions of Bounded Variations and Free Discontinuity Problems. Oxford University Press, Oxford (2000)
2. Attouch, H., Buttazzo, G., Michaille, G.: Variational Analysis in Sobolev and BV Spaces, Application to PDE and Optimization. MPS/SIAM Series in Optimization. SIAM, Philadelphia (2004)
3. Brach, R.: Friction, restitution and energy loss in planar collision. ASME J. Appl. Mech. **51**, 164–170 (1984)
4. Brogliato, B.: Nonsmooth Mechanics. Springer, Berlin (1999)
5. Caselli, F., Frémond, M.: Collisions of three balls on a plane. Comput. Mech. **43**(6), 743–754 (2009)

6. Caucci, A.M., Frémond, M.: Thermal effects of collisions: does rain turn into ice when it falls on a frozen ground? J. Mech. Mater. Struct. **4**(2), 225–244. http://pjm.math.berkeley.edu/jomms/2009/4-2/index.xhtml (2009)
7. Cholet, C.: Chocs de solides rigides, Ph.D. thesis, Université Pierre et Marie Curie, Paris (1998)
8. Chevoir, F., Cholet, C., Frémond, M.: Chocs de solides rigides. théorie et expériences, Impact in Mechanical Systems, Grenoble, Euromech colloquium 397 (1999)
9. Cholet, C.: Collisions d'un point et d'un plan. C. R. Acad. Sci., Paris **328**, 455–458 (1999)
10. Dimnet, E.: Collisions de solides déformables. Thèse de l'École nationale des Ponts et Chaussées, Paris (2000)
11. Dimnet, E.: Collision d'un rocher et d'un arbre, Bulletin des Laboratoires des Ponts et Chaussées, 262 (2006)
12. Ekeland, I., Temam, R.: Analyse convexe et problèmes variationnels, Dunod-Gauthier-Villars (1974)
13. Ekeland, I., Temam, R.: Convex analysis and variational problems. North Holland, Amsterdam (1976)
14. Frémond, M.: Rigid bodies collisions. Phys. lett. A **204**, 33–41 (1995)
15. Frémond, M.: Phase change with temperature discontinuities, Gakuto Inter. Ser. Math. Sci. Appl. **14**, 125–134 (2000)
16. Frémond, M.: Internal constraints in mechanics. In: Pfeiffer, F.G. (ed.) Non-Smooth Mechanics. Philosophical Transactions of the Royal Society, Mathematical, Physical and Engineering Sciences, série A, Londres, vol. 359, n. 1789, pp. 2309–2326 (2001)
17. Frémond, M.: La mécanique des collisions de solides. In: Lagnier, J. (ed.) La Mécanique des Milieux Granulaires. Hermès, Paris (2001)
18. Frémond, M.: Non-Smooth Thermomechanics. Springer, Berlin (2002)
19. Frémond, M.: Collisions, Edizioni del Dipartimento di Ingegneria Civile, Università di Roma "Tor Vergata" (2007). ISBN 978-88-6296-000-7
20. Frémond, M.: Phase Change in Mechanics, UMI-Springer Lecture Notes Series n. 13, ISBN 978-3-642-24608-1. http://www.springer.com/mathematics/book/978-3-642-24608-1 (2011). doi:10.1007/978-3-642-24609-8
21. Frémond, M.: Meccanica dei Materiali e della Fratturà, Lecture Notes, Università di Roma "Tor Vergata" (2015)
22. Frémond, M., Valenzi, P.I.: Sthenic incompatibilities in rigid boby motions. In: Wriggers, P., Nackenhorst, U. (eds.) Analysis and Simulation of Contact Problems, vol. 1, pp. 145–152. Springer, Heidelberg (2006). doi:10.1007/3-540-31761-9_17
23. Germain, P., Nguyen, Q.S., Suquet, P.: Continuum thermodynamics. J. Appl. Mech., ASME **50**, 1010–1021 (1983)
24. Jellet, J.H.: Treatise on the Theory of Friction. Foster and Co, Hodges (1872)
25. Kane, T.R.: A dynamic puzzle, Standford Mechanics Alumni Club Newsletter (1984)
26. Klein, F.: Zu Painlevés Kritik der Coulombschen Reibungsgesetze. Zeitschrift fur Mathematik und Physik **58**(1), 186–191 (1910)
27. Halphen, B., Son, N.Q.: Sur les matériaux standards généralisés. J. Mech. **14**(1), 39–63 (1975)
28. Lassoued, R.: Comportement hivernal des chaussées. Modélisation thermique, Thèse de l'École nationale des Ponts et Chaussées, Paris (2000)
29. Monteiro Marques, M.D.P.: Differential Inclusions in Nonsmooth Mechanical Problems, Shocks and Dry Friction. Birkhaüser, Basel (1993)
30. Moreau, J.J.: Sur les lois de frottement, de viscosité et de plasticité. C. R. Acad. Sci., Paris **271**, 608–611 (1970)
31. Moreau, J.J.: Bounded variation in time, chap I. In: Moreau, J.J., Panagiotopoulos, P.D., Strang, G. (eds.) Topics in Non-Smooth Mechanics, pp. 1–71. Birkhauser, Basel (1988)
32. Moreau, J.J.: Fonctionnelles convexes, Edizioni del Dipartimento di Ingegneria Civile, Università di Roma "Tor Vergata", 2003, ISBN 978-88-6296-001-4 and Séminaire sur les équations aux dérivées partielles. Collège de France, Paris (1966)
33. Painlevé, P.: Sur les lois du frottement de glissement. C. R. Acad. Sci. **121**(1), 112–115 (1905)
34. Painlevé, P.: Sur les lois du frottement de glissement. C. R. Acad. Sci. **141**(1), 401–405 (1905)

35. Painlevé, P.: Sur les lois du frottement de glissement. C. R. Acad. Sci. **141**(1), 546–552 (1905)
36. Pérès, J.: Mécanique générale. Masson, Paris (1953)
37. Pfeiffer, F.G.: Non-smooth mechanics. Philos. Trans. R. Soc., Math., Phys. Eng. Sci. A **359**(1789) (2001)
38. Pfeiffer, F.G., Glocker, C.: Multybody Dynamics with Unilateral Contacts. Wiley Series in Nonlinear Sciences. Wiley, New York (1996)

Chapter 3
The Theory: Mechanics and Thermics. An Example: Collision of Two Balls

Michel Frémond

3.1 Introduction

Let us consider two balls moving on a line, Fig. 3.1. For the sake of simplicity, we assume they are points with mass m_i. They have position $x_i(t)$ and velocity $U_i(t) = (dx_i/dt)(t)$. We assume the collisions of the points are instantaneous. Thus the velocities can be discontinuous with respect to time.

The velocity before a collision at time t is $U_i^-(t)$ and the velocity after is $U_i^+(t)$.

3.2 The Velocities and the Velocities of Deformation

It is easy to write the equations of motion for the two points. But in order to be precise and have results which can be easily adapted to more general settings, we derive these equations by using the principle of virtual work. Before we introduce it, let us remark that there is no reason to speak of deformation when dealing with an isolated point. But if we consider the *system* made of the two points, its *form changes* because the distance of the two points may change. Thus it is wise to consider that the *system is deformable*. A way to characterize the system velocity of deformation is to consider the relative velocity of the two points

$$D(U) = U_1 - U_2, \tag{3.1}$$

where $U = (U_1, U_2)$ is the set of the two actual velocities of the points. A *rigid system set of velocities* is such that the form of the system does not change: it is easy to see that they are characterized by

$$D(U) = U_1 - U_2 = 0, \tag{3.2}$$

M. Frémond, *Collisions Engineering: Theory and Applications*,
Springer Series in Solid and Structural Mechanics 6,
DOI 10.1007/978-3-662-52696-5_3

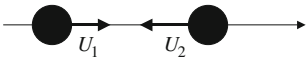

Fig. 3.1 Two balls schematized by points move on an axis (their mass moments of inertia are 0). The mass of the balls are m_1 and m_2, they have velocities U_1 and U_2

because when the form of the system does not change, the velocities of the two points are equal.

3.3 The Principle of Virtual Work and the Equations of Motion

The principle has been introduced in Chap. 2 with some experimental justification. We write it with in its classical form:

The virtual work of the acceleration forces, $\mathcal{W}_{acc}$, is equal to the sum of the virtual work of the internal forces, $\mathcal{W}_{int}$, and of the virtual work, $\mathcal{W}_{ext}$, of the external forces.

The principle is

$$\forall V, \forall t_1, \forall t_2, \tag{3.3}$$

$$\mathcal{W}_{acc}(t_1, t_2, V) = \mathcal{W}_{int}(t_1, t_2, V) + \mathcal{W}_{ext}(t_1, t_2, V), \tag{3.4}$$

where $V = (V_1, V_2)$ is a set of two virtual velocities.

For the sake of simplicity, we choose actual and virtual velocities to be discontinuous at only one time t with $t_1 < t < t_2$.

Remark 3.1 The principle of virtual work we use here is not to be confused with the principle of virtual power where the velocities are understood as small displacements (this relationship is often also called misleadingly the principle of virtual work).

3.4 The Virtual Works

Now we may introduce *generalized internal forces to the deformable system*. A productive way is to *define these generalized forces by their work* (or by duality in terms of mathematics). The work of the internal forces of the system between times t_1 and t_2, with discontinuity time t, $t_1 < t < t_2$, is a linear function of the velocity of deformation. We choose as virtual work of the internal forces

$$\mathcal{W}_{int}(t_1, t_2, V) = -\int_{t_1}^{t_2} R^{int}(\tau) D(V)(\tau) d\tau - P^{int}(t) D\left(\frac{V^+(t) + V^-(t)}{2}\right), \tag{3.5}$$

which is a linear function of $D(V) = (V_1 - V_2)$. Sign minus has no importance, it is chosen in accordance with habits of continuum mechanics. Its advantage will appear down below where a classical inequality has its classical sign, see relationship (3.46). The virtual work defines an internal force $R^{int}(\tau)$ which intervenes in the smooth evolution when the two points evolve without colliding. It defines also an internal percussion $P^{int}(t)$ which intervenes when collisions occur.

Remark 3.2 The linear function of $D(V)$ we have chosen is not the more general. The choice involving

$$- P^{int+}(t)D(V^+)(t) - P^{int-}(t)D(V^-)(t), \tag{3.6}$$

does not give much more opportunities, [8].

Let us note that $\mathcal{W}_{int}(t_1, t_2, V) = 0$ for any rigid system velocity, i.e., for $D(V) = (V_1 - V_2) = 0$.

The virtual work of the acceleration forces is

$$\mathcal{W}_{acc}(t_1, t_2, V) \tag{3.7}$$

$$= \sum_{i=1}^{2} \left\{ \int_{t_1}^{t_2} m_i \frac{dU_i}{dt}(\tau) V_i(\tau) d\tau \right\} + \sum_{i=1}^{2} \left\{ m_i \left[U_i(t)\right] . \frac{V_i^+(t) + V_i^-(t)}{2} \right\}, \tag{3.8}$$

where $[U(t)] = U^+(t) - U^-(t)$ is the velocity discontinuity. It is clear that this work is a linear function of V.

3.4.1 The Theorem of Kinetic Energy

Let us compute the actual work of the acceleration forces

$$\mathcal{W}_{acc}(t_1, t_2, U) \tag{3.9}$$

$$= \sum_{i=1}^{2} \left\{ \int_{t_1}^{t_2} m_i \frac{dU_i}{dt}(\tau) U_i(\tau) d\tau + m_i \left[U_i(t)\right] . \frac{U_i^+(t) + U_i^-(t} {2} \right\} \tag{3.10}$$

$$= \sum_{i=1}^{2} \left\{ \int_{t_1}^{t_2} m_i \frac{dU_i}{dt}(\tau) U_i(\tau) d\tau + \frac{m_i}{2} \left[(U_i(t))^2 \right] \right\} \tag{3.11}$$

$$= \sum_{i=1}^{2} \left\{ \frac{m_i}{2} \left(U_i^-(t_2)\right)^2 - \frac{m_i}{2} \left(U_i^+(t_1)\right)^2 \right\} = \mathcal{K}(U^-(t_2)) - \mathcal{K}(U^+(t_1)) \tag{3.12}$$

$$= \mathcal{K}^-(t_2) - \mathcal{K}^+(t_1), \tag{3.13}$$

which is equal to the variation of kinetic energy $\mathcal{K}$ between times t_1 and t_2. At any time we have kinetic energies $\mathcal{K}^-$ and $\mathcal{K}^+$ in case there is a collision.

The virtual work of the external forces is a linear function of the virtual velocities V. We choose

$$\mathcal{W}_{ext}(t_1, t_2, V) \tag{3.14}$$

$$= \sum_{i=1}^{2} \left\{ \int_{t_1}^{t_2} F_i(\tau) V_i(\tau) d\tau + P_i^{ext}(t) \frac{V_i^+(t) + V_i^-(t)}{2} \right\}. \tag{3.15}$$

External force F_i may be the gravity force. External percussion P_i^{ext} may represent hammer blows applied to the points.

3.5 The Equations of Motion

Interval $]t_1, t_2[$ is split in distinct intervals $]t_1, t[$ and $]t, t[$ where there is no discontinuity of U. By choosing smooth virtual velocities with compact support in interval $]t_1, t[$, we get from principle (3.4)

$$\sum_{i=1}^{2} \int_{t_1}^{t} m_i \frac{dU_i}{dt}(\tau) V_i(\tau) d\tau = -\int_{t_1}^{t} R^{int}(\tau) D(V)(\tau) d\tau + \sum_{i=1}^{2} \int_{t_1}^{t} F_i(\tau) V_i(\tau) d\tau. \tag{3.16}$$

The fundamental lemma of variation calculus gives

$$m_1 \frac{dU_1}{dt} = -R^{int} + F_1, \ a.e.\ in\ ]t_1, t[, \tag{3.17}$$

$$m_2 \frac{dU_2}{dt} = R^{int} + F_2, \ a.e.\ in\ ]t, t_2[. \tag{3.18}$$

Due to relationships (3.18), the principle becomes

$$\forall V, \ \sum_{i=1}^{2} m_i \left[U_i(t)\right] \frac{V_i^+(t) + V_i^-(t)}{2} \tag{3.19}$$

$$= -P^{int}(t) D\left(\frac{V^+(t) + V^-(t)}{2} \right) + \sum_{i=1}^{2} P_i^{ext}(t) \frac{V_i^+(t) + V_i^-(t)}{2}. \tag{3.20}$$

We get by choosing virtual velocities V with compact support in $]t_1, t_2[$

$$m_1 \left[U_1(t)\right] = -P^{int}(t) + P_1^{ext}(t), \tag{3.21}$$

$$m_2 \left[U_2(t)\right] = P^{int}(t) + P_2^{ext}(t). \tag{3.22}$$

Because at time $\tau \neq t$ there is neither velocity discontinuity nor external percussion, relationships (3.22) are satisfied at any time

$$m_1 [U_1(\tau)] = -P^{int}(\tau) + P_1^{ext}(\tau), \ \forall \tau \in]t_1, t_2[, \tag{3.23}$$

$$m_2 [U_2(\tau)] = P^{int}(\tau) + P_2^{ext}(\tau), \ \forall \tau \in]t_1, t_2[. \tag{3.24}$$

Let us recall that a detailed derivation of the equations of motion is given in [8].

3.6 Smooth Evolution of Two Balls with Thermal Effects

The system may receive heat from the outside and the two balls may exchange heat, for instance through an elastic string that connect them. We investigate the evolution of the temperatures T_1 and T_2 of the balls.

3.6.1 Laws of Thermodynamics for a Ball

The first law for ball 1 with internal energy $\mathcal{E}_1$ and kinetic energy $\mathcal{K}_1$ is

$$\frac{d\mathcal{E}_1}{dt} + \frac{d\mathcal{K}_1}{dt} = \mathcal{P}^1_{ext} + T_1(Q_1 + Q_{12}), \tag{3.25}$$

where $\mathcal{P}^1_{ext}$ is the actual power of the external forces to ball 1, Q_1 is the entropy received from from the external of the system and Q_{12} the entropy received from ball 2. The principle of virtual power for ball 1 with the actual velocities and the first law give

$$\frac{d\mathcal{K}_1}{dt} = \mathcal{P}^1_{int} + \mathcal{P}^1_{ext} = \mathcal{P}^1_{ext}, \tag{3.26}$$

because there is no internal force for a ball which is not deformable. The two previous relationships give

$$\frac{d\mathcal{E}_1}{dt} = T_1(Q_1 + Q_{12}). \tag{3.27}$$

The second law for ball 1 with entropy $\mathcal{S}_1$ is

$$\frac{d\mathcal{S}_1}{dt} \geq Q_1 + Q_{12}, \ T_1 > 0. \tag{3.28}$$

By combining relationships (3.27) and (3.28), we get

$$\frac{d\mathcal{E}_1}{dt} - T_1 \frac{d\mathcal{S}_1}{dt} \leq 0. \tag{3.29}$$

And because the only state quantity of ball 1 is its temperature T_1, relationship $\mathcal{E}_1(\mathcal{S}_1) = T_1\mathcal{S}_1 + \Psi_1(T)$ where $\Psi_1(T)$ is the free energy of ball 1 gives

$$\frac{d\mathcal{E}_1}{dt} = T_1\frac{d\mathcal{S}_1}{dt} + (\mathcal{S}_1 + \frac{d\Psi_1}{dT_1})\frac{dT_1}{dt} = T_1\frac{d\mathcal{S}_1}{dt}. \tag{3.30}$$

Thus relationship (3.29) is an equality

$$\frac{d\mathcal{S}_1}{dt} = Q_1 + Q_{12}, \tag{3.31}$$

and the evolution of a ball is nondissipative as expected.

3.6.2 *Laws of Thermodynamics for the System*

The first law is

$$\frac{d\mathcal{E}_1}{dt} + \frac{d\mathcal{E}_2}{dt} + \frac{d\mathcal{E}_{int}}{dt} + \frac{d\mathcal{K}_1}{dt} + \frac{d\mathcal{K}_2}{dt} = \mathcal{P}_{ext} + T_1Q_1 + T_2Q_2, \tag{3.32}$$

where $\mathcal{E}_{int}$ is the interaction internal energy between the two balls, and $\mathcal{P}_{ext}$ is the actual power of the external forces. The principle of virtual power for the system with the actual velocities

$$\frac{d\mathcal{K}_1}{dt} + \frac{d\mathcal{K}_2}{dt} = \mathcal{P}_{int} + \mathcal{P}_{ext}, \tag{3.33}$$

gives with relationship (3.32)

$$\frac{d\mathcal{E}_1}{dt} + \frac{d\mathcal{E}_2}{dt} + \frac{d\mathcal{E}_{int}}{dt} = -\mathcal{P}_{int} + T_1Q_1 + T_2Q_2. \tag{3.34}$$

The first laws for the balls give with the previous relationship

$$\frac{d\mathcal{E}_{int}}{dt} = -\mathcal{P}_{int} - T_1Q_{12} - T_2Q_{21} \tag{3.35}$$

$$= -\mathcal{P}_{int} - \delta T\left(\frac{Q_{21} - Q_{12}}{2}\right) - \Theta\left(Q_{12} + Q_{21}\right), \tag{3.36}$$

with

$$\delta T = (T_2 - T_1),\ \Theta = \frac{T_1 + T_2}{2}. \tag{3.37}$$

The second law is

$$\frac{d\mathcal{S}_1}{dt} + \frac{d\mathcal{S}_2}{dt} + \frac{d\mathcal{S}_{int}}{dt} \geq Q_1 + Q_2, \tag{3.38}$$

where $\mathcal{S}_{int}$ is the interaction entropy. By using the second laws for the balls, the relationships (3.31) where there is equality, we get

$$\frac{d\mathcal{S}_{int}}{dt} \geq -Q_{12} - Q_{21}. \tag{3.39}$$

With relationships (3.36) and (3.39), we get

$$\frac{d\mathcal{E}_{int}}{dt} - \Theta\frac{d\mathcal{S}_{int}}{dt} \leq -\mathcal{P}_{int} - \delta T\left(\frac{Q_{21} - Q_{12}}{2}\right) = R^{int}D(U) - \delta T\left(\frac{Q_{21} - Q_{12}}{2}\right). \tag{3.40}$$

The interaction free energy $\Psi^{int}(\Theta, g)$ satisfies relationship

$$\Psi^{int}(\Theta, g) = \mathcal{E}^{int}(\mathcal{S}^{int}, g) - \Theta\mathcal{S}^{int}, \tag{3.41}$$

where

$$g(t) = x_1(t) - x_2(t), \tag{3.42}$$

is the distance between the two balls we choose as state quantity of the system. We get

$$\frac{\partial\Psi^{int}}{\partial g}D(U) \leq R^{int}D(U) - \delta T\left(\frac{Q_{21} - Q_{12}}{2}\right). \tag{3.43}$$

By defining the dissipative R^{intd} and non dissipative R^{intnd} internal forces,

$$R^{int} = R^{intnd} + R^{intd}, \tag{3.44}$$

$$R^{intnd} = \frac{\partial\Psi^{int}}{\partial g}, \tag{3.45}$$

the previous relationship gives

$$0 \leq R^{intd}D(U) - \delta T\left(\frac{Q_{21} - Q_{12}}{2}\right). \tag{3.46}$$

Remark 3.3 The difference between the two sides of relationship (3.39) is easily computed

$$\frac{d\mathcal{S}_{int}}{dt} + Q_{12} + Q_{21} = \frac{1}{\Theta}\left\{R^{intd}D(U) - \delta T\left(\frac{Q_{21} - Q_{12}}{2}\right)\right\}. \tag{3.47}$$

It is also easy to show that this equation is equivalent to the first law (3.36).

3.6.3 The Constitutive Laws

The constitutive laws are defined with a pseudo-potential of dissipation $\Phi(D(U), \delta T)$

$$(R^{intd}, -\frac{Q_{21} - Q_{12}}{2}) \in \partial\Phi(D(U), \delta T). \tag{3.48}$$

3.6.4 An Example

Let consider two balls connected by an elastic string with length l. Let recall the distance g between the two balls

$$g(t) = x_1(t) - x_2(t), \tag{3.49}$$

where $x_1(t)$ and $x_2(t)$ are the positions of the two balls, is a state quantity.

When the gap $|g|$ between the two balls is lower than l, there is no interaction between the two balls. When the gap $|g|$ is larger than l, there is an elastic interaction proportional to

$$\text{pp}\{|g| - l\} == \text{pp}\{|x_1 - x_2| - l\}, \tag{3.50}$$

where pp{.} is the positive part function, see definition (A.2.1) in the Appendix. The free energy we choose are

$$\Psi_1(T_1) = -C_1 T_1 \ln T_1, \ \Psi_2(T_2) = -C_2 T_2 \ln T_2, \tag{3.51}$$

$$\Psi^{int}(\Theta, g) = -C^{int}\Theta \ln \Theta + \frac{k}{2}(\text{pp}\{|g| - l\})^2, \tag{3.52}$$

giving the nondissipative force

$$R^{intnd}(E) = \frac{d\Psi}{dg}(g) = ksgn(g)(\text{pp}\{|g| - l\}). \tag{3.53}$$

where sgn is the sign graph, defined by formula (A.4.2).

Remark 3.4 When $g = 0$, we have $\text{pp}\{|g| - l\} = 0$ and

$$R^{intnd}(E) = ksgn(0)0 = 0. \tag{3.54}$$

We choose

$$\Phi(D(U), \delta T, \chi) = \frac{f(\chi)}{2} D^2 + \frac{\lambda}{4} (\delta T)^2, \tag{3.55}$$

depending on the parameter $\chi = |g| - l$ with

$$f(\chi) = cH(\chi), \tag{3.56}$$

where H is the Heaviside graph. Quantity λ is the thermal conductivity of the string and c is the viscosity of the string. This choice implies that the mechanical problem is decoupled from the thermal problem. But of course the thermal problem depends on the mechanical dissipation $R^{intd}D(U)$.

We get the dissipative force

$$R^{intd}(D, \chi) = \frac{\partial \Phi}{\partial D}(D, \chi) = f(\chi)\, D. \tag{3.57}$$

Remark 3.5 When $\chi = 0$, we have $|g| - l = 0$ and

$$\frac{dg}{dt} = D(U) = 0. \tag{3.58}$$

giving

$$R^{intd}(0, 0) == cH(0)0 = 0. \tag{3.59}$$

3.6.4.1 The Motion

The equations of motion and constitutive laws give the equations for the positions $x_1(t)$ and $x_2(t)$

$$m_1 \frac{d^2x_1}{dt^2} = -k\text{pp}\{|x_1 - x_2| - l\} - cH(\chi)(\frac{dx_1}{dt} - \frac{dx_2}{dt}) + F_1, \tag{3.60}$$

$$m_2 \frac{d^2x_2}{dt^2} = k\text{pp}\{|x_1 - x_2| - l\} + cH(\chi)(\frac{dx_1}{dt} - \frac{dx_2}{dt}) + F_2. \tag{3.61}$$

With the positions of the balls as shown in Fig. 3.1, the equations of motions are

$$m_1 \frac{d^2x_1}{dt^2} = F_1, \tag{3.62}$$

$$m_2 \frac{d^2x_2}{dt^2} = F_2, \tag{3.63}$$

if $-l < g = x_1(t) - x_2(t) < 0$ and

$$m_1\frac{d^2x_1}{dt^2} = -k(x_1(t) - x_2(t) - l) - c(\frac{dx_1}{dt} - \frac{dx_2}{dt}) + F_1, \tag{3.64}$$

$$m_2\frac{d^2x_2}{dt^2} = k(x_1(t) - x_2(t) - l) + c(\frac{dx_1}{dt} - \frac{dx_2}{dt}) + F_2. \tag{3.65}$$

if $g = x_1(t) - x_2(t) < -l$.

When $x_1(t) - x_2(t)$ becomes 0 a collision occurs as one may see on Fig. 3.1.

Remark 3.6 The same motion with at a distance interaction in $2D$ or $3D$ is easily investigated. When considering a system made of two disks attached together by an elastic wire, there are at a distance interactions if the distance of the two disks is greater than the length of the wire. Such a model may represent two pedestrians holding hands. This idea is developed in Chap. 6 devoted to the motion of crowds. Such type of equations are easily solved.

3.6.4.2 The Temperatures

The thermal constitutive law is

$$\frac{Q_{21} - Q_{12}}{2} = -\frac{\lambda}{2}\delta T. \tag{3.66}$$

This relationship means that the entropy (or the heat) goes from the warm ball toward the cold one.

The equations to find the temperatures T_1 and T_2 are

$$\frac{d\mathcal{E}_1}{dt} = T_1(Q_1 + Q_{12}),\ \frac{d\mathcal{E}_2}{dt} = T_2(Q_2 + Q_{21}),$$
$$\frac{d\mathcal{E}_{int}}{dt} = -\mathcal{P}_{int} - \delta T\left(\frac{Q_{21} - Q_{12}}{2}\right) - \Theta\left(Q_{12} + Q_{21}\right).$$

They are completed by the thermal relations of the balls with the exterior. For instance, if there is no heat exchange

$$T_1Q_1 = T_2Q_2 = 0. \tag{3.67}$$

Remark 3.7 It may be chosen a more realistic description of the thermal exchanges with the exterior, we may have

$$T_1Q_1 = -\lambda_{ext}(T_1 - T_{ext}), \tag{3.68}$$

the exchanged heat is proportional to the difference of temperature between the ball and the exterior.

The free energies (3.52) give internal energies resulting in the equations

$$C_1 \frac{dT_1}{dt} = T_1 Q_{12},\ C_2 \frac{dT_2}{dt} = T_2 Q_{21}, \tag{3.69}$$

$$C^{int} \frac{d\Theta}{dt} = -\mathcal{P}_{int} + \frac{\lambda}{2} (\delta T)^2 - \Theta (Q_{12} + Q_{21}), \tag{3.70}$$

$$Q_{21} - Q_{12} = -\lambda \delta T. \tag{3.71}$$

The four unknowns are the two temperatures $T_1(t)$ and $T_2(t)$ and the two entropies $Q_{12}(t)$ and $Q_{21}(t)$.

In case the heat capacity of the spring is negligible, $C^{int} = 0$, and assuming the small perturbation assumption, the equations are

$$C_1 \frac{dT_1}{dt} + C_2 \frac{dT_2}{dt} = T_1 Q_{12} + T_2 Q_{21} = \Theta (Q_{12} + Q_{21}) = T_0 (Q_{12} + Q_{21}) = -\mathcal{P}_{int}, \tag{3.72}$$

$$\frac{C_1}{T_0} \frac{dT_1}{dt} - \frac{C_2}{T_0} \frac{dT_2}{dt} = Q_{12} - Q_{21} = \lambda \delta T = \lambda (T_2 - T_1). \tag{3.73}$$

They give

$$C_1 \frac{dT_1}{dt} = -\frac{\mathcal{P}_{int}}{2} + \lambda (T_2 - T_1), \tag{3.74}$$

$$C_2 \frac{dT_2}{dt} = -\frac{\mathcal{P}_{int}}{2} - \lambda (T_2 - T_1). \tag{3.75}$$

The mechanical effect $-\mathcal{P}_{int}$, the power of the internal forces is distributed between the two balls. If it is positive, it increases the temperature whereas the thermal conductivity equalizes them: the heat goes from the warm ball toward the cold one through the string.

Remark 3.8 It is possible to solve the same problem by using the entropy balances (3.31), and (3.47)

$$\frac{d\mathcal{S}_1}{dt} = Q_1 + Q_{12},\ \frac{d\mathcal{S}_2}{dt} = Q_2 + Q_{21}, \tag{3.76}$$

$$\frac{d\mathcal{S}_{int}}{dt} + Q_{12} + Q_{21} = \frac{1}{\Theta} \left\{ R^{intd} D(U) - \delta T \left(\frac{Q_{21} - Q_{12}}{2} \right) \right\} = \frac{1}{\Theta} \{ -\mathcal{P}_{intd} \}, \tag{3.77}$$

$$Q_{21} - Q_{12} = -\lambda \delta T. \tag{3.78}$$

by denoting

$$-\mathcal{P}_{intd} = \left\{ R^{intd} D(U) - \delta T \left(\frac{Q_{21} - Q_{12}}{2} \right) \right\}, \tag{3.79}$$

the dissipated power. The entropies are

$$\mathcal{S}_1 = C_1(1 + \ln T_1),\ \mathcal{S}_2 = C_2(1 + \ln T_2), \tag{3.80}$$

$$\mathcal{S}_{int} = C_{int}(1 + \ln \Theta). \tag{3.81}$$

Thus the equations become

$$C_1 \frac{d \ln T_1}{dt} = Q_1 + Q_{12},\ C_2 \frac{d \ln T_2}{dt} = Q_2 + Q_{21}, \tag{3.82}$$

$$C_{int} \frac{d \ln \Theta}{dt} + Q_{12} + Q_{21} = \frac{1}{\Theta} \left\{ R^{intd} D(U) - \delta T \left(\frac{Q_{21} - Q_{12}}{2} \right) \right\} = \frac{1}{\Theta} \{ -\mathcal{P}_{intd} \}, \tag{3.83}$$

$$Q_{21} - Q_{12} = -\lambda \delta T. \tag{3.84}$$

Let us note that the unknowns are the logarithms of the temperatures. Thus the existence of solutions implies that the temperatures are positive. This is an important advantage of this way of solving the physical problem. We think this way of doing, detailed in [1, 2, 8], is good both from the theoretical point of view: the laws of thermodynamics involve only one differential equation and from the practical and numerical point of view: the temperatures are positive. The notion of entropy is not more difficult to think of than the notion of internal energy.

With the assumptions of the example: no heat exchange with the exterior and the small perturbation assumption, we get

$$\frac{C_1}{T_0} \frac{dT_1}{dt} = Q_{12},\ \frac{C_2}{T_0} \frac{dT_2}{dt} = Q_{21}, \tag{3.85}$$

$$\frac{C^{int}}{T_0} \frac{d\Theta}{dt} = \frac{1}{T_0} \{ -\mathcal{P}_{intd} \} + Q_{12} + Q_{21}, \tag{3.86}$$

$$Q_{21} - Q_{12} = -\lambda \delta T. \tag{3.87}$$

The resulting equations are

$$C_1 \frac{dT_1}{dt} = -\frac{\mathcal{P}_{intd}}{2} + \lambda (T_2 - T_1), \tag{3.88}$$

$$C_2 \frac{dT_2}{dt} = -\frac{\mathcal{P}_{intd}}{2} - \lambda (T_2 - T_1). \tag{3.89}$$

The dissipated power $-\mathcal{P}_{intd}$ is positive: it increases the temperatures of the system whereas the thermal conductivity equalizes them.

3.7 Collisions of Two Balls with Thermal Effects

Assuming the collisions are instantaneous, the temperatures of the balls are also discontinuous with respect to time, [5, 7, 8]. Four temperatures appear in collisions: T_i^+ and T_i^- temperatures of the points after and before collision. We denote

$$[T_1] = T_1^+ - T_1^-, \ [T_2] = T_2^+ - T_2^-. \tag{3.90}$$

These differences are analog to the temperature time derivative dT/dt when the temperature is smooth. Let us recall that there is no dissipation with respect to this quantity because of Helmholtz relationship

$$s = -\frac{\partial \Psi}{\partial T}(T, \chi), \tag{3.91}$$

resulting from the definition of the internal energy $e(s, \chi)$ when the variables $E = (T, \chi)$ are chosen independent

$$e(s, \chi) = Ts + \Psi(T, \chi), \tag{3.92}$$

where s is the entropy and χ are other quantities. We denote some average temperatures

$$\bar{T}_1 = \frac{T_1^+ + T_1^-}{2}, \ \bar{T}_2 = \frac{T_2^+ + T_2^-}{2}, \bar{\Theta} = \frac{T_1^+ + T_1^- + T_2^+ + T_2^-}{4} = \frac{\bar{T}_1 + \bar{T}_2}{2}. \tag{3.93}$$

The temperature difference

$$\delta \bar{T} = \bar{T}_2 - \bar{T}_1, \tag{3.94}$$

is the analog of the spatial thermal gradient in a smooth situation. Let us also recall that there is dissipation with respect to this quantity: the almost universal example is the Fourier law. In the following investigation of the thermal effects of collisions, analogous choices are made remembering that they sum up what occur during the duration of collisions when Fourier law and Helmholtz relationship are assumed.

In the sequel, we consider sums which are transformed in the following way

$$T^+\mathcal{B}^+ + T^-\mathcal{B}^- = \bar{T}\,\Sigma(\mathcal{B}) + [T]\,\Delta(\mathcal{B}), \tag{3.95}$$

with

$$\bar{T} = \frac{T^+ + T^-}{2}, \ [T] = T^+ - T^-, \ \Sigma(\mathcal{B}) = \mathcal{B}^+ + \mathcal{B}^-, \ \Delta(\mathcal{B}) = \frac{\mathcal{B}^+ - \mathcal{B}^-}{2}. \tag{3.96}$$

3.7.1 First Law of Thermodynamics for a Ball

The laws of thermodynamics are the same for the two points. For point 1, the first law is

$$[\mathcal{E}_1] + [\mathcal{K}_1] = \mathcal{W}_{ext1}(U) + \mathcal{C}_1, \tag{3.97}$$

where $\mathcal{W}_{ext1}(U)$ is the actual work of the percussions which are exterior to point 1 and $\mathcal{C}_1$ is the amount of heat received by the point in the collision. This heat involves the heats $T_1\mathcal{B}_1$ received from the exterior to the system and the heats $T_1\mathcal{B}_{12}$ received from the interior of the system, i.e., from the other point. We assume that these heats are received at temperatures either T_1^+ or T_1^-

$$\mathcal{C}_1 = T_1^+\left(\mathcal{B}_1^+ + \mathcal{B}_{12}^+\right) + T_1^-\left(\mathcal{B}_1^- + \mathcal{B}_{12}^-\right) \tag{3.98}$$

$$= \bar{T}_1\left(\Sigma\left(\mathcal{B}_1\right) + \Sigma\left(\mathcal{B}_{12}\right)\right) + [T_1]\left(\Delta\left(\mathcal{B}_1\right) + \Delta\left(\mathcal{B}_{12}\right)\right). \tag{3.99}$$

The theorem of kinetic energy for point 1 is

$$[\mathcal{K}_1] = \mathcal{W}_{acc1}(U) = \mathcal{W}_{ext1}(U). \tag{3.100}$$

It gives with the energy balance

$$[\mathcal{E}_1] = \mathcal{C}_1 = \bar{T}_1\left(\Sigma\left(\mathcal{B}_1\right) + \Sigma\left(\mathcal{B}_{12}\right)\right) + [T_1]\left(\Delta\left(\mathcal{B}_1\right) + \Delta\left(\mathcal{B}_{12}\right)\right). \tag{3.101}$$

In the right hand side, there is no mechanical quantity because a point has no internal force, the work of which could contribute to the internal energy evolution.

3.7.2 Second Law of Thermodynamics for a Ball

It is

$$[\mathcal{S}_1] \geq \mathcal{B}_1^+ + \mathcal{B}_1^- + \mathcal{B}_{12}^+ + \mathcal{B}_{12}^- = \Sigma\left(\mathcal{B}_1\right) + \Sigma\left(\mathcal{B}_{12}\right), \ T_1^+ > 0. \tag{3.102}$$

We already know that temperature, T_1^-, before collision is positive. Temperature T_1^+ will be positive due to the formula giving the free energy.

3.7.3 A Useful Inequality for a Ball

Second law and relationship (3.101) give

$$[\mathcal{E}_1] - \bar{T}_1[\mathcal{S}_1] \leq [T_1]\left(\Delta\left(\mathcal{B}_1\right) + \Delta\left(\mathcal{B}_{12}\right)\right), \tag{3.103}$$

or by introducing free energy $\Psi = \mathcal{E} - T\mathcal{S}$

$$[\Psi_1] + \bar{\mathcal{S}}_1 [T_1] \leq [T_1] \Delta (\mathcal{B}_1) + [T_1] \Delta (\mathcal{B}_{12}) , \tag{3.104}$$

with

$$\bar{\mathcal{S}}_1 = \frac{\mathcal{S}_1^+ + \mathcal{S}_1^-}{2} \tag{3.105}$$

We denote

$$[\Psi_1] + \bar{\mathcal{S}}_1 [T_1] = -S_1 [T_1] \tag{3.106}$$

remembering that when $[T_1] \to 0$ we have $[\Psi_1] / [T_1] + \bar{\mathcal{S}}_1 \to 0$ because $\partial\Psi/\partial T + s = 0$. Then we have

$$0 \leq [T_1] (\Delta (\mathcal{B}_1) + \Delta (\mathcal{B}_{12}) + S_1). \tag{3.107}$$

Due to Helmholtz relationship, it is reasonable to assume no dissipation with respect to $[T_1]$ which is, as already said, the analog to dT/dt

$$\Delta (\mathcal{B}_1) + \Delta (\mathcal{B}_{12}) + S_1 = 0. \tag{3.108}$$

We deduce

$$[\mathcal{S}_1] = \Sigma (\mathcal{B}_1) + \Sigma (\mathcal{B}_{12}) . \tag{3.109}$$

3.7.4 The First Law for the System

The internal energy and entropy of the system are the sums of the internal energies and entropies of its components $\mathcal{E}_1$, $\mathcal{S}_1$ and $\mathcal{E}_2$, $\mathcal{S}_2$, to which interaction internal energy and entropy $\mathcal{E}^{int}$, $\mathcal{S}^{int}$ are added:

$$\mathcal{E} = \mathcal{E}_1 + \mathcal{E}_2 + \mathcal{E}^{int}, \tag{3.110}$$

$$\mathcal{S} = \mathcal{S}_1 + \mathcal{S}_2 + \mathcal{S}^{int}. \tag{3.111}$$

The first law for the system is

$$[\mathcal{E}] + [\mathcal{K}] = \mathcal{W}_{ext}(U) + \mathcal{C}, \tag{3.112}$$

where $\mathcal{C}$ is the heat received by the system in collision

$$\mathcal{C} = T_1^+ \mathcal{B}_1^+ + T_1^- \mathcal{B}_1^- + T_2^+ \mathcal{B}_2^+ + T_2^- \mathcal{B}_2^- . \tag{3.113}$$

The theorem of kinetic energy is

$$[\mathcal{K}] = \mathcal{W}_{acc}(U) = \mathcal{W}_{int}(D(U)) + \mathcal{W}_{ext}(U). \tag{3.114}$$

It gives with the first law

$$[\mathcal{E}] = -\mathcal{W}_{int}(D(U)) + \mathcal{C}. \tag{3.115}$$

The first laws for each point (3.101) and for the system (3.115) give

$$[\mathcal{E}] = [\mathcal{E}_1] + [\mathcal{E}_2] + \left[\mathcal{E}^{int}\right] \tag{3.116}$$

$$= \left[\mathcal{E}^{int}\right] + \bar{T}_1 \left(\Sigma\left(\mathcal{B}_1\right) + \Sigma\left(\mathcal{B}_{12}\right)\right) + [T_1]\left(\Delta\left(\mathcal{B}_1\right) + \Delta\left(\mathcal{B}_{12}\right)\right) \tag{3.117}$$

$$+\bar{T}_2 \left(\Sigma\left(\mathcal{B}_2\right) + \Sigma\left(\mathcal{B}_{21}\right)\right) + [T_2]\left(\Delta\left(\mathcal{B}_2\right) + \Delta\left(\mathcal{B}_{21}\right)\right) \tag{3.118}$$

$$= P^{int} D\left(\frac{U^+ + U^-}{2}\right) + T_1^+ \mathcal{B}_1^+ + T_1^- \mathcal{B}_1^- + T_2^+ \mathcal{B}_2^+ + T_2^- \mathcal{B}_2^- \tag{3.119}$$

$$= P^{int} D\left(\frac{U^+ + U^-}{2}\right) + \bar{T}_1 \Sigma\left(\mathcal{B}_1\right) + [T_1]\,\Delta\left(\mathcal{B}_1\right) + \bar{T}_2 \Sigma\left(\mathcal{B}_2\right) + [T_2]\,\Delta\left(\mathcal{B}_2\right). \tag{3.120}$$

Then

$$\left[\mathcal{E}^{int}\right] = P^{int} D\left(\frac{U^+ + U^-}{2}\right) - \bar{T}_1 \Sigma\left(\mathcal{B}_{12}\right) - [T_1]\,\Delta\left(\mathcal{B}_{12}\right) - \bar{T}_2 \Sigma\left(\mathcal{B}_{21}\right) - [T_2]\,\Delta\left(\mathcal{B}_{21}\right). \tag{3.121}$$

This relationship is interesting because only internal quantities intervene.

3.7.5 *The Second Law for the System*

It is

$$[\mathcal{S}] \geq \mathcal{B}_1^+ + \mathcal{B}_1^- + \mathcal{B}_2^+ + \mathcal{B}_2^- = \Sigma\left(\mathcal{B}_1\right) + \Sigma\left(\mathcal{B}_2\right), \tag{3.122}$$

where

$$[\mathcal{S}] = [\mathcal{S}_1] + [\mathcal{S}_2] + \left[\mathcal{S}^{int}\right] \geq \Sigma\left(\mathcal{B}_1\right) + \Sigma\left(\mathcal{B}_2\right), \tag{3.123}$$

which gives with (3.109)

$$\left[\mathcal{S}^{int}\right] \geq -\Sigma\left(\mathcal{B}_{12}\right) - \Sigma\left(\mathcal{B}_{21}\right). \tag{3.124}$$

In this relationship only internal heat exchanges intervene. Together with the first law (3.121), it gives an inequality coupling the mechanical and thermal dissipations.

3.7.6 A Useful Inequality for the System

We have with (3.121) and (3.124)

$$\left[\mathcal{E}^{int}\right] - \bar{\Theta}\left[\mathcal{S}^{int}\right] \leq P^{int} D\left(\frac{U^+ + U^-}{2}\right) - \bar{T}_1 \Sigma\left(\mathcal{B}_{12}\right) - [T_1]\, \Delta\left(\mathcal{B}_{12}\right) \tag{3.125}$$

$$-\bar{T}_2 \Sigma\left(\mathcal{B}_{21}\right) - [T_2]\, \Delta\left(\mathcal{B}_{21}\right) + \bar{\Theta}\left(\Sigma\left(\mathcal{B}_{12}\right) + \Sigma\left(\mathcal{B}_{21}\right)\right). \tag{3.126}$$

We define the interaction free energy: $\Psi^{int} = \mathcal{E}^{int} - \Theta \mathcal{S}^{int}$. It gives with the preceding relationship

$$\left[\Psi^{int}\right] + \bar{\mathcal{S}}^{int}\left[\Theta\right] \leq P^{int} D\left(\frac{U^+ + U^-}{2}\right) \tag{3.127}$$

$$-\bar{T}_1 \Sigma\left(\mathcal{B}_{12}\right) - [T_1]\, \Delta\left(\mathcal{B}_{12}\right) - \bar{T}_2 \Sigma\left(\mathcal{B}_{21}\right) - [T_2]\, \Delta\left(\mathcal{B}_{21}\right) + \bar{\Theta}\left(\Sigma\left(\mathcal{B}_{12}\right) + \Sigma\left(\mathcal{B}_{21}\right)\right), \tag{3.128}$$

with

$$\bar{\mathcal{S}}^{int} = \frac{\mathcal{S}^{int+} + \mathcal{S}^{int-}}{2}. \tag{3.129}$$

Remembering that we have denoted

$$[\Theta] = \frac{1}{2}\left([T_1] + [T_2]\right), \tag{3.130}$$

we define

$$\left[\Psi^{int}\right] + \bar{\mathcal{S}}^{int}\left[\Theta\right] = -S_{int}\left[\Theta\right]. \tag{3.131}$$

We obtain

$$0 \leq P^{int} D\left(\frac{U^+ + U^-}{2}\right) - \bar{T}_1 \Sigma\left(\mathcal{B}_{12}\right) - [T_1]\left(\Delta\left(\mathcal{B}_{12}\right) - \frac{S_{int}}{2}\right) \tag{3.132}$$

$$-\bar{T}_2 \Sigma\left(\mathcal{B}_{21}\right) - [T_2]\left(\Delta\left(\mathcal{B}_{21}\right) - \frac{S_{int}}{2}\right) + \bar{\Theta}\left(\Sigma(\mathcal{B}_{12}) + \Sigma(\mathcal{B}_{21})\right). \tag{3.133}$$

It is reasonable not to have dissipation with respect to $[T_1]$ and $[T_2]$ which are temperature variations with respect to time and not with respect to space

$$\Delta\left(\mathcal{B}_{12}\right) - \frac{S_{int}}{2} = 0,\ \Delta\left(\mathcal{B}_{21}\right) - \frac{S_{int}}{2} = 0. \tag{3.134}$$

Then

$$0 \leq P^{int} D\left(\frac{U^+ + U^-}{2}\right) - \bar{T}_1 \Sigma\left(\mathcal{B}_{12}\right) - \bar{T}_2 \Sigma\left(\mathcal{B}_{21}\right) + \bar{\Theta}\left(\Sigma\left(\mathcal{B}_{12}\right) + \Sigma\left(\mathcal{B}_{21}\right)\right) \tag{3.135}$$

but

$$\bar{T}_1 \Sigma(\mathcal{B}_{12}) + \bar{T}_2 \Sigma(\mathcal{B}_{21}) = \bar{\Theta}(\Sigma(\mathcal{B}_{12}) + \Sigma(\mathcal{B}_{21})) + \delta\bar{T}\frac{\Sigma(\mathcal{B}_{21}) - \Sigma(\mathcal{B}_{12})}{2}, \tag{3.136}$$

recalling that $\delta\bar{T} = \bar{T}_2 - \bar{T}_1$. Thus we get

$$0 \leq P^{int} D\left(\frac{U^+ + U^-}{2}\right) - \delta\bar{T}\frac{\Sigma(\mathcal{B}_{21}) - \Sigma(\mathcal{B}_{12})}{2}. \tag{3.137}$$

This relationship is important due to the quantities which intervene : the one which characterizes the mechanical evolution $D\left((U^+ + U^-)/2\right)$, and the other one which characterizes the spatial thermal heterogeneity $\delta\bar{T}$. Let us stress its analogy with the spatial thermal gradient in smooth situation. Relationship (3.137) is a guide to choose the quantities which are to be related to the internal forces. When dealing with experimental results relationship (3.137) is useful to choose the quantities which are to be plotted ones versus the others: P^{int} versus $D\left(U^+ + U^-\right)$ and $\Sigma(\mathcal{B}_{21}) - \Sigma(\mathcal{B}_{12})$ versus $\delta\bar{T}$.

Let us recall that on our way we have assumed no dissipation with respect to the temperature time variation.

3.7.7 The Constitutive Laws

Quantities which describe the mechanical evolution and thermal heterogeneity are $D\left((U^+ + U^-)/2\right)$ and $\delta\bar{T}$. We define the constitutive laws with a pseudo-potential of dissipation

$$\hat{\Phi}\left(D(\frac{U^+ + U^-}{2}), \delta\bar{T}, \chi\right). \tag{3.138}$$

The quantity $\chi = D\left(U^-/2\right)$ which depends on the past is used to take into account the non-interpenetration of the points. Let us recall a pseudo-potential of dissipation is a convex function, [4, 10], of $\left(D(\frac{U^+ + U^-}{2}), \delta\bar{T}\right)$ which is positive with value 0 at the origin. Then the constitutive laws are

$$\left(P^{int}, \frac{\Sigma(\mathcal{B}_{21}) - \Sigma(\mathcal{B}_{12})}{2}\right) \in \partial\hat{\Phi}\left(D(\frac{U^+ + U^-}{2}), \delta\bar{T}, D(\frac{U^-}{2})\right), \tag{3.139}$$

where the subdifferential set is computed with respect to the two first variables. It is easy to show that inequality (3.137) is satisfied. The choice of the pseudo-potential of dissipation is to be guided by experiments.

3.7.8 An Example of Thermal Effects Due to Collisions

We choose a pseudo-potential which does not couple the two first variables insuring that the mechanical problem is decoupled from the thermal one, for instance

$$\hat{\Phi}\left(D(\frac{U^+ + U^-}{2}), \delta\bar{T}, D(\frac{U^-}{2})\right) \tag{3.140}$$

$$= \hat{\Phi}_{meca}\left(D(\frac{U^+ + U^-}{2}), D(\frac{U^-}{2})\right) + \frac{\lambda}{4}\left(\delta\bar{T}\right)^2. \tag{3.141}$$

The pseudo-potential $\hat{\Phi}_{meca}$ gives the percussion P^{int}. The mechanical problem is not investigated in this Chapter but three examples have been given in Sect. 2.8 of Chap. 2. Other examples are given in Chap. 4. Complete investigation and results may be found in [8].

The thermal constitutive law is

$$\Sigma\left(\mathcal{B}_{21}\right) - \Sigma\left(\mathcal{B}_{12}\right) = -\lambda\delta\bar{T}. \tag{3.142}$$

We choose the simple free energy for the points $\Psi = -CTLogT$ and a zero interaction free energy, $\Psi^{int} = 0$. This choice gives

$$S_{int} = 0, \tag{3.143}$$

and with (3.134)

$$\Delta\left(\mathcal{B}_{12}\right) = 0, \ \Delta\left(\mathcal{B}_{21}\right) = 0. \tag{3.144}$$

Note that the free energy formula proves that the temperatures after collision are positive

$$T_1^+ > 0, \ T_2^+ > 0. \tag{3.145}$$

Let us assume that the mechanical problem is solved, i.e., the work $P^{int}D\left(\frac{U^+ + U^-}{2}\right)$ is known. The thermal equations are

$$[\mathcal{S}_1] = CLog\frac{T_1^+}{T_1^-} = \Sigma\left(\mathcal{B}_1\right) + \Sigma\left(\mathcal{B}_{12}\right), \tag{3.146}$$

$$[\mathcal{S}_2] = CLog\frac{T_2^+}{T_2^-} = \Sigma\left(\mathcal{B}_2\right) + \Sigma\left(\mathcal{B}_{21}\right), \tag{3.147}$$

$$[\mathcal{E}_1] = C\left[T_1\right] = \bar{T}_1\left(\Sigma\left(\mathcal{B}_1\right) + \Sigma\left(\mathcal{B}_{12}\right)\right) + \left[T_1\right]\Delta\left(\mathcal{B}_1\right), \tag{3.148}$$

$$[\mathcal{E}_2] = C\left[T_2\right] = \bar{T}_2\left(\Sigma\left(\mathcal{B}_2\right) + \Sigma\left(\mathcal{B}_{21}\right)\right) + \left[T_2\right]\Delta\left(\mathcal{B}_2\right), \tag{3.149}$$

$$0 = \left[\mathcal{E}^{int}\right] = P^{int} D\left(\frac{U^+ + U^-}{2}\right) - \bar{T}_1 \Sigma\left(\mathcal{B}_{12}\right) - \bar{T}_2 \Sigma\left(\mathcal{B}_{21}\right). \tag{3.150}$$

These equations are coupled with the description of the thermal exchanges with the exterior of the system. For instance, collision is isentropic

$$\Sigma\left(\mathcal{B}_1\right) = \Sigma\left(\mathcal{B}_2\right) = 0, \tag{3.151}$$

or adiabatic

$$T_1^+ \mathcal{B}_1^+ + T_1^- \mathcal{B}_1^- = \bar{T}_1 \Sigma\left(\mathcal{B}_1\right) + [T_1]\, \Delta\left(\mathcal{B}_1\right) = 0, \tag{3.152}$$

$$\bar{T}_2 \Sigma\left(\mathcal{B}_2\right) + [T_2]\, \Delta\left(\mathcal{B}_2\right) = 0. \tag{3.153}$$

The solution of these equations gives the temperatures T_i and the different entropy fluxes $\mathcal{B}_i$ and $\mathcal{B}_{ij}$.

3.7.8.1 The Isentropic Case

The equations give

$$C Log \frac{T_1^+}{T_1^-} = \Sigma\left(\mathcal{B}_{12}\right), \; C Log \frac{T_2^+}{T_2^-} = \Sigma\left(\mathcal{B}_{21}\right), \tag{3.154}$$

$$C\left[T_1\right] = \bar{T}_1 \Sigma\left(\mathcal{B}_{12}\right) + [T_1]\, \Delta\left(\mathcal{B}_1\right), \; C\left[T_2\right] = \bar{T}_2 \Sigma\left(\mathcal{B}_{21}\right) + [T_2]\, \Delta\left(\mathcal{B}_2\right), \tag{3.155}$$

$$P^{int} D\left(\frac{U^+ + U^-}{2}\right) = \bar{T}_1 \Sigma\left(\mathcal{B}_{12}\right) + \bar{T}_2 \Sigma\left(\mathcal{B}_{21}\right), \tag{3.156}$$

$$\Sigma\left(\mathcal{B}_{21}\right) - \Sigma\left(\mathcal{B}_{12}\right) = -\lambda \delta \bar{T}. \tag{3.157}$$

Then we have

$$C\left[T_1\right] = \bar{T}_1 \Sigma\left(\mathcal{B}_{12}\right) + [T_1]\, \Delta\left(\mathcal{B}_1\right), \tag{3.158}$$

$$C\left[T_2\right] = \bar{T}_2 \Sigma\left(\mathcal{B}_{21}\right) + [T_2]\, \Delta\left(\mathcal{B}_2\right), \tag{3.159}$$

$$P^{int} D\left(\frac{U^+ + U^-}{2}\right) = \bar{T}_1 C Log \frac{T_1^+}{T_1^-} + \bar{T}_2 C Log \frac{T_2^+}{T_2^-}, \tag{3.160}$$

$$C Log \frac{T_2^+}{T_2^-} + \lambda \bar{T}_2 = C Log \frac{T_1^+}{T_1^-} + \lambda \bar{T}_1. \tag{3.161}$$

The two last equations give the temperatures T_1^+ and T_2^+ after a collision. The first two give the thermal exchanges with the exterior : they are computed with $\Delta\left(\mathcal{B}_1\right)$ and $\Delta\left(\mathcal{B}_2\right)$.

3.7.8.2 The Adiabatic Case

The equations give

$$[\mathcal{S}_1] = C\,Log\frac{T_1^+}{T_1^-} = \Sigma\left(\mathcal{B}_1\right) + \Sigma\left(\mathcal{B}_{12}\right), \tag{3.162}$$

$$[\mathcal{S}_2] = C\,Log\frac{T_2^+}{T_2^-} = \Sigma\left(\mathcal{B}_2\right) + \Sigma\left(\mathcal{B}_{21}\right), \tag{3.163}$$

and

$$C\left[T_1\right] = \bar{T}_1\Sigma\left(\mathcal{B}_{12}\right),\ C\left[T_2\right] = \bar{T}_2\Sigma\left(\mathcal{B}_{21}\right), \tag{3.164}$$

and

$$P^{int}D\left(\frac{U^+ + U^-}{2}\right) = C\left[T_1\right] + C\left[T_2\right], \tag{3.165}$$

$$C\frac{[T_2]}{\bar{T}_2} - C\frac{[T_1]}{\bar{T}_1} = -\lambda\delta\bar{T}. \tag{3.166}$$

The two last equations give the temperatures T_1^+ and T_2^+ after a collision. The first two give the entropic exchanges $\Sigma\left(\mathcal{B}_1\right)$ and $\Sigma\left(\mathcal{B}_2\right)$ with the exterior.

3.7.8.3 The Small Perturbation Case

Computations of temperatures T_1^+ and T_2^+ in the two preceding situations may be performed with numerics or with closed form solutions which are sophisticated. A case is easily solved: we assume that the collision occurs at the ambient temperature and that the temperature variations are negligible compared with the ambient temperature. We may say that we assume small perturbations. This is the case for an every day experiment. In both isentropic and adiabatic cases, we have

$$Log\frac{T^+}{T^-} \simeq \frac{[T]}{T^-},\quad \frac{[T]}{\bar{T}} \simeq \frac{[T]}{T^-}. \tag{3.167}$$

In both cases we have

$$P^{int}D\left(\frac{U^+ + U^-}{2}\right) = C\left[T_1\right] + C\left[T_2\right], \tag{3.168}$$

$$C\frac{[T_2]}{T_2^-} - C\frac{[T_1]}{T_1^-} = -\lambda\delta\bar{T} \tag{3.169}$$

$$= -\lambda(T_2^- - T_1^- + \frac{[T_2]}{2} - \frac{[T_1]}{2}). \tag{3.170}$$

These relationships give

$$P^{int} D\left(\frac{U^+ + U^-}{2}\right) = C\,[T_1] + C\,[T_2]\,, \tag{3.171}$$

$$\left(\frac{C}{T_2^-} + \frac{\lambda}{2}\right)[T_2] - \left(\frac{C}{T_1^-} + \frac{\lambda}{2}\right)[T_1] = -\lambda(T_2^- - T_1^-). \tag{3.172}$$

To simplify again, let us assume that λ is small compared to C/T. It results

$$P^{int} D\left(\frac{U^+ + U^-}{2}\right) = C\,[T_1] + C\,[T_2]\,, \tag{3.173}$$

$$\frac{C}{T_2^-}[T_2] - \frac{C}{T_1^-}[T_1] = -\lambda(T_2^- - T_1^-), \tag{3.174}$$

which gives

$$C\,[T_1] = \frac{T_1^-}{T_2^- + T_1^-}\left(P^{int} D\left(\frac{U^+ + U^-}{2}\right) + \lambda T_2^-(T_2^- - T_1^-)\right), \tag{3.175}$$

$$C\,[T_2] = \frac{T_2^-}{T_2^- + T_1^-}\left(P^{int} D\left(\frac{U^+ + U^-}{2}\right) - \lambda T_1^-(T_2^- - T_1^-)\right). \tag{3.176}$$

These formulae show that the mechanical work

$$\frac{T_i^-}{T_2^- + T_1^-} P^{int} D\left(\frac{U^+ + U^-}{2}\right) \geq 0, \tag{3.177}$$

tends to warm up the two points and that the conduction effect

$$\frac{T_i^-}{T_2^- + T_1^-}\left(\pm\lambda T_j^-(T_2^- - T_1^-)\right) \tag{3.178}$$

tends to equalize their temperatures ($i, j = 1, 2,\ i \neq j$).

3.8 Phase Change and Collisions

Let us consider rain falling on deeply frozen soil. The rain droplets may freeze or remain liquid when colliding the soil, [3]. This problem may be addressed with the tools presented in the previous section. The energy of the droplet involves the phase latent heat quantity. The predictive theory of the occurrence of dangerous black ice is developed in [7] with predictions of the thermal evolution of highways, [9], for the winter viability. An analogous problem is the collision of a hail droplet with a warm soil, [7]. This problem is investigated in Chap. 7, where the collisions of two solids with the possibility of phase change is investigated.

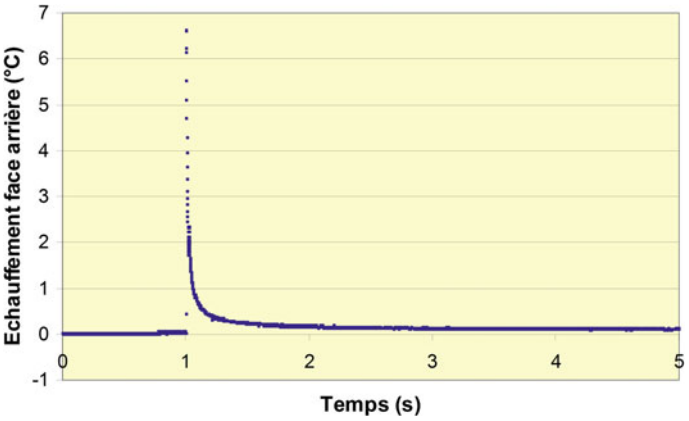

Fig. 3.2 A metallic ball with 3 mm diameter collides a metallic plate with 0,85 mm thickness. The kinetic energy of the ball is 0, 27 J. Temperature of the plate back face versus time is discontinuous at the time scale of the measurements, [11]

3.9 Experimental Results

As far as we know, there are almost no thermal measurements in collisions. Nevertheless some results are available. For instance, temperature of the back face of a metallic plate collided by a steel ball has been measured with an infrared camera, [11, 12]. A temperature increase up to $7°C$ in less than a hundredth of a second is reported in Fig. 3.2. At the engineering scale, temperature is actually discontinuous, even if at a finer time scale it is continuous.

If we assume the plate and the steel ball have the same temperature before collision, the formulae (3.176) within the small perturbation assumption give

$$2C\,[\theta] = P^{int}\,D\left(\frac{U^+ + U^-}{2}\right), \tag{3.179}$$

where C is the heat capacity of the steel ball and θ its temperature. This result may be used to have information on the mechanical constitutive law.

References

1. Bonetti, E., Colli, P., Frémond, M.: A phase field model with thermal memory governed by the entropy balance. Math. Models and Methods Appl. Sci. **13**, 231–256 (2003)
2. Bonetti, E., Frémond, M.: A phase transition model with the entropy balance. Math. Methods Appl. Sci. **26**, 539–556 (2003)

3. Caucci, A.M., Frémond, M.: Thermal effects of collisions: does rain turn into ice when it falls on a frozen ground? J. Mech. Mater. Struct. **4**(2), 225–244 (2009). http://pjm.math.berkeley.edu/jomms/2009/4-2/index.xhtml
4. Ekeland, I., Temam, R.: Convex Analysis and Variational Problems. North Holland, Amsterdam (1976)
5. Frémond, M.: Phase change with temperature discontinuities, Gakuto Inter. Ser. Math. Sci. Appl. **14**, 125–134 (2000)
6. Frémond, M.: La mécanique des collisions de solides. In: Lagnier, J. (ed.) La Mécanique des Milieux Granulaires. Hermès, Paris (2001)
7. Frémond, M.: Non-smooth Thermomechanics. Springer, Berlin (2002)
8. Frémond, M.: Collisions, Edizioni del Dipartimento di Ingegneria Civile, Università di Roma Tor Vergata, ISBN 978-88-6296-000-7 (2007)
9. Lassoued, R.: Comportement hivernal des chaussées. Modélisation thermique, Thèse de l'École nationale des Ponts et Chaussées, Paris (2000)
10. Moreau, J.J.: Fonctionnelles convexes, Edizioni del Dipartimento di Ingegneria Civile, Università di Roma "Tor Vergata", 2003, ISBN 978-88-6296-001-4 and Séminaire sur les équations aux dérivées partielles. Collège de France, Paris (1966)
11. Pron, H., Application des effets photothermiques et thermomécaniques à l'analyse des contraintes appliquées et résiduelles, thèse de l'Université de Reims Champagne-Ardenne (2000)
12. Pron, H., Henry, J.F., Bouferra, R., Bissieux, C., Beaudouin, J.L.: Etude par thermographie infrarouge du grenaillage de précontrainte ou shot-penning, Congrès français de thermique, SFT 2002, Vittel (2002)

Chapter 4
Collisions of Rigid Solids: Three Disks in a Plane

Federica Caselli and Michel Frémond

4.1 Introduction

We consider three rigid solids and we intend to build a predictive theory of their motion. When the solids do not interact or interact smoothly, the description of their motion is given by analytical mechanics without any major difficulty. We focus here on the collision problem: If only two of the solids collide, the results of Chaps. 2 and 3 apply with minor modifications. If all the three solids collide, there may be at a distance interactions between them. This is the case we want to consider. In particular, in this chapter the 2D problem of three rigid disks moving in a plane is investigated. The 3D problem of three rigid balls evolving in $\mathbb{R}^3$ is considered in Chap. 5. We address this widely studied topic (see, for instance, [2]) with a new point of view: *the system made of the three solids is deformable* because the relative distances of material points vary. In order to focus on the main ideas, we assume that the solids have smooth boundaries at collision points. The case of non-smooth boundaries is addressed in [6, 7].

The geometry of the system is depicted in Fig. 4.1: three identical disks with radius R and centers O_i, $i = 1, 2, 3$, evolve in a plane. One may think of coins sliding on a very smooth planar surface. An orthonormal basis $(\mathbf{e}_1, \mathbf{e}_2, \mathbf{e}_3)$ is introduced such that the unit vector $\mathbf{e}_1$ is parallel to $\mathbf{O_1O_2}$ and the unit vector $\mathbf{e}_3$ is orthogonal to the plane. The angle between $\mathbf{e}_1$ and $\mathbf{O_2O_3}$ is denoted by θ. At collision time disks 1 and 2 are in contact at point A and disks 2 and 3 are in contact at point B. We denote $l(\theta)$ the distance between point A and point B

$$l(\theta) = 2R\cos\frac{\theta}{2}\,. \tag{4.1}$$

Moreover, $\mathbf{N}_{12}$ denotes the outer normal vector to disk 1 at point A and $\mathbf{N}_{23}$ denotes the outer normal vector to disk 2 at point B. The case the disks are not identical, e.g. they have different radii and/or different masses, and the case of other geometric arrangements can be treated with straightforward extension of the theory presented in the following.

M. Frémond, *Collisions Engineering: Theory and Applications*,
Springer Series in Solid and Structural Mechanics 6,
DOI 10.1007/978-3-662-52696-5_4

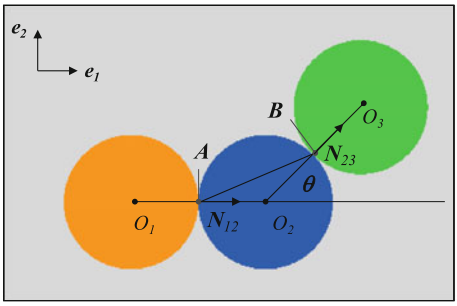

Fig. 4.1 The system at collision time

4.2 The Velocities

The actual linear velocities of the centers O_i of the disks are denoted by $\mathbf{U}_i(O_i)$ and $\mathbf{U} = (\mathbf{U}_1(O_1), \mathbf{U}_2(O_2), \mathbf{U}_3(O_3))$. Each $\mathbf{U}_i$ has two components, $U_{i,1}$ and $U_{i,2}$. The actual angular velocities of the disks are denoted by $\Omega_i \mathbf{e}_3$ and $\Omega = (\Omega_1, \Omega_2, \Omega_3)$. Similarly, virtual velocities are $\mathbf{V} = (\mathbf{V}_1(O_1), \mathbf{V}_2(O_2), \mathbf{V}_3(O_3))$ and $\omega = (\omega_1, \omega_2, \omega_3)$.

At geometric point A the velocities of the material points of disks 1 and 2 are

$$\mathbf{U}_1(A) = \mathbf{U}_1(O_1) + \Omega_1 \mathbf{e}_3 \times \mathbf{O_1A} = \begin{pmatrix} U_{1,1} \\ U_{1,2} + R\Omega_1 \end{pmatrix}, \tag{4.2}$$

$$\mathbf{U}_2(A) = \mathbf{U}_2(O_2) + \Omega_2 \mathbf{e}_3 \times \mathbf{O_2A} = \begin{pmatrix} U_{2,1} \\ U_{2,2} - R\Omega_2 \end{pmatrix}. \tag{4.3}$$

Similarly, at geometric point B we have

$$\mathbf{U}_2(B) = \mathbf{U}_2(O_2) + \Omega_2 \mathbf{e}_3 \times \mathbf{O_2B} = \begin{pmatrix} U_{2,1} - R\Omega_2 \sin\theta \\ U_{2,2} + R\Omega_2 \cos\theta \end{pmatrix}, \tag{4.4}$$

$$\mathbf{U}_3(B) = \mathbf{U}_3(O_3) + \Omega_3 \mathbf{e}_3 \times \mathbf{O_3B} = \begin{pmatrix} U_{3,1} + R\Omega_3 \sin\theta \\ U_{3,2} - R\Omega_3 \cos\theta \end{pmatrix}. \tag{4.5}$$

At collision time t, we denote with a minus superscript the actual and virtual velocities before collision

$$\mathbf{U}^- = (\mathbf{U}_1^-(\mathbf{O}_1), \mathbf{U}_2^-(\mathbf{O}_2), \mathbf{U}_3^-(\mathbf{O}_3)), \quad \Omega^- = (\Omega_1^-, \Omega_2^-, \Omega_3^-), \tag{4.6}$$

$$\mathbf{V}^- = (\mathbf{V}_1^-(\mathbf{O}_1), \mathbf{V}_2^-(\mathbf{O}_2), \mathbf{V}_3^-(\mathbf{O}_3)), \quad \omega^- = (\omega_1^-, \omega_2^-, \omega_3^-), \tag{4.7}$$

and with a plus superscript the actual and virtual velocities after collision

$$\mathbf{U}^{+} = (\mathbf{U}_1^{+}(\mathbf{O}_1), \mathbf{U}_2^{+}(\mathbf{O}_2), \mathbf{U}_3^{+}(\mathbf{O}_3)) , \quad \Omega^{+} = (\Omega_1^{+}, \Omega_2^{+}, \Omega_3^{+}) , \tag{4.8}$$

$$\mathbf{V}^{+} = (\mathbf{V}_1^{+}(\mathbf{O}_1), \mathbf{V}_2^{+}(\mathbf{O}_2), \mathbf{V}_3^{+}(\mathbf{O}_3)) , \quad \omega^{+} = (\omega_1^{+}, \omega_2^{+}, \omega_3^{+}) . \tag{4.9}$$

Moreover, for a generic (scalar or vectorial) quantity $\mathbf{W}$, we introduce the notations

$$[\mathbf{W}] = \mathbf{W}^{+} - \mathbf{W}^{-} , \quad \overline{\mathbf{W}} = \frac{\mathbf{W}^{+} + \mathbf{W}^{-}}{2} , \tag{4.10}$$

where $\mathbf{W}^{+}$ and $\mathbf{W}^{-}$ are the values after and before collision, respectively.

4.3 The Velocities of Deformation

The system we consider is the system made of the three solids. This system is deformable. The deformation linear and angular velocities depend on virtual velocities $\mathbf{V}_i(P)$ at different points P of the solids and on virtual angular velocities $\omega = (\omega_1, \omega_2, \omega_3)$. The choice of the deformation velocities is guided by the wish to represent all the phenomena occurring in the motion. They may be chosen as follows:

- the relative velocities of the solids at contact points

$$\mathbf{D}_{12}(\mathbf{V}, \omega) = \mathbf{V}_1(A) - \mathbf{V}_2(A) , \quad \mathbf{D}_{23}(\mathbf{V}, \omega) = \mathbf{V}_2(B) - \mathbf{V}_3(B) , \tag{4.11}$$

- the at a distance velocity of deformation D_{13} *which accounts for interaction of solid 3 with solid 1*

$$D_{13}(\mathbf{V}, \omega) = 2(\mathbf{V}_1(A) - \mathbf{V}_3(B)) \cdot \mathbf{BA} , \tag{4.12}$$

- the relative angular velocities of the solids

$$\hat{D}_{12}(\omega) = \omega_1 - \omega_2 , \quad \hat{D}_{23}(\omega) = \omega_2 - \omega_3 , \quad \hat{D}_{31}(\omega) = \omega_3 - \omega_1 , \tag{4.13}$$

  where $\hat{D}_{31}$ is a non local velocity of deformation analogous to D_{13}.

In our point of view, all the velocities of deformation are useful and all of them may be needed to describe the evolution of the system. This point of view allows to describe easily the numerous phenomena occurring in solids collisions: for instance, either the carreau phenomenon [3], or the superball effect [1, 8].

Remark 4.1 There are relationships between the velocities of deformation, internal constraints in mechanical parlance

$$\hat{D}_{12} + \hat{D}_{23} + \hat{D}_{31} = 0\,, \tag{4.14}$$

$$D_{13} - 2(\mathbf{D}_{12} + \mathbf{D}_{23}) \cdot \mathbf{BA} = 0\,. \tag{4.15}$$

Since these internal constraints are satisfied by any set of virtual velocities they do not intervene in the constitutive laws [3].

4.4 The Work of the Interior Forces

The work of the interior forces is given by

$$\begin{aligned}\mathcal{T}_{int}\left(\overline{\mathbf{V}}, \overline{\omega}\right) = &- \mathbf{P}_{12} \cdot \mathbf{D}_{12}\left(\overline{\mathbf{V}}, \overline{\omega}\right) - \mathbf{P}_{23} \cdot \mathbf{D}_{23}\left(\overline{\mathbf{V}}, \overline{\omega}\right) - MD_{13}\left(\overline{\mathbf{V}}, \overline{\omega}\right) \\ &- C_{12}\hat{D}_{12}\left(\overline{\omega}\right) - C_{23}\hat{D}_{23}\left(\overline{\omega}\right) - C_{31}\hat{D}_{31}\left(\overline{\omega}\right)\,.\end{aligned} \tag{4.16}$$

It introduces generalized internal forces: percussions $\mathbf{P}_{12}$ and $\mathbf{P}_{23}$ applied at points A and B, respectively; an a distance percussion $2M\mathbf{BA}$; torque percussions C_{12}, C_{23} and C_{31}. We emphasize *the importance of the at a distance velocity of deformation* D_{13} *which accounts for interaction of solid 3 with solid 1 and introduces the at a distance internal percussions* $-2M\mathbf{BA}$, *applied at point A, and* $2M\mathbf{BA}$, *applied at point B. Let us stress again that this velocity of deformation may be introduced as well as the local velocities of deformation* $\mathbf{D}_{12}$ *and* $\mathbf{D}_{23}$ *which account for interaction of the solids in contact.* The same holds for the non local velocity of deformation $\hat{D}_{31}$.

4.5 The Work of the Acceleration Forces

The work of the acceleration forces is given by

$$\mathcal{T}_{acc}\left(\overline{\mathbf{V}}, \overline{\omega}\right) = \sum_{i=1}^{3} m\left[\mathbf{U}_i(O_i)\right] \cdot \overline{\mathbf{V}}_i(O_i) + \sum_{i=1}^{3} I\left[\Omega_i\right]\overline{\omega}_i\,, \tag{4.17}$$

where m and I denote the mass and the mass moment of inertia of the disks, respectively. Let us note that the actual work of the acceleration forces is equal to the variation of the kinetic energy

$$\mathcal{T}_{acc}\left(\overline{\mathbf{U}}, \overline{\Omega}\right) = \sum_{i=1}^{3} \frac{m}{2}\left[\mathbf{U}_i(O_i)^2\right] + \sum_{i=1}^{3} I\left[\Omega_i^2\right]\,. \tag{4.18}$$

This relationship is important for the kinetic energy theorem. For the sake of simplicity, we assume that there are no exterior actions at collision time.

4.6 The Equations of Motion

The equations of motion result from the principle of virtual power

$$\forall \overline{\mathbf{V}}, \forall \overline{\omega}\,, \qquad \mathcal{T}_{acc}\left(\overline{\mathbf{V}}, \overline{\omega}\right) = \mathcal{T}_{int}\left(\overline{\mathbf{V}}, \overline{\omega}\right)\,. \tag{4.19}$$

They are

$$\begin{aligned}
m\left[\mathbf{U}_1(O_1)\right] &= -\mathbf{P}_{12} - 2M\mathbf{BA}\,,\\
m\left[\mathbf{U}_2(O_2)\right] &= \mathbf{P}_{12} - \mathbf{P}_{23}\,,\\
m\left[\mathbf{U}_3(O_3)\right] &= \mathbf{P}_{23} + 2M\mathbf{BA}\,,\\
I\left[\Omega_1\right]\mathbf{e}_3 &= -\mathbf{O_1A} \times \mathbf{P}_{12} - 2M\mathbf{O_1A} \times \mathbf{BA} - C_{12}\mathbf{e}_3 + C_{31}\mathbf{e}_3\,,\\
I\left[\Omega_2\right]\mathbf{e}_3 &= \mathbf{O_2A} \times \mathbf{P}_{12} - \mathbf{O_2B} \times \mathbf{P}_{23} + C_{12}\mathbf{e}_3 - C_{23}\mathbf{e}_3\,,\\
I\left[\Omega_3\right]\mathbf{e}_3 &= \mathbf{O_3B} \times \mathbf{P}_{23} + 2M\mathbf{O_3B} \times \mathbf{BA} - C_{31}\mathbf{e}_3 + C_{23}\mathbf{e}_3\,.
\end{aligned} \tag{4.20}$$

We note that gravity does not intervene in collisions, because it has a density with respect to the Lebesgue measure.

4.7 The Constitutive Laws

For the sake of simplicity, we choose quadratic pseudopotentials augmented by indicator functions which provide basic physical behaviour. They yield the following constitutive laws

$$\begin{aligned}
\mathbf{P}_{12} &= k\mathbf{D}_{12}\left(\overline{\mathbf{U}}, \overline{\Omega}\right) + \mathbf{R}_{12}^{reac}\,,\\
\mathbf{P}_{23} &= k\mathbf{D}_{23}\left(\overline{\mathbf{U}}, \overline{\Omega}\right) + \mathbf{R}_{23}^{reac}\,,\\
M &= \nu D_{13}\left(\overline{\mathbf{U}}, \overline{\Omega}\right)\,,\\
C_{12} &= \hat{k}\hat{D}_{12}\left(\overline{\Omega}\right)\,,\\
C_{23} &= \hat{k}\hat{D}_{23}\left(\overline{\Omega}\right)\,,\\
C_{31} &= \hat{\nu}\hat{D}_{31}\left(\overline{\Omega}\right)\,,
\end{aligned} \tag{4.21}$$

where $\mathbf{R}_{12}^{reac}$ and $\mathbf{R}_{23}^{reac}$ are impenetrability reactions defined as

$$\begin{aligned}
&\mathbf{R}_{12}^{reac} = R_{12}^{reac}\mathbf{N}_{12}\,,\\
&\mathbf{R}_{23}^{reac} = R_{23}^{reac}\mathbf{N}_{23}\,,\\
&R_{12}^{reac} \in \partial I_{-}(\mathbf{D}_{12}(\mathbf{U}^{+},\Omega^{+})\cdot\mathbf{N}_{12}) = \partial I_{-}((\mathbf{U}_{1}^{+}(A)-\mathbf{U}_{2}^{+}(A))\cdot\mathbf{N}_{12})\,,\\
&R_{23}^{reac} \in \partial I_{-}(\mathbf{D}_{23}(\mathbf{U}^{+},\Omega^{+})\cdot\mathbf{N}_{23}) = \partial I_{-}((\mathbf{U}_{2}^{+}(B)-\mathbf{U}_{3}^{+}(B))\cdot\mathbf{N}_{23})\,. \qquad (4.22)
\end{aligned}$$

The parameters k, $\hat{k}$, ν and $\hat{\nu}$ in the linear terms in equations (4.21) represent dissipative parameters and are positive quantities. In particular, ν and $\hat{\nu}$ quantify the intensity of the at a distance interactions between balls 1 and 3 related to the velocities D_{13} and $\hat{D}_{31}$, respectively. Function I_{-} in (4.22) is the indicator function of $\mathbb{R}^{-}$ which takes into account the impenetrability conditions.

Observe that the impenetrability reactions are active only when there is risk of interpenetration. Let us consider for instance R_{12}^{reac}: it is 0 if contact is not maintained after collision (i.e., $(\mathbf{U}_{1}^{+}(A)-\mathbf{U}_{2}^{+}(A))\cdot\mathbf{N}_{12}<0$) and it is positive, $R_{12}^{reac}\in\partial I_{-}(0)=\mathbb{R}^{+}$, if contact is maintained after collision (i.e., $(\mathbf{U}_{1}^{+}(A)-\mathbf{U}_{2}^{+}(A))\cdot\mathbf{N}_{12}=0$).

Other constitutive laws may be found in the literature, such as, for instance, Coulomb's law for collisions [4, 8, 9], which has been established with experiments. However, using this constitutive law, the equations of motion are quite involved and uniqueness of the evolution is not guaranteed. This makes the numerical methods tricky. On the contrary, thanks to convex analysis and monotone operator theory, with the present approach the problem of finding the velocities after collision has one and only one solution [3]. Moreover, as shown in the following, the solution may be easily computed by solving linear systems, and the obtained results are in agreement with everyday experience.

Remark 4.2 Parameter values may be measured through simple experiments: k may be measured performing two balls collisions; parameter ν, or function $\nu(\theta)$ in a more sophisticated theory, with three balls collisions.

4.7.1 Solution of the Equations

The equations to get velocities after collision $(\mathbf{U}^{+},\Omega^{+})$ as functions of velocities before collision $(\mathbf{U}^{-},\Omega^{-})$ result from the equations of motion and constitutive laws. They have one and only one solution [3]. This result is the basis of the method used to solve the equations. At collision time, there is contact between disks at geometric points A and B. Considering for instance A, there are two possible cases according to the contact status at such point after collision:

1. contact is not maintained: $\mathbf{D}_{12}(\mathbf{U}^+, \Omega^+) \cdot \mathbf{N}_{12} < 0$ and reaction $R_{12}^{reac} = 0$. The unknowns at point A are the two normal velocities $\mathbf{U}_1^+(A) \cdot \mathbf{N}_{12}$ and $\mathbf{U}_2^+(A) \cdot \mathbf{N}_{12}$ and the two tangential velocities;
2. contact is maintained: $\mathbf{D}_{12}(\mathbf{U}^+, \Omega^+) \cdot \mathbf{N}_{12} = 0$, reaction $R_{12}^{reac} \neq 0$. The unknowns at point A are the common normal velocity $\mathbf{U}_1^+(A) \cdot \mathbf{N}_{12} = \mathbf{U}_2^+(A) \cdot \mathbf{N}_{12}$, the reaction $R_{12}^{reac} \neq 0$ and the two tangential velocities.

If $\mathbf{D}_{12}(\mathbf{U}^+, \Omega^+) \cdot \mathbf{N}_{12} = 0$ and $R_{12}^{reac} = 0$, the two possibilities both hold. In any case, the unknowns satisfy a linear system resulting from the equations of motion and constitutive laws. There are $2 \times 2 = 4$ contact status (2 at point A and 2 at point B): we assume one of them, then we solve the linear system and check if the solution is the physical one, i.e., at each point the impenetrability condition is satisfied (case 1) or the reaction has the correct sign (case 2). If all conditions are satisfied this is the unique solution, otherwise this is not the unique solution and we start again with a new contact status assumption. Thanks to the existence and uniqueness properties, within at most 4 trials, the solution is found.

4.8 Numerical Examples

We consider the following setting: disks 2 and 3 in contact and at rest; disk 1 collides disk 2 with velocity $\mathbf{U}_1^-$ parallel to $\mathbf{O_1O_2}$. We distinguish the two cases of finite or infinite mass moment of inertia.

4.8.1 The Mass Moment of Inertia Is Infinite: $I = \infty$

Figure 4.2 shows the effect of mass m and at a distance interaction ν on contact status after collision, in the hypothesis $\theta = 0, k = 2, \mathbf{U}_1^- = (1, 0), R = 1$. Observe that when the at a distance parameter ν is large enough, disks 2 and 3, which are in contact before collision, are no longer in contact after collision. Let us again emphasize that the at a distance interactions are responsible for this every day phenomenon: two solids in contact before they are collided by another one are no longer in contact after collision. Irrespective of the values of the other parameters, this behaviour cannot be reproduced with $\nu = 0$.

Consider now the effect of the dissipative parameter k. When it is small, the dissipation is mainly due to the impenetrability reactions $\mathbf{R}_{12}^{reac}$ and $\mathbf{R}_{23}^{reac}$, which are active only when contact is maintained after collision: thus contact is very often maintained in this case. When k is large, in most situation contact is not maintained after collision.

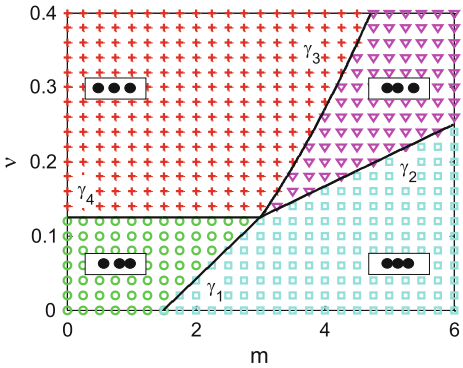

Fig. 4.2 Effect of mass m and at a distance interaction ν on contact status after collision for $\theta = 0$, $k = 2$, $\mathbf{U}_1^- = (1, 0)$, $R = 1$. In the four boxes it is shown a schematic representation of contact status after collision for parameter values in the corresponding region (the *black balls* in the *boxes* represent, from *left* to *right*, ball 1, ball 2 and ball 3)

In case the disks are aligned, analytical expressions may be found for the boundaries between the different regions (Fig. 4.2). They turn out to be lines and parabolas, namely:

$$\begin{aligned}
\gamma_1 &: \ \nu = \left(\frac{2m}{3} - \frac{k}{2}\right)\frac{1}{8R^2}\,, \\
\gamma_2 &: \ \nu = \frac{m}{24R^2}\,, \\
\gamma_3 &: \ \nu = \left(\frac{m^2}{3k} - \frac{k}{4}\right)\frac{1}{8R^2}\,, \\
\gamma_4 &: \ \nu = \frac{k}{16R^2}
\end{aligned} \tag{4.23}$$

(see [3, 8] for a detailed derivation).

Remark 4.3 In the review part of a PhD thesis, [5], it is mentioned that in 1995, all the many reviewed theories describing simultaneous collisions of three disks prove that two disks in contact before collisions remain in contact after collision with an other disk aligned with them. Experiments with three coins exclude these theories to predict the motion with multiple simultaneous collisions. Note that the concept of deformable system, introducing an at a distance velocity of deformation, allows to overcome the difficulty.

4.8.2 The Mass Moment of Inertia Is Finite: $I < \infty$

When the disks are aligned ($\theta = 0$), the angular velocity coupled to the friction at contact points A and B produces tangential percussions. Thus, after collision, disks 2 and 3 have a non null linear velocity along $\mathbf{e}_2$ and they also get an angular velocity. The effects of the at a distance parameter ν and of the local parameter k remain. When angle θ is not 0, the dispersion effect is accentuated. These results are illustrated in

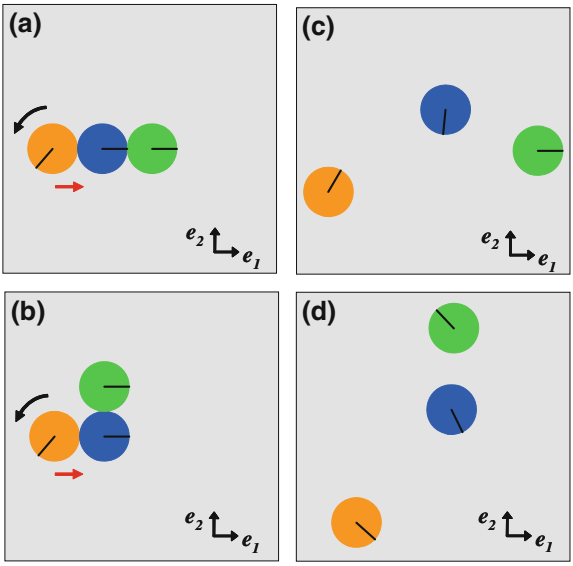

Fig. 4.3 The coupling of angular velocity and friction produces tangential percussions: **a** [resp. **b**] position of the disks at collision time for the case $\theta = 0$ [resp. $\theta = \pi/2$]; **c** [resp. **d**] position of the disks 5 s after collision. The *black* and *red arrows* in **a** and **b** show respectively angular velocity and velocity of the center of mass of ball 1 before collision ($\Omega_1^- = 1$, $\mathbf{U}_1^- = (1, 0)$). $R = 1$, $m = 1$, $k = \nu = 1$, $\hat{k} = \hat{\nu} = 0$

Fig. 4.3: Fig. 4.3(a) (resp. (b)) shows the position of the disks at collision time for the case $\theta = 0$ (resp. $\theta = \pi/2$); Fig. 4.3(c) (resp. (d)) shows the position of the disks 5 s after collision (here and in the following we assume that velocities remain constant after collision). In both cases we consider $R = 1$, $m = 1$, $k = \nu = 1$, $\hat{k} = \hat{\nu} = 0$, $\mathbf{U}_1^- = (1, 0)$, $\Omega_1^- = 1$. Animations of the numerical examples are available at http://dicii.uniroma2.it/?PG=25.26.73 or at http://extras.springer.com.

Remark 4.4 The theory may be applied to the motion of either boxes or bottles moving either in line or in groups on a conveyor belt. One may also think of pedestrians. Depending on the way they are seen, they may be either deformable bodies or points moving on a plane. An intermediate point of view is to consider they are disks with a mass moment of inertia. When the proper will of the pedestrians is not preponderant, it is wise to assume their motion results from natural attractions: the exit door of a theater, of a train, of an underground metropolitan station,… This point of view is developed in Chap. 6. One may also think that some pedestrians hold hands. Thus there are at a distance interactions both in the smooth motion and in the non-smooth motion. Smooth at a distance interactions are easily described as seen in Chap. 3.

References

1. Ben Mekki, O., Frémond, M.: Collision of four balls aligned. Vietnam J Mech, VAST **32**(3), 145–156 (2010)
2. Brogliato, B.: Nonsmooth Mechanics. Springer, Berlin (1999)

3. Caselli, F., Frémond, M.: Collisions of three balls on a plane. Comput Mech **43**(6), 743–754 (2009)
4. Dimnet, E.: Mouvement et collisions de solides rigides et déformables. Thèse de l'École nationale des Ponts et Chaussées, Paris (2002)
5. Durand, S.: Dynamique des systèmes à liaisons unilatérales avec frottement sec. Thèse de l'École nationale des Ponts et Chaussées, Paris (1996)
6. Frémond, M.: Collision of a wedge with a plane. Comput Appl Math **19**(2), 1–10 (2000)
7. Frémond, M.: Non-smooth Thermo-Mechanics. Springer, Berlin (2002)
8. Frémond, M.: Collisions, Edizioni del Dipartimento di Ingegneria Civile, Università di Roma "Tor Vergata" (2007). ISBN 978-88-6296-000-7
9. Jean, M., Moreau, J.J.: Unilaterality and dry friction in the dynamics of rigid body collections. In: Curnier, A. (ed.) Proceedings of Contact Mechanics International Symposium, pp. 31–48. Presses Polytechniques et Universitaires Romandes, Lausanne (1992)

Chapter 5
Collisions of Rigid Solids: Three Balls in a Box

Federica Caselli and Michel Frémond

5.1 Introduction

In this chapter the predictive theory presented in Chap. 4 is extended to the case of three rigid balls evolving in a three dimensional domain bounded by some constraints. One may think of balls in a box. We start with the case of three balls evolving on a plane [2, 3] and then we introduce the presence of walls. This is a 3D problem, because balls may jump.

5.2 Three Balls Evolving on a Plane

Three identical balls with radius R and centers O_i, $i = 1, 2, 3$, evolve on a plane with normal unit vector $\mathbf{e}_3$. The geometry of the system at collision time is shown in Fig. 5.1. The unit vector $\mathbf{e}_1$ is parallel to $\mathbf{O_1O_2}$ and the unit vector $\mathbf{e}_2$ is such that $(\mathbf{e}_1, \mathbf{e}_2, \mathbf{e}_3)$ is direct. The angle between $\mathbf{e}_1$ and $\mathbf{O_2O_3}$ is denoted by θ and belongs to $[0, 2\pi/3]$. At collision time balls 1 and 2 are in contact at point A and balls 2 and 3 are in contact at point B. We denote $l(\theta)$ the distance between point A and point B (4.1), $\mathbf{N}_{12}$ the outer normal vector to ball 1 at point A and $\mathbf{N}_{23}$ the outer normal vector to ball 2 at point B. Balls 1, 2 and 3 are in contact with the plane respectively at points C, D and E. This contact is unilateral, hence a ball may jump and have a positive vertical velocity after collision. $\mathbf{N}_4 = -\mathbf{e}_3$ denotes the downward normal vector to the plane.

The plane is assumed to be very massive, thus remaining immobile. The velocities of the centers of the balls $\mathbf{U}_i(O_i)$ as well as the angular velocities $\boldsymbol{\Omega}_i$ are vectors of $\mathbb{R}^3$. Thus any element $(\mathbf{U}, \boldsymbol{\Omega})$, where $\mathbf{U} = (\mathbf{U}_1(O_1), \mathbf{U}_2(O_2), \mathbf{U}_3(O_3))$ and $\boldsymbol{\Omega} = (\boldsymbol{\Omega}_1, \boldsymbol{\Omega}_2, \boldsymbol{\Omega}_3)$, has 18 components.

As in Chap. 4, we choose the following velocities of deformation:

- the relative velocities of the solids at contact points, $\mathbf{D}_{12}$ and $\mathbf{D}_{23}$;
- the at a distance velocity of deformation $D_{13} = 2(\mathbf{V}_1(A) - \mathbf{V}_3(B)) \cdot \mathbf{BA}$;
- the relative angular velocities of the solids $\hat{\mathbf{D}}_{12}$, $\hat{\mathbf{D}}_{23}$ and $\hat{\mathbf{D}}_{31}$ (which now are vectors of $\mathbb{R}^3$).

M. Frémond, *Collisions Engineering: Theory and Applications*,
Springer Series in Solid and Structural Mechanics 6,
DOI 10.1007/978-3-662-52696-5_5

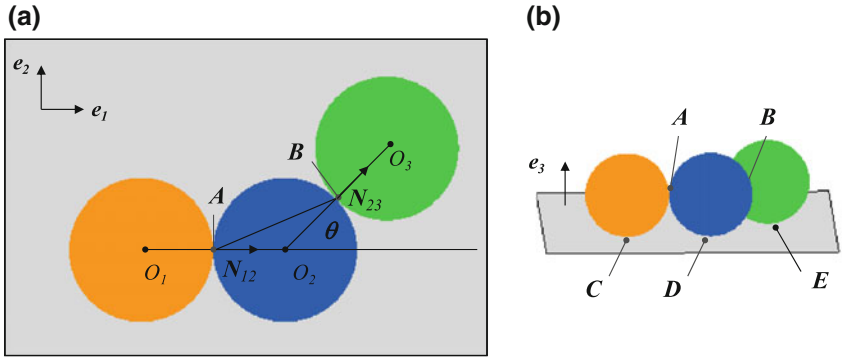

Fig. 5.1 The system at collision time: **a** top view; **b** 3D view

In addition, we choose three new velocities of deformation:

- the velocity of each ball with respect to the immobile plane

$$\mathbf{D}_{14}(\mathbf{V}, \boldsymbol{\omega}) = \mathbf{V}_1(C)\,, \quad \mathbf{D}_{24}(\mathbf{V}, \boldsymbol{\omega}) = \mathbf{V}_2(D)\,, \quad \mathbf{D}_{34}(\mathbf{V}, \boldsymbol{\omega}) = \mathbf{V}_3(E)\,, \tag{5.1}$$

  depending on the virtual velocities $\mathbf{V}$ and $\boldsymbol{\omega}$.

The latter introduce three new internal percussions $\mathbf{P}_{14}$, $\mathbf{P}_{24}$ and $\mathbf{P}_{34}$ applied respectively at the contact points C, D, and E.

The equations of motion become

$$\begin{aligned}
m\,[\mathbf{U}_1(O_1)] &= -\mathbf{P}_{12} - \mathbf{P}_{14} - 2M\mathbf{BA}\,,\\
m\,[\mathbf{U}_2(O_2)] &= \mathbf{P}_{12} - \mathbf{P}_{23} - \mathbf{P}_{24}\,,\\
m\,[\mathbf{U}_3(O_3)] &= \mathbf{P}_{23} - \mathbf{P}_{34} + 2M\mathbf{BA}\,,\\
I\left[\boldsymbol{\Omega}^1\right] &= -\mathbf{O_1A} \times \mathbf{P}_{12} - \mathbf{O_1C} \times \mathbf{P}_{14} - 2M\mathbf{O_1A} \times \mathbf{BA} - \mathbf{C}_{12} + \mathbf{C}_{31}\,,\\
I\left[\boldsymbol{\Omega}^2\right] &= \mathbf{O_2A} \times \mathbf{P}_{12} - \mathbf{O_2B} \times \mathbf{P}_{23} - \mathbf{O_2D} \times \mathbf{P}_{24} + \mathbf{C}_{12} - \mathbf{C}_{23}\,,\\
I\left[\boldsymbol{\Omega}^3\right] &= \mathbf{O_3B} \times \mathbf{P}_{23} - \mathbf{O_3E} \times \mathbf{P}_{34} + 2M\mathbf{O_3B} \times \mathbf{BA} - \mathbf{C}_{31} + \mathbf{C}_{23}\,.
\end{aligned} \tag{5.2}$$

The following simple constitutive laws are considered

$$\begin{aligned}
\mathbf{P}_{i4} &= k_4 \mathbf{D}_{i4}\left(\overline{\mathbf{U}}, \overline{\boldsymbol{\Omega}}\right) + \mathbf{R}_{i4}^{reac}\,,\\
\mathbf{R}_{i4}^{reac} &= R_{i4}^{reac}\mathbf{N}_4\,,\\
R_{i4}^{reac} &\in \partial I_{-}(\mathbf{D}_{i4}(\mathbf{U}^{+}, \boldsymbol{\Omega}^{+}) \cdot \mathbf{N}_4)\,,
\end{aligned} \tag{5.3}$$

where $\mathbf{R}_{i4}^{reac}$ is the impenetrability reaction of ball i and the plane, $i = 1, 2, 3$, and the parameter k_4 is a positive dissipative parameter. The indicator function I_{-} takes into account the impenetrability of balls and plane.

The equations for the 18 unknowns (the velocities $\mathbf{U}_i^+(O_i)$ and the angular velocities $\boldsymbol{\Omega}_i^+$) result combining equations of motion and constitutive laws. They have all the good properties already mentioned in Chap. 4: in particular, there is one and only one solution which may be computed by solving linear systems and checking the results. The number of contact status is $2^5 = 32$. The solution is obtained with at most 32 linear systems resolutions. In practice much less because it is possible to guess the status of some contacts.

Remark 5.1 The value of parameter k_4 may be measured through simple experiments of collisions of a ball with the plane.

5.2.1 Numerical Examples

In the numerical examples reported in this section, the terms $k\mathbf{D}_{12}$, $k\mathbf{D}_{23}$ and $k_4\mathbf{D}_{i4}$ are enhanced by distinguishing normal and tangential contributions: for instance $k\mathbf{D}_{12}$ is splitted in $k_N D_{12}^N$ and $k_T \mathbf{D}_{12}^T$, being $D_{12}^N = \mathbf{D}_{12} \cdot \mathbf{N}_{12}$ the normal velocity of deformation and $\mathbf{D}_{12}^T = \mathbf{D}_{12} - D_{12}^N \mathbf{N}_{12}$ the tangential one. In all the simulations we consider the following setting: before collision, balls 2 and 3 are in contact and at rest; at collision time, ball 1 collides ball 2. When not otherwise specified, we assume $R = 1, m = 0.1, k_N = k_T = k_{4N} = k_{4T} = 1, \nu = 1, \hat{k} = \hat{\nu} = 0$.

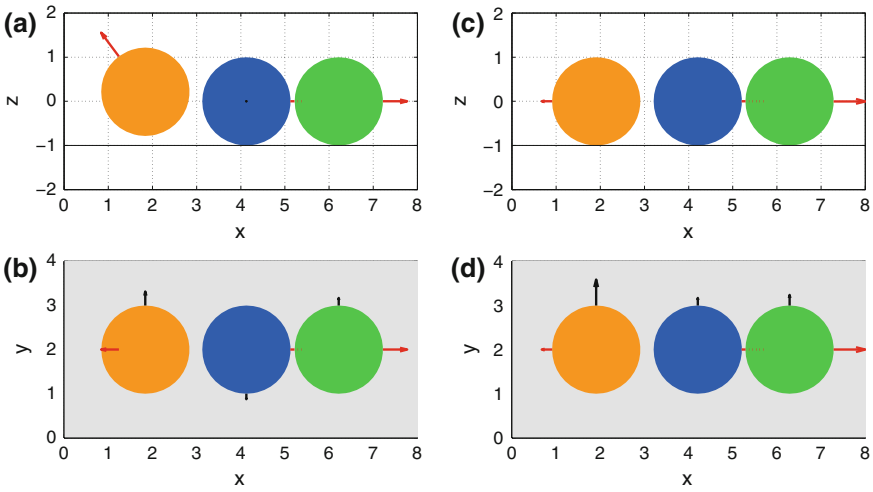

Fig. 5.2 The effect of friction between balls (position of the balls 0.4 s after collision). $\mathbf{U}_1^- = (1, 0, 0)$, $\boldsymbol{\Omega}_1^- = (0, 1, 0)$. **a**, **b** $k_T = 1$, ball 1 jumps; **c**, **d** $k_T = 0$, ball 1 remains in contact with the plane. **a**, **c** the balls are seen from the side; **b**, **d** the balls are seen from *above*. *Red* (resp. *black*) vector: velocity of ball center of mass (resp. ball angular velocity)

We introduce a coordinate system x, y, z such that the directions of the axes are $\mathbf{e}_1$, $\mathbf{e}_2$, $\mathbf{e}_3$ respectively, and the coordinates of point O_1 at collision time are $(2, 2, 0)$. The plane is at $z = -R$. In the figures it will be shown the position of the balls 0.4 s after collision, assuming that post-collision velocities remain constant. The balls will be seen from the side in the plane xz, and from above in the grey plane xy. Red and black vectors will denote, respectively, the velocity of ball center of mass and ball angular velocity. Animations of the numerical examples are available at http://dicii.uniroma2.it/?PG=25.26.73 or at http://extras.springer.com.

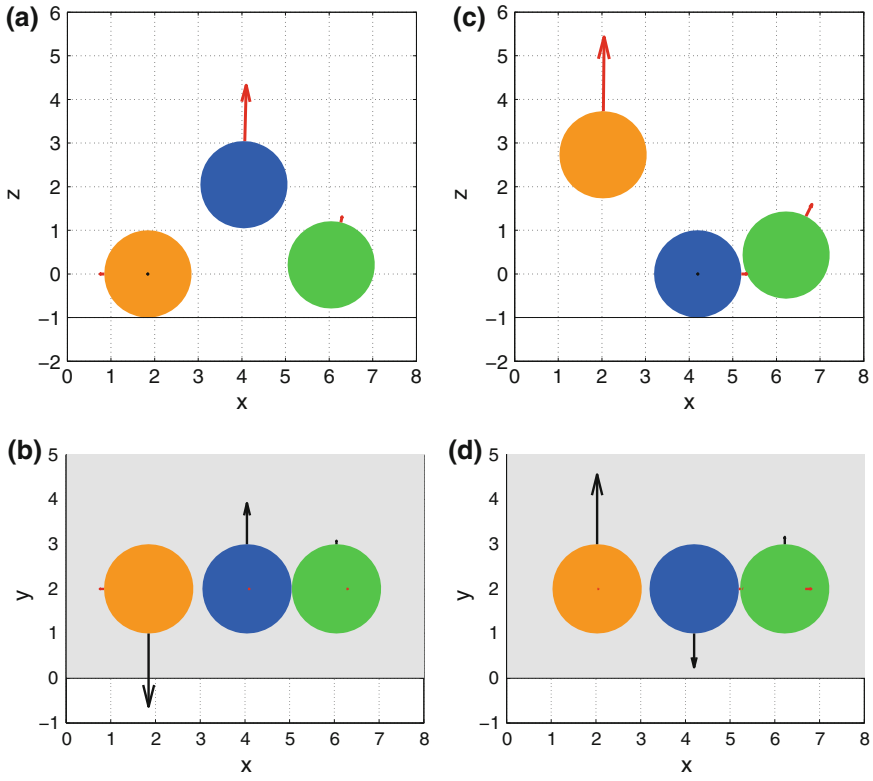

Fig. 5.3 The effect of the angular velocity (position of the balls 0.4 s after collision). $\mathbf{U}_1^- = (0.5, 0, -1)$, $k_{4T} = 0.01$. **a**, **b** $\boldsymbol{\Omega}_1^- = (0, -10, 0)$, ball 1 rotates anti-clockwise and ball 2 jumps as in the carreau effect of the French boule game; **c**, **d** $\boldsymbol{\Omega}_1^- = (0, 10, 0)$, ball 1 rotates clockwise and jumps whereas ball 2 remains in contact with the plane. In both cases ball 3 jumps. **a**, **c** the balls are seen from the side; **b**, **d** the balls are seen from *above*. *Red* (resp. *black*) vector: velocity of ball center of mass (resp. ball angular velocity) scaled by 0.25

5.2.1.1 The Balls Are Aligned

Effect of Tangential Friction Between Balls

The tangential dissipation or friction induces vertical reaction percussions at point A. This results in a jump of the colliding ball (ball 1) and in the gain of angular velocities by the collided balls (balls 2 and 3). In Fig. 5.2 we compare the results obtained with $k_T = 1$ (Fig. 5.2a, b) and $k_T = 0$ (Fig. 5.2c, d), in the hypothesis of initial velocities $\mathbf{U}_1^- = (1, 0, 0)$ and $\boldsymbol{\Omega}_1^- = (0, 1, 0)$ (ball 1 is rolling on the plane). As the picture shows, in case the tangential dissipative or friction coefficient k_T is large, ball 1 jumps, whereas when k_T is 0 it does not jump: this is due to the effect of the angular velocity which intervenes when the tangential coefficient k_T is not 0.

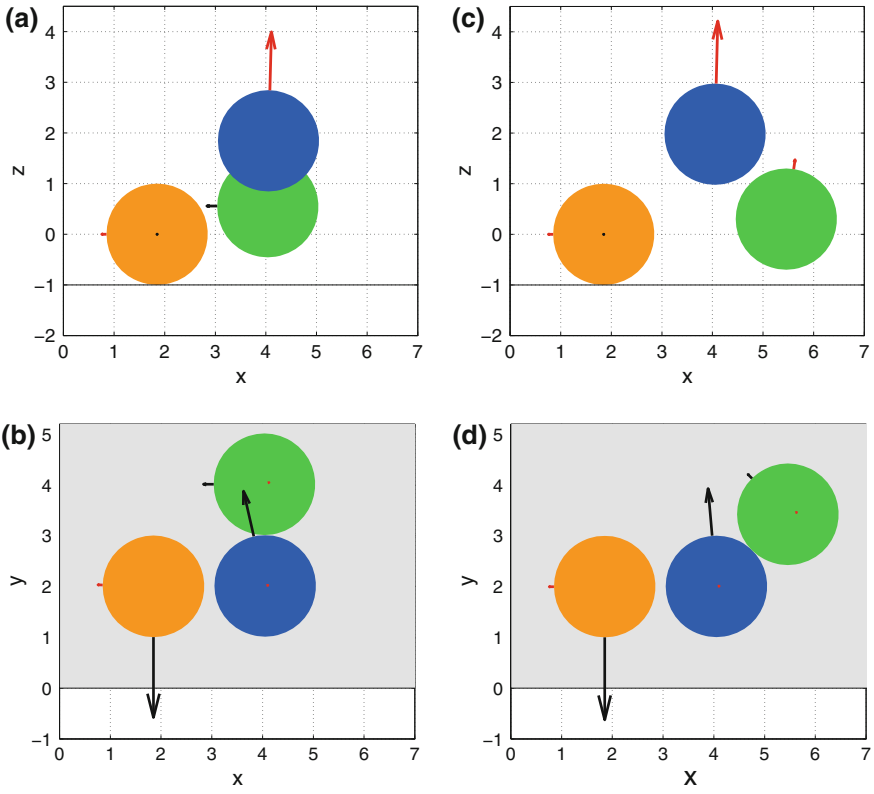

Fig. 5.4 The case of non aligned balls (position of the balls 0.4 s after collision). $\mathbf{U}_1^- = (0.5, 0, -1)$, $\boldsymbol{\Omega}_1^- = (0, -10, 0)$, $k_{4T} = 0.01$. **a**, **b** $\theta = \pi/2$; **c**, **d** $\theta = \pi/4$. The coupled effect of anti-clockwise velocity of ball 1 and friction result in jumps of balls 2 and 3. **a**, **c** the balls are seen from the side; **b**, **d** the balls are seen from *above*. *Red* (resp. *black*) vector: velocity of ball center of mass (resp. ball angular velocity) scaled by 0.25

Effect of the Angular Velocity

Now we investigate what happens if ball 1 is falling on the plane with velocity $\mathbf{U}_1^- = (0.5, 0, -1)$ and we compare what occurs in case ball 1 is simultaneously rotating anti-clockwise ($\boldsymbol{\Omega}_1^- = (0, -10, 0)$) or clockwise ($\boldsymbol{\Omega}_1^- = (0, 10, 0)$). In the first case (Fig. 5.3a, b), after collision ball 1 still rotates anti-clockwise and it remains in contact with the plane, whereas ball 2 jumps. This behavior may be found in the french boule game: the effect of the pre-collision anti-clockwise angular velocity is called the *carreau effect* (*fermo* in Italian) [5]. In the second case (Fig. 5.3c, d), after collision ball 1 rotates clockwise and jumps, whereas ball 2 remains in contact with the plane. Ball 3 jumps in both cases. We are assuming $k_{4T} = 0.01$.

5.2.1.2 The Balls Are Not Aligned

In Fig. 5.4 we consider again $\mathbf{U}_1^- = (0.5, 0, -1)$, $\boldsymbol{\Omega}_1^- = (0, -10, 0)$, and $k_{4T} = 0.01$, but we look at the case of non aligned balls: $\theta = \pi/2$ (Fig. 5.4a, b) and $\theta = \pi/4$ (Fig. 5.4c, d). As the picture shows, the carreau effect is present and the coupling of anti-clockwise angular velocity of ball 1 and friction at contact points makes balls 2 and 3 rotate and jump.

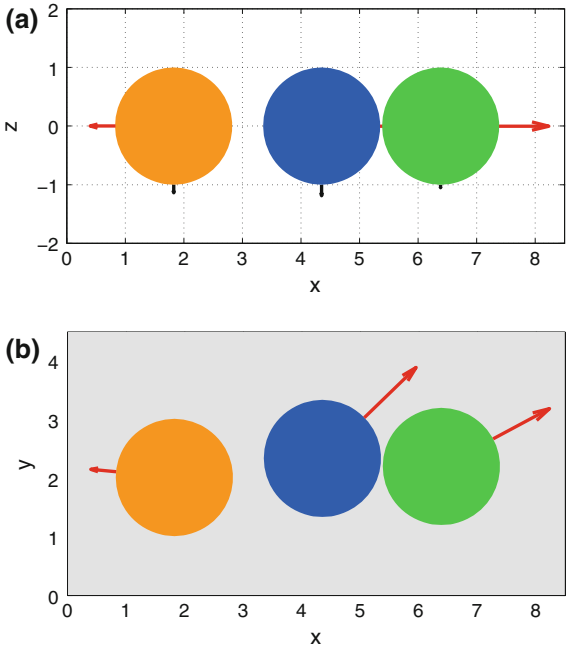

Fig. 5.5 The case of $\mathbf{U}_1^-$ not parallel to $\mathbf{O_1O_2}$ (position of the balls 0.4 s after collision). $\mathbf{U}_1^- = (\sqrt{2}, \sqrt{2}, 0)$, $\theta = 0$, $k_{4T} = 0$, $\boldsymbol{\Omega}_1^- = (0, 0, 0)$. Balls 2 and 3 are pushed by ball 1 and they rotate slightly. **a** the balls are seen from the side; **b** the balls are seen from *above*. *Red* (resp. *black*) vector: velocity of ball center of mass (resp. ball angular velocity)

5.2.1.3 Velocity $\mathbf{U}_1^-$ is not Parallel to $\mathbf{O_1O_2}$

The predictive theory gives realistic behavior also when velocity $\mathbf{U}_1^-$ is not parallel to $\mathbf{O_1O_2}$. Figure 5.5 shows the case $\mathbf{U}_1^- = (\sqrt{2}, \sqrt{2}, 0)$ (for $\theta = 0$, $k_{4T} = 0$, $\boldsymbol{\Omega}_1^- = (0, 0, 0)$): balls 2 and 3 are pushed by incoming ball 1 and due to tangential friction they rotate slightly.

5.3 Three Balls Evolving in a Box

In this section we take into account the presence of two rigid walls, i.e. we add two other constraints to the three-dimensional space the balls are evolving in (Figs. 5.6 and 5.7). One wall is parallel to the plane $\mathbf{e}_1\mathbf{e}_3$ and the other wall is parallel to the plane $\mathbf{e}_2\mathbf{e}_3$. They are denoted $wall_1$ and $wall_2$, respectively. At collision time ball 3 is in contact with $wall_1$ at point F and with $wall_2$ at point G. The vectors $\mathbf{N}_5 = \mathbf{e_1}$ and $\mathbf{N}_6 = \mathbf{e_2}$ are the normal vectors to $wall_1$ and $wall_2$, respectively. The walls are assumed to be very massive, thus remaining immobile. We notice that, from the point of view of collisions, the walls play exactly the same role as the plane.

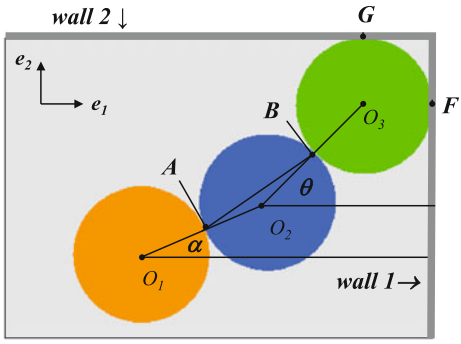

Fig. 5.6 The system at collision time in presence of walls (top view)

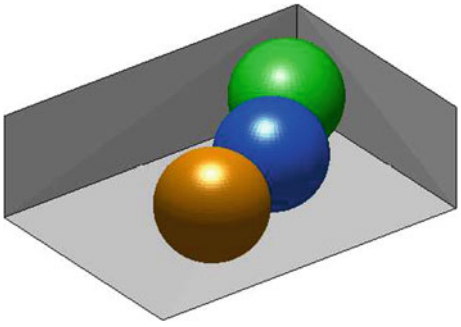

Fig. 5.7 The system at collision time in presence of walls (3D view)

We introduce two new velocities of deformation: the velocities of ball 3 with respect to the walls, that is,

$$\mathbf{D}_{35}(\mathbf{V},\boldsymbol{\omega}) = \mathbf{V}_3(F)\,, \quad \mathbf{D}_{36}(\mathbf{V},\boldsymbol{\omega}) = \mathbf{V}_3(G)\,, \tag{5.4}$$

depending on the virtual velocities $\mathbf{V}$ and $\boldsymbol{\omega}$. They in turn introduce the two internal percussions $\mathbf{P}_{35}$ and $\mathbf{P}_{36}$ applied at contact points F and G, respectively.

The equations of motion become

$$\begin{aligned}
m\,[\mathbf{U}_1(O_1)] &= -\mathbf{P}_{12} - \mathbf{P}_{14} - 2M\mathbf{BA}\,,\\
m\,[\mathbf{U}_2(O_2)] &= \mathbf{P}_{12} - \mathbf{P}_{23} - \mathbf{P}_{24}\,,\\
m\,[\mathbf{U}_3(O_3)] &= \mathbf{P}_{23} - \mathbf{P}_{34} - \mathbf{P}_{35} - \mathbf{P}_{36} + 2M\mathbf{BA}\,,\\
I\left[\boldsymbol{\Omega}^1\right] &= -\mathbf{O_1A}\times\mathbf{P}_{12} - \mathbf{O_1C}\times\mathbf{P}_{14} - 2M\mathbf{O_1A}\times\mathbf{BA} - \mathbf{C}_{12} + \mathbf{C}_{31}\,,\\
I\left[\boldsymbol{\Omega}^2\right] &= \mathbf{O_2A}\times\mathbf{P}_{12} - \mathbf{O_2B}\times\mathbf{P}_{23} - \mathbf{O_2D}\times\mathbf{P}_{24} + \mathbf{C}_{12} - \mathbf{C}_{23}\,,\\
I\left[\boldsymbol{\Omega}^3\right] &= \mathbf{O_3B}\times\mathbf{P}_{23} - \mathbf{O_3E}\times\mathbf{P}_{34} - \mathbf{O_3F}\times\mathbf{P}_{35} - \mathbf{O_3G}\times\mathbf{P}_{36}\\
&\quad + 2M\mathbf{O_3B}\times\mathbf{BA} - \mathbf{C}_{31} + \mathbf{C}_{23}\,.
\end{aligned} \tag{5.5}$$

The following simple constitutive laws are considered

$$\mathbf{P}_{35} = k_5\mathbf{D}_{35}(\mathbf{U}^{\pm},\boldsymbol{\Omega}^{\pm}) + \mathbf{R}_{35}^{reac}\,,$$

$$\mathbf{R}_{35}^{reac} = R_{35}^{reac}\mathbf{N}_5, \quad R_{35}^{reac} \in \partial I\_(\mathbf{D}_{35}(\mathbf{U}^{+},\boldsymbol{\Omega}^{+})\cdot\mathbf{N}_5) = \partial I\_(\mathbf{U}_3^{+}(F)\cdot\mathbf{N}_5), \tag{5.6}$$

$$\mathbf{P}_{36} = k_6\mathbf{D}_{36}(\mathbf{U}^{\pm},\boldsymbol{\Omega}^{\pm}) + \mathbf{R}_{36}^{reac}\,,$$

$$\mathbf{R}_{36}^{reac} = R_{36}^{reac}\mathbf{N}_6, \quad R_{36}^{reac} \in \partial I\_(\mathbf{D}_{36}(\mathbf{U}^{+},\boldsymbol{\Omega}^{+})\cdot\mathbf{N}_6) = \partial I\_(\mathbf{U}_3^{+}(G)\cdot\mathbf{N}_6). \tag{5.7}$$

where $\mathbf{R}_{35}^{reac}$ and $\mathbf{R}_{36}^{reac}$ are impenetrability reactions and the parameters k_5 and k_6 are positive dissipative parameter. The indicator function $I\_$ takes into account the impenetrability of ball 3 and the walls, $\mathbf{U}_3^{+}(F)\cdot\mathbf{N}_5 \le 0$ and $\mathbf{U}_3^{+}(G)\cdot\mathbf{N}_6 \le 0$.

The equations for the 18 unknowns (the velocities $\mathbf{U}_i^{+}(O_i)$ and the angular velocities $\boldsymbol{\Omega}_i^{+}$) result combining equations of motion and constitutive laws. Again, there is one and only one solution which may be computed by solving linear systems and checking the results. The number of contact status is 2^7. The solution is obtained with at most 2^7 linear systems resolutions. In practice much less because it is possible to guess the status of some contacts.

Remark 5.2 The value of parameters k_5 and k_6 may be measured through simple experiments of collisions of a ball with a wall.

It is left as an exercise to the interested Reader the generalization of the present theory to different settings, such as the one depicted in Fig. 5.8. As the picture shows, in such case, ball 2 and ball 1 are in contact with a wall, say $wall_3$ (with unit normal $\mathbf{N}_7 = -\mathbf{e}_2$ and dissipative parameter k_7), respectively at points H and I. Ball 3 is in contact only with $wall_1$ at point F. We have a total of eight contact points. The

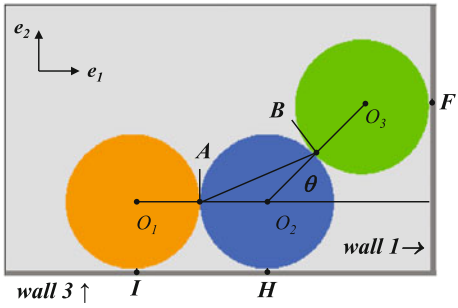

Fig. 5.8 The system at collision time in presence of walls (top view), alternative setting

angle α is zero; should it be lower than zero, the contact point would be seven (i.e., no contact point I).

The present theory for collisions, combined with the well-known theory for smooth evolutions and with a collision-detection algorithm, can be used to simulate, for instance, the billiard game. As already said, the present theory has been source of inspiration in crowd movement modeling for pedestrians who hold hands [6] (see also Chap. 6). In case of granular material modelling, where thousands of particles interact, the mechanical ideas presented here can still be applied, however computational aspects demand for special treatments [1, 7]. In that case, homogenization techniques are also appealing [4].

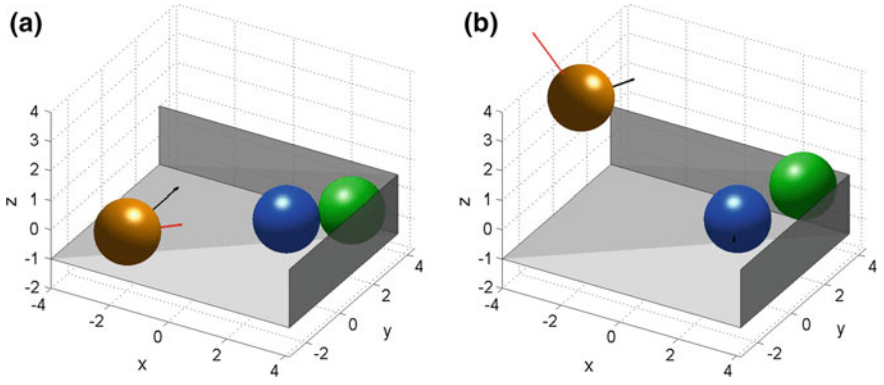

Fig. 5.9 An example relevant to the system with walls (Fig. 5.6), with $\alpha = \pi/6$, $\theta = \pi/4$. $\mathbf{U}_1^- = (2\sqrt{2}, 2\sqrt{2}, 0)$, $\boldsymbol{\Omega}_1^- = (0, 8, 0)$. **a** The system 0.7 s before collision and **b** 0.7 s after collision. *Red* (resp. *black*) vector: velocity of ball center of mass (resp. ball angular velocity), scaled by 1/3

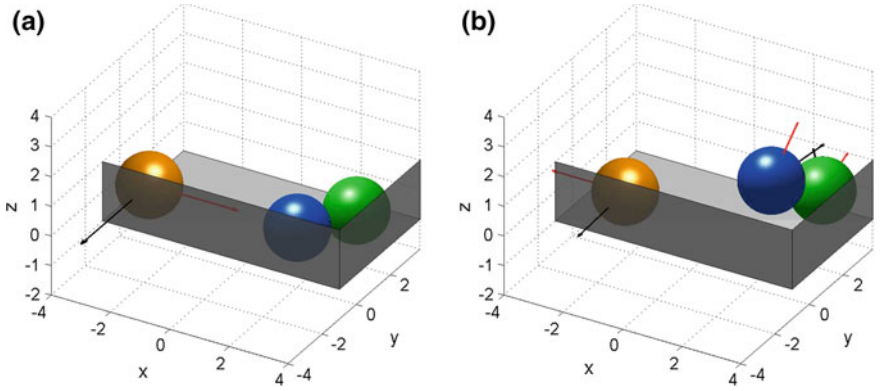

Fig. 5.10 An example relevant to the system with walls in the alternative setting (Fig. 5.8), with $\theta = \pi/3$. $\mathbf{U}_1^- = (2, 0, 0)$, $\boldsymbol{\Omega}_1^- = (0, -3, 0)$. **a** The system 1.5 s before collision and **b** 1.5 s after collision. *Red* (resp. *black*) vector: velocity of ball center of mass (resp. ball angular velocity)

5.3.1 Numerical Examples

In this section two numerical examples are reported. The parameter values indicated in Sect. 5.2.1 are assumed, except for $k_T = 10$ and $k_{4T} = 0.01$. In addition, $k_{5N} = k_{6N} = k_{7N} = 1$ and $k_{5T} = k_{6T} = k_{7T} = 0.01$.

The first example is relevant to the geometric setting in Figs. 5.6 and 5.7, with $\alpha = \pi/6, \theta = \pi/4$. The velocities of ball 1 before collision are $\mathbf{U}_1^- = (2\sqrt{2}, 2\sqrt{2}, 0)$, $\boldsymbol{\Omega}_1^- = (0, 8, 0)$. Figure 5.9a, b show the system 0.7 s before and 0.7 s after collision, respectively. As can be noticed, ball 1 and ball 3 jump after collision.

The second example is relevant to the geometric setting in Fig. 5.8, with $\theta = \pi/3$. The velocities of ball 1 before collision are $\mathbf{U}_1^- = (2, 0, 0)$, $\boldsymbol{\Omega}_1^- = (0, -3, 0)$. Figure 5.10a, b show the system 1.5 s before and 1.5 s after collision, respectively. As can be noticed, ball 2 and ball 3 jump after collision, while ball 1 goes back along $-x$.

Additional examples, inspired by the carambola game, can be visualized at http://dicii.uniroma2.it/?PG=25.26.73 or http://extras.springer.com. They are courtesy of Mrs. Stella Brach.

Acknowledgments The Authors express their sincere gratitude to Dr. Stella Brach for her kind collaboration.

References

1. Alart, P.: 2015, How to overcome indetermination and interpenetration in granular systems via nonsmooth contact dynamics. An exploratory investigation. Comput. Methods Appl. Mech. Eng. **270**, 3756 (2014)
2. Caselli, F., Frémond, M.: Collisions of three balls on a plane. Comput. Mech. **43**(6), 743–754 (2009)

3. Caselli, F., Frémond, M.: Collision of three balls moving on a plane. In: Proceedings of the International Conference on Computational Contact Mechanics, Lecce, Italy, 16–18 september 2009
4. Maury, B.: A time-stepping scheme for inelastic collisions. Numerische Mathematik **102**(4), 649–679 (2006)
5. https://en.wikipedia.org/wiki/P%C3%A9tanque or https://it.wikipedia.org/wiki/P%C3%A9tanque
6. Pécol, P., Argoul, P., Dal Pont, S., Erlicher, S.: A new crowd movement modeling for pedestrians who hold hands. In: Poceedings of the XVIIIth Symposium Vibrations, Chocs et Bruit, ASTELAB. EDF, Clamart, France (2012)
7. Visseq, V., Martin, A., Dureisseix, D., Dubois, F., Alart, P.: Distributed nonsmooth contact domain decomposition (NSCDD): algorithmic structure and scalability. Lect. Notes Comput. Sci. Eng. 01/2014; **98**, 529–536 (2014). doi: 10.1007/978-3-319-05789-7_60

Chapter 6
Pedestrian Trajectories and Collisions in Crowd Motion

Pierre Argoul and Bachar Kabalan

A 2D microscopic approach for crowd movement modeling has been studied and applied for ten years now. This collective research is reported in [3, 9, 10, 53–55, 66, 79–84].

The first idea was to use a granular media flow model based on the collision theory introduced in 1995 by Michel Frémond [31] and described in Chap. 2.

In this model the movement of the granular particles is in a 2D space and the particles, in the initial version, are rigid. Philippe Pécol [79], improved the granular media flow model to manage collisions in the trajectories of pedestrians. He compared the results of his model and other models to experiments in the case of urgent evacuations. The evacuation times given by his model are very satisfactory in the case of emergency.

More recently, Bachar Kabalan [53] addressed three new aspects. The first one concerns pedestrian navigation towards a final destination, the second one consists of managing pedestrian-pedestrian interactions and the last aspect is the validation and verification of the model.

The basis of this model is presented in what follows. Current research tracks are finally introduced but not detailed.

6.1 Definitions—Phenomena of Typical Crowd Self-Organization

A crowd is defined in the dictionary as a multitude of people united in the same location. A group of people in a crowd shares the idea of geographic proximity, but also possesses a collective conscience and intelligence. The thoughts and actions of each member of this group are all oriented toward the same goal, for example, the evacuation of a room. This is the primary characteristic of a crowd, unlike in a group in which varying motivations exist. Furthermore, the overall intelligence of a

M. Frémond, *Collisions Engineering: Theory and Applications*,
Springer Series in Solid and Structural Mechanics 6,
DOI 10.1007/978-3-662-52696-5_6

crowd is generally inferior to that of any one of its members. Reactions are guided by primary emotions (fear, anger, desire, joy) more than by reflective consideration of the circumstances.

Between isolated pedestrians and a dense crowd, other design scenarios include: light to heavy pedestrian traffic, groups of people walking together, parades, religious and political demonstrations, and sporting events such as marathons.

Usually, for relative dense crowds, the number of individuals, the time period of their movements, and the crowd density (people/m^2) are chosen in a way so as to exclude movements during which interaction is non-existent or only present for very short periods of time. In [27], for engineering practice, the authors even precised the definition of a crowd as a large group of individuals ($\geq$100 people) within the same space at the same time, whose movements are for a prolonged period of time ($\geq$60 s), and who is dependent on predominantly local interactions (density $\geq$ 1 people/m^2).

Each individual in a crowd usually behaves according to his or her own motivations, without conforming to a leader's orders or following a pre-established plan (Fig. 6.1a). Nevertheless, the behavior of an individual in a crowd is heavily influenced by that of the other individuals nearby. Although each individual is independent, all are interconnected by a vast network of interactions as illustrated in Fig. 6.1b. All the local interactions between nearby individuals give way to the global dynamic of the system. Such a system possesses emergent properties, i.e. collective behaviors that spontaneously appear on the group scale, without having been explicitly intended by the individuals. Accordingly, the movements of a crowd, as well as many other collective human behaviors (for example, automobile traffic, the spread of a rumor [59], the spread of sickness on networks [69, 74], or the evolution of opinions during an election, [62]), obey certain self-organization processes, several of which are described in the following paragraphs. Self-organization can be defined as the spontaneous emergence of a global structure triggered by local interactions between members of a system. There are four main mechanisms that play a role in self-organized systems, [15]:

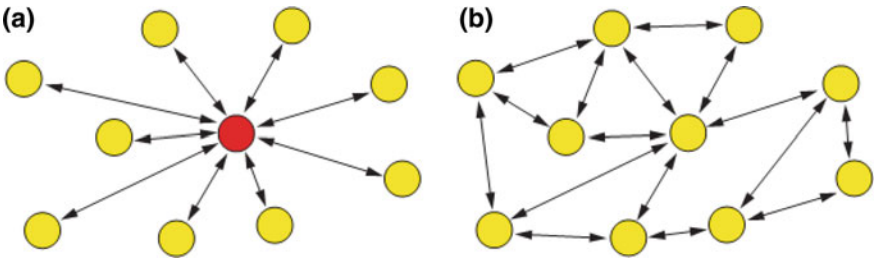

Fig. 6.1 Two systems using **a** a centralized and **b** a decentralized mechanism [70]

- positive feedback or the snow ball effect, [70]: It is when an individual is encouraged to do a certain act since those who surround him are already doing it. Take for example the Mexican wave. It starts with a small group of fans then gets amplified to encompass the whole crowd of a football stadium;
- negative feedback: without this mechanism, positive feedback leads the system to a state of dynamic amplification without control. This mechanism counteracts the amplification effect to bring the system back to a stable state;
- random perturbations: if all members of a system had identical behavior, no positive and negative feedback can occur. Paradoxically, without random perturbations, no self-organization could take place, [44].
- multiple interactions: interaction between two individuals occurs when one acquires new information from another leading the former to modify his/her behavior in light of what he/she had just learned. These interactions can be direct without leaving a trace (visual, audio, or sensory signs) or indirect leaving a trace (trails, chemical deposits,...).

The first studies describing the behaviour of pedestrians walking in a crowd include both qualitative (e.g., the determination of pedestrians' preferences) and quantitative (e.g., the walking speed or walking pace[1] of pedestrians) observations. These observations allow us to list certain behavioral characteristics of pedestrians as well as highlight and describe several phenomena of a crowd's self-organization that occur in certain specific situations. The main goal of these studies was to develop guidelines for planning and designing pedestrian facilities. Before 1995, a number of simulation models have been proposed, e.g. queuing models and models for the route choice behaviour of pedestrians. None of these approaches adequately takes into account the self-organization effects occurring in pedestrian crowds. These may, however, lead to unexpected obstructions due to mutual disturbances of pedestrian flows, [38]. Since then, the different kinds of spatio-temporal collective motion patterns formed by pedestrian crowds due to the sensitive dependence of emerging pedestrian flows on the geometrical shape of pedestrian facilities have been investigated in detail. More recently, Hoogendoorn et al. [49], proposed a theory predicting self-organization, as well as results from experimental research that provide more insight into these dynamic phenomena. This theory of self-organization in pedestrian flow is based on the assumption that each pedestrian aims to minimize his or her predicted disutility of walking. So of all the available options (e.g. accelerating, decelerating, changing direction, doing nothing), a pedestrian tries to choose the one that will yield the smallest predicted disutility. It is referred to the principle of least effort, i.e. an individual will try to adapt to his or her environment or will try to change the environment to suit its needs, whichever is easier. The experimental research performed by these authors provides more insight into these dynamic phenomena as well as exposing other forms of self-organization, i.e. in case of over-saturated

[1]Walking speed or walking pace describe how fast the pedestrian is walking; walking speed is expressed as kilometers per hour and walking pace as minutes per kilometer. For a person with excellent fitness, an approximate moderate walking pace is 9 min per kilometer and the corresponding approximate moderate walking speed is 6.4 km per hour.

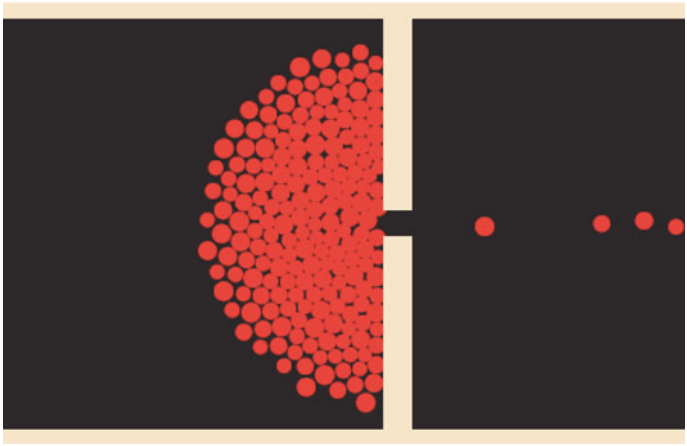

Fig. 6.2 Arch phenomenon in front of a door, based on [39]

bottlenecks or crossing pedestrian flows. The resulting structures are similar to states that occur in granular matter and solids, including their imperfections (voids in granular flow also so-called vacancies[2]). Groups of pedestrians that are homogeneous in terms of desired walking speeds and direction seem to form structures consisting of overlapping layers. This basic pattern forms the basis of other more complex patterns emerging in multi-directional pedestrian flow: in a bi-directional pedestrian flow, dynamic lanes are formed which can be described by the layer structure. Diagonal patterns can be identified in crossing pedestrian flows. In [49], the authors both described these structures and the conditions under which they emerge, as well as the implications for theory and modeling of pedestrian flows.

Self-organization phenomena are macroscopic effects reflecting the pedestrians' microscopic interactions. Some of the frequently observed ones are presented below.

When a pedestrian pathway narrows into a bottleneck, the individuals become more nervous and want to move faster. Individuals will push each other, causing the movement to become less fluid, the crowd denser, and the time necessary to traverse the bottleneck longer. This is the effect of **faster is slower**.

Furthermore, when a dense crowd wants to traverse a narrow space, such as a door, the small space quickly becomes blocked and an arch of people forms around it. This is **the partial blockage and arch phenomenon,** illustrated in Fig. 6.2. In a pedestrian flow at the bottleneck entry, this effect may be caused by inefficient merging behaviour, e.g. due to overly polite or aggressive behaviour. Finally, when the crowd becomes very dense and immobile, the individuals shuffle in place. This is called **the gridlock phenomenon**.

[2] A vacancy in solid-state physics is defined by a lattice position that is vacant because an atom is missing.

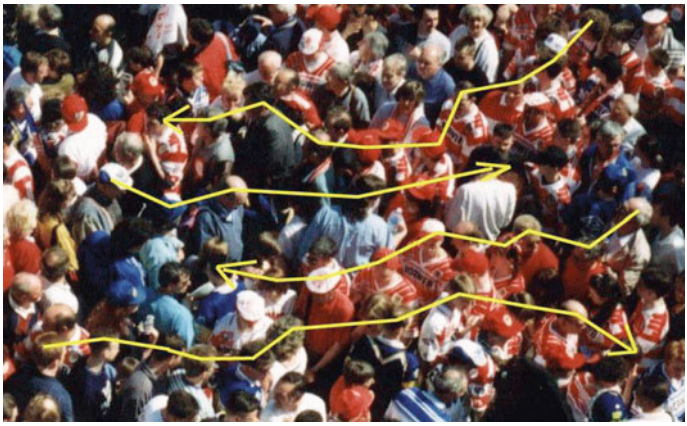

Fig. 6.3 Lane formation in counter flow, based on [97]

Fig. 6.4 Formation of a single file during an evacuation, based on [81]

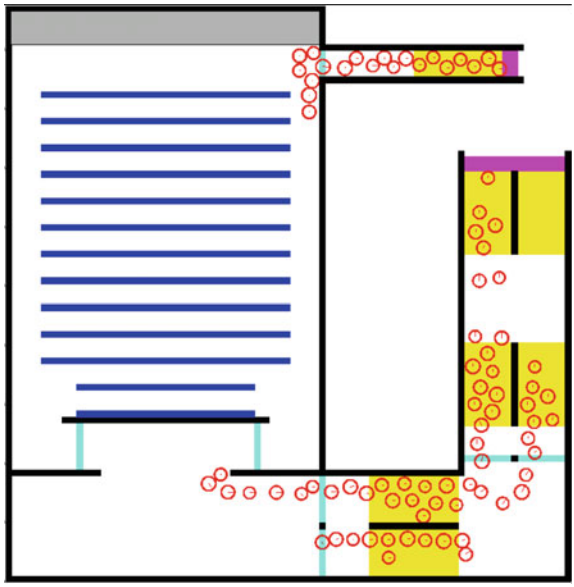

In crowds of pedestrians moving along the same pathway but into opposite directions, lines of uniform walking direction are formed if the pedestrian density exceeds a critical value. These lines of pedestrians walking in a single line[3] are naturally formed. They reduce pedestrian collision while increasing the pedestrians' speed. This phenomenon is in Fig. 6.3, and will be called **lane formation in counter flow.**

[3]Which is sometimes called an "Indian file ", pedestrians walking one behind the other.

In addition, during an evacuation through one exit, the individuals will also arrange themselves one behind the other, **in single file**. This phenomenon is illustrated in Fig. 6.4.

Moreover, if the evacuation exit is traversed simultaneously by two crowds moving in opposite directions, the individuals composing each crowd go through the exit alternately, creating the oscillations. Oscillatory variations of the walking direction develop at narrow passages (corridors, staircases, or doors). The average oscillation frequency increases with growing width and decreasing length of the passage. This phenomenon is illustrated in Fig. 6.5, and will be called **the oscillations phenomenon**. It can be observed by watching the video on the following link (file oscillation.avi are available at https://ifsttar.libcast.com/mast-sdoa or at http://extras.springer.com). In this video, two groups arrive at a constant flow rate from two opposite sides of an opening. Each group want to pass to the other side, giving rise to an oscillation phenomenon around the opening.

Another effect is **corner hugging**, illustrated in Fig. 6.6: when pedestrians turn around an angle or a corner, they slow down and get closer to the corner thus increasing the local density of the crowd.

When individuals are in competition to evacuate a given space, the evacuation becomes ineffective, or individuals behave inappropriately, sometimes even aggressively. We describe this type of behaviour as competitive.

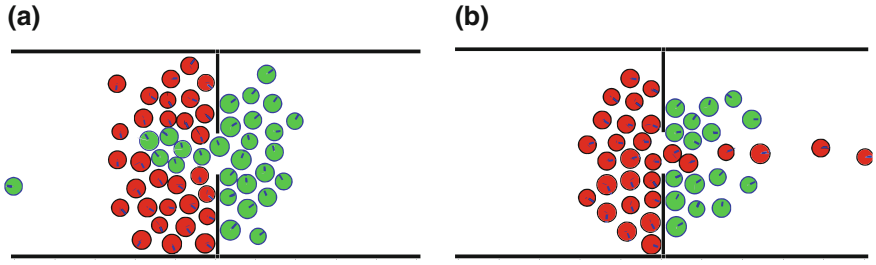

Fig. 6.5 Oscillations phenomenon

Fig. 6.6 Corner hugging based on [97]

6.2 The Current Methods for Modeling Crowd Movement

Due to its complex nature, crowd movement does not lend itself easily to mathematical modeling. The wide variation in walking styles, the unpredictable behaviour of one isolated individual, and the large number of individuals potentially interacting with each other make any rigorous formalization of crowd phenomena difficult.

Despite the complexity of human behaviour, numerous models have been developed in recent years, hoping to accurately simulate crowd behaviours and situations. Crowd movement models are ideally designed to reproduce every behaviour exhibited by pedestrians as well as all the observed phenomena of crowds, in particular those mentioned in the preceding section. Of course, the complexity of behaviors and observed phenomena forces each model to target only one or two specific applications. Modeling of all of these levels of behaviour necessitates a complex and demanding formalization, integrating a large number of cognitive processes such as perception, motor control, individual motivations, memory, capacity for reason, etc. In [27], the authors compared a large number (27) of crowd motion models of the last decades, thereby providing an overview of the current literature on crowd motion models of that time. Moreover, this type of models could provide interesting research tools for other domains such as artificial intelligence, experimental psychology and cognitive neuroscience; though the aims of these various fields differ and lie outside this work's area of application.

Crowd movement models in comparison with those of the flow of granular media have certain **specific features** of which the two main ones are: pedestrian scheduling and route choice, and pedestrian-pedestrian interaction.

Pedestrian Scheduling and Route Choice

Some of the most interesting and challenging theoretical and practical problems in describing pedestrians behaviour are route choice and activity scheduling. Specific terms must be first defined in order to clarify how they will be employed in this work. According to [12], a $route$ is a chain of consecutive nodes joined by links, connecting the origin, the intermediate destinations, and the final destination. This definition can be applied to discrete networks that are made up of links and nodes. However, pedestrians usually move freely in their environment choosing a route from an infinite set of alternatives without being restricted to certain lanes or nodes. In this case, a route is the trajectory of a pedestrian that started at an origin and ended at a destination. Compared to other modes of transportation, a characteristic feature of pedestrian route choice is that the trajectories are continuous in time and space. Since a pedestrian chooses a route from an infinite set of alternatives, appropriate theories and models describing the pedestrian route choice are required. A $trajectory$ is the graphical representation of the motion of an object, in our case an individual. A pedestrian's trajectory is usually obtained by saving his coordinates at each time step and finally connecting all the points (see Fig. 6.7). A *shy away distance* is the minimum distance that pedestrians keep with different elements of

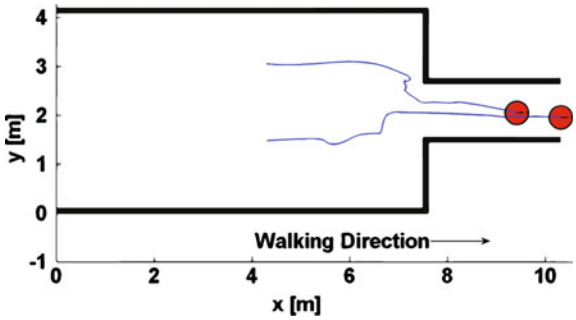

Fig. 6.7 Pedestrian trajectories in the case of a bottleneck

the surrounding environment (walls, obstacles, other pedestrians...). This distance depends on obstacle characteristics and the available space for pedestrians [23].

Pedestrian activity scheduling pertains to which, in which order, and where pedestrians perform activities. Pedestrian activity scheduling has not been studied comprehensively in the past. There are some indications that pedestrians somehow optimize the order in which they perform their activities, and that directness plays an important role [48]. Hill [45] has analyzed in 1982 pedestrian strategies for choosing and describing routes. He concluded that, like most walking processes, route selection strategies are largely subconscious. Furthermore, directness is the most prevalent reason for choosing a particular route. Route directness pertains not only to the length of the route, but also to its complexity (in terms of direction changes). Pedestrians appear to frequently choose the shortest route, though they are seldom aware that they have chosen to minimize distance as a primary strategy in route choice ([34, 92]). Observations carried out in Jerusalem by Guy [34], showed a strong tendency, by about two thirds of the subjects, toward the shortest distance route. Other studies indicated that besides distance, pleasantness is an important route attribute. The two attributes together produce a high correlation with the route preferences [12]. Other factors deemed important in route choice behaviour are habit, number of crossings, pollution and noise levels, safety and shelter from poor weather conditions, and stimulation of the environment. The extent to which these route attributes play a substantial role in his/her route choice behaviour depends greatly on trip purpose [12], e.g. scenery is very important for recreational trips, but it plays no role for work-related walking trips. Cheung and Lam [16] study pedestrians choosing between escalators and stairways in subway stations and its dependency on the differences in travel times. The authors showed that pedestrians are more susceptible to delays in the descending direction than in the ascending direction, and are more inclined to use the escalator in the latter case.

Given the complexity of the pedestrian route choice problem, it was necessary to divide it into sub problems. This has been done by creating different levels of route choice, identifying pedestrian behaviors in each one and finally modeling them.

Two main approaches for classifying route choice behaviour can be found in literature. In the first approach [23], pedestrian behaviour is classified into three categories : (i) the strategic level, which encompasses decisions an individual makes concerning general organization of his or her activities, such as first going to buy a train ticket and then going to buy a magazine [100]; (ii) the tactical level, which entails the integration of local topology and trip planning so as to complete all planned activities along the way [23, 47]; and finally (iii) the operational level, which concerns the short-term movements of the pedestrian and his or her interactions with the individuals who cross his or her path [37, 72, 101]. In the second approach, pedestrian behaviour is classified based on navigation as a function of distance. According to [35], three spatial scales exist for pedestrian navigation: (i) long range ($10 \sim 200$ m), (ii) medium range ($5 \sim 50$ m), and (iii) short range ($1 \sim 10$ m).

The two approaches are very similar where the main difference is in the used notations. The first approach was used by Hoogendoorn [46, 47] to develop the normative pedestrian behaviour theory and is much more widespread in the literature. For this reason, it will be developed below. However, the second approach seems to us to be much simpler and easier to be conveyed and has been chosen in [53].

The Strategic Level

In most models, a pedestrian's behaviour is influenced strictly by his/her surroundings or his/her local environment. In reality, people decide on which activities they want to perform and in what order even before entering a certain facility. Therefore they compute a preliminary path that will allow them to accomplish their objectives. For example, before arriving to a train station, a passenger might have already decided to first buy the ticket, then buy a newspaper and finally head to the platform. If the passenger is familiar with the environment, he/she would have already planned his route. If not, he/she can consult the train station's plan. In [50], it is considered that this process takes place at a strategic level.

The Tactical Level

At the strategic level, a preliminary path is planned that passes by the chosen intermediary and final destinations. In the tactical level, at each decision point (intermediate destination) everything that was chosen at the strategical level is reexamined according to local conditions and circumstances such as weather, topology, traffic, etc. At this level, pedestrians might cancel certain activities and change their route. A traveler who risks missing his/her train would cancel all activities and head directly to the platform. To model this behaviour, an algorithm should be capable of organizing the activities to be done (obligatory or optional), localizing the areas where they can be accomplished (familiar with the environment or not), and computing the corresponding route.

The operational level

At the operational level, pedestrians interact with their surroundings. Once on the path chosen at the upper levels, an individual interacts with other pedestrians and obstacles that he/she crosses on his/her way. Therefore the pedestrian is forced to deviate from his/her original route. This can be observed by comparing an individual's trajectory with his/her planned path. At this level, a pedestrian decides to walk, wait, or accomplish a task.

Pedestrian-Pedestrian Interaction

Among the different forms of interaction between pedestrians, the act of avoidance stands out as an essential component of the coordination of collective movement. This action constitutes a central element of the majority of pedestrian movement models.

Existing experimental studies allow one to compare predictions from a model with certain observed global characteristics, such as flow intensity, velocity distribution or emerging collective arrangements. However, in these experiments, the lack of control of the observed situation creates a major obstacle for the identification of interaction laws and the validation of underlying hypotheses. In a natural environment, the result of an interaction on a pedestrian's spontaneous behaviour is difficult to quantify, given that the observer neither controls the terms of the interaction nor knows the pedestrian's desired direction, attention level, or comfort velocity.

Several approaches have been developed to take into account avoidance in crowd movement modeling. The first one is based on physics: pedestrians are considered as particles moving according to a set of forces. An attractive force pulls the pedestrians towards their destination and a repulsive one allows them to keep a distance with other pedestrians and obstacles in order to avoid collisions. Force-based models have had great success in the academic world for many years. However, important limitations have then been identified. Indeed, it is hard to objectively evaluate the intensity of the different forces applied on pedestrians. Moreover, those models turned out to be unreliable for fitting experimental data. For instance, collisions are not well simulated: pedestrians tend to rebound against each other like rigid particles, which is of course far away from the observed phenomenon. A radically different approach has been recently developed [71]. It is based on cognitive science: the pedestrian is now considered as a cognitive agent, who is able to gather information from his/her environment through a defined vision field. His/her behaviour is then led by two decisions based on the presence of other pedestrians and obstacles and of course the position of his/her destination point. First, the pedestrian chooses the most direct path to his/her destination, taking into account the possible collisions with obstacles. Second, he/she maintains a minimal security distance to the first obstacle, in order to have enough time for an emergency stop. Thanks to the implementation of these behaviors, the cognitive models seem to be more consistent with empirical data than the force-based models.

The introduction of social physchological forces (repulsive forces) in the proposed model will be only presented here. Different approaches exist and are under study (cf. [53]).

Empirical evidence of the complexity of pedestrian behaviour within a rather dense crowd, as previously mentioned (clustering, lanes and queues), leads us to consider the first important distinction between the different methodological approaches: pedestrians as a flow and pedestrians as a set of individuals or agents.

Thus we distinguish two large categories: the **macroscopic** models and the **microscopic** models. In the first category, the crowd is described with fluid-like properties, giving rise to macroscopic approaches. Macroscopic models describe how density and velocity of the pedestrian flow change over time, using partial differential equations (Navier-Stokes or Boltzmann-like equations). This approach is based on analogies observed at medium and high densities. The second category concerns microscopic models, where collective phenomena will emerge from the complex local interactions between many individuals (self-organizing effects).

In this section, we are interested in pedestrian behaviour on the operational level, such as collision or jostling avoidance. Modelling methods that focus on the operational level can be classified according to various criteria (Table 6.1): the crowd representation, the pedestrians' movement space representation, the pedestrian representation, the pedestrian contact representation, the pedestrian movement representation, the crowd phenomenon targeted for analysis, the type of crowd examined, etc. We have chosen to classify and present the operational level models according to the method of crowd representation.

Table 6.1 Criteria for classifying crowd movement models

Crowd representation	Macroscopic
	Microscopic
Pedestrians' movement space representation	Continuous space
	Discretized space
Contact representation	By using regularization laws
	By solving a local non linear problem
Pedestrian's movement representation	Rules
	Data
	Forces
Phenomenon targeted for analysis	Counterflow lines
	Evacuation
Crowd's type of walking	Normal walking velocity
	Emergency walking

6.2.1 Macroscopic Models

In macroscopic models, pedestrians demonstrate a collective behaviour and the crowd is considered as a single entity. These models can be classified into two sub-categories: regression models and models of fluid dynamics (liquid or gas).

Regression Models

In regression models, the significant pedestrian variables are generally the flow rate and the mean speed. The global movement of the pedestrians is formulated using statistical relations between the different variables of flow and depends upon the studied infrastructure and the specific circumstances of the movement [33, 65]. Different regression models are discussed in [75]. In order to better understand how this type of model functions, we examine the historical approach of service levels, introduced by Fruin [33]. To characterize each place of contact, Fruin develops a gradation of service levels. Each level corresponds to an interval of crowd density at an observed average flow, going from A, for the best, to F, for the worst (Table 6.2).

The characterization of each service level, with regard to the behaviour of the pedestrians, is as follows:

A: Up to this density, each traveler can move at his or her desired speed, since collisions remain unlikely.
B-C: The travelers can still move with relative ease, avoid conflicts and choose their speed.
C-D: Passing other pedestrians becomes more difficult. The small distance separating one person from another causes the pedestrians to reduce their speed.
D-E: This critical zone brings about a slow general speed. The travelers movement becomes irregular, up to the point where movement and other changes of direction are nearly impossible.
E-F: Contact between pedestrians becomes unavoidable, preventing pedestrians from passing each other.

Table 6.2 Levels of service for walking from Fruin [33]

Service levels		Densities		Rate of flow people/min/m
		People/m^2	m^2/people	
A	Free flow	<0.3	>3.2	<23
B	Reasonably free flow	0.3 to 0.4	2.3 to 3.2	23 to 33
C	Stable flow	0.4 to 0.7	1.4 to 2.3	33 to 49
D	Approaching unstable flow	0.7 to 1.1	0.9 to 1.4	49 to 66
E	Unstable flow	1.1 to 2	0.5 to 0.9	66 to 82
F	Forced or breakdown flow	>2	<0.5	Variable

Fluid Dynamics Models

To illustrate fluid dynamics models [6, 9, 13, 51, 52, 87, 88], we have chosen the crowd model of Bodgi [9] as an example, in which pedestrians are represented as an entity by a compressible fluid. This approach is often found in vehicle traffic models. The crowd behaviour is observed at point M given by the coordinates (x, y, z) in an inertial or Galilean frame of reference. The variables used are local and dependent upon both the time t and the position of point M. In [9], the author considers only the spatial coordinate x ($x \in [0\ ;\ L]$ if one considers the longitudinal position of the pedestrians over a footbridge of length L). In this case, the crowd behaviour is similar to that of a compressible liquid governed by the partial derivative equation of the conservation of mass:

$$\frac{\partial \eta}{\partial t} + \frac{\partial}{\partial x}(\eta\, v) = 0 \tag{6.1}$$

where η represents the local density of pedestrians and v their local velocity.

Since there are two unknown variable functions η and v, a second partial differential equation is necessary to complete the system. This equation is generally called the closure equation, and relates the variables η and v. Other fluid dynamics models are presented in [75].

In conclusion, macroscopic models are limited in that they cannot take into account the characteristics of each individual pedestrian, such as his or her position, direction of movement and physical attributes. Furthermore, if one considers the observation that the majority of individuals in a crowd move in small groups, this type of model is no longer well adapted to reproduce crowd behaviour. On the other hand, these models prove to be useful when the crowd is dense and one is interested in the movement of the crowd as a whole. Because of this, Bodgi [10] succeeded in using an analytical study deduced from her macroscopic model, to determine both the critical number of pedestrians that will trigger synchronization with a particular footbridge, and the displacement of the latter when the combined crowd-structure system reaches a stationary state.

6.2.2 Microscopic Models

In microscopic models, the movement of each individual is represented in space and time. Each individual behaves, makes decisions and interacts with others in a specific way. These models can be classified into five sub-categories: rule-based models, social force models, cellular automata models, discrete choice models, and completely mathematical models.

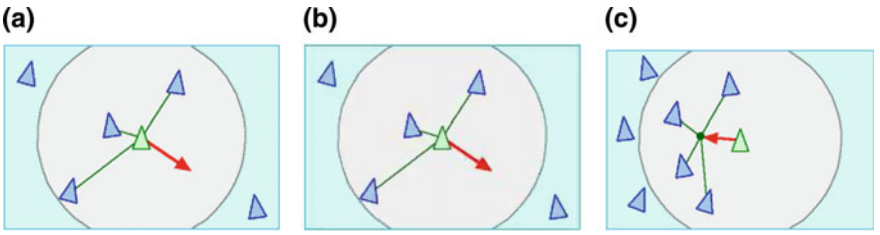

Fig. 6.8 The three rules describing the behaviour of birds [90]: **a** separation, **b** alignment, and **c** cohesion

Rule-Based Models

Rule-based models, introduced by Reynolds [90], draw from the flight patterns of birds in a group in order to model a crowd. For this scenario, three rules describe the behaviour of birds keeping a certain distance from each other (Fig. 6.8): (i) separation: the birds do not collide; (ii) alignment: the birds attempt to maintain a common direction and speed; and (iii) cohesion: the birds try to remain united. The first rule, consisting in the avoidance of collision between birds (or pedestrians), has the consequence of allotting no importance to each individual's shape or form.

Social Force Models

The social force model [4, 36, 37, 39, 40, 60, 72, 76–78, 85], developed principally by Helbing, allows one to control the movement of each pedestrian by the use of three forces: acceleration, repulsion and (optionally) attraction (Fig. 6.9). In this model, a disc represents the pedestrian. If a pedestrian's motion is not disturbed, the driving force of acceleration allows him or her to move toward his or her desired destination, with the acceleration oriented at every instant toward this target.

The introduction of repulsive forces is inspired from a granular approach [21]. Each pedestrian has a specific mass and direction, and a particular manner of walking he or she adopts depending on the surrounding environment (obstacles and other pedestrians). Because there is no spatial discretization in the zone of movement, the pedestrian can move continuously in a 2D environment.

This model is predominately used to simulate evacuation situations. Though it holds the advantage of a low complexity, it is not adaptable to situations of high-density crowds. In these scenarios, the pedestrians in the model oscillate in place due to the repulsive distance-creating force [85].

Cellular Automata Models

In cellular automata models, the 2D movement zone of the pedestrians is discretized [8, 56, 57, 96, 103–105]. A uniform grid of cells contains inaccessible cells (obstacles), occupied cells (pedestrians), and empty cells (Fig. 6.10). At each time step, the pedestrians shift into a neighboring cell according to certain rules. There are two ways of moving pedestrians at each time step. In one way, the pedestrians move in turn (individual by individual) in a random manner. The model thus

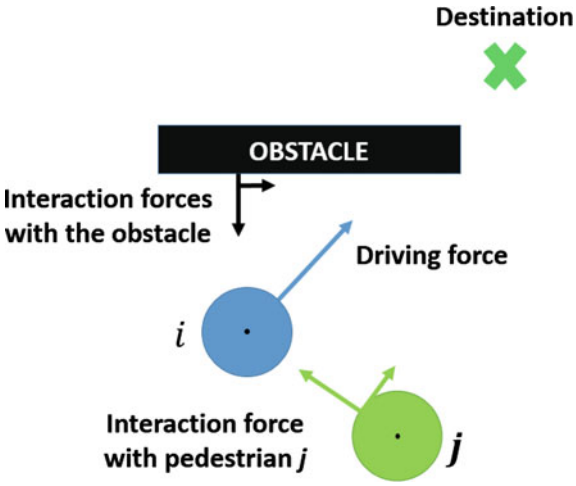

Fig. 6.9 Social forces acting on pedestrian i. The plotted forces are: **the driving force of acceleration** allowing the pedestrian to move in a certain direction with the desired velocity, **the at a distance interaction force** due to pedestrian j, and a similar force due to an obstacle; non plotted are **repulsive forces** allowing to avoid certain pedestrians or obstacles and attractive forces allowing to approach certain objects or people. The introduction of last forces allows to introduce more realistic behaviours in the crowd movement [37]

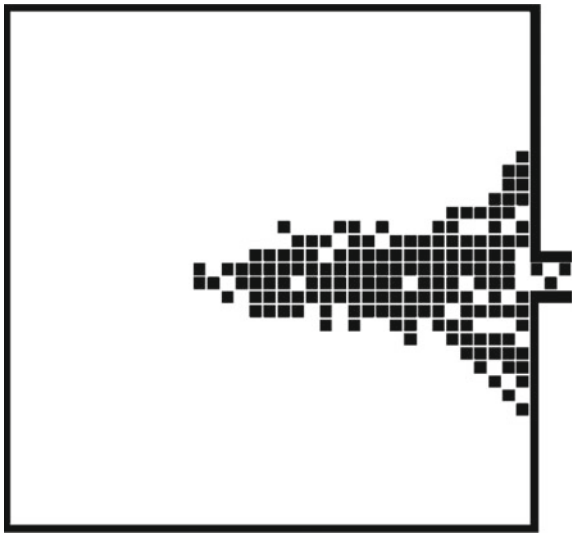

Fig. 6.10 Example of a simulation of a room evacuation performed with a cellular automata model [96]

intrinsically controls for contact, since a pedestrian cannot move into an occupied cell. In the other, the positions of the pedestrians are updated globally (at the same time), and a random choice is made if two pedestrians wish to move into the same cell. One advantage of cellular automata models is their capacity to create simulations in broad spaces with a large number of pedestrians, due to the reduced time needed to calculate the simulations. Their largest inconvenience is their lack of realism: pedestrian movement is constrained by the grid and contact between pedestrians is not directly controlled.

Completely Mathematical Models

In Venel's mathematical model of crowd movement [10], the pedestrians are represented by discs, move with their own directions and speeds, and are able to sidestep each other and obstacles. Contact between individuals is controlled by a geometrical constraint that prevents the overlapping of two pedestrians. The velocity of a pedestrian is computed by placing the spontaneous velocity within the set of admissible velocities (i.e., the velocities that do not violate the non-overlapping constraint). A desired velocity, updated at every instant, allows the pedestrians to go in the shortest direction to reach their destination. This simulation draws from a model of granular interactions, in which contacts between grains are inelastic collisions. The mathematical model is well adapted for dense crowds in evacuation situations.

6.3 The Proposed 2D Discrete Model

The non-smooth approach proposed by Frémond [24, 25, 31, 32] that has mainly been applied to the movement of granular media, has already been proven successful in managing collisions between rigid particles. This original approach was selected to treat the contact and to control the type of collisions among particles. It is based on the theory of collisions of rigid bodies, first proposed by Frémond [31, 32] in a rigorous thermodynamic framework, accounting for the dissipative aspects of collisions, see Chaps. 2–5. The description of the behaviour of a collection of discrete bodies is based on the consideration that the system made of the discrete bodies, even if they are rigid, is deformable because their relative distances vary. Frémond introduces the concept of the coefficient of dissipation to handle the rebound and the velocities of particles after each collision. Local interactions between particles are managed by the use of pseudo-potentials of dissipation, [68]. A further kinematic impenetrability condition is introduced to avoid overlapping, see Chaps. 2–5.

Thus our idea was to adapt it so as to represent pedestrians and their strategy of displacement. The developed model will handle local interactions, such as pedestrian-pedestrian and pedestrian-obstacle, in order to reproduce the global and real dynamics of pedestrian traffic. First, to control the crowd movement on the ground in this model, four targets had to be managed: (i) multiple simultaneous collisions, i.e. to detect and to treat each local interaction, such as pedestrian-pedestrian and pedestrian-obstacle; (ii) the desire of each pedestrian to move in a particular direction with a specific speed

at each time; (iii) the possibility to add forces to make the behaviour of the pedestrians more realistic (social forces, subgroup forces, etc.); and (iv) the possibility to study the interaction of the pedestrians with the structure under crossing.

Only the first three targets will be presented in this section. Concerning the pedestrian-structure coupling, a differential equation of Kuramoto [89], allows one to manage the evolution of the pedestrians' phase. This equation will allow the convergence of the instantaneous angular frequency of each pedestrian towards that of the structure under certain conditions. Preliminary results for the Millenium Bridge are given in [83].

Analytical studies are also developed in [9, 10, 79] to determine the critical number of pedestrians among which synchronization may be triggered and the displacement amplitude of the footbridge when the crowd-structure system has reached a stationary state. Pécol [79] performed similar analyses deduced from his microscopic model and both fully coupled approaches are compared in [55]. While both models used an equation of type Kuramoto to model the synchronization of the induced pedestrian force with the bridge's movement, each one adopted a different sensitivity parameter. Bodgi [9] proved mathematically that pedestrians are sensitive to the acceleration of the bridge while Pécol [79] chose Strogatz's approach [98] where pedestrians are sensitive to the displacement amplitude of the bridge.

6.4 Multiple Contacts' Detection

In a discrete 2D crowd movement model, if the particles (pedestrians) are numerous and able to continually move in the studied space, an effective method of detecting contacts and nearby neighbors is necessary. Without such a method, the time needed for calculation would be much too long. In the following, we will consider only particle-particle interactions, since particle-obstacle interactions can be generated analogously.

To detect contacts between particles, two stages must be isolated:

- the determination of particle couples susceptible to coming into contact;
- the calculation of the distance between these two particles.

The complexity of this second stage depends upon the form of the modeled particles. Since pedestrians are represented by convex shapes, we will choose the particles to be circular, with a fairly large size. This is for two reasons. First, a disc represents decently well an individual seen from above and is a very simple shape. Second, from a more practical point of view, this shape reduces the calculation cost of the simulations, since it allows one to define in a simple fashion certain notions such as particles normal to each other and the relative distance between two particles. Nonetheless, it would be very much possible to consider other representations.

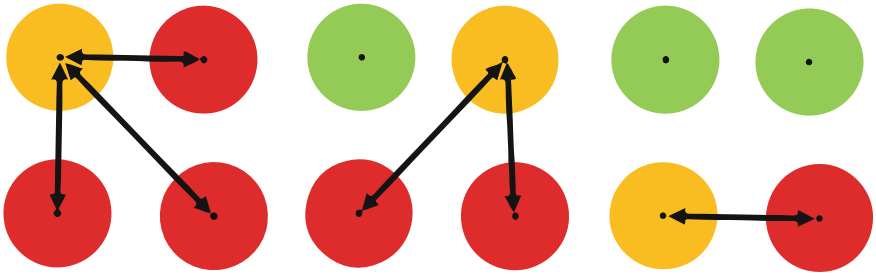

Fig. 6.11 Test of all possible contacts. The particle is *red* when its hasn't been tested yet, *yellow* when it is being tested, and *green* when the possible contacts are found

The relative distance D_{ij} between the particles i and j, in a system of N particles moving in space, is directly defined by:

$$D_{ij}(\mathbf{x}) = |\mathbf{x}_j - \mathbf{x}_i| - (r_i + r_j) \tag{6.2}$$

where r_i is the radius of particle i, and $|\mathbf{x}_j - \mathbf{x}_i| = \sqrt{\left(q_j^x - q_i^x\right)^2 + \left(q_j^y - q_i^y\right)^2}$.

There is a contact between the particles i and j when $D_{ij}(\mathbf{x}) = 0$, and an overlap when $D_{ij}(\mathbf{x}) < 0$.

The first option is to test all the possible contacts (Fig. 6.11). This method is, of course, the most crude and basic. For a system of N particles, it would be necessary to test $\frac{N(N-1)}{2}$ particle couples, an operation number on the order of $O(N^2)$. For example, when the number of considered particles is around or greater than 10^4, it becomes necessary to calculate at least 49995000 distances for each time step of the integration scheme. In terms of calculation time, this would be very costly.

Proposing a method that identifies all of the potential contacts creates a difficulty. This method must be efficient as to not consume the largest part of the calculation time. One can find numerous methods such as Delaunay triangulation [19, 99], Linked Cell Method (LCM) or Manhattan Boxes [30, 102], Verlet Neighbor List (VNL) [2, 73], Linked Linear List (LLL) or Sweep and Prune [73, 86, 91, 102] and robust methods [11, 28, 29, 73], often appearing as extensions of the methods previously cited. Some of these possess parallel versions that allow one to benefit from super-calculators [19]. The different detection algorithms will not be detailed here, even if they are of great interest.

In the following, we will briefly present several methods of contact detection.

Delaunay Triangulation [19, 99]

This method consists in creating a triangular network between the centers of the bodies in the system. This allows one to obtain directly all the edges corresponding to potential contacts (Fig. 6.12). The contacts are then determined by calculating the relative distance between particles in potential contact.

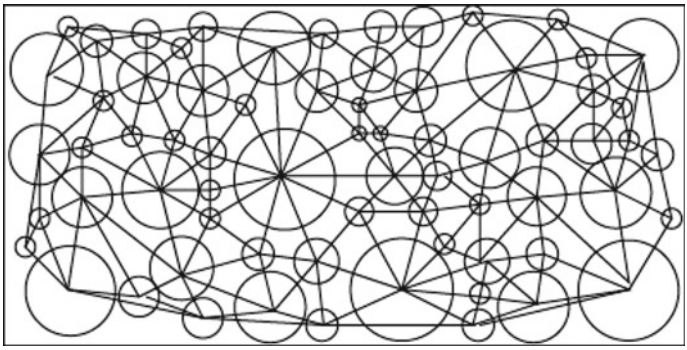

Fig. 6.12 Delaunay triangulation

Linked Cell Method (LCM) or Manhattan Boxes [30, 102]

This method consists in cutting up the particle evolution space into boxes of the same size, as a function of the size of the particles (Fig. 6.13). The particles are then distributed in their corresponding boxes. Contacts between particles, whether of the same box or of adjacent boxes, are determined by calculating the relative distance between these particles. If one follows the route of the boxes, not all the adjacent boxes will need to be covered, since detections between boxes could already have been made. This allows one to limit the number of tests realized. This method is more suitable for systems composed of equivalently sized particles. In an optimal configuration, the number of operations necessary to find the potential contacts is in the order of $O(N)$.

Fig. 6.13 Manhattan boxes [102]

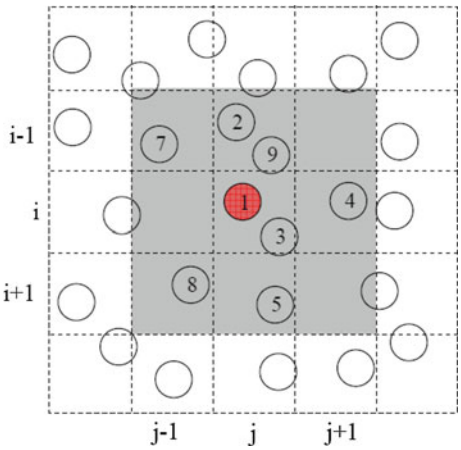

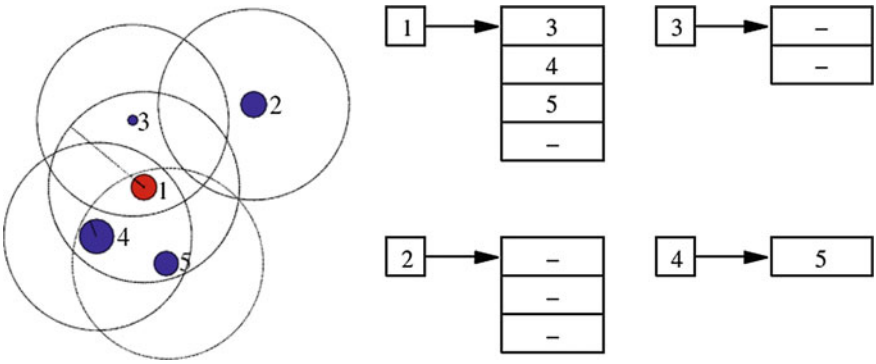

Fig. 6.14 VNL—imaginary circles and storage of particles in lists [73]

Verlet Neighbor List (VNL) [2, 73]

The main idea of this method is to design an imaginary circle around each particle in the system and then create a list of neighboring particles within the circle (Fig. 6.14). The relative distances between the particles are then calculated. The optimal extension of the circular zone around the particles depends on their speed and the density of the total system. Creating the list of neighboring particles necessitates $\frac{N(N-1)}{2}$ calculations, a number of operations of the order $O(N^2)$. This method is thus more suited for quasi-static systems, in which the list does not need to be updated for all time steps. The frequency of updates depends on the density of the system, the velocity of the particles and the radii of the imaginary circles.

Linked Linear List (LLL) or Sweep and Prune [73, 86, 91, 102]

This method plays out in three stages. The first consists in creating rectangular boxes that completely encompass each particle, and which have sides aligned in parallel along an axial system. In the second stage, each box is separately projected onto the axial system. Finally, a potential contact is determined for all boxes whose projections overlap the two axes (Fig. 6.15). This method is difficult to implement. However, in an optimal configuration [102], the number of operations necessary to find the potential contacts is in the order of $O(N)$. This method is well suited for systems composed of differently sized particles.

Finally, the capabilities of these methods are compared in [73, 99]. The methods of Manhattan boxes and Delaunay triangulation demonstrate the best performances. In the model presented below, we have chosen to use Delaunay triangulation.

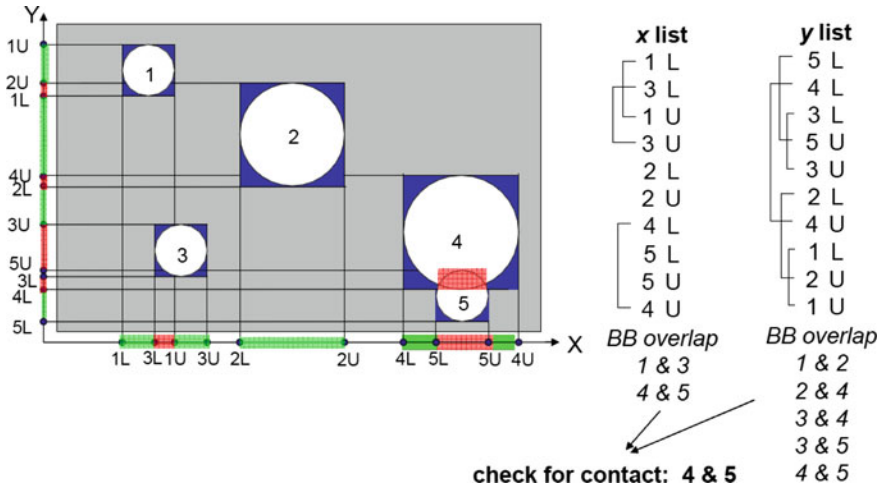

Fig. 6.15 LLL—visualisation of encompassing boxes, their projections onto the axial system, the determination of the overlapping of the projections on the axes, and the determination of potential contacts [102]

6.5 Presentation of Three Approaches to Granular Media

A granular medium is defined as a set of particles subjected to gravity that interact with each other via contact, with or without friction and with or without cohesion. In this section, three approaches generally applied to modelling granular media will be briefly presented and compared. They are denoted by *DEM* (Discrete Element Model), *NSM*1 (Non Smooth Model 1) and *NSM*2 (Non Smooth Model 2).

We assume then that the particles are restricted to moving in a plane, circular with a fairly large size, and with negligible rotation. One can refer to [24] for supplementary research on particles of more complex shapes and to [3, 79] for the full 2D case with rotation.

Let us consider a system of N circular particles moving in a plane. The center position of the ith particle is described by the vector ${}^t\mathbf{x}_i = (q_i^x, q_i^y) \in \mathbb{R}^2$, r_i is its radius, and $\mathbf{U}_i(t) = \frac{d\mathbf{x}_i(t)}{dt}$ is its velocity. When the generalized displacement vector $\mathbf{x}$ of size $2N$, ${}^t\mathbf{x} = ({}^t\mathbf{x}_1, {}^t\mathbf{x}_2, ..., {}^t\mathbf{x}_N)$, is assumed to be a regular function of time, the dynamics equation for each particle can be written as the following differential system

$$\begin{cases} \dot{\mathbf{x}}(t) = \mathbf{U}(t) \\ \mathbf{M}\dot{\mathbf{U}}(t) = \mathbf{f}(t) + \mathbf{g}(t) \end{cases} \tag{6.3}$$

where $\mathbf{M}$ is the $2N \times 2N$ mass matrix of all the particles; $\dot{\mathbf{x}}$ denotes the generalized velocity vector of size $2N$, ${}^t\dot{\mathbf{x}} = ({}^t\dot{\mathbf{x}}_1, {}^t\dot{\mathbf{x}}_2, ..., {}^t\dot{\mathbf{x}}_N)$, ${}^t\mathbf{U} = ({}^t\mathbf{U}_1, {}^t\mathbf{U}_2, ..., {}^t\mathbf{U}_N)$, and $\mathbf{f}$

(resp. $\mathbf{g}$) is the vector of at a distance forces (resp. contact forces) of size $2N$ applied to the system, or ${}^t\mathbf{f} = ({}^t\mathbf{f}_1, {}^t\mathbf{f}_2, ..., {}^t\mathbf{f}_N)$ (resp. ${}^t\mathbf{g} = ({}^t\mathbf{g}_1, {}^t\mathbf{g}_2, ..., {}^t\mathbf{g}_N)$).

Two major steps exist in each of the three approaches: the detection and the treatment (processing) of every contact. We will analyze only particle-particle interactions, since particle-obstacle interactions can be handled analogously.

In the case of circular particles, the detection of contact is straightforward. Let us introduce the unit vector $\mathbf{e}_{ij}$ directed from particle i to particle j by $\mathbf{e}_{ij} = \frac{\mathbf{x}_j - \mathbf{x}_i}{\|\mathbf{x}_j - \mathbf{x}_i\|}$. The distance D_{ij} between two particles i and j can be expressed as:

$$D_{ij}(\mathbf{x}) = \|\mathbf{x}_j - \mathbf{x}_i\| - (r_i + r_j) \tag{6.4}$$

where $\|\mathbf{x}_j - \mathbf{x}_i\| = \sqrt{\left(q_j^x - q_i^x\right)^2 + \left(q_j^y - q_i^y\right)^2}$.

When particles i and j are in contact: $D_{ij}(\mathbf{x}) = 0$ and when they overlap: $D_{ij}(\mathbf{x}) < 0$. If the number of considered particles increases, an efficient method of detection of contacts [28], or closest neighbors becomes necessary to reduce computation time. However, due to the relatively small number of considered particles in the simulations presented in this section, the use of such a method is not necessary in our research.

The next step is to determine the contact force vector $\mathbf{g}(t)$ in order to find $\mathbf{U}(t)$ and $\mathbf{x}(t)$. In *DEM*, the local contact force between two particles i and j is chosen to be proportional to D_{ij}, whereas in *NSM*1, it is defined so that particles never overlap, i.e., there is a constraint on the particles' position. Additionally, in *NSM*2, the local contact force is determined by a constraint on the relative deformation velocity between particles. Differences and similarities in contact treatment (processing) among the three approaches are detailed both analytically and numerically in the following sections. It will be shown that both the discretization of the *NSM*1 and *NSM*2 approaches constitute constrained minimization problems.

6.5.1 Theoretical Aspects of the Three Approaches

DEM

In the smooth approach introduced by Cundall in the seventies [21, 22], contact is treated using regular forces. The expression of the repulsive force applied to particle i, which represents local interaction via contact between particles i and j, is given by:

$$\mathbf{g}_{ij}(t) = k \min\left(0, D_{ij}(\mathbf{x}(t))\right) \mathbf{e}_{ij}(t) \tag{6.5}$$

where k is a stiffness constant. For crowd simulations, $k = 1.2 \times 10^5\,\mathrm{kg\,s^{-2}}$ is chosen by Helbing et al. [39].

The total contact force applied to particle i is thus:

$$\mathbf{g}_i(t) = \sum_{\substack{j=1 \\ j \neq i}}^{N} \mathbf{g}_{ij}(t) \ . \tag{6.6}$$

With this approach, overlapping is required to control the contact. If there is no overlap between particles i and j ($D_{ij}(\mathbf{x}) > 0$), then $\mathbf{g}_{ij} = \mathbf{0}$.

*NSM*1

In this approach [63], contact between circular particles is treated as purely inelastic collisions, i.e., no rebound is considered. Extension of this approach to include other types of collisions (elastic collisions) is not straightforward, as mentioned by [63]. The particles' positions must always be admissible, i.e., there should never be any overlap between particles. At the instant of collision, there is a discontinuity in the velocity $\mathbf{U}$. Hence, the velocity after collision, $\mathbf{U}^+$, is determined such that the position of colliding particles is feasible, i.e., $\mathbf{U}^+$ has a geometric meaning rather than a physical meaning.

The particles velocities after contact, $\mathbf{U}^+$, must belong to the set of admissible velocities defined by:

$$C_{\mathbf{x}} = \left\{ \mathbf{v} \in \mathbb{R}^{2N} : \forall i < j, \ {}^t\mathbf{G}_{ij}(\mathbf{x})\, \mathbf{v} \geq 0 \text{ as soon as } D_{ij}(\mathbf{x}) = 0 \right\} \tag{6.7}$$

$$\begin{aligned} \text{where} \quad {}^t\mathbf{G}_{ij}(\mathbf{x}) &= \nabla D_{ij}(\mathbf{x}) \\ &= \big(0, ..., 0, \underset{\substack{\uparrow \\ \text{particle } i}}{-\,{}^t\mathbf{e}_{ij}}, 0, ..., 0, \underset{\substack{\uparrow \\ \text{particle } j}}{{}^t\mathbf{e}_{ij}}, 0, ..., 0\big) \in \mathbb{R}^{2N} \ . \end{aligned} \tag{6.8}$$

Thus, since overlapping is forbidden by virtue of the condition ${}^t\mathbf{G}_{ij}(\mathbf{x})\, \mathbf{U}^+ \geq 0$, two particles i and j already in contact can only increase or preserve their relative distance. The polar cone $N_{\mathbf{x}}$ of $C_{\mathbf{x}}$ is then introduced [63, 67]:

$$\begin{aligned} N_{\mathbf{x}} &= \left\{ \mathbf{w} \in R^{2N}, \ {}^t\mathbf{w}\, \mathbf{v} \leq 0 \quad \forall \mathbf{v} \in C_{\mathbf{x}} \right\} \\ &= \left\{ -\sum_{i<j} \mu_{ij}\, \mathbf{G}_{ij}(\mathbf{x}), \ \ \mu_{ij} = 0 \text{ if } D_{ij}(\mathbf{x}) > 0, \ \mu_{ij} \in R^+ \text{ if } D_{ij}(\mathbf{x}) = 0 \right\} \ . \end{aligned} \tag{6.9}$$

The system (6.3) is rewritten using a differential inclusion:

$$\begin{cases} \mathbf{M}\ \dot{\mathbf{U}} + N_{\mathbf{x}} \ni \mathbf{f}, \\ \mathbf{U}^+ = P_{C_{\mathbf{x}}}\, \mathbf{U}^-, \end{cases} \tag{6.10}$$

where $P_{C_{\mathbf{x}}}$ is the Euclidean projection onto the closed convex cone $C_{\mathbf{x}}$. A solution of this problem was shown to exist [7, 64].

When there is no contact, the first equation of (6.10) reads as the ordinary differential equation $\mathbf{M}\ \dot{\mathbf{U}} = \mathbf{f}$. When there is a contact, the previous equation can be read as $\exists \mathbf{g} \in -N_{\mathbf{x}}$, such that $\mathbf{M}\ \dot{\mathbf{U}} = \mathbf{f} + \mathbf{g}$, where the expression of the total contact force is $\mathbf{g} = \sum_{1 \leq i < j \leq N} \mu_{ij} \mathbf{G}_{ij}(\mathbf{x})$. The second equation of (6.10) provides the collision model. The velocity after contact $\mathbf{U}^+$ is then defined as the Euclidean projection of the velocity before contact $\mathbf{U}^-$ on the set $C_{\mathbf{x}}$. This approach allows us solve the following constrained minimization problem:

$$\mathbf{U}^+ = \underset{\mathbf{v} \in C_{\mathbf{x}}}{\arg\min} \left[\frac{1}{2} \|\mathbf{v} - \mathbf{U}^-\|^2_{\mathbf{M}} \right] \tag{6.11}$$

where $\|\mathbf{y}\|^2_{\mathbf{M}} = {}^t\mathbf{y}\ \mathbf{M}\ \mathbf{y}$.

NSM2

NSM2 is an original approach based on the theory of the collisions of rigid bodies, first proposed in [31, 32] a rigorous thermodynamic frame highlighting the dissipative character of collisions. The numerical aspects were later developed in [24, 25].

Let us consider the set of N particles as a deformable system composed of N rigid solids. Collisions among particles can be inelastic or elastic. Friction forces can also be considered, [25, 32]. The relative deformation velocity between the ith and jth particles in contact at point $A_{i,j}$ is defined by

$$\boldsymbol{\Delta}_{ij}(\mathbf{U}(t)) = \mathbf{U}_i(G_i) + \boldsymbol{\Omega}_i \wedge \mathbf{G_i}\,\mathbf{A_{i,j}} - \left(\mathbf{U}_j(G_j) + \boldsymbol{\Omega}_j \wedge \mathbf{G_j}\,\mathbf{A_{i,j}}\right) \tag{6.12}$$

where G_i and $\boldsymbol{\Omega}_i$ are the center of mass and the angular velocity of the ith particle, respectively, see Chap. 5. When the rotation of the particles is neglected, the previous Eq. 6.12 becomes:

$$\begin{aligned} \boldsymbol{\Delta}_{ij}(\mathbf{U}(t)) &= \mathbf{U}_i(G_i) - \mathbf{U}_j(G_j) \\ &= \mathbf{U}_i(t) - \mathbf{U}_j(t)\ . \end{aligned} \tag{6.13}$$

The motion equations are written as:

$$\mathbf{M}\ \dot{\mathbf{U}}(t) = -\mathbf{f}^{int}(t) + \mathbf{f}^{ext}(t) \quad \text{almost everywhere} \tag{6.14}$$

$$\mathbf{M}\ \left(\mathbf{U}^+(t) - \mathbf{U}^-(t)\right) = -\mathbf{P}^{int}(t) + \mathbf{P}^{ext}(t) \quad \text{everywhere} \tag{6.15}$$

where $\mathbf{f}^{ext}(t)$ and $\mathbf{f}^{int}(t)$ are respectively the exterior and interior forces vectors of dimension $2N$ applied to the deformable system.

The existence of a solution of the system given by Eqs. (6.14) and (6.15) is proven in [17, 24, 31]. Equation (6.14) describes the smooth evolution of the multi-particle system, whereas Eq. (6.15) describes its non-smooth evolution during a collision. Hence, Eq. (6.14) applies everywhere, except at the instant of the collision, where it is replaced by Eq. (6.15). When contact is detected, velocities of colliding particles are discontinuous. Thus, in Eq. (6.15), the percussions $\mathbf{P}^{int}(t)$ and $\mathbf{P}^{ext}(t)$, interior and exterior to the system, respectively, are introduced, resulting from the variation of the linear momentum for the duration of the collision. By definition, percussions have the dimension of a force multiplied by a time. The $\mathbf{P}^{int}(t)$ percussions are unknown; these percussions take into account the dissipative interactions between two factors: the colliding particles (dissipative percussions) and the reaction forces that permit the avoidance of overlapping among particles (reactive percussions) [31, 32] defined the velocity of deformation at the moment of impact as $\frac{\boldsymbol{\Delta}(\mathbf{U}^+)+\boldsymbol{\Delta}(\mathbf{U}^-)}{2}$ and showed that $\mathbf{P}^{int}$ is defined in duality with $\frac{\boldsymbol{\Delta}(\mathbf{U}^+)+\boldsymbol{\Delta}(\mathbf{U}^-)}{2}$ according to the work of internal forces. He then introduced a pseudo-potential of dissipation Φ that allows us to express $\mathbf{P}^{int}$ as:

$$\mathbf{P}^{int} \in \partial\Phi\left(\frac{\boldsymbol{\Delta}(\mathbf{U}^+) + \boldsymbol{\Delta}(\mathbf{U}^-)}{2}\right) \tag{6.16}$$

where the operator ∂ is the sub-differential that generalizes the derivative for convex functions [32].

The convex function Φ [68] is defined as the sum of two pseudo-potentials: $\Phi = \Phi^d + \Phi^r$, where Φ^d and Φ^r characterize the dissipative and reactive interior percussions respectively. Φ^r allows to define the reactive percussions which ensure the non-interpenetration between particles. It is defined as: $\Phi^r = I_C\left(\frac{{}^t(\Delta(U^+)+\Delta(U^-))N}{2}\right)$ where N is the normal vector to the plane tangent to the contact point between the two particles, I_C is the characteristic function of the set C defined by $\left[\frac{{}^t\Delta(U^-)N}{2}, +\infty\,[\text{or}]\,-\infty, \frac{{}^t\Delta(U^-)N}{2}\right]$, according to the selected sense for the normal vector. The pseudo-potential Φ^d is chosen to be quadratic: $\Phi^d(y) = \frac{K}{2}y^2$, where K is a coefficient of dissipation. This choice allows one to find the classical results when using the coefficient of restitution. Other choices of Φ^d allow one to obtain a large variety of behaviors after impact [17, 32].

With the definition of the interior percussions given by Eq. (6.16), the existence and unicity of the solution of the system given by Eqs. (6.14) and (6.15) is proven in [18, 25, 32].

In Eq. (6.15), the problem becomes determining the velocity $\mathbf{U}^+$ after particle collision. To determine $\mathbf{U}^+$, we have to solve the following constrained minimization problem:

$$\mathbf{X} = \underset{\mathbf{Y}\in\mathbf{R}^{2N}}{\arg\min}\left[{}^t\mathbf{Y}\,\mathbf{M}\,\mathbf{Y} + \Phi(\boldsymbol{\Delta}(\mathbf{Y})) - {}^t(2\mathbf{U}^- + \mathbf{M}^{-1}\mathbf{P}^{ext})\mathbf{M}\;\mathbf{Y}\right] \tag{6.17}$$

where the solution $\mathbf{X} = \frac{\mathbf{U}^+ + \mathbf{U}^-}{2}$.

In this approach, the velocity of a particle after a contact ($\mathbf{U}^+$) has a physical meaning. Proof of the existence and uniqueness of this velocity after the simultaneous collisions of several rigid solids, as well as the dissipativity of the collisions, is presented in [24, 25, 31, 32].

6.5.2 Numerical Aspects of the Three Approaches

The time interval $[0, T]$ is discretized into N_{int} regular intervals $[t^n, t^{n+1}]$ of length $h = \frac{T}{N_{int}}$. Let $\mathbf{x}^0 = \mathbf{x}(0)$ and $\mathbf{U}^0 = \mathbf{U}(0)$ respectively be the initial positions and velocities of the particles. Given $\mathbf{x}^n$ and $\mathbf{U}^n$ at time t^n, we have to find $\mathbf{x}^{n+1}$ and $\mathbf{U}^{n+1}$ at time t^{n+1} for each approach.

For both *NSM*1 and *NSM*2, after making some assumptions, the contact problem can be written with the same formalism as that used in plasticity. The evolution equations of classical elastoplasticity, define a unilaterally constrained problem of evolution. Simo [94] showed that by applying an implicit backward-Euler difference scheme, this continuum problem is transformed into a constrained-optimization problem, governed by discrete Kuhn–Tucker conditions. Thus, this constrained problem of evolution collapses to the iterative solution of a convex mathematical programing problem.

Denoting σ the stress tensor and C the elasticity tensor respectively, the discrete constrained-optimization problem in the case of plasticity can be written as [93]:

$$\sigma^{n+1} = \underset{\sigma}{\arg\min} \left[\frac{1}{2} \|\sigma - \sigma_{predicted}\|^2_{\boldsymbol{C}^{-1}} + \Delta\lambda f(\sigma) \right] \quad \text{with } \sigma_{predicted} = \sigma^n + \mathsf{C} : \Delta\boldsymbol{\varepsilon} \tag{6.18}$$

where C^{-1} is the compliance tensor, $\|\mathsf{X}\|^2_{\mathsf{C}^{-1}} = {}^t\mathsf{X} : \mathsf{C}^{-1} : \mathsf{X}$ is the energy norm and X is a stress tensor, $\Delta\boldsymbol{\varepsilon} = \boldsymbol{\varepsilon}^{n+1} - \boldsymbol{\varepsilon}^n$ is the total strain increment, $\Delta\lambda$ is the plasticity multiplier, $f(\sigma)$ is the elastic domain, and $\Delta\lambda$ and σ satisfy the inequalities:

$$\begin{cases} f(\sigma^{n+1}) \leq 0 \\ \Delta\lambda \geq 0 \\ \Delta\lambda f(\sigma^{n+1}) = 0 \,. \end{cases} \tag{6.19}$$

In other words, the minimization problems obtained with *NSM*1 and *NSM*2 can also be solved using the well-known algorithms proposed, for example, in [93].

DEM

The positions and velocities of particles at time t^{n+1} are given by the explicit scheme:

$$\begin{cases} \mathbf{U}^{n+1} = \mathbf{U}^n + h\mathbf{M}^{-1}(\mathbf{f}^n + \mathbf{g}^n) \\ \mathbf{x}^{n+1} = \mathbf{x}^n + h\mathbf{U}^{n+1} \end{cases} \tag{6.20}$$

where $\mathbf{f}^n$ is the vector of at a distance forces and $\mathbf{g}^n$ is the vector of contact forces at time t^n (Eq. (6.3)). Based on Eqs. (6.5) and (6.6), the contact force applied to the particle i at time t^n is given by:

$$\mathbf{g}_i^n = \sum_{\substack{j=1 \\ j \neq i}}^{N} k \min(0, D_{ij}(\mathbf{x}^n)) \mathbf{e}_{ij}^n \, . \tag{6.21}$$

The overlap and stability of the time integration scheme depend on the chosen time step denoted by h [21, 81, 84]. The choice of this parameter is thus essential.

NSM1

The positions of particles at time t^{n+1} are obtained by the iterative equation:

$$\mathbf{x}^{n+1} = \mathbf{x}^n + h\mathbf{U}^{n+1} \tag{6.22}$$

where $\mathbf{U}^{n+1}$ needs to be found such that $D_{ij}(\mathbf{x}^{n+1}) \geq 0$.

As D_{ij} is convex, the following relationship can be established:

$$D_{ij}(\mathbf{x}^{n+1}) = D_{ij}(\mathbf{x}^n + h\mathbf{U}^{n+1}) \geq D_{ij}(\mathbf{x}^n) + h^t \mathbf{G}_{ij}(\mathbf{x}^n)\mathbf{U}^{n+1} \geq 0 \, . \tag{6.23}$$

Therefore, we search for $\mathbf{U}^{n+1}$ such that the approximation of the final distance between each pair of particles $D_{ij}(\mathbf{x}^n) + h^t \mathbf{G}_{ij}(\mathbf{x}^n)\mathbf{U}^{n+1}$ is either positive or zero.

To calculate $\mathbf{U}^{n+1}$, we have to solve the constrained minimization problem:

$$\mathbf{U}^{n+1} = \underset{\mathbf{v}^{n+1} \in R^{2N}}{\arg\min} \left[\frac{1}{2} \|\mathbf{v}^{n+1} - \mathbf{V}_{predicted}\|_{\mathbf{M}}^2 - \sum_{1 \leq i < j \leq N} \mu_{ij}^{n+1} (D_{ij}(\mathbf{x}^n) + h^t \mathbf{G}_{ij}(\mathbf{x}^n)\mathbf{v}^{n+1}) \right]$$
$$\text{with } \mathbf{V}_{predicted} = \mathbf{U}^n + h\mathbf{M}^{-1}\mathbf{f}^{,n} \tag{6.24}$$

where μ_{ij}^{n+1} is a Lagrange multiplier and has the dimension of a force. μ_{ij}^{n+1} and $\mathbf{U}^{n+1}$ must satisfy the Kuhn–Tucker conditions:

$$\begin{cases} \mu_{ij}^{n+1} \geq 0 \\ D_{ij}(\mathbf{x}^n) + h^t \mathbf{G}_{ij}(\mathbf{x}^n)\mathbf{U}^{n+1} \geq 0 \\ \mu_{ij}^{n+1} \left(D_{ij}(\mathbf{x}^n) + h^t \mathbf{G}_{ij}(\mathbf{x}^n)\mathbf{U}^{n+1} \right) = 0 \, . \end{cases} \tag{6.25}$$

The convergence of the numerical scheme given by Eqs. (6.22), (6.24), and (6.25) is proven in [7]. The inelastic collision law is implicitly included in the constrained minimization problem (6.24). The constraint affects the particle positions at the end of the considered time step, and $\mathbf{U}^{n+1}$ is computed such that these positions are admissible.

The expressions of $\mathbf{U}^{n+1}$ and μ_{ij}^{n+1} are related by:

$$\mathbf{M}\,\mathbf{U}^{n+1} = \mathbf{M}\;\mathbf{U}^{n} + h\mathbf{f}^{n} + h\sum_{1\le i<j\le N}\mu_{ij}^{n+1}\mathbf{G}_{ij}(\mathbf{x}^{n}) \tag{6.26}$$

where μ_{ij}^{n+1} and $\mathbf{U}^{n+1}$ satisfy the Kuhn–Tucker conditions Eq. (6.25).
NSM2

On each interval $[t^n, t^{n+1}]$, smooth forces are substituted by percussions applied at the time $\theta_n = t^n + \frac{h}{2}$. All the non-smooth forces, or the percussions applied during the collision, are applied to the system at θ_n. Hence, interior (resp. exterior) percussions to the deformable system are the sum of two factors: the interior (resp. exterior) percussions during contacts, and the percussions obtained from smooth forces exerted on the system during the system's smooth evolution [25]. It follows that the velocities are discontinuous at times θ_n when percussions are applied to the system, but elsewhere are constant. This idea is represented by a piecewise affine function, constant on $[t^n, \theta_n[$ and $]\theta_n, t^{n+1}]$ and with a jump discontinuity at θ_n (see Fig. 6.16).

The equation governing a discontinuity on $[t^n, t^{n+1}]$ is:

$$\mathbf{U}^{n+1}(\theta_n) - \mathbf{U}^{n}(\theta_n) = \mathbf{M}^{-1}\left(-\mathbf{P}^{int}\left(\frac{\boldsymbol{\Delta}(\mathbf{U}^{n+1}(\theta_n)) + \boldsymbol{\Delta}(\mathbf{U}^{n}(\theta_n))}{2}\right) + \mathbf{P}^{ext}(\theta_n)\right). \tag{6.27}$$

Let $\mathbf{X}^{n+1} = \frac{\mathbf{U}^{n+1}(\theta_n)+\mathbf{U}^{n}(\theta_n)}{2}$ so that Eq. (6.27) becomes:

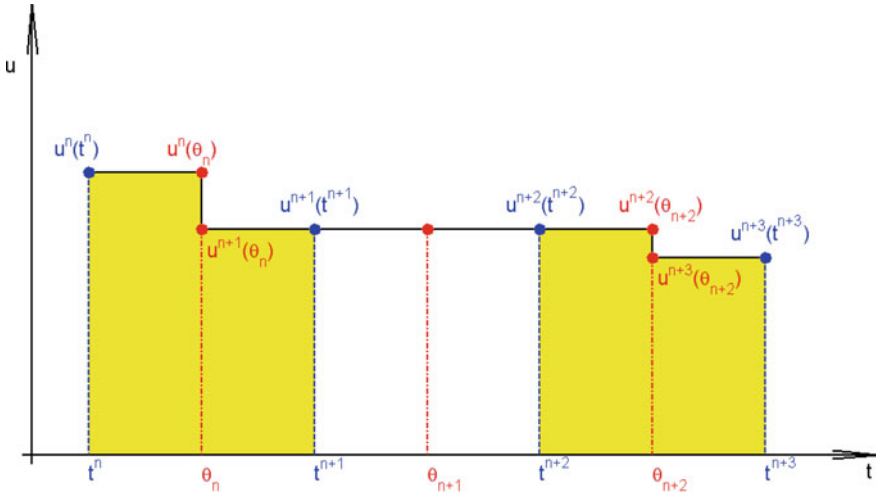

Fig. 6.16 *NSM2*—velocity of the pedestrian i. Time intervals in *yellow* correspond to those where there is a contact and/or nonzero smooth force applied to the ith particle and where there is a jump discontinuity in the velocity

$$2\mathbf{X}^{n+1} + \mathbf{M}^{-1}\mathbf{P}^{int}(\boldsymbol{\Delta}(\mathbf{X}^{n+1})) = 2\mathbf{U}^n(\theta_n) + \mathbf{M}^{-1}\mathbf{P}^{ext}(\theta_n)\,. \tag{6.28}$$

From Eqs. (6.17) and (6.28), $\mathbf{X}^{n+1}$ can be obtained by solving the constrained minimization problem:

$$\mathbf{X}^{n+1} = \underset{\mathbf{Y}^{n+1} \in \mathbf{R}^{2N}}{\arg\min} \left[{}^t\mathbf{Y}^{n+1}\mathbf{M}\,\mathbf{Y}^{n+1} + \Phi(\mathbf{x}^n, \boldsymbol{\Delta}(\mathbf{Y}^{n+1})) - {}^t(2\mathbf{U}^n(\theta_n) + \mathbf{M}^{-1}\mathbf{P}^{ext}(\theta_n))\mathbf{M}\,\mathbf{Y}^{n+1}\right] \tag{6.29}$$

where $\mathbf{Y}^{n+1} = \frac{\mathbf{U}^{n+1}(\theta_n)+\mathbf{U}^n(\theta_n)}{2}$.

The constitutive law used is the linear law corresponding to the quadratic pseudo-potential:

$$\Phi^d(\mathbf{x}^n, \boldsymbol{\Delta}(\mathbf{Y}^{n+1})) = \sum_{1\le i<j\le N} \tfrac{1}{2}K_T \left({}^t\boldsymbol{\Delta}_{ij}(\mathbf{Y}^{n+1})\,{}^{\perp}\mathbf{e}^n_{ji}\right)^2 + \tfrac{1}{2}K_N \left({}^t\boldsymbol{\Delta}_{ij}(\mathbf{Y}^{n+1})\mathbf{e}^n_{ji}\right)^2 \tag{6.30}$$

where $\mathbf{e}^n_{ji}$ is the normal vector at the contact point, ${}^{\perp}\mathbf{e}^n_{ji}$ is the tangent vector at the contact point, and K_N and K_T respectively are the coefficients of dissipation for the normal and tangential components of percussions. K_N reflects the inelastic nature of collisions between particles. A collision between a particle and a wall is elastic for $K_N \to \infty$ [32]. Practically, a value of $K_N > 10^4\,\mathrm{kg}$ is well suited in the case of dense crowds. K_T is due to the atomization of viscous friction and its value is often chosen to be zero. Its influence is shown in [53] and illustrated for the case of a pedestrian flow through a bottleneck.

The following inequality has to be verified when there is a contact between two particles i and j:

$$-\,{}^t\boldsymbol{\Delta}_{ij}(\mathbf{Y}^{n+1})\mathbf{e}^n_{ji} + {}^t\boldsymbol{\Delta}_{ij}(\frac{\mathbf{U}^n(\theta_n)}{2})\mathbf{e}^n_{ji} \le 0\,. \tag{6.31}$$

The dual formulation of the no interpenetration condition in Eq. (6.31) is used to express the potential Φ^r in the following form:

$$\Phi^r(\mathbf{x}^n, \boldsymbol{\Delta}(\mathbf{Y}^{n+1})) = \sum_{1\le i<j\le N} \mu^{n+1}_{ij}\left[-\,{}^t\boldsymbol{\Delta}_{ij}(\mathbf{Y}^{n+1})\mathbf{e}^n_{ji} + {}^t\boldsymbol{\Delta}_{ij}(\frac{\mathbf{U}^n(\theta_n)}{2})\mathbf{e}^n_{ji}\right] \tag{6.32}$$

where μ^{n+1}_{ij} is a Lagrange multiplier and has the dimension of a percussion. μ^{n+1}_{ij} and $\mathbf{U}^{n+1}$ must satisfy the Kuhn–Tucker conditions:

$$\begin{cases} \mu^{n+1}_{ij} \ge 0 \\ {}^t\boldsymbol{\Delta}_{ij}(\mathbf{Y}^{n+1})\mathbf{e}^n_{ji} - {}^t\boldsymbol{\Delta}_{ij}(\frac{\mathbf{U}^n(\theta_n)}{2})\mathbf{e}^n_{ji} \ge 0 \\ \mu^{n+1}_{ij}\left[{}^t\boldsymbol{\Delta}_{ij}(\mathbf{Y}^{n+1})\mathbf{e}^n_{ji} - {}^t\boldsymbol{\Delta}_{ij}(\frac{\mathbf{U}^n(\theta_n)}{2})\mathbf{e}^n_{ji}\right] = 0\,. \end{cases} \tag{6.33}$$

The velocities and positions at the end of time steps are solutions of:

$$\begin{cases} \mathbf{U}^{n+1}(\theta_n) = \mathbf{U}^{n+1}(\theta_{n+1}) = 2\mathbf{X}^{n+1} - \mathbf{U}^n(\theta_n) \\ \mathbf{x}^{n+1} = \mathbf{x}^n + h\frac{\mathbf{U}^{n+1}(\theta_n)+\mathbf{U}^n(\theta_n)}{2} \end{cases}. \tag{6.34}$$

The minimization problems (6.24) and (6.29) are solved using the classical Uzawa algorithm [20, 25, 26, 32].

To write Eq. (6.29) with the same formalism as Eqs. (6.18) and (6.24), only purely inelastic collisions need to be considered, as in *NSM*1. We choose, then, $K_N = K_T = 0$ in Eq. (6.30). Thus Eq. (6.29) becomes:

$$\mathbf{U}^{n+1} = \underset{\mathbf{V}^{n+1} \in R^{2N}}{\arg\min} \left[\frac{1}{2}\|\mathbf{V}^{n+1}(\theta_n) - \mathbf{V}_{predicted}\|^2_{\mathbf{M}} - \sum_{1\le i<j\le N} \mu_{ij}^{n+1}\, {}^t\mathbf{G}_{ij}(\mathbf{x}^n)\mathbf{V}^{n+1}(\theta_n) \right] \text{ with } \mathbf{V}_{predicted} = \mathbf{U}^n(\theta_n) + \mathbf{M}^{-1}\mathbf{P}^{ext}(\theta_n) \tag{6.35}$$

Consequently, with $K_N = K_T = 0$, the expressions of $\mathbf{U}^{n+1}$ and of μ_{ij}^{n+1} are related by:

$$\mathbf{M}\,\mathbf{U}^{n+1}(\theta_n) = \mathbf{M}\,\mathbf{U}^n(\theta_n) + \mathbf{P}^{ext}(\theta_n) + \sum_{1\le i<j\le N} \mu_{ij}^{n+1}\mathbf{G}_{ij}(\mathbf{x}^n) \tag{6.36}$$

where μ_{ij}^{n+1} and $\mathbf{U}^{n+1}$ satisfy the Kuhn–Tucker conditions Eq. (6.33).

Equations (6.26) and (6.36) have similar expressions; however, the calculation of the Lagrange multiplier μ_{ij}^{n+1} is different for each. For $NSM1$, the constraint is on the position of the particle and is dependent on the time step, so overlapping is always avoided. The velocity of the particle has a "geometrical meaning" since it is computed from the previously found position. However, for *NSM*2, the constraint

Table 6.3 Analogies between minimization problems in the case of plasticity and when using *NSM*1 or *NSM*2

	Main unknown variable	Predicted value	External agency	Constraint	Lagrange multiplier
*NSM*1	$\mathbf{U}^{n+1}$	$\mathbf{V}_{predicted} = \mathbf{U}^n + h\mathbf{M}^{-1}\mathbf{f}^n$	$h\,\mathbf{f}^n$	$D_{ij}(\mathbf{x}^n) + h\,{}^t\mathbf{G}_{ij}(\mathbf{x}^n)\mathbf{U}^{n+1} \ge 0(m)$	$\mu_{ij}^{n+1}(N)$
*NSM*2	$\mathbf{U}^{n+1}(\theta_n)$	$\mathbf{V}_{predicted} = \mathbf{U}^n(\theta_n) + \mathbf{M}^{-1}\mathbf{P}^{ext}(\theta_n)$	$\mathbf{P}^{ext}(\theta_n)$	${}^t\mathbf{G}_{ij}(\mathbf{x}^n)\mathbf{U}^{n+1}(\theta_n) \ge 0(m\cdot s^{-1})$	$\mu_{ij}^{n+1}(N\cdot s)$
Plasticity	σ^{n+1}	$\sigma_{predicted} = \sigma^n + \mathsf{C} : \Delta\boldsymbol{\varepsilon}$	$\Delta\boldsymbol{\varepsilon} = \boldsymbol{\varepsilon}^{n+1} - \boldsymbol{\varepsilon}^n$	$f(\sigma^{n+1}) \le 0$	$\Delta\lambda$

is on the velocity of the particle and is independent of the time step, so overlapping is possible. The velocity now has a greater physical meaning, and it can be accepted that the position of the particle after contact can violate the overlapping condition.

Table 6.3 shows the analogies between minimization problems in the case of plasticity and when using $NSM1$ or $NSM2$ (Eqs. (6.18), (6.24), and (6.35)).

The difference in contact treatment between $NSM1$ and $NSM2$ can be illustrated with the following example. In the xy-plane, we consider a particle of radius $r = 0.22\,\text{m}$, initial position $\mathbf{x}_{initial} = {}^t(0.5, 0.5)$, and initial velocity $\mathbf{U}_{initial} = {}^t(\frac{1}{\sqrt{2}}, -\frac{1}{\sqrt{2}})$. The ground corresponds to $y = 0$. We choose $K_N = K_T = 0\,\text{kg}$, $T = 0.8\,\text{s}$, and $h = 10^{-3}\,\text{s}$. No exterior force is applied to the particle. The particle's position in the xy-plane after a collision with the ground, and the time evolution of its velocity along the y-axis, are given for both $NSM1$ and $NSM2$ in Fig. 6.17. Considering the spatial trajectory of the particle's center in the xy-plane, we illustrate previously made remarks about Eqs. (6.26) and (6.36) in the following figures. Figure 6.17b (a zoomed-in-on section of Fig. 6.17a) shows that unlike $NSM1$, a light numerical overlapping can exist with $NSM2$. Figure 6.17d (a zoomed-in-on section of Fig. 6.17c) shows that when the contact is detected, one intermediate velocity with no physical meaning is found just after the collision with $NSM1$.

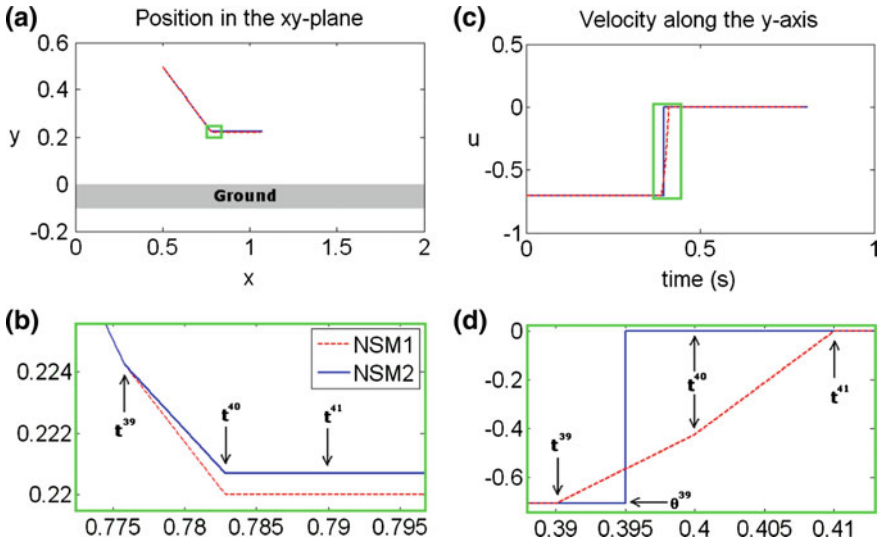

Fig. 6.17 Collision of a particle with the ground for $NSM1$-$NSM2$. Subplots **a** and **b** show the trajectory in the xy-plane of the particle's center (radius $r = 0.22\,\text{m}$) after collision with the ground as a function of time. Subplots **c** and **d** show the time evolution of the velocity along the y-axis of the particle's center after collision with the ground. Subplots **b** and **d** are magnifications of the *green rectangles* in subplots (**a**) and (**c**), respectively. The curve for $NSM1$ is the *red dotted line* and the curve for NSM2 is the *blue line*

6.6 Adaptation of a Granular Approach to the Crowd

The 2D approach of rigid particles movement, in particular the one proposed by Frémond, can be adapted to crowd movement. A pedestrian can be represented as a particle by being given a willingness, i.e., a desire to move in a particular direction with a specific speed at each moment. To adapt the granular approach proposed by Frémond to a crowd, two steps need to be considered: first, the introduction into the model of the desired velocity of each pedestrian, in order to portray crowd movement; and second, the definition of the desired velocity of each pedestrian.

6.6.1 Introduction of the Desired Velocity of Each Pedestrian into the Particle Movement Approach

In order to introduce the willingness of each pedestrian to move at his or her desired velocity, an acceleration force is added to the particle movement approach. We can note: $\mathbf{f}^{int}(t) = \mathbf{f}^{a}(t)$, where $\mathbf{f}^{a}(t)$ is the acceleration force [37] allowing one to give a desired direction and velocity amplitude to each pedestrian. Each component $\mathbf{f}_i^{a}(t)$ of the vector force of dimension $2N$: ${}^{t}\mathbf{f}^{a} = ({}^{t}\mathbf{f}_1^{a}, {}^{t}\mathbf{f}_2^{a}, ..., {}^{t}\mathbf{f}_N^{a})$ is associated with pedestrian i and can be expressed as:

$$\mathbf{f}_i^{a}(t) = m_i \frac{\|\mathbf{U}_{d,i}\|\mathbf{e}_{d,i}(t) - \mathbf{U}_i(t)}{\tau_i} \tag{6.37}$$

where $\mathbf{U}_{d,i}$ is the desired velocity of the pedestrian i; $\mathbf{e}_{d,i}$ is his or her desired direction; $\mathbf{U}_i$ is the pedestrian's current velocity; and τ_i is a relaxation time, allowing the pedestrian i to recover his or her desired velocity after a collision. Smaller values of τ_i let the pedestrians walk more aggressively [39]. For this variable, Helbing chose $\tau = 0.5\,\mathrm{s}$. An example of the post-collision trajectories as a function of τ for two identical pedestrians i and j moving in opposite directions is illustrated in Fig. 6.18. The expressions of $\|\mathbf{U}_{d,i}\|$ and $\mathbf{e}_{d,i}(t)$ need to be defined in order to find $\mathbf{f}_i^{a}(t)$. This is the purpose of the next paragraph.

6.6.2 Definition of the Desired Velocity

The amplitude $\|\mathbf{U}_{d,i}\|$ of the desired velocity represents the speed at which the ith pedestrian wants to move on the considered structure, and can be influenced by the pedestrian's level of nervousness. Generally, this velocity is chosen following a normal distribution with an average of $1.34\,\mathrm{m\,s^{-1}}$ and standard deviation of $0.26\,\mathrm{m\,s^{-1}}$ [43].

Several definitions of the desired trajectory $\mathbf{e}_{d,i}(t)$ of pedestrian i are possible: (i) the most comfortable trajectory, where he or she exerts the least effort (e.g., by

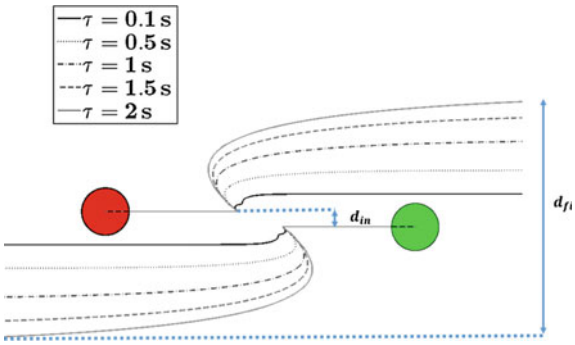

Fig. 6.18 Trajectories of two identical pedestrians i and j moving in opposite directions for different values of τ. After the collision, the external acceleration force allows each pedestrian to gradually change from the current post-collision velocity to the desired velocity, depending on the values of τ_i and τ_j. In this example, $\tau_i = \tau_j = \tau$

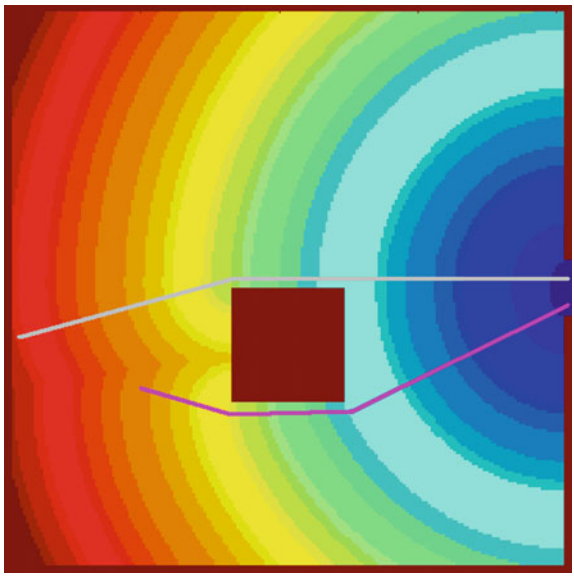

Fig. 6.19 Geodesic distances to the exit of a room containing an obstacle. Two examples of shortest trajectory are plotted as a function of the initial position of the pedestrian in the room

avoiding stairs) and changes direction the least frequently, etc.; (ii) the shortest path; or (iii) the fastest path to move from one place to another [50]. It is possible to combine two strategies in the same simulation or to change the preferred strategy for any reason during the simulation.

The strategy of the shortest path from one point to another [58] is implemented through a Fast Marching algorithm and can be used to obtain $\mathbf{e}_{d,i}$. This direction depends on the space or terrain (whether there are obstacles, etc.), the time, and also the characteristics of the individual (gender, age, slowed or hurried steps, etc.). It is defined by: $\mathbf{e}_{d,i}(t) = \frac{\mathbf{U}_{d,i}(t)}{\|\mathbf{U}_{d,i}\|}$. Figure 6.19 illustrates an example of the geodesic

distances to the exit of a room containing an obstacle. Two examples of shortest trajectory are plotted as a function of the initial position of the pedestrian in the room.

6.6.3 The Influence of the Relaxation Time Parameter τ

Here we consider the trajectories of two pedestrians moving in opposite directions after a collision. A study is performed to determine the influence of the relaxation time parameter τ on two post-collision variables: the time t_{fi} that the pedestrian needs to recover his or her desired trajectory, and the final distance d_{fi} resulting from the shock (Fig. 6.18).

When the initial distance d_{in} is small and the value of τ is less than 0.5 s, several contacts may occur since the pedestrians walk aggressively and recover their desired velocity immediately after a collision.

When the value of τ is more than 0.5 s, there will only be one collision, and t_{fi} and d_{fi} increase linearly as a function of τ (Fig. 6.20).

Observing the results obtained after the collision between two pedestrians of different radii but with the same velocity (Fig. 6.21), one can notice that the lighter pedestrian (with a radius closer to 0.20 m) needs more time after the contact to resume his or her desired trajectory, while the heavier pedestrian (with a radius closer to 0.25 m) attains this trajectory faster. Simulations conducted for the case of pedestrians with different initial velocities have produced the same kind of results as those of pedestrians with the same velocities [79].

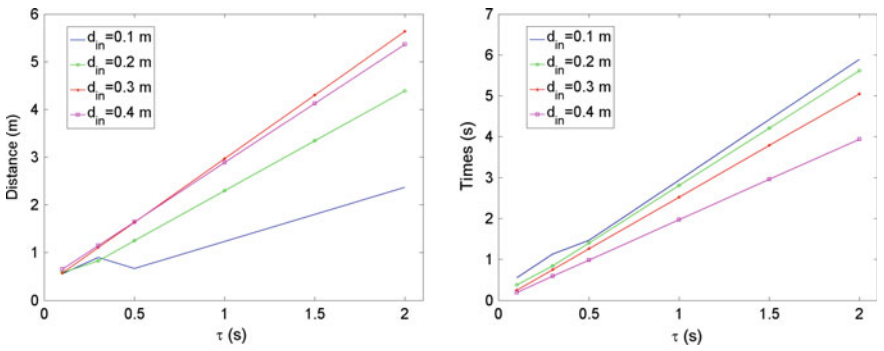

Fig. 6.20 The final distance d_{fi} as a function of τ and d_{in} (*left*); the time t_{fi} as a function of τ and d_{in} (*right*). The velocity of the pedestrians is 1.5 m s^{-1} and their radii are 0.25 m

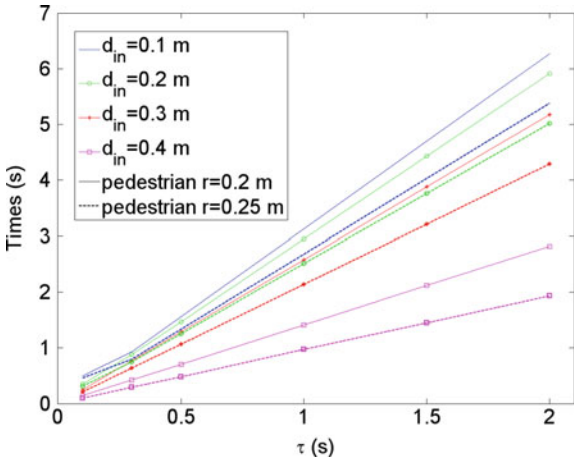

Fig. 6.21 t_{fi} as a function of τ and d_{in}. The velocity of the pedestrians is 1.5 m s^{-1} and their radii are 0.2 m and 0.25 m

6.7 Making the Behaviour of Pedestrians More Realistic

To make the behaviour of the pedestrians more realistic, several forces can be added to obtain $\mathbf{f}^{int}(t)$. For instance, $\mathbf{f}^{int}(t) = \mathbf{f}^{a}(t) + \mathbf{f}^{soc}(t) + \mathbf{f}^{sgr}(t)$, where $\mathbf{f}^{soc}(t)$ is a socio-psychological force [39] that reflects the tendency of pedestrians to keep a certain distance from other pedestrians, and $\mathbf{f}^{sgr}(t)$ is a subgroup force [95] that allows one to take into account the subgroup behaviour of crowd movement. Both of these forces are detailed in the following paragraphs.

6.7.1 The Socio-Psychological Force

The expression of the socio-psychological force [36, 39], applied to the ith pedestrian interacting with pedestrian j, is given by:

$$\mathbf{f}_{ij}^{soc}(t) = A_i \exp\left(\frac{-D_{ij}(\mathbf{x}(t))}{B_i}\right)\left(\Lambda_i + (1-\Lambda_i)\frac{1+\cos\varphi_{ij}}{2}\right)\mathbf{e}_{ij} \tag{6.38}$$

where A_i denotes the interaction strength; B_i the range of the repulsive interaction; $\Lambda_i < 1$ the anisotropic character of pedestrian interactions, as the situation in front of a pedestrian has a larger impact on behavior than what is occurring behind; and φ_{ij} the angle between the direction $\mathbf{e}_{d,i}(t)$ of the desired motion and the direction $-\mathbf{e}_{ij}$ of the pedestrian exerting a repulsive force. Figure 6.22 shows an example of a pedestrian-pedestrian interaction with and without the socio-psychological force. A video at the following link shows head-on encounter of 2 couples of pedestrians (file repulsionCollision.avi are available at https://ifsttar.libcast.com/mast-sdoa or at

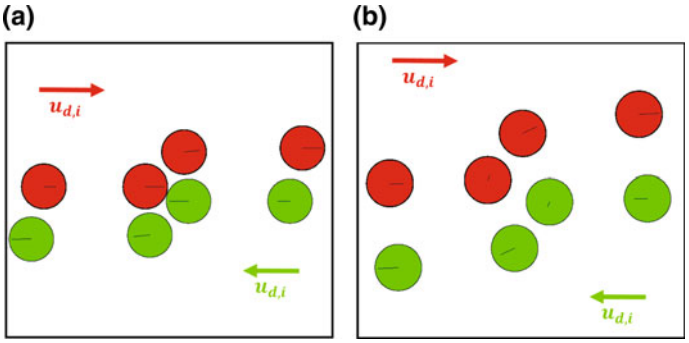

Fig. 6.22 Pedestrian-pedestrian interaction, **a** without and **b** with the socio-psychological force

http://extras.springer.com). The pedestrians on the bottom avoid each other because the repulsive force is activated while the ones on the top collide since the repulsive force is not activated.

One can notice that in Fig. 6.22 (left), which illustrates an interaction without the socio-psychological force, a pedestrian-pedestrian collision occurs. On the other hand, in Fig. 6.22 (right), which includes this force, there is no collision. Pedestrians avoid each other by turning around.

6.7.2 Subgroups: Pedestrians Holding Hands

A group is defined as a physical collection of people following the same way, but who may be or not a part of the same social group. A subgroup is defined as people within the same physical group who want to stay together [95] like those of friends or a family. Several studies have revealed that smaller subgroups constitute the majority of the people in a crowd [5, 95]. However, very few studies are able to model the subgroup behaviour [72, 95]. A particular subgroup concerns pedestrians who hold hands. It is recognized that holding hands is the most effective way of keeping children safe from traffic injury.

To describe the particular subgroup behaviour of the holding hands pedestrians, we were inspired by the article [14] describing the interactions between rigid particles as an "at-a-distance" velocity of deformation. This velocity is the derivative with respect to time of the squared distance between linked shoulders, i.e. points A_i and A_j for pedestrians i and j (Fig. 6.23). This model takes into account the effects of the subgroup as a continuous deformation within the subgroup of pedestrians who hold hands while existing methods in literature describe the cohesion of the subgroup with external forces [72, 95]. This new subgroup model [3] needs that pedestrians be oriented. The rotation of the pedestrians around themselves has been integrated in the 2D model to obtain an improvement of the microscopic approach proposed in [79–82]. It is noteworthy that the pedestrians orientation is rarely used in literature [1, 61]. Therefore, the center position of the ith particle is now described by the vector

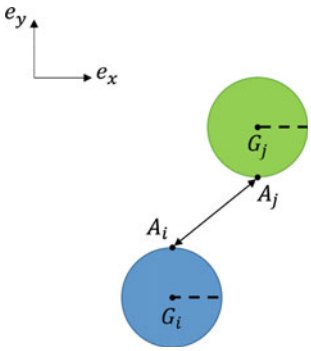

Fig. 6.23 Two pedestrians holding hands- Example of linked shoulders

${}^t\mathbf{x}_i = (q_i^x, q_i^y, \theta_i(t)) \in R^3$, where $\theta_i(t) \in [-\pi, \pi]$ represents the walking direction of the particles about the $\mathbf{e}_z$-axis ($\theta_i(t) = 0$ when the particle's walking direction is parallel to the x-axis in the positive direction, $\theta_i(t) > 0$ when the particle turns counterclockwise), $\dot{\theta}_i(t) = d\theta_i/dt$ its rotational velocity, and $\boldsymbol{\Omega}_i(t) = [0, 0, \dot{\theta}_i(t)]$. A mass moment of inertia I_i about a particle's vertical axis is integrated in the inertial matrix of the set of particles making it of size $3N \times 3N$.

Analogous to the acceleration force given by Eq. (6.37), a restoring torque must also be introduced to return the pedestrian to his desired direction after a perturbation. It is modeled as the combination of a linear rotational spring and of a linear rotational damper [3], and is defined for the ith pedestrian by:

$$I_i^a = k_i\left(\theta_i - \theta_{d,i}\right) + c_i\dot{\theta}_i = -I_i\ddot{\theta}_i \tag{6.39}$$

where $\theta_{d,i}$ is the angle between $\mathbf{e}_{d,i}$ and the reference direction $\mathbf{e}_x = [1; 0]$, I_i (in kg.m^2) is the moment of inertia, k_i (in kg $\cdot$ m^2 $\cdot$ s^{-2} $\cdot$ rd^{-1}) is the torsional stiffness, c_i (in kg $\cdot$ m^2 $\cdot$ s^{-1} $\cdot$ rd^{-1}) is the rotational damping, and $\omega_i = \sqrt{\frac{k_i}{I_i}}$ (in rd $\cdot$ s^{-1}) is the undamped resonant frequency for pedestrian i. After a perturbation, a particle returns the fastest without oscillations to its desired direction when its rotation is critically damped ($\zeta_i = \frac{c_i}{2\sqrt{I_i k_i}} = 1$). For $\zeta_i > 1$, the individual returns more slowly to its desired position (Fig. 6.24a, b). For $\zeta_i < 1$, it oscillates before returning to its desired direction (Fig. 6.24c, d). The collision in Fig. 6.24 occurs at $t = 0.1$ s and the time step is $\Delta t = 0.01$ s. The solid line plotted inside the particle represents the pedestrian's desired direction while the dotted line represents his current walking direction. We have chosen $\zeta_i = 1$.

The maximum rotation must also be controlled so that pedestrians won't rotate in an unrealistic manner after a shock. By solving Eq. (6.39), we obtain the rotation time-evolution of an individual about himself:

$$\theta_i(t) = \dot{\theta}_0(K_T, K_N)te^{-\omega_i t} + \theta_{d,i} \tag{6.40}$$

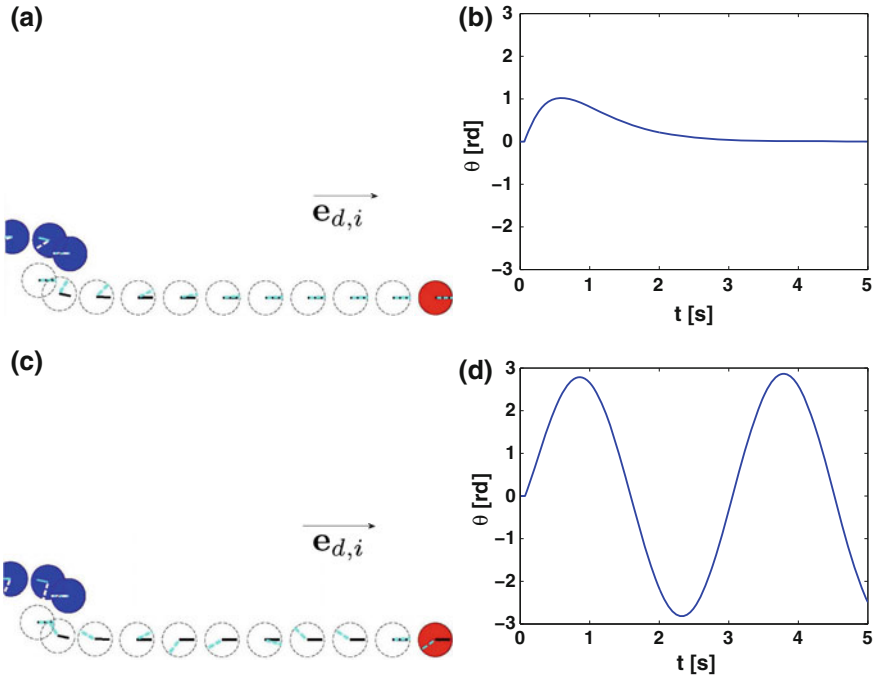

Fig. 6.24 Pedestrian-pedestrian interaction without repulsive forces: the *left column* shows the pedestrian's movement after "collision" for $\zeta_i = 1$ (*top*) and $\zeta_i = 0$ (*bottom*), where $\theta_{d,i} = 0$. The *right column* is a plot of the pedestrian's rotation as a function of time

where $\dot{\theta}_0(K_T, K_N)$ is calculated by the model (by solving Eq. (6.29)) after a shock takes place and $k_i = I_i \cdot \omega_i^2$, the torsional stiffness (Eq. (6.39)), is introduced by the user ($k_i = k$ for the sake of simplicity). Figure 6.25 shows that the value of $\dot{\theta}_0$, calculated after a shock, varies with K_T and is independent of K_N for values greater than 2×10^3 kg. From Eq. (6.40), we can easily obtain the expression of θ_{max}:

$$\theta_{max} = \frac{\dot{\theta}_0(K_T)}{\omega_i \cdot e} + \theta_{d,i} \tag{6.41}$$

By varying k (in $\mathrm{kg} \cdot \mathrm{m}^2 \cdot \mathrm{s}^{-2} \cdot \mathrm{rd}^{-1}$) between [0.5, 18.5], and for each value of $\dot{\theta}_0$ obtained from Fig. 6.25 (each value of $\dot{\theta}_0$ corresponds to a value of K_T), Eq. (6.41) gives the surface illustrated in Fig. 6.26. Now the user can specify the desired value of θ_{max} by choosing from Fig. 6.26 a point $(\dot{\theta}_0, k)$ which corresponds to a couple (K_T, k). The couple must be on or below the isoline representing the chosen value of the maximal rotation.

Now that the rotation is introduced into the model, the at a distance velocity of deformation is, see Chap. 5 and [32]:

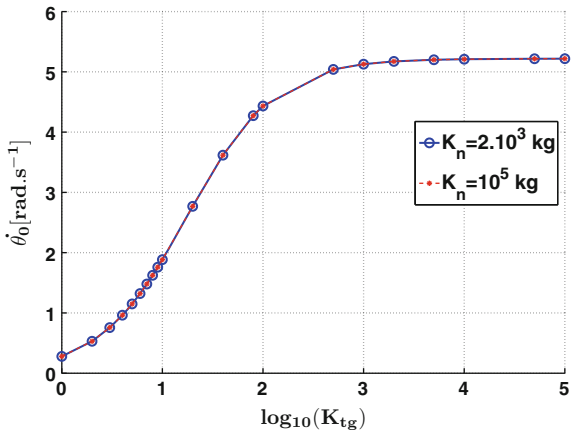

Fig. 6.25 Variation of $\dot{\theta}_0$ as a function of $\log_{10}(K_T)$

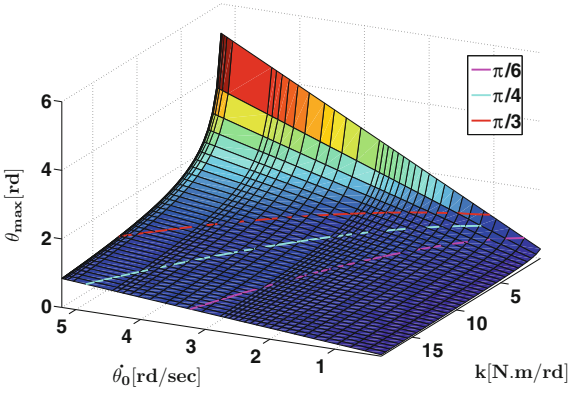

Fig. 6.26 Variation of θ_{max} as a function of $\dot{\theta}_0$ and k

$$\boldsymbol{\Delta}^*_{ij}\left(\mathbf{x}(t), \mathbf{U}(t)\right) = 2\left(\mathbf{U}_i(t) - \mathbf{U}_j(t)\right) \cdot \mathbf{A}_j \mathbf{A}_i. \tag{6.42}$$

In the previous expression of the pseudo-potential of dissipation, a new quadratic term function of the at a distance velocity of deformation is added:

$$\begin{aligned} \Phi^d(\mathbf{x}, \mathbf{Y}) = & \frac{1}{2} \sum_{1 \le i \le j \le N} \left[K_N \left({}^t\boldsymbol{\Delta}_{ij}(\mathbf{Y}) \cdot \mathbf{e}^n_{ji} \right)^2 + K_T \left({}^t\boldsymbol{\Delta}_{ij}(\mathbf{Y}) \cdot {}^{\perp}\mathbf{e}^n_{ji} \right)^2 \right] \\ & + \sum_{1 \le i \le j \le N_{subgroup}} \frac{1}{2} K_V \left(\boldsymbol{\Delta}^*_{ij}(\mathbf{x}, \mathbf{Y}) \right)^2 \end{aligned} \tag{6.43}$$

where K_V is the coefficient of viscous dissipation. A numerical study of the influence of K_v is performed in [79]. It is shown that the higher the value of K_v is, the more rigid the bond between the holding hands pedestrian is; thus a free pedestrian colliding the subgroup wont be able to break the bond.

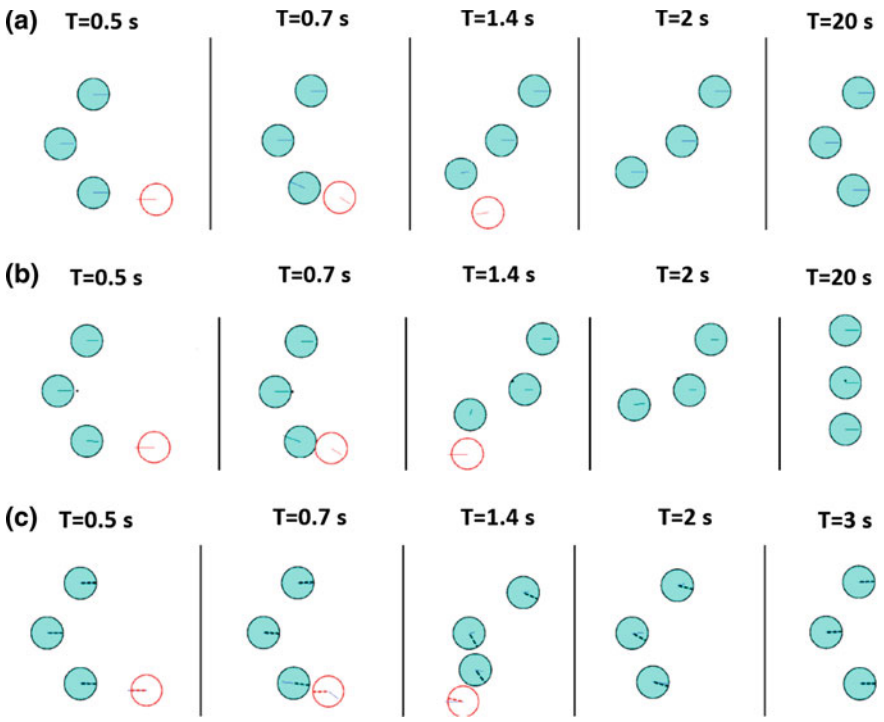

Fig. 6.27 Example of a three holding hands pedestrians (in *light blue*) subgroup colliding with a fourth pedestrian (in *red*), each row correspond to an approach: Singh [95] *top line*, Moussaïd [72] *middle line*, and our approach [3, 79] *bottom line*

On a same example illustrated in Fig. 6.27, a comparison has been done between different subgroup approaches: Singh [95], Moussaïd [72], and our approach for pedestrians holding hands with $K_v = 100\,\mathrm{Kgm}^{-1}$. A subgroup composed of three pedestrians collides with a fourth pedestrian. It is shown that, with the proposed subgroup approach, the subgroup is re-formed faster after a collision than with the other approaches. Moreover, only the proposed approach allows to keep the shape of the subgroup throughout the whole simulation [3, 79].

6.8 Simulations of Crowd Movement

In Fig. 6.28, one can find the different stages of the MATLAB program of the discrete crowd movement model. The simulations of crowd movement that were undertaken are split into four categories: (i) the reproduction of observed phenomena of crowd self-organization (see Sect. 6.1); (ii) the simulation of emergency evacuation exercises, with comparisons between the experimental and numerical results; (iii) the use

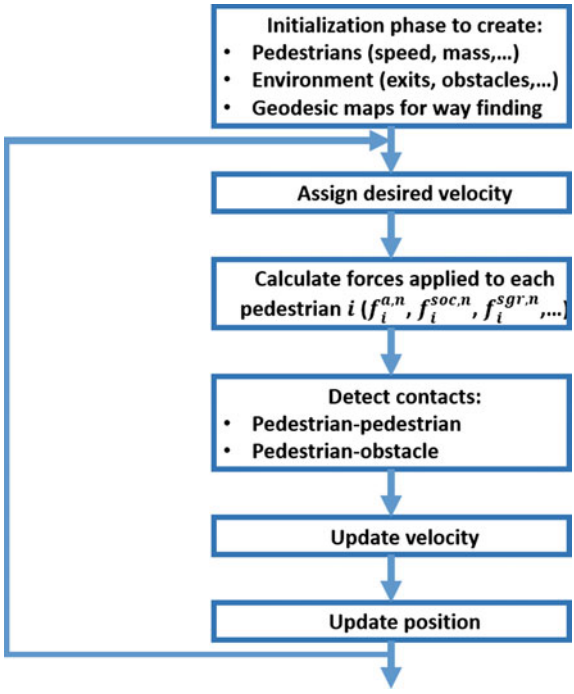

Fig. 6.28 Discrete crowd movement model—stages in MATLAB program

of the model to improve the service quality of a studied space; and (iv) the modeling of sub-group movements.

Three parameters are proposed and calculated in order to compare and then comment on the different results: (i) the evacuation curve, which represents the temporal evolution of the number of pedestrians leaving a given location through one of several exits; (ii) the average rate of flow Q of pedestrians going across an exit, obtained via a temporal derivation of the previous curve; and (iii) the evacuation time from an initial position, or the average time necessary for a person to evacuate a structure, in function of their starting location.

6.8.1 Phenomena of Crowd Self-Organization

The first way to validate a crowd movement model is to attempt to reproduce real-life observed self-organization phenomena [39]. By adapting the three approaches, we have aimed to reproduce two classical phenomena [40, 101]: lane formation in counter flow and arch formation.

Lane Formation in Counter Flow

Observations show that when two groups of pedestrians, going in opposite directions, meet, the pedestrians begin to walk in a line in order to advance as effectively as possible. This phenomenon is called lane formation in counter flow.

We have tried to reproduce this type of situation with our crowd movement model. To do this, we have simulated a throng of 1500 pedestrians. At the beginning, the pedestrians are randomly positioned in a 80 m by 20 m rectangle. Half the pedestrians, represented by blue filled-in circles, wish to move to the right, and the other 750 pedestrians, represented by red empty circles, wish to move to the left (Fig. 6.29a). Since social forces are not introduced in this simulation, only the interior acceleration force is considered. Only this force, therefore, allows the pedestrians to move to their desired destination after a collision. The pedestrians all have identical characteristics (size, mass, desired speed, etc.). To keep the number of pedestrians walking in the considered space constant, as soon as a pedestrian leaves via one side, an identical pedestrian enters the space via a random position on the y-axis of the other side.

In Fig. 6.29b, we can see the phenomenon of lane formation. This phenomenon can be observed in the video at the following link (file melee1500p.avi are available at https://ifsttar.libcast.com/mast-sdoa or at http://extras.springer.com). The number of lanes that are formed depends on the length of the considered space and the density of the pedestrians present [36, 37, 40]. This phenomenon has never been quantified in experimental conditions.

The simulations seem to demonstrate that with successive collisions (or successive avoidances when social forces are added), a pedestrian ends up falling behind

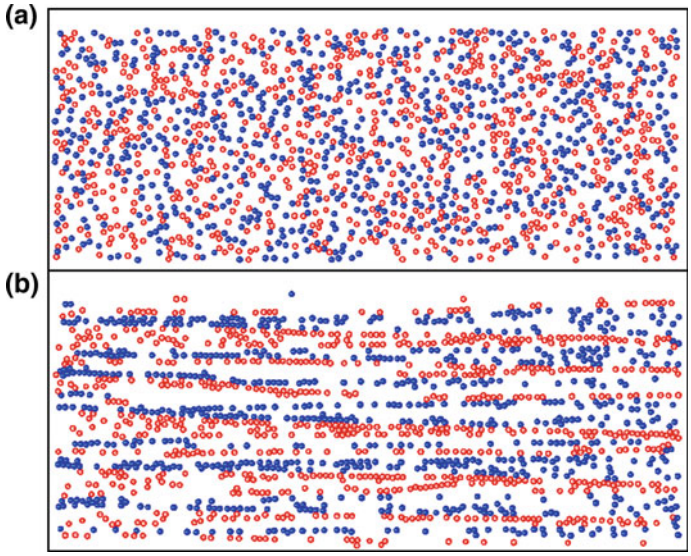

Fig. 6.29 Simulation of a throng of 1500 pedestrians—**a** $t = 0\,\text{s}$, **b** $t = 40\,\text{s}$

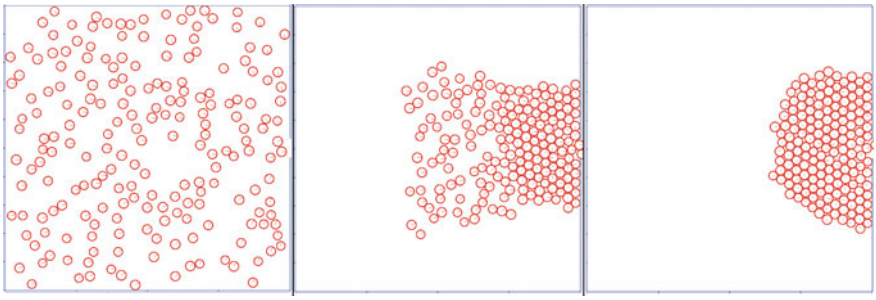

Fig. 6.30 Simulation of an evacuation from a room—arch formation—$t = 0$ s, 200 people wish to evacuation (*left*); $t = 6$ s, 187 people still need to evacuate (*middle*); $t = 12$ s, 166 people still need to evacuate (*right*)

another one moving in the same direction. This walking position no longer demands avoidance of other pedestrians. As the lanes of pedestrians form, it becomes more and more difficult to walk anywhere except in lane. This behaviour is not explicitly planned for by any single pedestrian, but is rather the result of the collected behaviors of all the members in the crowd.

Arch Formation

Observations of pedestrians show that when a dense crowd wishes to go through a narrow opening, the pedestrians place themselves around this opening to exit as quickly as possible: one thus observes the formation of an arch around the exit.

Our crowd movement model allows one to reproduce this type of phenomenon. We have considered 200 pedestrians wishing to evacuate a 20 m by 20 m square room with a 1 m-wide opening on the right side (Fig. 6.30a). Social forces are not introduced. The pedestrians all have identical characteristics (size, mass, desired speed, etc.).

In Fig. 6.30, we can see the formation of an arch, a phenomenon experimentally observed in emergency evacuations. The corresponding simulation can be watched at the following link (file evacuation200p.avi are available at https://ifsttar.libcast.com/mast-sdoa or at http://extras.springer.com).

6.8.2 Evacuation Exercises: Comparison Between Numerical and Experimental Results

In this part, we will present comparisons between results obtained from real-life experiments and results from numerical simulations. Evacuations simulations are analyzed from four different locations: a room, a classroom, a movie theater and an elementary school.

Evacuation of a Room

The objective of this section is to compare an evacuation situation simulated with the three adapted approaches, considering only their manner of handling pedestrian-pedestrian and pedestrian-obstacle local contacts. Social forces are thus not introduced.

Let us consider a square room with sides of 5 m containing 20 pedestrians who wish to leave through an 82 cm-wide door. The parameters used in the simulations are given in Table 6.4.

Since the parameters of the pedestrians are generated randomly within a given interval (Table 6.4), 50 simulations are realized (Fig. 6.31) with the respective time steps $h = 10^{-2}$ s, $h = 10^{-3}$ s and $h = 10^{-4}$ s for each adapted approach. For every approach, the initial conditions of these simulations are identical. Figure 6.31 shows the straight line obtained from a linear regression of the 50 simulations with the adapted NSM2 approach, for $h = 10^{-2}$ s. The slope of this line allows one to determine the average flow rate Q of pedestrians crossing the exit. Table 6.5 contains both the values of Q obtained from the simulations that were realized with the three approaches and different time steps, and from a real-life exercise imitating emergency evacuation conditions [42].

In Table 6.5, one can see that the influence of the chosen time step on Q is negligible, as long as the temporal integration scheme is stable. In addition, one can observe that the value of Q obtained with the adapted NSM2 approach is very close to the value acquired from the emergency evacuation exercise. The pedestrians evacuate faster with the adapted NSM1 approach than with the other two approaches. These results are likely due to the manner of handling contact: perfectly inelastic for the adapted NSM1 approach, and elastic for the adapted DEM and NSM2

Table 6.4 Evacuation from a room—parameters used in the evacuation simulations of the square room (*uniformly distributed within the given interval); the response time is the time necessary for pedestrian i to begin evacuating the room after the start of the evacuation movement

Parameter		Symbol	Value	Unit
Pedestrian i	Speed*	$\|\mathbf{U}_{d,i}\|$	[1.5, 2]	$\mathrm{m} \cdot \mathrm{s}^{-1}$
	Radius*	r_i	[0.2, 0.25]	m
	Mass*	m_i	[60, 100]	kg
	Response time	$t_{r,i}$	0	s
	Relaxation time*	τ_i	[0.1, 0.5]	s
DEM approach	Stiffness constant	k	1.2×10^5	$\mathrm{kg} \cdot \mathrm{s}^{-2}$
NSM2 approach	Normal dissipation coefficient	K_N	10^5	kg
	Tangential dissipation coefficient	K_T	0	kg
	Time step	h	$10^{-2}, 10^{-3}, 10^{-4}$	s

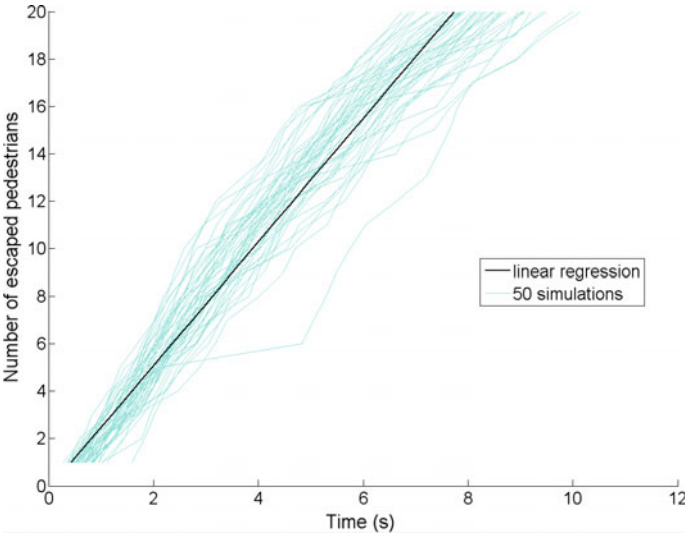

Fig. 6.31 Evacuation of a room—evacuation curves for NSM2, with $h = 10^{-2}$ s. The *cyan-colored curves* are the results of the 50 simulations. The linear regression of these simulations (the *straight black line*) allows one to obtain the average rate of flow for pedestrians exiting through the door

Table 6.5 Evacuation of room—average flow rate Q (ppl/min) of pedestrians leaving through the exit

Simulations or real-life experiment	Q (ppl/min)		
	$h = 10^{-2}$ s	$h = 10^{-3}$ s	$h = 10^{-4}$ s
Simulations with adapted DEM approach	182	182	181
Simulations with adapted NSM1 approach	279	276	278
Simulations with adapted NSM2 approach	156	154	155
Real experiment	160		

approaches. For these last two approaches, the difference between the values of Q could be caused by the phenomenon of overlapping, necessary for treating contact in the adapted DEM approach. Thus, in order to take into account pedestrians bumping into each other, it seems necessary to employ elastic collisions.

Evacuation of a Classroom

In this section, we will compare between a real-life exercise of a classroom evacuation and numerical simulations. The evacuation exercise, with a classroom of 30 students, is presented in [41]. The width of the classroom is 5.85 m and its length 6.75 m. The room contains 30 desks, organized into six rows and five columns. The longitudinal and transversal distances between the desks are, respectively, 0.9 and 1.35 m. The only door for entering or exiting the room is 0.5 m wide. The evacuation exercise is recorded by two video cameras. At the signal of the cameraman, all of the students

Table 6.6 Evacuation of a classroom—parameters used in the simulations (*uniformly distributed within the given interval); the response time is the time necessary for student i to begin evacuating after the start of the evacuation movement

Parameter		Symbol	Value	Unit
Student i	Speed*	$\|\mathbf{U}_{d,i}\|$	[1.2, 2]	$\mathrm{m} \cdot \mathrm{s}^{-1}$
	Radius*	r_i	[0.18, 0.22]	m
	Mass*	m_i	[50, 75]	kg
	Response time	$t_{r,i}$	0	s
	Relaxation time*	τ_i	[0.1, 0.5]	s
Approach	Normal dissipation coefficient	K_N	10^5	kg
NSM2	Tangential dissipation coefficient	K_T	0	kg
	Time step	h	0.01	s

stand up from their chairs and rush towards the exit. The parameters used in the numerical simulations are given in Table 6.6. Some of these parameters are uniformly distributed within a given interval. Fifty simulations have been realized.

Figure 6.32 shows examples of the progression of two numerical simulations obtained with the NSM1 and NSM2 adapted approaches. Since the progression obtained with the DEM approach is similar to that attained with the NSM2 approach, the former is not given. For all three adapted methods, a formation of an arch around the exit door is observed. For the DEM and NSM2 approaches, the students evacuate the classroom (first line of Fig. 6.32) without problem, whereas for the NSM1 approach, the students often are blocked (second line of Fig. 6.32).

The adapted NSM1 approach does not appear to be effective for this situation. Because of this, we will limit our study to the other two methods. Figure 6.33 gives the average evacuation time of the students starting from their initial position (i.e., the desks). The average evacuation times acquired from the real evacuation exercise are given at the top, those from the 50 numerical simulations realized with the adapted DEM approach in the middle, and those with the adapted NSM2 approach at the bottom. One can observe similarities between the average evacuation times obtained from the evacuation exercise and those from the numerical simulations. First of all, if we consider each column, the average evacuation time increases as a function of the distance d_{b-s}: desk position—exit. Next, even if the evacuation times increase in function of d_{b-s}, the students in the two first columns (those closest to the door) require a disproportionate time in order to evacuate. Helbing [41], using the real-life evacuation exercise, explains this phenomenon with the fact that students naturally use the aisles between the desks that are closest to the door. If the students are seated at the desks and wish to move toward the exit, this would be the aisle to their left. Therefore, the students seated in the first two columns use the same aisle, increasing

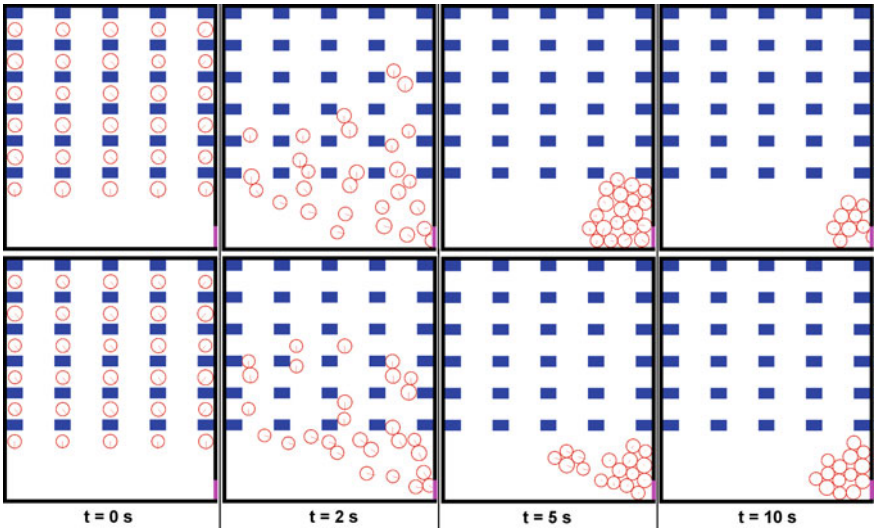

Fig. 6.32 Evacuation of a classroom—example of the progression of two numerical simulations at different moments. The first line is obtained with the adapted NSM2 approach and the second with the adapted NSM1 approach. The walls are represented in *black*, the desks in *blue*, the exit door in *magenta* and the individuals by *red circles*

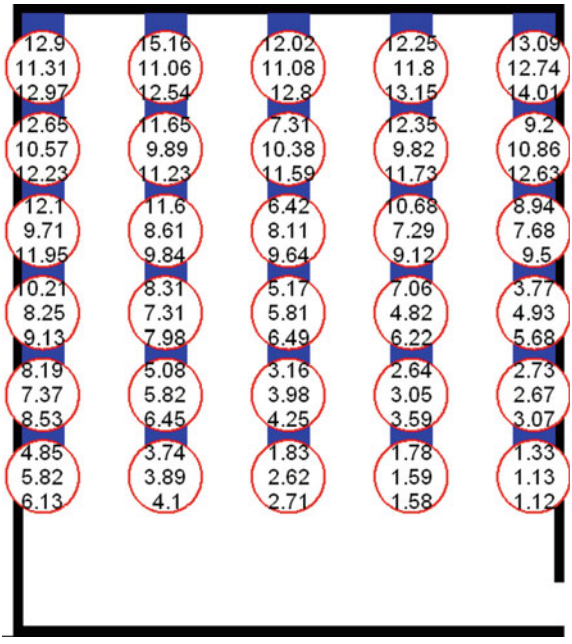

Fig. 6.33 Evacuation of a classroom—average evacuation time of the students starting from their initial positions. The three results presented in each circle give the average evacuation times according to the real-life evacuation exercise (at the *top*) and according to the numerical simulations (adapted DEM approach in the middle and adapted NSM2 approach at the *bottom*)

the density of people in this aisle and thus their evacuation time. However, using the simulations, we can give a different explanation. During the emergency evacuation, the density of the students around the narrow door becomes too great. Therefore, the students who arrive in front of the door can more easily exit than those who arrive from one of the two sides. The latter have difficulty inserting themselves into the flow of their peers who are leaving.

Evacuation of a Movie Theater

Similarly, we will undertake in the following a comparison between a real-life exercise and numerical simulations realized with the adapted NSM2 approach, this time for an evacuation from a movie theater. The evacuation exercise is presented in [57]. A cinema with 174 seats contains 101 seated students whose initial positions are fixed. Two evacuation routes are available, through either exit A or exit B (Fig. 6.34). Everyone in the cinema is asked to act cautiously in order to avoid injuries. After the alarm is set off, the students begin to evacuate in function of their reaction time.

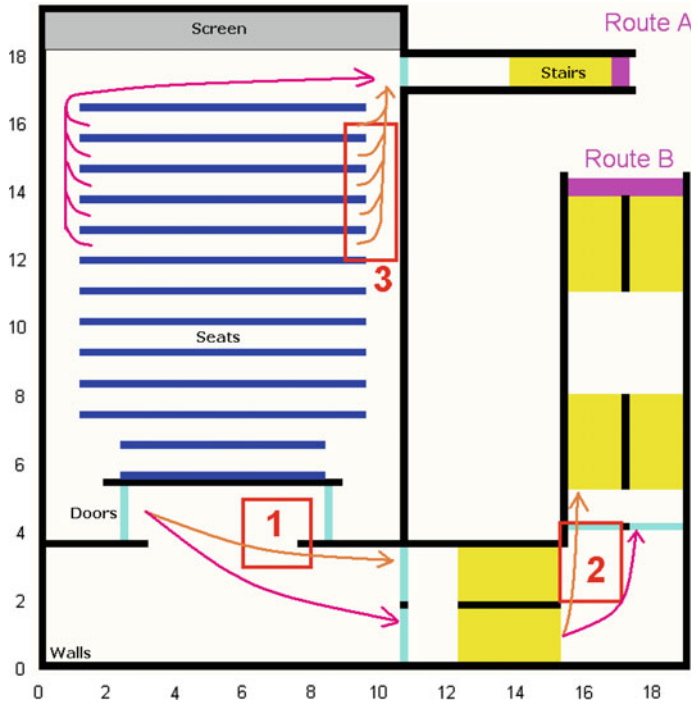

Fig. 6.34 Representation of the movie theater during a numerical simulation. Seats are portrayed as *blue*, walls as *black*, the movie screen as *gray*, the stairs as *yellow*, the doors as *cyan* and the exits as *magenta* (exit A at the *top* and exit B at the *bottom*). In function of the number of people in the *red rectangles* (the control zones numbered 1, 2 or 3), the moviegoers change from moving in the direction of the beige arrow to that of the *magenta arrow*

The evacuation times of the students are the results of this real-life evacuation exercise. The parameters used in the simulations are in accordance with the observations made in the exercise and are summarized in Table 6.7. Some of the parameters are uniformly distributed within a given interval.

One hundred numerical simulations are realized with the adapted NSM2 approach. This approach contains both the interior acceleration and socio-psychological forces presented in Sect. 6.7.1. To evacuate, the pedestrians use the shortest route. Several control zones are added in order to make the pedestrian movement more realistic and to avoid the appearance of areas of congestion (Fig. 6.34).

If the number of people is greater or equal to 5 in the first and second red rectangles, or greater or equal to 15 in the third, the other pedestrians move in the direction of the magenta arrow instead of that of the beige arrow.

Table 6.7 Evacuation of a movie theater—parameters used in the simulations (*uniformly distributed within the given interval)

Parameter		Symbol	Value	Unit
Pedestrian i	Speed*	$\|\mathbf{U}_{d,i}\|$	[1.2, 2]	$\mathrm{m} \cdot \mathrm{s}^{-1}$
	Speed when on stairs	$\|\mathbf{U}_{d,i}\|$	0.5	$\mathrm{m} \cdot \mathrm{s}^{-1}$
	Radius*	r_i	[0.2, 0.25]	m
	Mass*	m_i	[60, 100]	kg
	Response time*	$t_{r,i}$	[0, 4]	s
	Relaxation time*	τ_i	[0.1, 0.5]	s
Approach	Normal dissipation coefficient	K_N	10^5	kg
NSM2	Tangential dissipation coefficient	K_T	0	kg
Social force for student i	Amplitude of interaction	A_i	2000	N
	Range of repulsive interaction	B_i	0, 08	m
	Anisotropic character of interactions	Λ_i	0	
	Angle between $\mathbf{e}_{d,i}(t)$ and $-\mathbf{e}_{ij}$	φ_{ij}	90	Degree
	Time step	h	0.01	s

The response time is the time necessary for student i to begin evacuating after the start of the evacuation movement

An example of the progression of a numerical simulation is shown in Fig. 6.35 and can be watched at the following link (file evacuationMovieTheater.avi are available at https://ifsttar.libcast.com/mast-sdoa or at http://extras.springer.com).

The results of the real-life exercise and of the numerical simulations are summarized in Table 6.8. From the results summarized in the table, we can see there is practically no difference between the results from the experimental exercise and the results from the numerical simulations; or, at least, the differences are acceptable.

Figure 6.36 shows that the curve of the number of evacuated pedestrians in function of time, obtained from the numerical simulations, is very close to its counterpart from the real-life exercise.

Evacuation of an Elementary School

We next will apply the adapted NSM2 approach to an evacuation exercise in an elementary school, presented in [57]. This example demonstrates that it is possible to study a 3D problem while using a 2D approach. The building is composed of

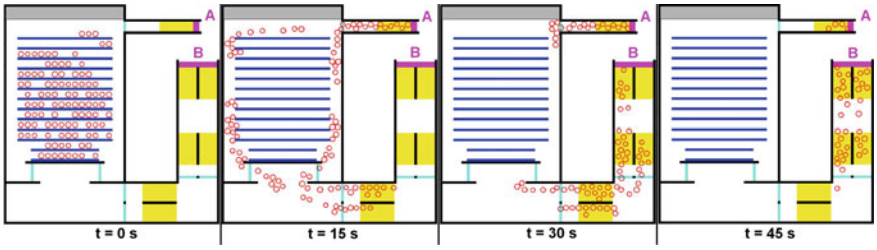

Fig. 6.35 Example of the progression of a numerical simulation at different times. The *red circles* represent the pedestrians

Table 6.8 Comparison between experimental exercise and numerical simulations for the evacuation of a movie theater

	Real-life exercise	Numerical simulations
Number of students	101	101
Number of seats	174	174
Number of simulations	1	100
Exit A		
Evacuation time (last person)	45 s	49.4 s
Average evacuation time	31.1 s	30.7 s
Exit B		
Evacuation time (last person)	66 s	62 s
Average evacuation time	53.1 s	48.6 s
Both exits		
Evacuation time (last person)	66 s	62 s
Average evacuation time	44 s	41.9 s

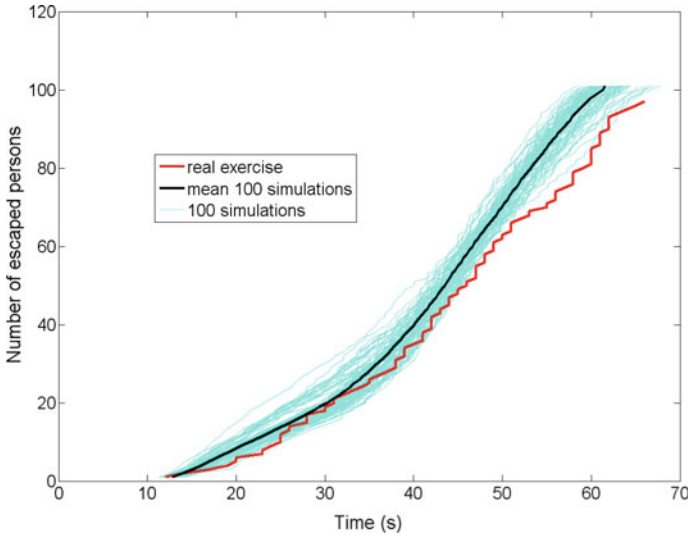

Fig. 6.36 Comparison between the results of the experimental exercise and the results of the numerical simulations: number of evacuated pedestrians as a function of time. The 100 numerical simulations are the *cyan-colored curves*, the average of these is the *black curve*, and the curve from the real exercise is in *red*

three floors and contains six classrooms, with a total of 130 pupils (from 6 to 10 years old). The initial number of people in each classroom is given in [57]. After the alarm is set off, the pupils begin the evacuation. Each class of pupils follows its respective teacher. Video footage is taken throughout the evacuation exercise and is used to determine the experimental results. To simulate this exercise, we propose the parameters summarized in Table 6.9. These parameters, meant to represent any given population, are obtained from [39, 57]. Some of these parameters are uniformly distributed within a given interval.

One hundred numerical simulations are made with the adapted NSM2 approach. This approach contains both the interior acceleration and socio-psychological forces presented in Sect. 6.7.1. To evacuate, the pedestrians use the shortest route. An example of the progression of such a numerical simulation is shown in Fig. 6.37 and can be watched on the following link (file evacuationPrimarySchool.avi are available at https://ifsttar.libcast.com/mast-sdoa or at http://extras.springer.com).

Figure 6.38 shows the curves of the number of evacuated pedestrians as a function of time, obtained from the results of the experimental exercise and from the average of the results of the numerical simulations. Since the parameters of the numerical simulations hold true for any standard population, the results of these simulations are very close to those obtained from the experimental exercise. One can notice that on the evacuation curve obtained from the exercise, the flow suddenly decreases at $t \simeq 38\,\text{s}$, then increases again after $t \simeq 48\,\text{s}$. This phenomenon (possibly a jam or

Table 6.9 Evacuation of an elementary school—parameters used in the simulations (*uniformly distributed in the given interval)

Parameter		Symbol	Value	Unit
Pedestrian i	Speed*	$\|\mathbf{U}_{d,i}\|$	[1.2, 2]	$\mathrm{m} \cdot \mathrm{s}^{-1}$
	Speed when on stairs	$\|\mathbf{U}_{d,i}\|$	[0.5, 1]	$\mathrm{m} \cdot \mathrm{s}^{-1}$
	Radius*	r_i	[0.2, 0.25]	m
	Mass*	m_i	[60, 100]	kg
	Response time*	$t_{r,i}$	[0, 10]	s
	Relaxation time*	τ_i	[0.1, 0.5]	s
Approach	Normal dissipation coefficient	K_N	10^5	kg
NSM2	Tangential dissipation coefficient	K_T	0	kg
Social force for pedestrian i	Amplitude of interaction	A_i	2000	N
	Range of repulsive interaction	B_i	0, 08	m
	Anisotropic character of the interactions	Λ_i	0	
	Angle between $\mathbf{e}_{d,i}(t)$ and $-\mathbf{e}_{ij}$	φ_{ij}	90	Degree
	Time step	h	0.01	s

The response time is the time necessary for person i to begin evacuating after the start of the evacuation movement

back-up) is not reproduced by our model. One possible explanation is that the pupils become blocked at some part of the building, probably when two classes meet in the stairwell. The fact that the pupils are grouped next to their teacher could add to this blockage.

6.8.3 A Predictive Model

This section has the objective of demonstrating that the adapted *NSM*2 approach can be used to improve the service quality of a studied space. In the first study, we will look to see if the addition of a well-placed obstacle in front of a door can improve the service quality of its associated area. In the second study, we will seek to determine if the proposed crowd model can be used to locate in a considered space the zones that could give rise to pedestrian injury during an emergency evacuation. Finally, the

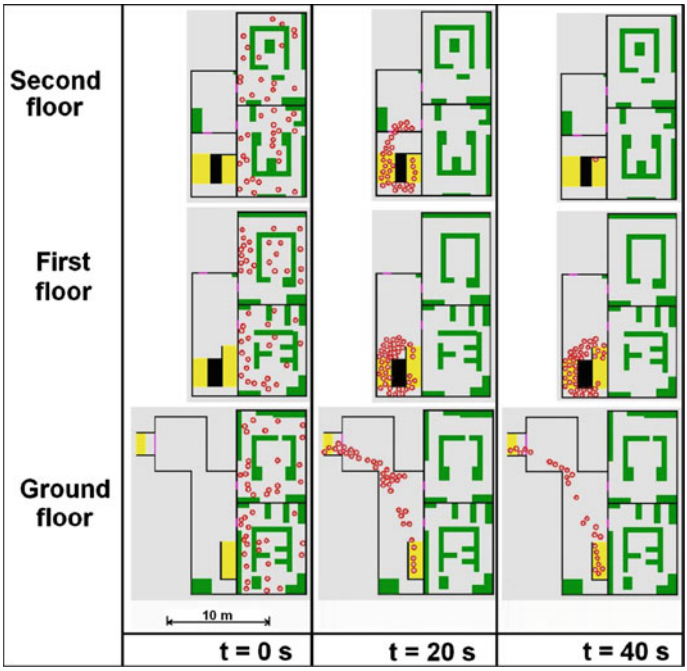

Fig. 6.37 Evacuation of an elementary school—example of the progression of a numerical simulation at different moments. The walls are represented by *black*, the obstacles by *green*, the stairs by *yellow*, the doors by *magenta* and the pedestrians by *red circles*

third study will concern the modeling of travelers switching from train to platform or vice versa. This study will propose a solution to facilitate the evacuation of train platforms.

Addition of an Obstacle in Front of a Door

Let us consider a crowd that wishes to evacuate a room via a narrow door. For these types of geometries, called bottlenecks, researchers pay close attention to clogging or blockage, an effect that can arise at or close to the door. Theoretically, human behaviour during panic situations leads to arching and clogging as shown in Fig. 6.2 or 6.39a, respectively. In normal situations, pedestrians don't rush toward the exit and a funnel shape is obtained rather than an arch (see Fig. 6.39b). Both phenomena can be watched on the following links (files clogging.avi and funnel.avi are available at https://ifsttar.libcast.com/mast-sdoa or at http://extras.springer.com).

Clogging results in a reduction in the efficiency of the evacuation and creates strong pressures within the backed-up crowd. One possible remedy for this problem would be to place an obstacle in front of the door, as Helbing [36] has experimentally tested. In [106], experimental results have been presented about the effect that an obstacle has in the granular flow through an orifice. Previous authors showed that if the position of the obstacle is properly selected, a dramatic decrease of the clogging

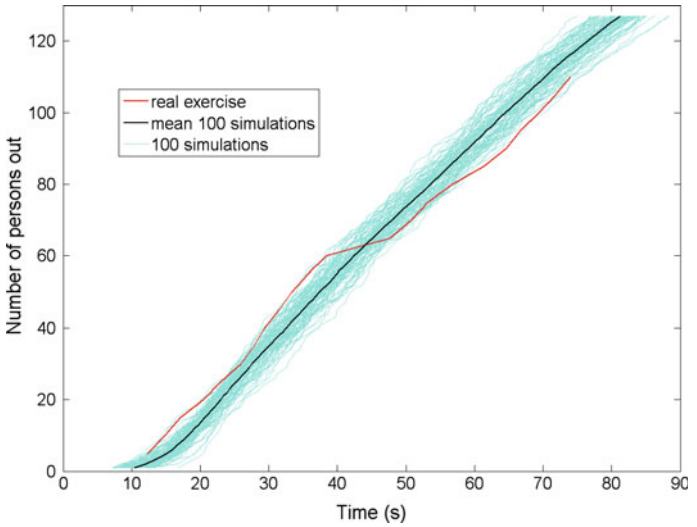

Fig. 6.38 Comparison between results from the real-life exercise and those from the numerical simulations: evacuation of an elementary school—number of evacuated people as a function of time. The *cyan curves* represent the 100 numerical simulations, the *black curve* the average of these simulations, and the *red curve* the experimental exercise

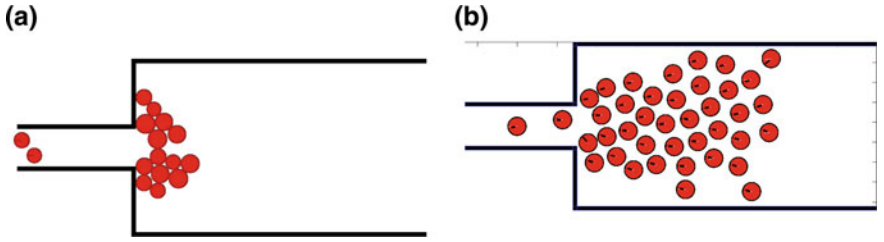

Fig. 6.39 Simulation of **a** an urgent and **b** a normal evacuation through a bottleneck

probability can be obtained. Interestingly, the clogging reduction effect is not caused by a net reduction of the flow rate, neither by a reduction of the density of particles at the very outlet. Instead, it is suggested that the introduction of an obstacle induces a strong reduction of the pressure above the outlet. This behaviour, which is proposed to be the one behind the clogging reduction, could have an analogy in the flow of crowds through bottlenecks, where it has been typically assumed that the main role of a column behind a door is to prevent straight motion of people towards the exit.

Continuing these considerations, in this section we will attempt to determine if our adapted *NSM*2 approach is able to model this type of problem and to show how a space's service quality can be improved during an emergency evacuation. Let us consider a 5 by 5 m square room that contains 20 people wishing to exit through a door 82 cm wide. In some of the simulations, an obstacle (for example, a pillar, etc.) will be placed in front of the exit.

Table 6.10 Evacuation of a square room with or without an obstacle—parameters used in the simulations (*uniformly distributed in the given interval)

Parameter		Symbol	Value	Unit
Pedestrian i	Speed*	$\|\mathbf{U}_{d,i}\|$	[1.2, 2]	$\mathrm{m} \cdot \mathrm{s}^{-1}$
	Radius*	r_i	[0.2, 0.25]	m
	Mass*	m_i	[60, 100]	kg
	Response time	$t_{r,i}$	0	s
	Relaxation time*	τ_i	[0.1, 0.5]	s
Approach	Normal dissipation coefficient	K_N	10^5	kg
NSM2	Tangential dissipation coefficient	K_T	0	kg
Obstacle	Position {not central, central}	p_1	{0, 0.41}	m
	Distance to the exit	p_2	{0.7, 0.9}	m
	Width (rectangle)	l_o	0.45	m
	Length (rectangle)	L_o	{0.45, 0.636, 0.8, 1}	m
	Diameter (circle)	D_o	{0.45, 0.636}	m
	Time step	h	0.01	s

The response time is the time necessary for pedestrian i to begin to evacuate after the setting off of the evacuation movement

The parameters used in the simulations are given in Table 6.10 and are uniformly distributed in their mentioned interval.

The flow rate J of people going through the exit was first calculated for every run. J (people/min) represents the number of pedestrians $\triangle N$, that passes a certain facility (in our case the narrow door) within a certain time interval $\triangle t$: $J = \frac{J}{b} = \frac{\triangle N}{\triangle t}$. The average flow rate J_{mean} of J is then obtained and determined by τ and the parameters of the obstacle (position, distance from the exit, form and size).

Numerical simulations are carried out using the adapted *NSM*2 approach, without introducing social forces. In emergency evacuation situations, pedestrians use the shortest path to evacuate. Several cases are simulated for different values of τ and varying positions, shapes and lengths of the rectangular obstacle that maintains a width of 0.45 m throughout the simulations (Fig. 6.40). Fifty simulations are executed for each position of the obstacle.

The values of J_{mean} for the different simulations are presented in Table 6.11.

According to these results, when τ varies from 0.5 to 0.1 s, the number of evacuated pedestrian increased considerably. Smaller values of τ indicate more aggressive pedestrians who do not hesitate to rush and quickly regain their desired speed after a collision. When $\tau = 0.1$ s and the obstacle is central ($p_1 = 0.41$ m), J_{mean} increases in relation to the dimensions of the obstacle. However, the evacuation of the pedestrians is only facilitated when the obstacle is close enough to the exit ($p_2 = 0.7$ m). On the other hand, when $\tau = 0.5$ s and the obstacle is far from the exit ($p_2 = 0.9$ m), the

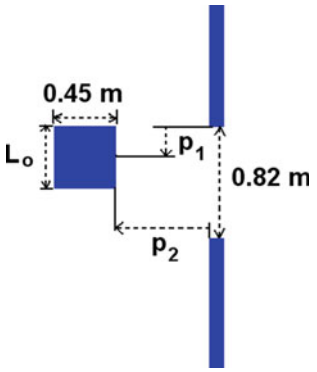

Fig. 6.40 Different positions of the obstacle in function of L_o, p_1 and p_2

Table 6.11 Evacuation of a square room with or without an obstacle—average flow J_{mean} (pedestrian/min) of pedestrians going through the door as a function of τ, p_1, p_2, obstacle's shape (rectangular or circular) and obstacle's size (L_o or D_o)

τ			0.1 s			0.5 s		
p_1			0.41 m		0 m	0.41 m		0 m
p_2			0.7 m	0.9 m	0.7 m	0.7 m	0.9 m	0.7 m
Q (ppl/min)	No obstacle		230	230	230	116	116	116
	Rectangular L_o	0.45 m	231	213	212	115	115	111
		0.636 m	247	217	206	109	116	107
		0.8 m	251	223	203	102	116	106
		1 m	264	222	200	101	112	106
	Circular D_o	0.45 m	202	222	222	112	114	110
		0.636 m	238	207	208	122	107	112

values of J_{mean} are practically the same with and without the obstacle; and when the obstacle is near the exit ($p_2 = 0.7$ m), there is no improvement in the quality of the evacuation service.

When the obstacle is not centered on the exit ($p_1 = 0$ m), in both cases $\tau = 0.1$ s and $\tau = 0.5$ s, J_{mean} decreases as the dimensions of the obstacle increase.

The simulations show that an obstacle centered near the exit increased J_{mean} in proportion to the length of the obstacle.

Numerical simulations have also been carried out with a circular obstacle. Depending on the values of the parameters τ, p_1, p_2, and D_o, the circular obstacle can increase the average flow of evacuating pedestrians J_{mean}, improving the evacuation process in some cases (e.g. $\tau = 0.1$ s, $p_1 = 0.41$ m, $p_2 = 0.7$ m, and $D_o = 0.636$ m). More research will need to be conducted to determine the optimal parameters τ, p_1, p_2, and L_o/D_o for a circular and rectangular obstacle.

Evacuation of a Room with Two Adjacent Exits

The goal of this section is to show that the proposed crowd model can be used to estimate the areas and pedestrians in a room that are subjected to strong pressure during an emergency evacuation. Human tolerance for pressures and forces depends on the amplitude, duration, direction, and location of the contact force. For example, receiving a slap to the face can briefly generate hundreds of g (acceleration of gravity) locally, but does not produce any real damage; however, constant application of 16 g for one minute can be fatal. The position, age, and health of the pedestrian may also affect their tolerance. Because of the large number of varying properties possessed by the contact force and the pedestrian, determining whether a collision between two pedestrians can result in an injury is a complex problem. Therefore, only the areas of the room where the contact percussion is at its highest during evacuation will be studied.

The evacuation of a room containing 500 people who want to evacuate through two adjacent exits is simulated; the distance between the two exits is 4 m. The parameters used in the simulation are summarized in Table 6.12.

Figure 6.41 presents an example of an evacuation simulation.

The formation of an arch as a function of the value of the contact percussion is observed in front of each exit. The pedestrians exiting are not under pressure in the doorway, as if they were being protected by other pedestrians. Similarly, the pedestrians the farthest from the exits cannot be injured because they are not subjected to strong pressures. The people trapped between the two exits by the two streams of evacuating pedestrians are subject to strong pressures. In this area, a pedestrian could be injured (area defined by green rectangle on Fig. 6.41).

Modeling Travellers Moving Between Platform and Subway Car

This application of the model is the result of a pre-project for the RATP (RATP is the large Paris public transportation company) aimed at reducing evacuation time of a subway car in subway stations with a single exit. This project suggests the instillation of flashing arrows in such stations that indicate the direction of the exit when the train is stopped and are completely invisible when turned off.

Table 6.12 Evacuation of a room with two adjacent exits - parameters used in the simulations (*uniformly distributed over the given interval)

Parameter		Symbol	Value	Unit
Pedestrian i	Desired speed*	$\|\mathbf{U}_{d,i}\|$	[1.2, 2]	$\mathrm{m} \cdot \mathrm{s}^{-1}$
	Radius*	r_i	[0.2, 0.25]	m
	Mass*	m_i	[60, 100]	kg
	Relaxation time*	τ_i	[0.1, 0.5]	s
Approach	Normal dissipation coefficient	K_N	10^5	kg
NSM2	Tangential dissipation coefficient	K_T	0	kg
	Time step	h	0.01	s

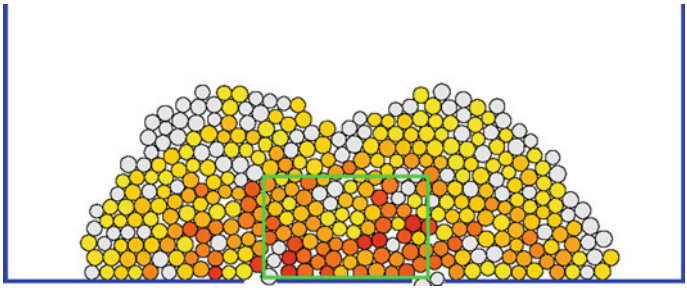

Fig. 6.41 Evacuation of a room with two adjacent exits—pedestrians are colored according to the value of the contact percussion: *gray* when the pedestrian is not in contact with anything in their immediate environment, and otherwise, a color spectrum from *yellow* to *red* as their contact percussion increases. The *green rectangle* is the area in which pedestrians could be injured

This system is supposed to decrease the amount of time commuters spend moving between train and platform, using the numerical analysis to optimize the device. It should be noted that estimating the flows of people in the stations and subway cars in real time would require comprehensive (appropriate) software, according to the RATP.

Two scenarios are considered: with and without the presence of the indication arrow. Two times are compared in the two scenarios considered: the time required for a pedestrian starting outside the subway car to board a subway car and the time required for the pedestrians starting inside the subway car to exit onto the platform.

We will consider one part of a platform and one subway car. To simulate the two scenarios, we use the parameters given in Table 6.13 to represent a standard population. Some parameters are uniformly distributed over the given interval.

Fifty numerical simulations of the two scenarios are carried out using the adapted *NSM*2 approach. For each simulation, the initial conditions are exactly the same for the two scenarios, i.e. 20 pedestrians want to enter into the subway car and 25 pedestrians out of the 34 randomly positioned in the car want to get out.

The two scenarios, with and without the indication arrow, proceed as follows:

* $0 \Rightarrow 10$ s: the subway car arrives and the indication arrow begins flashing.
* $10 \Rightarrow 15$ s: the indication arrow continues flashing as the pedestrians position themselves around the doors.
* 15 s: the doors open and pedestrians begin to exit the subway car, the pedestrians outside the car wait for the pedestrians inside to exit, allowing them to board.
* $15 \Rightarrow 20$ s: the indication arrow remains illuminated.
* 20 s: if the pedestrians have not finished exiting the subway car, the people outside the car force their entry.

Table 6.13 Modeling travellers moving between platform and subway car- parameters used in the simulations (*uniformly distributed over the given interval); the response time is the time necessary for pedestrian i to begin to evacuate after the start of the evacuation

Parameter		Symbol	Value	Unit
Pedestrian i	Desired speed*	$\|\mathbf{U}_{d,i}\|$	[1.2, 1.5]	$\mathrm{m} \cdot \mathrm{s}^{-1}$
	Speed when on stairs	$\|\mathbf{U}_{d,i}\|$	0.5	$\mathrm{m} \cdot \mathrm{s}^{-1}$
	Radius*	r_i	[0.2, 0.25]	m
	Mass*	m_i	[60, 100]	kg
	Response time*	$t_{r,i}$	0	s
	Relaxation time*	τ_i	[0.1, 0.5]	s
Approach	Normal dissipation coefficient	K_N	10^5	kg
*NSM*2	Tangential dissipation coefficient	K_T	0	kg
Social force for the pedestrian i	Strength of the interaction	A_i	2000	N
	Range of repulsive interaction	B_i	0, 08	m
	Anisotropic character of the interactions	Λ_i	0	
	Angle between $\mathbf{e}_{d,i}(t)$ and $-\mathbf{e}_{ij}$	φ_{ij}	90	degree
	Time step	h	0.01	s

Once the pedestrians have reached the yellow tactile strip:

* With the indication arrow: the pedestrians move randomly amongst themselves for 0.5 s (standard reaction time) before heading towards the exit to the right of the platform.
* Without the indication arrow: the pedestrians move randomly amongst themselves for 3 s (standard reaction time + looking for the exit), slowing down to look for the exit before heading towards the exit to the right of the platform.

An example simulation of a platform/subway car exchange with and without an indication arrow is represented in Fig. 6.42 and can be watched at the following link (files metro_with_arrow.mp4 and metro_without_arrow.mp4 are available at https://ifsttar.libcast.com/mast-sdoa or at http://extras.springer.com). The dimensions of the car are the same as those of RATP cars. The people in blue are men, and those in pink are women. Once a person has found the exit of the platform, they will be colored in beige.

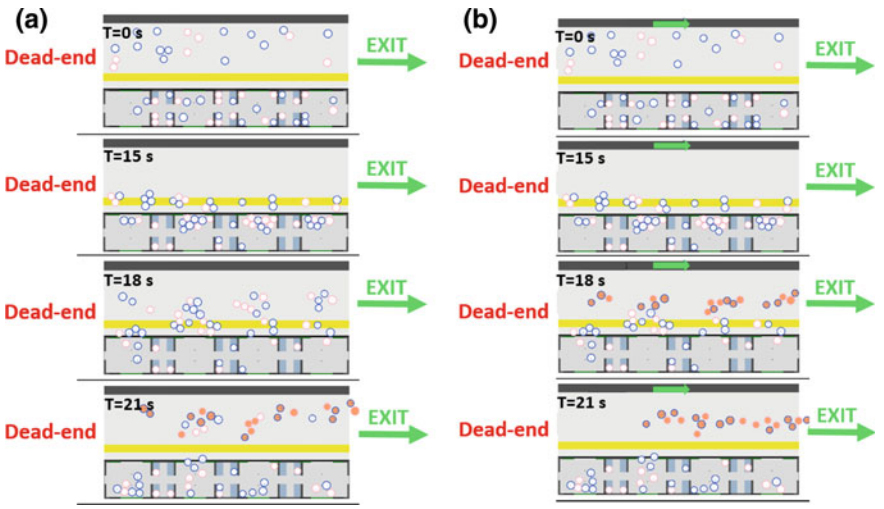

Fig. 6.42 Example of a simulation of a platform/subway car exchange **a** without and **b** with indication *arrow*

Table 6.14 Results of the simulations of a platform/subway car exchange with and with indication arrow

	Average time for the last pedestrian to enter the subway car (s)	Average time for the last pedestrian to reach the exit to the right of the platform (s)
Scenario without the indication arrow	≃21.5	≃31
Scenario with the indication arrow	≃21.5	≃28.5

The results obtained from the simulations of a platform/subway car exchange for the two scenarios are summarized in Table 6.14.

The presence of the blue arrow does not change the speed of the pedestrians boarding the subway car, but does help pedestrians exiting the subway car evacuate the platform.

Modeling Subgroup Movement

The adapted *NSM*2 approach is currently used to model the sub-group movement. The specific instances of counter-current movement by several sub-groups have been filmed. The video clips were chosen from [95]. Parameters such as the number of people, the number of sub-groups and the physical considerations were recorded. Situations in which members of sub-groups walking against the flow of pedestrian traffic, in groups of 2 to 4 people, have had to take evasive, measures have been selected.

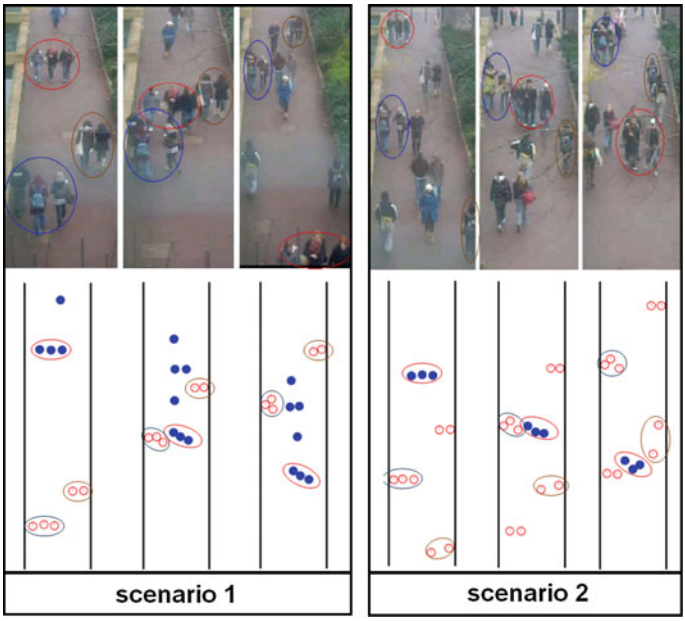

Fig. 6.43 Modeling sub-group movement in a crowd of pedestrians- Comparison between video sequences and numeric simulations. Corresponding sub-groups are circled in the same color

The selected situations are reproduced with the proposed crowd movement model. The simulations are also performed with the Singh sub-group model [95]. The values of the parameters are: $d_{l,f} = 0.7\,\text{m}$, $\varphi_{l,f} = \pm\frac{\pi}{2}$ and $k_{sgr} = 0.15\,\text{s}^{-1}$ [72, 95].

Two simulated scenarios are presented in Fig. 6.43. Our results correlate strongly with the videos and digital simulations. For more details, see [79].

Conclusions

The 2D model based on the theory developed by Michel Frémond and adapted to crowd movement showed its efficacy in treating collisions between pedestrians and in estimating the time and flow of pedestrians to evacuate in an emergency situation, [54]. Thanks to its mechanical formulation using the principle of virtual work and the treatment of collisions by means of non smooth mechanics, this model has proved to correctly represent a wide variety of behaviors (elastic and inelastic collisions with rebound or not, pedestrians holding hands, etc.). However, in urgent evacuations or even highly dense events, it is important to evaluate the pressure applied to the pedestrians' bodies in congested areas. This allows us to test measures and solutions aimed at preventing the pressure from reaching fatal levels. In order to achieve this, the particles representing pedestrians must be rendered deformable. This subject is currently in progress.

Whereas in high density crowds collisions are inevitable, in a sparse crowd pedestrians don't appreciate the contact and prefer to avoid touching and maintain a personal space. Our model must be then improved, in order to be consistent with the experimental observations.

Different approaches for avoidance behaviors are addressed in [53]. In the cognitive approach, a pedestrian can assess the remaining distance to the first possible collision and the global distance to destination. Then by assessing the two distances he/she dodges possible collisions (without any effect on neighboring individuals) while minimizing the traversed distance to destination. As for the social repulsive force, its interest lies in modeling pushing or aggressive behaviour. A combination of the two approaches seems to be of interest in certain applications such as in railway stations especially during alighting/boarding processes. The 2D model was recently used in a study aimed at estimating the train dwell time (the time a train spends at a scheduled stop) at the RER-A Noisy Champs station (RER-A is the line A of the Réseau Express Régional) have been investigated for a given demand of boarding and alighting passengers, [66]. Two simulations of about 30 pedestrians passing through the turnstiles and about 50 pedestrians boarding and alighting the train can be watched at the following links (files tourniquet.avi and NoisyChamp.avi are available at https://ifsttar.libcast.com/mast-sdoa or at http://extras.springer.com). This study has been a part of evaluating public transport in the Île-de-France region. With a rising demand for public transport, it has become crucial to assess the design of pedestrian areas in the region's railway and transfer stations as well as the impact of changes in the timetables of public transit systems. This is one of the objectives of the Grand Paris project that aims to modernize the existing transport network, to improve residents quality of life, and build a sustainable city.

References

1. Antonini, G., Bierlaire, M., Weber, M.: Simulation of pedestrian behavior using a discrete choice model calibrated on actual motion data. In: 4th Swiss Transport Research Conference. Monte Verita, Ascona, Switzerland (2004)
2. Allen, M.P., Tildesley, D.J.: Computer Simulation of Liquids. Oxford University Press, Oxford (1987)
3. Argoul, P., Pécol, P., Cumunel, G., Erlicher, S.: A discrete crowd movement model for holding hands pedestrians. In: EUROMECH - Colloquium 548, Direct and Variational Methods for Nonsmooth Problems in Mechanics, 24–26 June 2013
4. Apel, M.: Simulation of pedestrian flows based on the social force model using the verlet link cell algorithm. Ph.D. thesis, Poznan University of Technology (2004)
5. Aveni, A.: The not-so-lonely crowd: friendship groups in collective behaviour. Sociometry **40**(1), 96–99 (1977)
6. Bellomo, N., Coscia, V., Delitala, M.: On the mathematical theory of vehicular traffic flow I. fluid dynamic and kinetic modelling. Math. Models Methods Appl. Sci. **12**(12), 1801–1843 (2002)
7. Bernicot, F., Lefebvre-Lepot, A.: Existence results for non-smooth second order differential inclusions, convergence result for a numerical scheme and application to the modelling of inelastic collisions. Confluentes Mathematici **2**, 445–471 (2010)

8. Blue, V., Adler, J.: Cellular automata microsimulation of bi-directional pedestrian flows. J. Transp. Res. Board **1678**, 135–141 (2000)
9. Bodgi, J.: Synchronisation piétons-structure: application aux vibrations des passerelles souples. Ph.D. thesis, École nationale des Ponts et Chaussées (2008)
10. Bodgi, J.: Synchronization piétons-passerelle: modèle macroscopique et étude analytique. In: Proceedings of 27^{émes} rencontres de l' AUGC, Saint Malo, France(2009)
11. Bruneel, H.C.J., De Rycke, I.: Quicktrace: a fast algorithm to detect contact. Int. J. Numer. Methods Eng. **54**(2), 299–316 (2002)
12. Bovy, P.H.L., Stern, E.: Route Choice: Wayfinding in Transport Networks, vol. 9. Kluwer Academic Publishers, Dordrecht (1990)
13. Bruno, L., Venuti, F.: Crowd-structure interaction in footbridges: modelling, application to a real case-study and sensitivity analyses. J. Sound Vib. **323**, 475–493 (2009)
14. Caselli, F., Frémond, M.: Collisions of three balls on a plane. Comput. Mech. **43**(6), 743–754 (2009)
15. Camazine, S., Franks, N.R., Sneyd, J., Bonabeau, E., Deneubourg, J.L., Theraula, G.: Self-Organization in Biological Systems. Princeton University Press, Princeton (2001)
16. Cheung C.Y., Lam W.H.K.: Pedestrian route choices between escalator and stairway in MTR stations, J. Transp. Eng. **124**(3), 277–285 (1998)
17. Cholet, C.: Chocs de solides rigides. Ph.D. thesis, Université Pierre et Marie Curie, Paris (1998)
18. Cholet, C.: Collision d'un point et d'un plan. C. R. Acad. Sci. Paris **328**, 455–458 (1999)
19. Chrisochoides, N., Nave, D.: Parallel Delaunay mesh generation kernel. Int. J. Numer. Methods Eng. **58**, 161–176 (2003)
20. Ciarlet, P.: Introduction to Numerical Linear Algebra and Optimisation. Cambridge University Press, Cambridge (1989)
21. Cundall, P.A.: A computer model for simulating progressive large scale movements of blocky rock systems. In: Proceedings of the Symposium of the International Society of Rock Mechanics, vol. 2, pp. 129–136. Nancy, France (1971)
22. Cundall, P.A., Strack, O.D.L.: A discrete numerical model for granular assemblies. Geotechnique **29**(1), 47–65 (1979)
23. Daamen, W.: Modelling passenger flows in public transport facilities. Ph.D. thesis, Technische Universiteit Delft (2004)
24. Dal Pont, S., Dimnet, E.: A theory for multiple collisions of rigid solids and numerical simulation of granular flow. Int. J. Solids Struct. **43**(20), 6100–6114 (2006)
25. Dal Pont, S., Dimnet, E.: Theoretical approach to instantaneous collisions and numerical simulation of granular media using the A-CD2 method. Appl. Math. Comput. Sci. Berkeley **3/1**, 1–24 (2008)
26. Dimnet, E.: Collisions de solides déformables. Ph.D. thesis, École nationale des Ponts et Chaussées (2002)
27. Duives, D.C., Daamen, W., Hoogendoorn, S.P.: State-of-the-art crowd motion simulation models. Transp. Res. Part C - Emerg. Technol. **37**, 193–209 (2013)
28. Ericson, C.: Real Time Collision Detection. Morgan Haufmann Publishers, San Francisco (2004)
29. Feng, Y.T., Han, K., Owen, D.R.J.: Filling domains with disks: an advancing front approach. Int. J. Numer. Methods Eng. **56**(5), 699–713 (2003)
30. Fortin, J., Coorevits, P.: Selecting contact particles in dynamics franular mechanics systems. In: ACOMEN, Liège, 28–31 May 2002
31. Frémond, M.: Rigid bodies collisions. Phys. Lett. A **204**, 33–41 (1995)
32. Frémond, M.: Collisions, Edizioni del Dipartimento di Ingegneria Civile dell'Université di Roma Tor Vergata (2007)
33. Fruin, J.J.: Designing for pedestrians: a level of service concept. Highw. Res. Rec. **355**, 1–15 (1971)
34. Guy, Y.: Pedestrian route choice in central Jerusalem. Technical report, Department of Geography, Ben-Gurion University of The Negev, Beer Sheva (1987)

35. Hartmann, D., Hasel, P.: Efficient dynamic floor field methods for microscopic pedestrian crowd simulations. Commun. Comput. Phys. **16**(1), 264–286 (2014)
36. Helbing, D.: Traffic and related self-driven many-particle systems. Rev. Mod. Phys. **73**, 1067–1141 (2002)
37. Helbing, D., Molnar, P.: Social force model for pedestrian dynamics. Phys. Rev. E **51**(5), 4282–4286 (1995)
38. Helbing, D., Molnar, P.: Self-organization phenomena in pedestrian crowds. arXiv:cond-mat/9806152 [cond-mat.stat-mech], pp. 569–577 (1998)
39. Helbing, D., Farkas, I., Vicsek, T.: Simulating dynamic features of escape panic. Nature **407**, 487–490 (2000)
40. Helbing, D., Farkas, I., Molnar, P., Vicsek, T.: Simulation of pedestrians crowds in normal and evacuation situations. In: Schreckenberg, M., Deo Sarma, S. (eds.) Pedestrian and Evacuation Dynamics, pp. 21–58. Springer, Berlin (2002)
41. Helbing, D., Isobe, M., Nagatani, T., Takimoto, K.: Lattice gas simulation of experimentally studied evacuation dynamics. Phys. Rev. E **67**, 067101 (2003)
42. Helbing, D., Buzna, L., Johansson, A., Werner, T.: Self-organized pedestrian crowd dynamics: experiments, simulations, and design solutions. Transp. Sci. **39**, 1–24 (2005)
43. Henderson, L.F.: The statistics of crowd fluids. Nature **229**, 381–383 (1971)
44. Heylighen, F.: The science of self-organization and adaptivity. Encycl. Life Support Syst. **5**(3), 253–280 (2001)
45. Hill, M.R.: Spatial structure and decision-making of pedestrian route selection through an urban environment. Ph.D. thesis, University of Nebraska, Lincoln (1982)
46. Hoogendoorn, S.P.: Normative pedestrian behaviour theory and applications. Technical Report CTvk2001.002, Delft University of Technology (2001)
47. Hoogendoorn, S.P.: Walker behaviour modelling by differential games. In Proceedings of the Computational Physics of Transport and Interface Dynamics Seminar. Springer (2002)
48. Hoogendoorn, S.P., Bovy, P.H.L.: Pedestrian route-choice and activity scheduling theory and models, Trans. Res. B **38**, 169–190 (2004)
49. Hoogendoorn, S.P., Daamen, W.: Self-organization in pedestrian flow. In: Hoogendoorn, S.P., Luding, S., Bovy, P.H.L., Schreckenberg, M., Wolf, D.E. (eds.) Traffic and Granular Flow 03, pp. 373–382. Springer, Berlin (2005)
50. Hoogendoorn, S.P., Bovy, P.H.L., Daamen, W.: Microscopic pedestrian wayfinding and dynamics modelling. In: Schreckenberg, M., Sharma, S.D. (eds.) Pedestrian and Evacuation Dynamics, pp. 123–154. Springer, Berlin (2001)
51. Hughes, R.L.: A continuum theory for the flow of pedestrians. Transp. Res. Part B: Methodol. **36**, 507–535 (2002)
52. Hughes, R.L.: The flow of human crowds. Annu. Rev. Fluid Mech. **35**, 169–182 (2003)
53. Kabalan, B.: Crowd dynamics: modeling pedestrian movement and associated generated forces. Ph.D. thesis, Université Paris-Est, Champs-sur-Marne, France (2016)
54. Kabalan, B., Argoul, P., Cumunel, G., Erlicher, S., Christoforou, Z.: A 2D discrete crowd movement model: pedestrian dynamics - crowd-structure interaction. In: Final Conference COST Committee TU 1004: Public Transport Passenger Flows in the Era of ITS, 5 (2005)
55. Kabalan, B., Argoul, P., Erlicher, S.: Crowd-structure interaction in laterally vibrating footbridges: comparison of two fully coupled approaches. In: Proceedings of Footbridge: 5th International Conference - Footbridges: Past, Present and Future. Imperial College, London (2014)
56. Kirchner, A., Klüpfel, H., Nishinari, K., Schadschneider, A., Schreckenberg, M.: Simulation of competitive egress behavior: comparison with aircraft evacuation data. Phys. A **324**, 689–697 (2003)
57. Klüpfel, H.L.: A cellular automaton model for crowd movement and egress simulation. Ph.D. thesis, Universität Duisburg - Essen (2003)
58. Kimmel, R., Sethian, J.A.: Fast marching methods for computing distance maps and shortest paths. Technical report 669, CPAM, University of California, Berkeley (1996)

59. Lai, G., Wong, O.: The tie effect on information dissemination: the spread of a commercial rumor in Hong Kong. Soc. Netw. **24**, 49–75 (2002)
60. Lakoba, T.I., Finkelstein, N.M.: Modifications of the Helbing-Molnàr-Farkas-Vicsek social force model for pedestrian evolution. Simulation **81**(5), 339–352 (2005)
61. Langston, P.A., Masling, R., Asmar, B.N.: Crowd dynamics discrete element multi-circle model. Saf. Sci. **44**, 395–416 (2006)
62. Liggett, T.M.: Stochastic interacting systems: contact, voter and exclusion processes. Fundamental Principles of Mathematical Sciences, vol. 324. Springer, Berlin (1999)
63. Maury, B.: A time-stepping scheme for inelastic collisions. Numerische Mathematik **102**(4), 649–679 (2006)
64. Maury, B., Venel, J.: A discrete contact model for crowd motion. ESAIM: Math. Model. Numer. Anal. **45**, 145–168 (2011). doi:10.1051/m2an/2010035
65. Milazzo, J.S., Rouphail, N.M., Hummer, J.E., Allen, D.P.: The effect of pedestrians on the capacity of signalized intersections. Transp. Res. Rec. J. Transp. Res. Board **1646**, 37–46 (1998)
66. Mokhtary, S., Christoforou, Z., Leurent, F., Kabalan, B., Argoul, P., Cumunel, G.: Crowd dynamics and pedestrian trajectories in public transit, Railway Stations and Urban Integration. In: 5th Next Station Congress. Marrakech, Morocco (2015)
67. Moreau, J.J.: Décomposition orthogonale d'un espace hilbertien selon deux cônes mutuellement polaires. C. R. Acad. Sci. Paris Ser. I **255**, 238–240 (1962)
68. Moreau, J.J.: Sur les lois de frottement, de viscosité et de plasticité. C. R. Acad. Sci. Paris **271**, 608–611 (1970)
69. Moreno, Y., Pastor-Satorras, R., Vespignani, A.: Epidemic outbreaks in complex heterogeneous networks. Eur. Phys. J. B **26**, 521–529 (2002)
70. Moussaïd, M.: Étude expérimentale et modélisation des déplacements collectifs de piétons. Ph.D. thesis, Université Toulouse III, Paul Sabatier (2010)
71. Moussaid, M., Helbing, D., Theraulaz, G.: How simple rules determine pedestrian behavior and crowd disasters. Proc. Natl. Acad. Sci. USA (PNAS) **108**, 6884–6888 (2011)
72. Moussaïd, M., Perozo, N., Garnier, S., Helbing, D., Theraulaz, G.: The walking behaviour of pedestrian social groups and its impact on crowd dynamics. PLoS ONE **5**(4), e10047 (2010). doi:10.1371/journal.pone.0010047
73. Muth, B., Müller, M.K., Eberhard, P., Luding, S.: Collision detection and administration methods for many particles with different sizes. In: 4th International Conference on Discrete Element Methods, Brisbane, Australia (2007)
74. Newman, M.E.J.: Spread of epidemic disease on networks. Phys. Rev. E **66**, 016128 (2002)
75. Paris, S.: Characterisation of levels of services and modelling of flows of people inside exchange areas. Ph.D. thesis, Université de Rennes 1 (2007)
76. Parisi, D.R., Dorso, C.O.: Microscopic dynamics of pedestrian evacuation. Phys. A **354**, 606–618 (2005)
77. Parisi, D.R., Dorso, C.O.: Morphological and dynamical aspects of the room evacuation process. Phys. A **385**, 343–355 (2007)
78. Parisi, D.R., Gilman, M., Moldovan, H.: A modification of the social force model can reproduce experimental data of pedestrian flows in normal conditions. Phys. A **388**, 3600–3608 (2009)
79. Pécol, P.: Modélisation 2D discrète du mouvement des piétons - Application à l'évacuation des structures du génie civil et à l'interaction foule-passerelle. Ph.D. thesis, Université Paris-Est, Champs-sur-Marne, France (2011)
80. Pécol, P., Dal Pont, S., Erlicher, S., Argoul, P.: Modelling crowd-structure interaction, Mécanique and industries. EDP Sci. **11**(6), 495–504 (2010)
81. Pécol, P., Dal Pont, S., Erlicher, S., Argoul, P.: Discrete approaches for crowd movement modelling. Eur. J. Comput. Mech. **20**(1–4), 189–206 (2011)
82. Pécol, P., Dal Pont, S., Erlicher, S., Argoul, P.: Smooth/non-smooth contact modeling of human crowds movement: numerical aspects and application to emergency evacuations. Ann. Solid Struct. Mech. **2**(2–4), 69–85 (2011)

83. Pécol, P., Dal Pont, S., Erlicher, S., Bodgi, J., Argoul, P.: A 2D discrete model for crowd-structure interaction. In: Proceedings of the Fourth International Conference Footbridge. Wroclaw, Poland 6–9 July (2011)
84. Pécol, P., Argoul, P., Dal Pont, S., Erlicher, S.: The non smooth view for contact dynamics by Michel Frémond extended to the modeling of crowd movements. AIMS, Discret. Contin. Dyn. Syst. Ser. S **6**(2), 547–565 (2013)
85. Pelechano, N., Addler, J.M., Badler, N.I.: Controlling individual agents in high-density crowd simulation. In Proceedings of the 2007 ACM SIGGRAPH/Eurographics Symposium on Computer Animation, pp. 99–108 (2007)
86. Perkins, E., Williams, J.R.: A fast contact detection algorithm insensitive to object sizes. Eng. Comput. **18**(1/2), 48–61 (2001)
87. Piccoli, B., Tosin, A.: Pedestrian flows in bounded domains with obstacles. Contin. Mech. Thermodyn. **21**, 85–107 (2009)
88. Piccoli, B., Tosin, A.: Time-evolving measures and macroscopic modeling of pedestrian flow. Arch. Ration. Mech. Anal. **199**, 707–738 (2011)
89. Pikovsky, A., Rosenblum, M., Kurths, J.: Synchronization - A Universal Concept in Nonlinear Sciences, Series 12. Cambridge University Press, Cambridge (2001)
90. Reynolds, C.: Flocks, herds, and schools: a distributed behavioral model. Comput. Graph. **21**, 25–34 (1987)
91. Schinner, A.: Fast algorithms for the simulations of polygonal particles. Granul. Matter **2**(1), 35–43 (1999)
92. Senevarante, P.N., Morall, J.F.: Analysis of factors affecting the choice of route of pedestrians. Transp. Plan. Technol. **10**, 147–159 (1986)
93. Simo, J.C., Hughes, T.J.R.: Elastoplasticity and Viscoplasticity Computational Aspects. Springer, Berlin (1996)
94. Simo, J.C., Hughes, T.J.R.: Computational Inelasticity. Springer, Berlin (1998)
95. Singh, H., Arter, R., Dodd, L., Drury, J.: Modelling subgroup behavior in crowd dynamics dem simulation. Appl. Math. Model. **33**, 4408–4423 (2009)
96. Song, W.-G., Yu, Y.-F., Wang, B.-H., Fan, W.-C.: Evacuation behaviors at exit in CA model with force essentials: a comparison with social force model. Phys. A **371**, 658–666 (2006)
97. Still, G.K.: Crowd dynamics. Ph.D. thesis, University of Warwick, Department of Mathematics (2000)
98. Strogatz, S., Abrams, D., McRobie, A., Eckhardt, B., Ott, E.: Theoretical mechanics: crowd synchrony on the Millennium Bridge. Nature **438**, 43–44 (2005)
99. Tavares, D.L.M., Comba, J.L.D.: Broad-phase collision detection using Delaunay triangulation. Technical report, Universidade Federal do Rio Grande do Sul (2007)
100. Timmermans, H., Vanderhagen, X., Borgers, A.: Transportation systems, retail environments and pedestrian trip chaining behaviour: modelling issues and applications. Transp. Res. Part B **26**, 45–59 (1992)
101. Venel, J.: Modélisation mathématique des mouvements de foule. Ph.D. thesis, Laboratoire de Mathématiques, Université Paris XI, Orsay, France (2008)
102. Wassgren, C., Sarkar, A.: PSL DEM lecture 11: coarse contact detection, https://pharmahub.org/resources/255 (2008)
103. Yamamoto, K., Kokubo, S., Nishinari, K.: Simulation for pedestrian dynamics by real-coded cellular automata (RCA). Phys. A **379**, 654–660 (2007)
104. Yue, H., Hao, H., Chen, X., Shao, C.: Simulation of pedestrian flow on square lattice based on cellular automata model. Phys. A **384**, 567–588 (2007)
105. Zhao, D., Yang, L., Li, J.: Exit dynamics of occupant evacuation in an emergency. Phys. A **363**, 501–511 (2006)
106. Zuriguel, I., Janda, A., Garcimartìn, A., Lozano, C., Arévalo, R., Maza, D.: Silo clogging reduction by the presence of an obstacle. Phys. Rev. Lett. **107**, 278001–278005 (2011)

Chapter 7
Collisions of Deformable Solids

Michel Frémond

7.1 Introduction

Let us consider a piece of ice colliding with a warm soil. As seen in Chap. 3 when assuming collisions of two points, the dissipative work produces an increase of the temperatures. In the dimension three solids we are considering, the work is mostly dissipated on the colliding contact surface and in its neighbourhood. Thus the temperature discontinuity is more important in this zone and some melting may occur there and not elsewhere. In this Chapter, collisions of deformable solids are investigated together with the possible resulting phase changes. There are volume discontinuities of velocity and volume temperature discontinuities. In the collisions, there are also instantaneous evolutions of the volume fractions β_i. They result from the very fast motions at the microscopic level due to the very fast evolutions of the temperatures, [6–8]. Thermal evolutions are instantaneous and there may be instantaneous phase changes. Thus there are discontinuities of the volume fractions

$$[\beta_i] = \beta_i^+ - \beta_i^-, \tag{7.1}$$

in the solids which occupy domains $\Omega_1(t) = \Omega_1$ and $\Omega_2(t) = \Omega_2$ at collision time t. We introduce percussions related to volume velocity discontinuities and percussions works and percussion work fluxes related to phase volume fraction discontinuities.

We assume the contact surface of the colliding solids is conformal, i.e., it has a nonzero Lebesgue measure.

7.2 The Principle of Virtual Work

Let virtual macroscopic velocities, $\mathbf{V} = (\mathbf{V}_1, \mathbf{V}_2)$ and virtual volume fraction velocities $\gamma = (\gamma_1, \gamma_2)$. The actual velocities are $\mathbf{U} = (\mathbf{U}_1, \mathbf{U}_2)$ and $\dot{\beta} = (\dot{\beta}_1, \dot{\beta}_2)$. They have values before collision denoted with exponent $^-$ and values after collision

M. Frémond, *Collisions Engineering: Theory and Applications*,
Springer Series in Solid and Structural Mechanics 6,
DOI 10.1007/978-3-662-52696-5_7

denotes with exponent $^+$. We denote also $\mathsf{D}(\mathbf{V}_1)$, $\mathsf{D}(\mathbf{V}_2)$, the usual strain rates and $\mathbf{D}_s(\mathbf{V}) = \mathbf{V}_2 - \mathbf{V}_1$ the gap velocity on the contact surface. Based on the developments of the previous Chapters, we define with these quantities collision velocities of deformation

$$\mathsf{D}(\frac{\mathbf{V}_1^+ + \mathbf{V}_1^-}{2}),\ \mathsf{D}(\frac{\mathbf{V}_2^+ + \mathbf{V}_2^-}{2}), \tag{7.2}$$

$$\mathbf{D}_s(\frac{\mathbf{V}^+ + \mathbf{V}^-}{2}), \tag{7.3}$$

$$\left[\gamma_1\right],\ \left[\gamma_2\right], \tag{7.4}$$

$$\mathbf{grad}\left[\gamma_1\right],\ \mathbf{grad}\left[\gamma_2\right]. \tag{7.5}$$

Each of them has an obvious mechanical meaning. For instance,

$$\left[\gamma_1\right](t), \tag{7.6}$$

is the atomic part of the volume fraction velocity

$$\frac{d\gamma_i}{dt}. \tag{7.7}$$

The virtual work of the interior percussion forces, is a linear function of the velocities of deformation, [6–8]

$$\mathcal{T}_{int}(\Omega_1 \cup \Omega_2, \mathbf{V}, \gamma) \tag{7.8}$$

$$= -\int_{\Omega_1} \Sigma_1 : \mathsf{D}(\frac{\mathbf{V}_1^+ + \mathbf{V}_1^-}{2}) d\Omega_1 - \int_{\Omega_2} \Sigma_2 : \mathsf{D}(\frac{\mathbf{V}_2^+ + \mathbf{V}_2^-}{2}) d\Omega_2 \tag{7.9}$$

$$- \int_{\partial\Omega_1 \cap \partial\Omega_2} \mathbf{R}_p \cdot \mathbf{D}_s(\frac{\mathbf{V}^+ + \mathbf{V}^-}{2}) d\Gamma \tag{7.10}$$

$$- \int_{\Omega_1} B_{p1}\left[\gamma_1\right] + \mathbf{H}_{p1} \cdot \mathbf{grad}\left[\gamma_1\right] d\Omega_1 - \int_{\Omega_2} B_{p2}\left[\gamma_2\right] + \mathbf{H}_{p2} \cdot \mathbf{grad}\left[\gamma_2\right] d\Omega_2\ , \tag{7.11}$$

It introduces the internal forces, contact percussions $\mathbf{R}_p$, percussion stresses Σ and, percussion works B_p, percussion work flux vectors $\mathbf{H}_p$.

The virtual work of the acceleration forces is

$$\mathcal{T}_{acc}(\Omega_1 \cup \Omega_2, \mathbf{V}, \gamma) = \int_{\Omega_1} \rho_1 [\mathbf{U}_1] \cdot \frac{\mathbf{V}_1^+ + \mathbf{V}_1^-}{2} d\Omega_1 + \int_{\Omega_2} \rho_2 [\mathbf{U}_2] \cdot \frac{\mathbf{V}_2^+ + \mathbf{V}_2^-}{2} d\Omega_2 .$$

Remark 7.1 The mass balance equations are

$$[\rho] = 0 .$$

When the material are incompressible, the incompressibility conditions are taken into account by the pseudo-potentials of dissipation introducing percussion pressures, [3, 9].

The exterior forces have the virtual work

$$\begin{aligned} \mathcal{T}_{ext}(\Omega_1 \cup \Omega_2, \mathbf{V}, \gamma) &= \int_{\Omega_1} \mathbf{F}_{p1} \cdot \frac{\mathbf{V}_1^+ + \mathbf{V}_1^-}{2} d\Omega_1 + \int_{\Omega_2} \mathbf{F}_{p2} \cdot \frac{\mathbf{V}_2^+ + \mathbf{V}_2^-}{2} d\Omega_2 \\ &+ \int_{\partial\Omega_1} \mathbf{T}_{p1} \cdot \frac{\mathbf{V}_1^+ + \mathbf{V}_1^-}{2} d\Gamma_1 + \int_{\partial\Omega_2} \mathbf{T}_{p2} \cdot \frac{\mathbf{V}_2^+ + \mathbf{V}_2^-}{2} d\Gamma_2 \\ &+ \int_{\Omega_1} A_1 \left[\gamma_1\right] d\Omega_1 + \int_{\Omega_2} A_2 \left[\gamma_2\right] d\Omega_2 \\ &+ \int_{\partial\Omega_1} a_1 \left[\gamma_1\right] d\Gamma_1 + \int_{\partial\Omega_2} a_2 \left[\gamma_2\right] d\Gamma_2 . \end{aligned}$$

We assume that the surface exterior percussions $\mathbf{T}_p$ are applied to the whole boundary of each solid (they can be equal to zero in some parts of the boundaries). The $\mathbf{F}_p$ are the volume exterior percussions. The A and a are the volume and surface percussion work provided by the exterior by electrical, radiative,…actions. The equations of motion results from the principle of virtual work

$$\forall \mathbf{V} , \forall \gamma , \mathcal{T}_{acc}(\Omega_1 \cup \Omega_2, \mathbf{V}, \gamma) = \mathcal{T}_{int}(\Omega_1 \cup \Omega_2, \mathbf{V}, \gamma) + \mathcal{T}_{ext}(\Omega_1 \cup \Omega_2, \mathbf{V}, \gamma) .$$

Different choices of the virtual velocities $\mathbf{V} = (\mathbf{V}_1, \mathbf{V}_2)$ and $\gamma = (\gamma_1, \gamma_2)$ give

$$\rho_1 [\mathbf{U}_1] = \mathrm{div}\Sigma_1 + \mathbf{F}_{p1} , \ -B_{p1} + \mathrm{div}\mathbf{H}_{p1} + A_1 = 0 , \text{ in } \Omega_1 , \tag{7.12}$$

$$\rho_2 [\mathbf{U}_2] = \mathrm{div}\Sigma_2 + \mathbf{F}_{p2} , \ -B_{p2} + \mathrm{div}\mathbf{H}_{p2} + A_2 = 0 , \text{ in } \Omega_2 , \tag{7.13}$$

$$\Sigma_1 \mathbf{N}_1 = \mathbf{R}_p + \mathbf{T}_{p1},\ \mathbf{H}_{p1} \cdot \mathbf{N}_1 = a_1,\ \text{on } \partial\Omega_1 \cap \partial\Omega_2,$$
$$\Sigma_2 \mathbf{N}_2 = -\mathbf{R}_p + \mathbf{T}_{p2}\ ,\ \mathbf{H}_{p2} \cdot \mathbf{N}_2 = a_2\ ,\ \text{on } \partial\Omega_1 \cap \partial\Omega_2,$$
$$\Sigma_1 \mathbf{N}_1 = \mathbf{T}_{p1},\ \mathbf{H}_{p1} \cdot \mathbf{N}_1 = a_1\ ,\ \text{on } \partial\Omega_1 \backslash (\partial\Omega_1 \cap \partial\Omega_2)\,,$$
$$\Sigma_2 \mathbf{N}_2 = \mathbf{T}_{p2}\ ,\ \mathbf{H}_{p2} \cdot \mathbf{N}_2 = a_2,\ \text{on } \partial\Omega_2 \backslash (\partial\Omega_1 \cap \partial\Omega_2)\,.$$

7.3 The First Law of Thermodynamics

As in Chap. 3, we define

$$[T_2] = T_2^+ - T_2^-,\ [T_1] = T_1^+ - T_1^-.$$

Those two quantities are analogous to the velocity dT/dt in a smooth evolution. They are the atomic parts of the temperature time derivatives. We define also

$$\underline{T}_2 = \frac{T_2^+ + T_2^-}{2},\ \underline{T}_1 = \frac{T_1^+ + T_1^-}{2},$$

in Ω_1 and Ω_2, and

$$\delta\underline{T} = \underline{T}_2 - \underline{T}_1,\ \Theta = \frac{T_2 + T_1}{2},\ [\Theta] = \Theta^+ - \Theta^- = \frac{[T_1] + [T_2]}{2},$$
$$\underline{T}_m = \frac{\underline{T}_2 + \underline{T}_1}{2} = \frac{\Theta^+ + \Theta^-}{2} = \frac{1}{4}\left(T_2^+ + T_1^+ + T_2^- + T_1^-\right),$$

in $\partial\Omega_1 \cap \partial\Omega_2$.

Quantity $\delta\underline{T}$ at point $\mathbf{x}_1 = \mathbf{x}_2 = \mathbf{x} \in \partial\Omega_1 \cap \partial\Omega_2$ is analogous to $\mathbf{grad}T$ in a smooth situation. The states quantities of the solids are $E_1 = (T_1, \beta_1, \mathbf{grad}\ \beta_1, \varepsilon_1)$ and $E_2 = (T_2, \beta_2, \mathbf{grad}\ \beta_2, \varepsilon_2)$, where the deformation ε are continuous in the collision. The state quantities of the contact surface are $E^{\pm} = \Theta$ on $\partial\Omega_1 \cap \partial\Omega_2$.

The evolutions of the two solids are described by

$$\Delta E_1^{\pm} = (\mathsf{D}(\frac{\mathbf{U}_1^+ + \mathbf{U}_1^-}{2}), [\beta_1]\,, \mathbf{grad}\,[\beta_1]\,, \mathbf{grad}\underline{T}_1) \text{ in } \Omega_1,$$
$$\Delta E_2^{\pm} = (\mathsf{D}(\frac{\mathbf{U}_2^+ + \mathbf{U}_2^-}{2}), [\beta_2]\,, \mathbf{grad}\,[\beta_2]\,, \mathbf{grad}\underline{T}_2) \text{ in } \Omega_2.$$

The evolution of the contact surface is describe by

$$\delta E^{\pm} = (\mathbf{D}_s(\frac{\mathbf{U}^+ + \mathbf{U}^-}{2}), \delta\underline{T}) \text{ on } \partial\Omega_1 \cap \partial\Omega_2\ .$$

The free energies of the two solids are $\Psi_1(E_1)$ and $\Psi_2(E_2)$. The structure of the expression of the work of the interior percussions leads us to introduce surface free energies, Ψ_{1s}, Ψ_{2s}.

Now let us consider the thermal effects. We focus on the basic problem, the collision of two solids. Thus the equations which are considered are relative to a collision which occurs at time t. For the sake of simplicity, time t is deleted from the formulas. Following our rules, the heat intakes are equal to the entropy intakes multiplied by the temperatures at which the entropies are received, either at temperature T^+ or at temperature T^-. Let $\mathcal{D}_1 \cup \mathcal{D}_2$ be a subdomain of $\Omega_1 \cup \Omega_2$. Let us denote $O_1 = \partial\Omega_1 \cap \partial\mathcal{D}_1$, $O_2 = \partial\Omega_2 \cap \mathcal{D}_2$, and $O = O_1 \cap O_2$. When the solids collide, we assume that each solid receives heat impulses from the other through local actions. The heat impulse received by subdomain $\mathcal{D}_1 \cup \mathcal{D}_2$ is

$$\begin{aligned}
\mathcal{Q}(\mathcal{D}_1 \cup \mathcal{D}_2) &= \int_{\mathcal{D}_1} \Sigma(T_1\mathcal{B}_1)d\Omega_1 + \int_{\mathcal{D}_2} \Sigma(T_2\mathcal{B}_2)d\Omega_2 \\
&+ \int_{\partial\mathcal{D}_1\setminus O} \Sigma(T_1 Q_{p1})d\Gamma_1 + \int_{\partial\mathcal{D}_1} \Sigma(T_1\mathcal{B}_{s1})d\Gamma_1 \\
&+ \int_{\partial\mathcal{D}_2\setminus O} \Sigma(T_2 Q_{p2})d\Gamma_2 + \int_{\partial\mathcal{D}_2} \Sigma(T_2\mathcal{B}_{s2})d\Gamma_2 \\
&= \int_{\mathcal{D}_1} \Sigma(T_1\mathcal{B}_1)d\Omega_1 + \int_{\mathcal{D}_2} \Sigma(T_2\mathcal{B}_2)d\Omega_2 \\
&+ \int_{\partial\mathcal{D}_1} \Sigma\left(T_1\left(Q_{p1} + \mathcal{B}_{s1}\right)\right)d\Gamma_1 + \int_{\partial\mathcal{D}_2} \Sigma\left(T_2\left(Q_{p2} + \mathcal{B}_{s2}\right)\right)d\Gamma_2 \\
&- \int_O \Sigma\left(T_1 Q_{p1} + T_2 Q_{p2}\right)d\Gamma \ ,
\end{aligned}$$

where $\Sigma(X) = X^+ + X^-$. The TQ_p's are the heat impulses supplied by contact action from the exterior of the system to the surfaces, and the $T\mathcal{B}_s$'s are the exterior surface heat impulses, for instance, sources due to a chemical rapid reaction (the heat $T\mathcal{B}_s$ is present everywhere in the preceding expression, whereas the heat supplied by the exterior TQ_p is absent from part $\partial\mathcal{D}_1 \cap \partial\mathcal{D}_2$ where there is no heat supplied from the exterior by contact). The $T\mathcal{B}$'s are the volume heat impulses received from the exterior. The functions TQ_p are defined on $\partial\Omega_1 \cap \partial\Omega_2$: they are the heat supplied by one solid to another one by contact (this property can be seen by choosing one of the subdomains $\mathcal{D}$ empty).

The structure of the expression of the work of the interior forces and the structure of the expression of the received heat lead us to assume surface internal energies e_s besides the volume internal energies. The energy balance of the subdomain $\mathcal{D}_1 \cup \mathcal{D}_2$ at any time t, is

$$\begin{aligned}
&\int_{\mathcal{D}_1\cup\mathcal{D}_2} [e]d\Omega + \int_{O_1} [e_{s1}]d\Gamma_1 + \int_{O_2} [e_{s2}]d\Gamma_2 \\
&= -\mathcal{T}_{int}(\mathcal{D}_1 \cup \mathcal{D}_2, \mathbf{U}, \beta) + \mathcal{Q}(\mathcal{D}_1 \cup \mathcal{D}_2) \ ,
\end{aligned}$$

where $\mathcal{T}_{int}\ (\mathcal{D}_1 \cup \mathcal{D}_2, \mathbf{U}, \beta)$ is the actual work of the percussions interior to the subdomain $\mathcal{D}_1 \cup \mathcal{D}_2$. We get

$$\begin{aligned}
\int_{\mathcal{D}_1\cup\mathcal{D}_2} [e]d\Omega + \int_{O_1} [e_{s1}]d\Gamma_1 + \int_{O_2} [e_{s2}]d\Gamma_2 \\
= \int_O \mathbf{R}_p \cdot \mathbf{D}_s(\frac{\mathbf{U}^+ + \mathbf{U}^-}{2})d\Gamma \\
+ \int_{\mathcal{D}_1} \Sigma_1 : \mathsf{D}(\frac{\mathbf{U}_1^+ + \mathbf{U}_1^-}{2}) + B_{p1}[\beta_1] + \mathbf{H}_{p1} \cdot \mathbf{grad}[\beta_1]\, d\Omega_1 \\
+ \int_{\mathcal{D}_2} \Sigma_2 : \mathsf{D}(\frac{\mathbf{U}_2^+ + \mathbf{U}_2^-}{2}) + B_{p2}[\beta_2] + \mathbf{H}_{p2} \cdot \mathbf{grad}[\beta_2]\, d\Omega_2 \\
+ \mathcal{Q}(\mathcal{D}_1 \cup \mathcal{D}_2)\ .
\end{aligned}$$

The energy balance inside the solids is

$$\begin{aligned}
\int_{\mathcal{D}_1\cup\mathcal{D}_2} [e]d\Omega = \int_{\mathcal{D}_1} \Sigma_1 : \mathsf{D}(\frac{\mathbf{U}_1^+ + \mathbf{U}_1^-}{2}) + B_{p1}[\beta_1] + \mathbf{H}_{p1} \cdot \mathbf{grad}[\beta_1]\, d\Omega_1 \\
+ \int_{\mathcal{D}_2} \Sigma_2 : \mathsf{D}(\frac{\mathbf{U}_2^+ + \mathbf{U}_2^-}{2}) + B_{p2}[\beta_2] + \mathbf{H}_{p2} \cdot \mathbf{grad}[\beta_2]\, d\Omega_2 \\
- \int_{\partial\mathcal{D}_1} \Sigma(T_1\mathbf{Q}_{p1} \cdot \mathbf{N}_1)d\Gamma_1 - \int_{\partial\mathcal{D}_2} \Sigma(T_2\mathbf{Q}_{p2} \cdot \mathbf{N}_2)d\Gamma_2 \\
+ \int_{\mathcal{D}_1} \Sigma(T_1\mathcal{B}_1)d\Omega_1 + \int_{\mathcal{D}_2} \Sigma(T_2\mathcal{B}_2)d\Omega_2\ ,
\end{aligned}$$

where the subdomains $\mathcal{D}_1$ and $\mathcal{D}_2$ are interior to each solid and where $T_1\mathbf{Q}_{p1}$, $T_2\mathbf{Q}_{p2}$ are the heat flux vectors in Ω_1 and in Ω_2. With this relationship, we get

$$\begin{aligned}
\int_{O_1} [e_{s1}]d\Gamma_1 + \int_{O_2} [e_{s2}]d\Gamma_2 \\
= \int_O \mathbf{R}_p \cdot \mathbf{D}_s(\frac{\mathbf{U}^+ + \mathbf{U}^-}{2})d\Gamma \\
+ \int_{\partial\mathcal{D}_1} \Sigma\left\{T_1\left(\mathbf{Q}_{p1} \cdot \mathbf{N}_1 + Q_{p1} + \mathcal{B}_{s1}\right)\right\}d\Gamma_1 \\
+ \int_{\partial\mathcal{D}_2} \Sigma\left\{T_2\left(\mathbf{Q}_{p2} \cdot \mathbf{N}_2 + Q_{p2} + \mathcal{B}_{s2}\right)\right\}d\Gamma_2 \\
- \int_O \Sigma\left(T_1Q_{p1} + T_2Q_{p2}\right)d\Gamma\ .
\end{aligned}$$

This results in the energy balance in Ω_1

$$[e_1] + \mathrm{div}\Sigma\left(T_1\mathbf{Q}_{p1}\right) = \Sigma_1 : \mathsf{D}(\frac{\mathbf{U}_1^+ + \mathbf{U}_1^-}{2}) + B_{p1}\,[\beta_1] + \mathbf{H}_{p1}\cdot\mathbf{grad}\,[\beta_1] + \Sigma(T_1\mathcal{B}_1)$$
$$= \Sigma_1 : \mathsf{D}(\frac{\mathbf{U}_1^+ + \mathbf{U}_1^-}{2}) + B_{p1}\,[\beta_1] + \mathbf{H}_{p1}\cdot\mathbf{grad}\,[\beta_1] + \underline{T}_1\Sigma(\mathcal{B}_1) + [T_1]\,\Delta(\mathcal{B}_1)\ ,$$

or

$$[e_1] + \mathrm{div}\left(\underline{T}_1(\Sigma(\mathbf{Q}_{p1}))\right) + \mathrm{div}([T_1]\,\Delta(\mathbf{Q}_{p1}))$$
$$= [e_1] + \underline{T}_1\mathrm{div}(\Sigma(\mathbf{Q}_{p1})) + \mathbf{grad}\underline{T}_1\cdot\Sigma(\mathbf{Q}_{p1}) + [T_1]\,\mathrm{div}\Delta(\mathbf{Q}_{p1}) + \mathbf{grad}\,[T_1]\cdot\Delta(\mathbf{Q}_{p1})$$
$$= \Sigma_1 : \mathsf{D}(\frac{\mathbf{U}_1^+ + \mathbf{U}_1^-}{2}) + B_{p1}\,[\beta_1] + \mathbf{H}_{p1}\cdot\mathbf{grad}\,[\beta_1] + \underline{T}_1\Sigma(\mathcal{B}_1) + [T_1]\,\Delta(\mathcal{B}_1)\ ,$$

where we denote as usual $\Delta(X) = (X^+ - X^-)/2$, $\Sigma(X) = X^+ + X^-$ and we use the relationship $\Sigma(XY) = \Sigma(X)\underline{Y} + \Delta(X)[Y]$, with $\underline{Y} = (Y^+ + Y^-)/2$ and $[Y] = Y^+ - Y^-$.

We choose the volume free energies as

$$\Psi_1 = -C_1T_1\ln T_1 + \check{\Psi}_1\ ,$$

with

$$\check{\Psi}_1(T_1,\beta_1,\mathbf{grad}\beta_1) = -\beta_1\frac{L_1}{T_0}(T_1 - T_0) + \frac{k_1}{2}\,(\mathbf{grad}\beta_1)^2 + I(\beta_1)\ .$$

We have

$$\left[\check{\Psi}_1\right] = \check{\Psi}_1(T_1^+,\beta_1^+,\mathbf{grad}\beta_1^+) - \check{\Psi}_1(T_1^-,\beta_1^-,\mathbf{grad}\beta_1^-)$$
$$= \check{\Psi}_1(T_1^+,\beta_1^+,\mathbf{grad}\beta_1^+) - \check{\Psi}_1(T_1^+,\beta_1^-,\mathbf{grad}\beta_1^-)$$
$$+\check{\Psi}_1(T_1^+,\beta_1^-,\mathbf{grad}\beta_1^-) - \check{\Psi}_1(T_1^-,\beta_1^-,\mathbf{grad}\beta_1^-)\ ,$$

and

$$\check{\Psi}_1(T_1^+,\beta_1^-) - \check{\Psi}_1(T_1^-,\beta_1^-) = -\beta_1^-\frac{L_1}{T_0}\,[T_1]\ .$$

Thus

$$[\Psi_1] = [-C_1T_1\ln T_1] + \check{\Psi}_1(T_1^+,\beta_1^+) - \check{\Psi}_1(T_1^+,\beta_1^-) - \beta_1^-\frac{L_1}{T_0}\,[T_1]$$
$$\leq [-C_1T_1\ln T_1] - \beta_1^-\frac{L_1}{T_0}\,[T_1] + B_{p1}^{fe}\,[\beta_1] + \mathbf{H}_{p1}^{fe}\cdot\mathbf{grad}\,[\beta_1]\ ,$$

with

$$(B_{p1}^{fe}, \mathbf{H}_{p1}^{fe}) \in \partial\check{\Psi}_1(T_1^+, \beta_1^+, \mathbf{grad}\beta_1^+) = (-\frac{L_1}{T_0}(T_1^+ - T_0) + \partial I(\beta_1^+), k_1\mathbf{grad}\beta_1^+) \ , \tag{7.14}$$

where the subdifferential is computed with respect to β_1^+ and $\mathbf{grad}\beta_1^+$. Moreover

$$\begin{aligned}[e_1] = [\Psi_1 + T_1 s_1] = [\Psi_1] + \underline{s}_1[T_1] + \underline{T}_1\,[s_1] \\ \leq -S_1\,[T_1] + \underline{T}_1\,[s_1] + B_{p1}^{fe}\,[\beta_1] + \mathbf{H}_{p1}^{fe} \cdot \mathbf{grad}\,[\beta_1] \ ,\end{aligned}$$

by denoting

$$[-C_1 T_1 \ln T_1] - \beta_1^- \frac{L_1}{T_0}\,[T_1] + \underline{s}_1[T_1] = -S_1\,[T_1]\,.$$

Thus the energy balance in Ω_1 is

$$\begin{aligned}\underline{T}_1\,[s_1] + \underline{T}_1 \mathrm{div}(\Sigma(\mathbf{Q}_{p1})) \geq \Sigma_1 : \mathsf{D}(\frac{\mathbf{U}_1^+ + \mathbf{U}_1^-}{2}) \\ +(B_{p1} - B_{p1}^{fe})\,[\beta_1] + (\mathbf{H}_{p1} - \mathbf{H}_{p1}^{fe}) \cdot \mathbf{grad}\,[\beta_1] + \underline{T}_1 \Sigma(\mathcal{B}_1) \\ +\,[T_1]\left(\Delta(\mathcal{B}_1) + S_1 - \mathrm{div}\Delta(\mathbf{Q}_{p1})\right) - \mathbf{grad}\,[T_1] \cdot \Delta(\mathbf{Q}_{p1}) - \mathbf{grad}\underline{T}_1 \cdot \Sigma(\mathbf{Q}_{p1}) \ .\end{aligned}$$

When the temperature discontinuity is zero, S_1 is zero since

$$\frac{\partial \Psi}{\partial T} + s = 0 \ .$$

This relationship is extended by assuming that there is no dissipation with respect to $[T_1]$ and $\mathbf{grad}\,[T_1]$. Then

$$\Delta(\mathcal{B}_1) + S_1 - \mathrm{div}\Delta(\mathbf{Q}_{p1}) = 0 \ , \quad \Delta(\mathbf{Q}_{p1}) = 0 \ ,$$

which give

$$\Delta(\mathcal{B}_1) + S_1 = 0 \ , \ \mathbf{Q}_{p1}^+ = \mathbf{Q}_{p1}^- = \mathbf{Q}_{p1} \ . \tag{7.15}$$

The energy balance becomes

$$\begin{aligned}[s_1] + 2\mathrm{div}\mathbf{Q}_{p1} \\ \geq \frac{1}{\underline{T}_1}\left\{\Sigma_1 : \mathsf{D}(\frac{\mathbf{U}_1^+ + \mathbf{U}_1^-}{2}) + (B_{p1} - B_{p1}^{fe})\,[\beta_1] + (\mathbf{H}_{p1} - \mathbf{H}_{p1}^{fe}) \cdot \mathbf{grad}\,[\beta_1]\right\} \\ -\frac{2}{\underline{T}_1}\mathbf{grad}\underline{T}_1 \cdot \mathbf{Q}_{p1} + \Sigma(\mathcal{B}_1) \ ,\end{aligned} \tag{7.16}$$

In the same way, the energy balance in Ω_2 is

$$[s_2] + 2\mathrm{div}\mathbf{Q}_{p2}$$
$$\geq \frac{1}{\underline{T}_2}\left\{\Sigma_2 : \mathsf{D}(\frac{\mathbf{U}_2^+ + \mathbf{U}_2^-}{2}) + (B_{p2} - B_{p2}^{fe})\,[\beta_2] + (\mathbf{H}_{p2} - \mathbf{H}_{p2}^{fe}) \cdot \mathbf{grad}\,[\beta_2]\right\}$$
$$-\frac{2}{\underline{T}_2}\mathbf{grad}\underline{T}_2 \cdot \mathbf{Q}_{p2} + \Sigma(\mathcal{B}_2)\ , \quad (7.17)$$

with

$$\Delta(\mathcal{B}_2) + S_2 = 0\ , \quad \mathbf{Q}_{p2}^+ = \mathbf{Q}_{p2}^- = \mathbf{Q}_{p2}\ . \quad (7.18)$$

Remark 7.2 In this section the discontinuity of the free energy

$$\begin{aligned}[\Psi] &= \Psi(T^+, \beta^+, \mathbf{grad}\beta^+) - \Psi(T^-, \beta^-, \mathbf{grad}\beta^-)\\ &= \Psi(T^+, \beta^+, \mathbf{grad}\beta^+) - \Psi(T^+, \beta^-, \mathbf{grad}\beta^-)\\ &+\Psi(T^+, \beta^-, \mathbf{grad}\beta^-) - \Psi(T^-, \beta^-, \mathbf{grad}\beta^-)\ ,\end{aligned}$$

is split into two terms

$$\Psi(T^+, \beta^+, \mathbf{grad}\beta^+) - \Psi(T^+, \beta^-, \mathbf{grad}\beta^-) \quad (7.19)$$

and

$$\Psi(T^+, \beta^-, \mathbf{grad}\beta^-) - \Psi(T^-, \beta^-, \mathbf{grad}\beta^-) \quad (7.20)$$

The first one is treated by using the convexity of function

$$(\beta, \mathbf{grad}, \beta) \to \Psi(T^+, \beta, \mathbf{grad}, \beta). \quad (7.21)$$

The second one is replaced by

$$\left(\frac{[-C_1T_1\ln T_1]}{[T_1]} - \beta_1^-\frac{L_1}{T_0}\right)[T_1]\ ,$$

which is different from

$$\partial\Psi_T(T_1^-, \beta^-, \mathbf{grad}\beta^-)\,[T_1] = \left(-C_1(1 + \ln T_1^-) - \beta_1^-\frac{L_1}{T_0}\right)[T_1]\ .$$

This difference appears in Eq. (7.15) and in (10.29) of Chap. 10 where the two S which are slightly different, give $\Delta(\mathcal{B})$ or the allocation of the external entropy production $\mathcal{B}^+ + \mathcal{B}^-$ between temperatures T^+ and T^-. We think that the two way of doing are convenient: to use either the differential quotient or the derivative of $-C_1T_1\ln T_1$. This remark gives a hint to the way to deal with non convex free energies: in case

$(\beta, \mathbf{grad}\beta) \to \Psi(T^+, \beta, \mathbf{grad}\beta)$ is not convex, the discontinuities may be replaced by differential quotients. But it is a long and complicated task.

The energy balance on $\partial\Omega_1$ is

$$\begin{aligned}[e_{s1}] &= \underline{T}_1 2\mathbf{Q}_{p1} \cdot \mathbf{N}_1 + \Sigma\left\{T_1(Q_{p1} + \mathcal{B}_{s1})\right\} \\ &= \underline{T}_1 2\mathbf{Q}_{p1} \cdot \mathbf{N}_1 + \underline{T}_1 \Sigma\left(Q_{p1} + \mathcal{B}_{s1}\right) \\ &\quad + \Delta\left(Q_{p1} + \mathcal{B}_{s1}\right)[T_1] \ . \end{aligned} \tag{7.22}$$

Moreover due to the relationship $e_{s1} = \Psi_{s1} + s_{s1}T_1$

$$[e_{s1}] = [\Psi_{s1}] + \underline{s}_{s1}[T_1] + \underline{T}_1[s_{s1}] = -S_{s1}[T_1] + \underline{T}_1[s_{s1}],$$

by denoting

$$[\Psi_{s1}] + \underline{s}_{s1}[T_1] = -S_{s1}[T_1].$$

Then the energy balance is

$$\begin{aligned}\underline{T}_1[s_{s1}] &= \underline{T}_1 2\mathbf{Q}_{p1} \cdot \mathbf{N}_1 + \underline{T}_1 \Sigma\left(Q_{p1} + \mathcal{B}_{s1}\right) \\ &\quad + \left\{\Delta\left(Q_{p1} + \mathcal{B}_{s1}\right) + S_{s1}\right\}[T_1].\end{aligned}$$

Assuming as usual no dissipation with respect to $[T_1]$

$$\Delta\left(Q_{p1} + \mathcal{B}_{s1}\right) + S_{s1} = 0, \tag{7.23}$$

the energy balance becomes

$$\underline{T}_1[s_{s1}] = \underline{T}_1 2\mathbf{Q}_{p1} \cdot \mathbf{N}_1 + \underline{T}_1 \Sigma\left(Q_{p1} + \mathcal{B}_{s1}\right). \tag{7.24}$$

The different heat sources which produce the evolution of the internal energy are thermal. There is no mechanical source in Eq. (7.24).

The energy balance on $\partial\Omega_2$ is

$$[e_{s2}] = \underline{T}_2 2\mathbf{Q}_{p2} \cdot \mathbf{N}_2 + \Sigma\left\{T_2(Q_{p2} + \mathcal{B}_{s2})\right\}. \tag{7.25}$$

Then

$$\underline{T}_2[s_{s2}] = \underline{T}_2 2\mathbf{Q}_{p2} \cdot \mathbf{N}_2 + \underline{T}_2 \Sigma\left(Q_{p2} + \mathcal{B}_{s2}\right), \tag{7.26}$$

with no dissipation with respect to $[T_2]$

$$\Delta\left(Q_{p2} + \mathcal{B}_{s2}\right) + S_{s2} = 0, \tag{7.27}$$

where S_{s2} is defined by

$$[\Psi_{s2}] + \underline{s}_{s2}[T_2] = -S_{s2}\,[T_2]\ .$$

The energy balance on $\partial\Omega_1 \cap \partial\Omega_2$ is

$$\begin{aligned}[e_{s1}] + [e_{s2}] &= \mathbf{R}_p \cdot \mathbf{D}_s\Big(\frac{\mathbf{U}^+ + \mathbf{U}^-}{2}\Big) \\ +\Sigma(T_1\mathcal{B}_{s1}) + \Sigma\{T_2\mathcal{B}_{s2}\} &+ \underline{T}_1 2\mathbf{Q}_{p1}\cdot\mathbf{N}_1 + \underline{T}_2 2\mathbf{Q}_{p2}\cdot\mathbf{N}_2\ . \end{aligned} \tag{7.28}$$

We have

$$\begin{aligned}[e_{s1}] + [e_{s2}] &= \mathbf{R}_p \cdot \mathbf{D}_s\Big(\frac{\mathbf{U}^+ + \mathbf{U}^-}{2}\Big) \\ + [T_1]\,\Delta\,(\mathcal{B}_{s1}) + \underline{T}_1\,\Sigma\,(\mathcal{B}_{s1}) &+ [T_2]\,\Delta\,(\mathcal{B}_{s2}) + \underline{T}_2\,\Sigma\,(\mathcal{B}_{s2}) \\ &+\underline{T}_1 2\mathbf{Q}_{p1}\cdot\mathbf{N}_1 + \underline{T}_2 2\mathbf{Q}_{p2}\cdot\mathbf{N}_2\ . \end{aligned}$$

By subtracting relationships (7.22) and (7.25), it results

$$\begin{aligned} 0 &= \mathbf{R}_p \cdot \mathbf{D}_s\Big(\frac{\mathbf{U}^+ + \mathbf{U}^-}{2}\Big) - [T_1]\,\Delta(Q_{p1}) - \underline{T}_1\,\Sigma(Q_{p1}) - [T_2]\,\Delta(Q_{p2}) - \underline{T}_2\,\Sigma(Q_{p2}) \\ &= \mathbf{R}_p \cdot \mathbf{D}_s\Big(\frac{\mathbf{U}^+ + \mathbf{U}^-}{2}\Big) - [T_1]\,\Delta(Q_{p1}) - [T_2]\,\Delta(Q_{p2}) - \frac{\delta\underline{T}}{2}(\Sigma(Q_{p2}) - \Sigma(Q_{p1}) \\ &\qquad -\underline{T}_m(\Sigma(Q_{p2}) + \Sigma(Q_{p1})\ . \end{aligned}$$

Assuming as usual no dissipation with respect to the $[T]$'s, we let

$$\Delta(Q_{p1}) = 0\ ,\ \ \Delta(Q_{p2}) = 0\ . \tag{7.29}$$

Then $Q^+_{p1} = Q^-_{p1} = Q_{p1}$, $Q^+_{p2} = Q^-_{p2} = Q_{p2}$ and

$$0 = \mathbf{R}_p \cdot \mathbf{D}_s\Big(\frac{\mathbf{U}^+ + \mathbf{U}^-}{2}\Big) - \delta\underline{T}(Q_{p2} - Q_{p1}) - 2\underline{T}_m(Q_{p2} + Q_{p1})\ . \tag{7.30}$$

Remark 7.3 On $\partial\Omega_1 \cap \partial\Omega_2$, the relationships (7.23) and (7.27) become

$$\Delta\,(\mathcal{B}_{s1}) + S_{s1} = 0\ ,\ \ \Delta\,(\mathcal{B}_{s2}) + S_{s2} = 0\ ,$$

due to (7.29).

7.4 The Second Law of Thermodynamics

Surface entropies s_s are introduced. The second law of thermodynamics is

$$\begin{aligned}
&\int_{\mathcal{D}_1\cup\mathcal{D}_2}[s]d\Omega+\int_{O_1}[s_{s1}]d\Gamma_1+\int_{O_2}[s_{s2}]d\Gamma_2\\
&\geq-\int_{\partial\mathcal{D}_1\setminus O_1}2\mathbf{Q}_{p1}\cdot\mathbf{N}_1d\Gamma_1-\int_{\partial\mathcal{D}_2\setminus O_2}2\mathbf{Q}_{p2}\cdot\mathbf{N}_2d\Gamma_2\\
&\quad+\int_{\mathcal{D}_1}\Sigma(\mathcal{B}_1)d\Omega_1+\int_{\mathcal{D}_2}\Sigma(\mathcal{B}_2)d\Omega_2\\
&+\int_{O_1\setminus O}\Sigma(Q_{p1})+\Sigma(\mathcal{B}_{s1})d\Gamma_1+\int_{O_2\setminus O}\Sigma(Q_{p2})+\Sigma(\mathcal{B}_{s2})d\Gamma_2\\
&\quad+\int_O\Sigma(\mathcal{B}_{s1})d\Gamma_1+\int_O\Sigma(\mathcal{B}_{s2})d\Gamma_2\,.
\end{aligned}$$

By integrating by parts

$$\begin{aligned}
&\int_{\mathcal{D}_1}[s_1]+\operatorname{div}(2\mathbf{Q}_{p1})-\Sigma(\mathcal{B}_{s1})d\Omega_1+\int_{\mathcal{D}_2}[s_2]+\operatorname{div}(2\mathbf{Q}_{p2})-\Sigma(\mathcal{B}_{s2})d\Omega_2\\
&\quad+\int_{O_1}[s_{s1}]d\Gamma_1+\int_{O_2}[s_{s2}]d\Gamma_2\\
&\geq\int_{O_1\setminus O}2\mathbf{Q}_{p1}\cdot\mathbf{N}_1+\Sigma(Q_{p1})+\Sigma(\mathcal{B}_{s1})d\Gamma_1\\
&\quad+\int_{O_2\setminus O}2\mathbf{Q}_{p2}\cdot\mathbf{N}_2+\Sigma(Q_{p2})+\Sigma(\mathcal{B}_{s2})d\Gamma_2\\
&+\int_O2\mathbf{Q}_{p1}\cdot\mathbf{N}_1+\Sigma(\mathcal{B}_{s1})d\Gamma_1+\int_O2\mathbf{Q}_{p2}\cdot\mathbf{N}_2+\Sigma(\mathcal{B}_{s2})d\Gamma_2\,,
\end{aligned}$$

then

$$\begin{aligned}
&\int_{\mathcal{D}_1}[s_1]+\operatorname{div}(2\mathbf{Q}_{p1})-\Sigma(\mathcal{B}_{s1})d\Omega_1+\int_{\mathcal{D}_2}[s_2]+\operatorname{div}(2\mathbf{Q}_{p2})-\Sigma(\mathcal{B}_{s2})d\Omega_2\\
&\quad+\int_{O_1}[s_{s1}]d\Gamma_1+\int_{O_2}[s_{s2}]d\Gamma_2\\
&\geq\int_{O_1}\left\{2\mathbf{Q}_{p1}\cdot\mathbf{N}_1+\Sigma(Q_{p1})+\Sigma(\mathcal{B}_{s1})\right\}d\Gamma_1\\
&\quad+\int_{O_2}\left\{2\mathbf{Q}_{p2}\cdot\mathbf{N}_2+\Sigma(Q_{p2})+\Sigma(\mathcal{B}_{s2})\right\}d\Gamma_2\\
&\quad+\int_O\{-\Sigma(Q_{p1})-\Sigma(Q_{p2})\}d\Gamma\,.
\end{aligned}$$

The preceding inequality gives

$$[s_1] + \mathrm{div}(2\mathbf{Q}_{p1}) - \Sigma(\mathcal{B}_1) \geq 0 \ , \ \text{in } \Omega_1 \ , \quad (7.31)$$

$$[s_2] + \mathrm{div}(2\mathbf{Q}_{p2}) - \Sigma(\mathcal{B}_2) \geq 0 \ , \ \text{in } \Omega_2 \ , \quad (7.32)$$

$$[s_{s1}] - \left\{2\mathbf{Q}_{p1} \cdot \mathbf{N}_1 + \Sigma(Q_{p1}) + \Sigma(\mathcal{B}_{s1})\right\} \geq 0 \ , \ \text{on } \partial\Omega_1 \ , \quad (7.33)$$

$$[s_{s2}] - \left\{2\mathbf{Q}_{p2} \cdot \mathbf{N}_2 + \Sigma(Q_{p2}) + \Sigma(\mathcal{B}_{s2})\right\} \geq 0 \ , \ \text{on } \partial\Omega_2 \ , \quad (7.34)$$

$$[s_{s1}] + [s_{s2}]$$
$$- \left\{2\mathbf{Q}_{p1} \cdot \mathbf{N}_1 + \Sigma(\mathcal{B}_{s1})\right\} - \left\{2\mathbf{Q}_{p2} \cdot \mathbf{N}_2 + \Sigma(\mathcal{B}_{s2})\right\} \geq 0 \ , \ \text{on } \partial\Omega_1 \cap \partial\Omega_2 \ . \quad (7.35)$$

The energy balances (7.24) and (7.26) imply the inequalities (7.33) and (7.34) are satisfied (they are equalities). It results that (7.35) is equivalent to

$$\Sigma(Q_{p1}) + \Sigma(Q_{p2}) = 2(Q_{p2} + Q_{p1}) \geq 0 \ .$$

The energy balances (7.16), (7.17) and (7.30) induce to choose the basic assumptions to establish the constitutive laws:

$$\Sigma_1 : \mathsf{D}(\frac{\mathbf{U}_1^+ + \mathbf{U}_1^-}{2}) + (B_{p1} - B_{p1}^{fe})\,[\beta_1] + (\mathbf{H}_{p1} - \mathbf{H}_{p1}^{fe}) \cdot \mathbf{grad}\,[\beta_1]$$
$$- 2\mathbf{grad}\underline{T}_1 \cdot \mathbf{Q}_{p1} \geq 0 \ , \ \textit{in } \Omega_1 \ , \quad (7.36)$$

$$\Sigma_2 : \mathsf{D}(\frac{\mathbf{U}_2^+ + \mathbf{U}_2^-}{2}) + (B_{p2} - B_{p2}^{fe})\,[\beta_2] + (\mathbf{H}_{p2} - \mathbf{H}_{p2}^{fe}) \cdot \mathbf{grad}\,[\beta_2]$$
$$-2\mathbf{grad}\underline{T}_2 \cdot \mathbf{Q}_{p2} \geq 0 \ , \ \textit{in } \Omega_2 \ , \quad (7.37)$$

$$\mathbf{R}_p \cdot \mathbf{D}_s(\frac{\mathbf{U}^+ + \mathbf{U}^-}{2}) - \delta\underline{T}(Q_{p2} - Q_{p1}) \geq 0 \ , \ \textit{on } \partial\Omega_1 \cap \partial\Omega_2 \ . \quad (7.38)$$

7.5 The Constitutive Laws

We assume pseudo-potential of dissipation

$$\Phi_1(\Delta E_1^{\pm}, E_1^{\pm}, \chi) = \Phi_1(\mathsf{D}(\frac{\mathbf{U}_1^+ + \mathbf{U}_1^-}{2}), [\beta_1]\,, \mathbf{grad}\,[\beta_1]\,, \mathbf{grad}\underline{T}_1, E_1^{\pm}, \chi) \ ,$$

$$\Phi_2(E_2^{\pm}, \Delta E_2^{\pm}, \chi) = \Phi_2(\mathsf{D}(\frac{\mathbf{U}_2^+ + \mathbf{U}_2^-}{2})), [\beta_2]\,, \mathbf{grad}\,[\beta_2]\,, \mathbf{grad}\underline{T}_2, E_2^{\pm}, \chi) \ ,$$

$$\Phi_s(\delta E^{\pm}, E^{\pm}, \chi) = \Phi_s(\mathbf{D}_s(\frac{\mathbf{U}^+ + \mathbf{U}^-}{2}), \delta\underline{T}, E^{\pm}, \chi) \ ,$$

which imply relationships (7.36)–(7.38) are satisfied. The surface pseudo-potential of dissipation Φ_s takes into account the impenetrability condition

$$\mathbf{D}_s(\mathbf{U}^+) \cdot \mathbf{N}_1 \geq 0 \ ,$$

with the indicator function

$$I_+(\mathbf{D}_s(\mathbf{U}^+) \cdot \mathbf{N}_1) \ , \tag{7.39}$$

and we have

$$\Phi_s(\delta E^\pm, E^\pm, \chi) = \Phi_s(\delta E^\pm, E^\pm, \chi) + I_+(\mathbf{D}_s(\mathbf{U}^+) \cdot \mathbf{N}_1) \ ,$$

where quantities χ involve $\mathbf{D}_s(\mathbf{U}^-)$.

The constitutive laws are

$$\begin{aligned}
&(\Sigma_1, B_{p1} - B_{p1}^{fe}, \mathbf{H}_{p1} - \mathbf{H}_{p1}^{fe}, -2\mathbf{Q}_{p1}) \qquad (7.40)\\
&\in \partial\Phi_1(\mathsf{D}(\frac{\mathbf{U}_1^+ + \mathbf{U}_1^-}{2}), [\beta_1] \, , \mathbf{grad}\,[\beta_1] \, , \mathbf{grad}\underline{T}_1, E_1^\pm, \chi) \ ,\\
&(\Sigma_2, B_{p2} - B_{p2}^{fe}, \mathbf{H}_{p2} - \mathbf{H}_{p2}^{fe}, -2\mathbf{Q}_{p2}) \qquad (7.41)\\
&\in \partial\Phi_2(\mathsf{D}(\frac{\mathbf{U}_2^+ + \mathbf{U}_2^-}{2}), [\beta_2] \, , \mathbf{grad}\,[\beta_2] \, , \mathbf{grad}\underline{T}_2, E_2^\pm, \chi) \ ,\\
&\left(\mathbf{R}_p, -(Q_{p2} - Q_{p1})\right) \in \partial\Phi_s(\mathbf{D}_s(\frac{\mathbf{U}^+ + \mathbf{U}^-}{2}), \delta\underline{T}, E^\pm, \chi) \ ,
\end{aligned}$$

where the subdifferential are computed with respect to the first quantities and not with respect to the E's and χ. For example, we choose

$$\begin{aligned}
&\Phi_1(\mathsf{D}(\frac{\mathbf{U}_1^+ + \mathbf{U}_1^-}{2}), [\beta_1] \, , \mathbf{grad}\,[\beta_1] \, , \mathbf{grad}\underline{T}_1, E_1^\pm, \chi)\\
&= \Phi_1(\mathsf{D}(\frac{\mathbf{U}_1^+ + \mathbf{U}_1^-}{2}), [\beta_1] \, , \mathbf{grad}\,[\beta_1] \, , \mathbf{grad}\underline{T}_1, \underline{T}_1)\\
&= 2k_M \left(\mathsf{D}(\frac{\mathbf{U}_1^+ + \mathbf{U}_1^-}{2}\right)^2 + \frac{k}{2\underline{T}_1} \left(\mathbf{grad}\underline{T}_1\right)^2 + \frac{c}{2}\,[\beta_1]^2 + \frac{k_m}{2} \left(\mathbf{grad}\,[\beta_1]\right)^2 \ ,
\end{aligned}$$

and

$$\begin{aligned}
\Phi_s(\mathbf{D}_s(\frac{\mathbf{U}^+ + \mathbf{U}^-}{2}), \delta\underline{T}, E^\pm, \chi) &= \Phi_s(\mathbf{D}_s(\frac{\mathbf{U}^+ + \mathbf{U}^-}{2}), \delta\underline{T}, \underline{T}_1, \underline{T}_2, \mathbf{D}_s(\mathbf{U}^+))\\
&= k_{ls} \left(\mathbf{D}_s(\frac{\mathbf{U}^+ + \mathbf{U}^-}{2})\right)^2 + \frac{\underline{T}_1 + \underline{T}_2}{\underline{T}_1\underline{T}_2} \frac{k_{ps}^d}{2} \left(\delta\underline{T}\right)^2 + I_+(\mathbf{D}_s(\mathbf{U}^+) \cdot \mathbf{N}_1) \ ,
\end{aligned}$$

where the k's parameters and c denote different thermal conductivities and dissipative parameters. For the sake of simplicity, we assume $\Phi_1 \equiv \Phi_2$. The pseudo-potential of dissipation have been chosen in such a way that the constitutive laws are linear besides the compulsory impenetrability condition. We think that the basic physical phenomena are to be described by these laws. It is only when dealing with particular problems that sophisticated non linear constitutive laws are to be introduced.

Remark 7.4 The coefficient of $\left(\delta \underline{T}\right)^2$ in pseudo-potential Φ_s is

$$\frac{\underline{T}_1 + \underline{T}_2}{\underline{T}_1 \underline{T}_2} \frac{k_{ps}^d}{2} ,$$

whereas it is

$$\frac{\lambda}{4} ,$$

in pseudo-potential Φ of Sect. 3.7.8 of Chap. 3 for collisions of rigid balls. In the small perturbation assumption where the temperature have values close to T_0, we have

$$\lambda = \frac{4k_{ps}^d}{T_0} ,$$

if the rigid body collision is understood as an approximation of the deformable body collision. The coefficient in front of k_{ps}^d is useful to have rather simple boundary conditions (for instance, (7.65)).

The constitutive laws are

$$\begin{aligned} \Sigma_1 &= 2k_M \mathsf{D}\left(\mathbf{U}_1^+ + \mathbf{U}_1^-\right) , \\ B_{p1} - B_{p1}^{fe} = c\left[\beta_1\right] \ , \ \mathbf{H}_{p1} - \mathbf{H}_{p1}^{fe} &= k_m \mathbf{grad}\left[\beta_1\right] , \\ -\mathbf{Q}_{p1} &= \frac{k}{\underline{T}_1} \mathbf{grad} \underline{T}_1 , \text{ in } \Omega_1 , \end{aligned}$$

$$\begin{aligned} \Sigma_2 &= 2k_M \mathsf{D}\left(\mathbf{U}_2^+ + \mathbf{U}_2^-\right) , \\ B_{p2} - B_{p2}^{fe} = c\left[\beta_2\right] \ , \ \mathbf{H}_{p2} - \mathbf{H}_{p2}^{fe} &= k_m \mathbf{grad}\left[\beta_2\right] , \\ -\mathbf{Q}_{p2} &= \frac{k}{\underline{T}_2} \mathbf{grad} \underline{T}_2 , \text{ in } \Omega_2 , \end{aligned}$$

and

$$\begin{aligned} \mathbf{R}_p &= k_{ls}\left(\mathbf{U}_2^+ - \mathbf{U}_1^+ + \mathbf{U}_2^- - \mathbf{U}_1^-\right) + P^{dr}\mathbf{N}_1 \ , \\ -(Q_{p2} - Q_{p1}) &= \frac{\underline{T}_1 + \underline{T}_2}{\underline{T}_1\underline{T}_2} k_{ps}^d \delta\underline{T}, \ \text{on } \partial\Omega_1 \cap \partial\Omega_2 \ , \end{aligned} \tag{7.42}$$

where P^{dr} is the impenetrability reaction

$$P^{dr} \in \partial I_+(\mathbf{D}_s(\mathbf{U}^+) \cdot \mathbf{N}_1) = \partial I_+((\mathbf{U}_2^+ - \mathbf{U}_1^+) \cdot \mathbf{N}_1) \ .$$

Remark 7.5 The pseudo-potentials Φ_i does not have constraint on $[\beta_i]$, because β_i^+ is between 0 and 1 due to the definition of B_i^{nd} (see relationship (7.14) which involves $\partial I(\beta_1^+)$).

Note that the constitutive laws are only dissipative as are the constitutive laws for rigid bodies collisions. This property is characteristic of collisions where even the impenetrability reactions are dissipative in contrast with many other cases where the reactions to internal constraints are workless, [5, 7, 8]. The following theorem ensures that the second law of thermodynamics is satisfied with the constitutive laws that have just been chosen.

Theorem 7.1 *If the constitutive laws are satisfied and if the temperatures are positive, then*

- *the impenetrability internal constraint is satisfied, and*
- *the second law of thermodynamics is satisfied.*

Proof The proof is straightforward. □

7.6 Evolution in a Collision

The data of this problem are the state and the velocities before the collision, as well as the exterior actions: the percussions $\mathbf{F}_p$, $\mathbf{T}_p$, A, a, and the heat impulse sources $\Sigma(T\mathcal{B})$ in Ω_1 and Ω_2, $\Sigma T(Q_p)$ on $\partial\Omega_1\backslash(\partial\Omega_1 \cap \partial\Omega_2)$ and $\partial\Omega_2\backslash(\partial\Omega_1 \cap \partial\Omega_2)$, and $\Sigma T(\mathcal{B}_s)$ in $\partial\Omega_1$ and $\partial\Omega_2$. The unknowns are the state quantities (T, β) and the velocities after the collision. The mechanical equations are

$$\begin{aligned} \rho_1\,[\mathbf{U}_1] &= \mathrm{div}\Sigma_1 + \mathbf{F}_{p1} \ , \\ 0 &= \mathrm{div}\mathbf{H}_{p1} - B_{p1} + A_1 \ , \ \text{in } \Omega_1 \ , \end{aligned} \tag{7.43}$$

$$\begin{aligned} \rho_2\,[\mathbf{U}_2] &= \mathrm{div}\Sigma_2 + \mathbf{F}_{p2} \ , \\ 0 &= \mathrm{div}\mathbf{H}_{p2} - B_{p2} + A_2 \ , \ \text{in } \Omega_2 \ , \end{aligned} \tag{7.44}$$

$$\Sigma_1 \mathbf{N}_1 = \mathbf{R}_p + \mathbf{T}_{p1}\ ,\ \mathbf{H}_{p1}\cdot\mathbf{N}_1 = a_1\ ,$$
$$\Sigma_2 \mathbf{N}_2 = -\mathbf{R}_p + \mathbf{T}_{p2}\ ,\ \mathbf{H}_{p2}\cdot\mathbf{N}_2 = a_2\ ,\ \text{on}\ \partial\Omega_1\cap\partial\Omega_2\ , \tag{7.45}$$

$$\Sigma_1 \mathbf{N}_1 = \mathbf{T}_{p1}\ ,\ \mathbf{H}_{p1}\cdot\mathbf{N}_1 = a_1\ ,\ \text{on}\ \partial\Omega_1\backslash(\partial\Omega_1\cap\partial\Omega_2), \tag{7.46}$$

$$\Sigma_2 \mathbf{N}_2 = \mathbf{T}_{p2}\ ,\ \mathbf{H}_{p2}\cdot\mathbf{N}_2 = a_2\ ,\ \text{on}\partial\Omega_2\backslash(\partial\Omega_1\cap\partial\Omega_2)\ . \tag{7.47}$$

The thermal equations are

$$[e_1] + \text{div}(2\underline{T}_1\mathbf{Q}_{p1})$$
$$= \Sigma_1 : \mathsf{D}(\frac{\mathbf{U}_1^+ + \mathbf{U}_1^-}{2}) + B_{p1}\,[\beta_1] + \mathbf{H}_{p1}\cdot\mathbf{grad}\,[\beta_1] + \Sigma(T_1\mathcal{B}_1),\ \text{in}\ \Omega_1, \tag{7.48}$$

$$[e_2] + \text{div}(2\underline{T}_2\mathbf{Q}_{p2})$$
$$= \Sigma_2 : \mathsf{D}(\frac{\mathbf{U}_2^+ + \mathbf{U}_2^-}{2}) + B_{p2}\,[\beta_2] + \mathbf{H}_{p2}\cdot\mathbf{grad}\,[\beta_2] + \Sigma(T_2\mathcal{B}_2),\ \text{in}\ \Omega_2, \tag{7.49}$$
$$[e_{s1}] = \underline{T}_1 2\mathbf{Q}_{p1}\cdot\mathbf{N}_1 + \Sigma\{T_1(Q_{p1}+\mathcal{B}_{s1})\},\ \text{on}\ \partial\Omega_1,$$

Remark 7.6 The last relationship and the two following ones are boundary conditions for the partial differential equations which are to be satisfied by the temperature in Ω_1 and in Ω_2.

$$[e_{s2}] = \underline{T}_2 2\mathbf{Q}_{p2}\cdot\mathbf{N}_2 + \Sigma\{T_2(Q_{p2}+\mathcal{B}_{s2})\},\ \text{on}\ \partial\Omega_2\ ,$$
$$[e_{s1}] + [e_{s2}] = \mathbf{R}_p\cdot\mathbf{D}_s(\frac{\mathbf{U}^+ + \mathbf{U}^-}{2}) + \Sigma\{T_2\mathcal{B}_{s2}\} + \Sigma\{T_1\mathcal{B}_{s1}\}$$
$$+2\underline{T}_1\mathbf{Q}_{p1}\cdot\mathbf{N}_1 + 2\underline{T}_2\mathbf{Q}_{p2}\cdot\mathbf{N}_2,\ \text{on}\ \partial\Omega_1\cap\partial\Omega_2\ .$$

The equations are completed by the relationships

$$\Delta(\mathcal{B}_1) + S_1 = 0\ ,\ \textit{in}\ \Omega_1\ ,$$
$$\Delta(\mathcal{B}_2) + S_2 = 0\ ,\ \textit{in}\ \Omega_2\ ,$$
$$\Delta\left\{Q_{p1}+\mathcal{B}_{s1}\right\} + S_{s1} = 0\ ,\ \textit{on}\ \partial\Omega_1\ ,$$
$$\Delta\left(Q_{p2}+\mathcal{B}_{s2}\right) + S_{s2} = 0\ ,\ \textit{on}\ \partial\Omega_2\ ,$$
$$\Delta(Q_{p1}) = 0,\ \Delta(Q_{p2}) = 0\ ,\ \text{on}\ \partial\Omega_1\cap\partial\Omega_2\ .$$

Equations (7.15) with the data $\Sigma(T_1\mathcal{B}_1)$ give the two heat impulses $\mathcal{B}_1^+$ and $\mathcal{B}_1^-$ in Ω_1, depending on the temperatures T_1^+ and T_1^-. With the data $\Sigma(T_1Q_{p1})$, $\Sigma(T_1\mathcal{B}_{s1})$, and the Eq. (7.22), the two heat impulses $\mathcal{B}_1^+$ and $\mathcal{B}_1^-$ give the heat flux $\underline{T}_1 2\mathbf{Q}_{p1}\cdot\mathbf{N}_1$ on $\partial\Omega_1\backslash(\partial\Omega_1\cap\partial\Omega_2)$ which is the boundary condition for the equation

(7.48). Equations (7.22), (7.23), (7.25), (7.27), (7.28), the constitutive laws (7.42) and the data $\Sigma(T_1\mathcal{B}_{s1})$, $\Sigma(T_2\mathcal{B}_{s2})$ give the $\mathcal{B}_s$, Q_p, and the two heat fluxes $\underline{T}_1 2\mathbf{Q}_{p1}\cdot\mathbf{N}_1$ and $\underline{T}_2 2\mathbf{Q}_{p2}\cdot\mathbf{N}_2$ on $\partial\Omega_1\cap\partial\Omega_2$ depending on the temperatures and the mechanical works. The heat fluxes $\underline{T}_1 2\mathbf{Q}_{p1}\cdot\mathbf{N}_1$ and $\underline{T}_2 2\mathbf{Q}_{p2}\cdot\mathbf{N}_2$ on $\partial\Omega_1\cap\partial\Omega_2$ are the boundary conditions on $\partial\Omega_1\cap\partial\Omega_2$ for Eqs. (7.48) and (7.49). Thus the equations provide the boundary conditions for solving the two Eqs. (7.48) and (7.49) which give the two future temperatures T_1^+ and T_2^+. In the following sections examples of those mechanical and thermal equations are investigated.

7.6.1 *The Mechanical Evolution When Decoupled from the Thermal Evolution*

The equations of motion are (7.43)–(7.47). Let us recall that we have assumed that all the mechanical quantities are independent of the temperature and that the constitutive laws have been chosen simple in order to emphasize the properties of the equations

$$\begin{aligned}\Sigma_1 &= 2k_M\mathsf{D}\left(\mathbf{U}_1^+ + \mathbf{U}_1^-\right)\ ,\ \text{in } \Omega_1\ ,\\ \Sigma_2 &= 2k_M\mathsf{D}\left(\mathbf{U}_2^+ + \mathbf{U}_2^-\right)\ ,\ \text{in } \Omega_2\ ,\end{aligned}$$

the positive parameter k_M describes the dissipative properties of the material in a collision;

$$\mathbf{R}_p = k_{ls}\left(\mathbf{U}_2^+ - \mathbf{U}_1^+ + \mathbf{U}_2^- - \mathbf{U}_1^-\right) + P^{dr}\mathbf{N}_1\ ,\ \text{on } \partial\Omega_1\cap\partial\Omega_2\ ,$$

the positive parameter k_{ls} describes the dissipative properties of the contact surface in a collision. The properties of non-interpenetration reaction P^{dr} result from its definition

$$P^{dr}\in\partial I_+(\mathbf{D}_s(\mathbf{U}^+)\cdot\mathbf{N}_1) = \partial I_-((\mathbf{U}_2^+ - \mathbf{U}_1^+)\cdot\mathbf{N}_1)\ .$$

Introducing the constitutive laws in the equations of motion, it results by denoting $\Delta\mathbf{V}$ the laplacian of vector $\mathbf{V}$

$$\begin{aligned}\rho_1\mathbf{U}_1^+ &= k_M\left(\mathbf{grad}\mathrm{div}\mathbf{U}_1^+ + \Delta\mathbf{U}_1^+\right)\\ &+\mathbf{F}_{p1} + \rho_1\mathbf{U}_1^- + k_M\left(\mathbf{grad}\mathrm{div}\mathbf{U}_1^- + \Delta\mathbf{U}_1^-\right)\ ,\ \text{in } \Omega_1\ ,\end{aligned}\tag{7.50}$$

$$\begin{aligned}\rho_2\mathbf{U}_2^+ &= k_M\left(\mathbf{grad}\mathrm{div}\mathbf{U}_2^+ + \Delta\mathbf{U}_2^+\right)\\ &+\mathbf{F}_{p2} + \rho_2\mathbf{U}_2^- + k_M\left(\mathbf{grad}\mathrm{div}\mathbf{U}_2^- + \Delta\mathbf{U}_2^-\right)\ ,\ \text{in } \Omega_2\ ,\end{aligned}\tag{7.51}$$

$$\Sigma_1 \mathbf{N}_1 = k_{ls}\left(\mathbf{U}_2^+ - \mathbf{U}_1^+ + \mathbf{U}_2^- - \mathbf{U}_1^-\right) + P^{dr}\mathbf{N}_1,$$
$$\Sigma_2 \mathbf{N}_2 = -k_{ls}\left(\mathbf{U}_2^+ - \mathbf{U}_1^+ + \mathbf{U}_2^- - \mathbf{U}_1^-\right) + P^{dr}\mathbf{N}_2\ ,\ \text{on}\ \partial\Omega_1 \cap \partial\Omega_2\ , \tag{7.52}$$

$$\Sigma_1 \mathbf{N}_1 = \mathbf{T}_{p1}\ ,\ \text{on}\ \partial\Omega_1 \backslash (\partial\Omega_1 \cap \partial\Omega_2)\ , \tag{7.53}$$

and

$$\Sigma_2 \mathbf{N}_2 = \mathbf{T}_{p2}\ ,\ \text{on}\ \partial\Omega_2 \backslash (\partial\Omega_1 \cap \partial\Omega_2)\ . \tag{7.54}$$

The preceding Eqs. (7.50)–(7.54) have a variational formulation. Let C be the convex set of the kinematically admissible future velocities

$$C = \{(\mathbf{V}_1, \mathbf{V}_2) \in \mathcal{V}_1 \times \mathcal{V}_2 \,|\, (\mathbf{V}_2 - \mathbf{V}_1)\cdot \mathbf{N}_1 \geq 0\ ,\ on\ \partial\Omega_1 \cap \partial\Omega_2\}\ .$$

It is easy to show that a solution of the Eqs. (7.50)–(7.54) satisfies

$$\begin{aligned}(\mathbf{U}_1^+, \mathbf{U}_2^+) \in C\ ,\ \forall (\mathbf{V}_1, \mathbf{V}_2) \in C,\\ a_1(\mathbf{U}_1^+, \mathbf{V}_1 - \mathbf{U}_1^+) + a_2(\mathbf{U}_2^+, \mathbf{V}_2 - \mathbf{U}_2^+) + b(\mathbf{U}_2^+ - \mathbf{U}_1^+, \mathbf{V}_2 - \mathbf{V}_1 - (\mathbf{U}_2^+ - \mathbf{U}_1^+))\\ \geq L_1(\mathbf{V}_1 - \mathbf{U}_1^+) + L_2(\mathbf{V}_2 - \mathbf{U}_2^+) - b(\mathbf{U}_2^- - \mathbf{U}_1^-, \mathbf{V}_2 - \mathbf{V}_1 - (\mathbf{U}_2^+ - \mathbf{U}_1^+))\ ,\end{aligned} \tag{7.55}$$

with

$$a_1(\mathbf{U}, \mathbf{V}) = \int_{\Omega_1} 2k\mathsf{D}(\mathbf{U}) : \mathsf{D}(\mathbf{V}) d\Omega_1 + \int_{\Omega_1} \rho_1 \mathbf{U}\cdot\mathbf{V} d\Omega_1\ ,$$
$$b(\mathbf{U}, \mathbf{V}) = \int_{\partial\Omega_1 \cap \partial\Omega_2} k_{ls}\mathbf{U}\cdot\mathbf{V}) d\Gamma_1\ ,$$
$$L_1(\mathbf{V}) = \int_{\Omega_1} \mathbf{F}_{p1}\cdot\mathbf{V} d\Omega_1 + \int_{\partial\Omega_1 \backslash (\partial\Omega_1 \cap \partial\Omega_2)} \mathbf{T}_{p1}\cdot\mathbf{V} d\Gamma_1$$
$$- \int_{\Omega_1} 2k\mathsf{D}(\mathbf{U}_1^-) : \mathsf{D}(\mathbf{V}) d\Omega_1 + \int_{\Omega_1} \rho_1 \mathbf{U}_1^-\cdot\mathbf{V} d\Omega_1\ .$$

The functions a_2 and L_2 are defined in the same way. Problem (7.55) is a classical variational inequality which has a unique solution in a convenient functional framework [4, 10–12]. Thus the future velocities $\mathbf{U}^+$ are uniquely determined by the past.

7.6.2 An Example: Collision of a Bar with a Rigid Support

Consider the bar shown in Fig. 7.1 falling on a rigid fixed support ($\mathbf{U}_2 = 0$), [1]. The bar is assumed to be elastic when evolving smoothly (with Young modulus 2.5×10^{10} Pa, Poisson coefficient 0.3 and density 7877 kg/m^3). When colliding with the rigid support, it is dissipative.

The bar equation of motion when colliding the support is

$$\rho_1 \mathbf{U}_1^+ = k_M \mathbf{grad}\mathrm{div}\mathbf{U}_1^+ + k_M \Delta \mathbf{U}_1^+ + \rho_1 \mathbf{U}_1^- + k_M \mathbf{grad}\mathrm{div}\mathbf{U}_1^- + k_M \Delta \mathbf{U}_1^- \ ,$$

in the bar

$$\Sigma_1 \mathbf{N}_1 = -k_{ls} \left(\mathbf{U}_1^+ + \mathbf{U}_1^- \right) - P^{dr} \mathbf{N}_1 \ ,$$

on the contact surface, and

$$\Sigma_1 \mathbf{N}_1 = 0 \ ,$$

outside the contact surface. The dissipative parameters are chosen as: $k_M = 10^5$ Ns^2/m^2 and $k_{ls} = 8\ 10^6$ Ns^2/m^3. The velocities of the bar after the first collision where contact is not maintained, are not rigid body velocities. The bar vibrates afterwards. There is a competition between the slow rising motion after the collision and the fast vibrating motion resulting from the elasticity of the bar. The first oscillations are such that the bar which has not risen far above the support collides with it other times, six times in this example, [1, 2]. The vertical position of a point of the lower

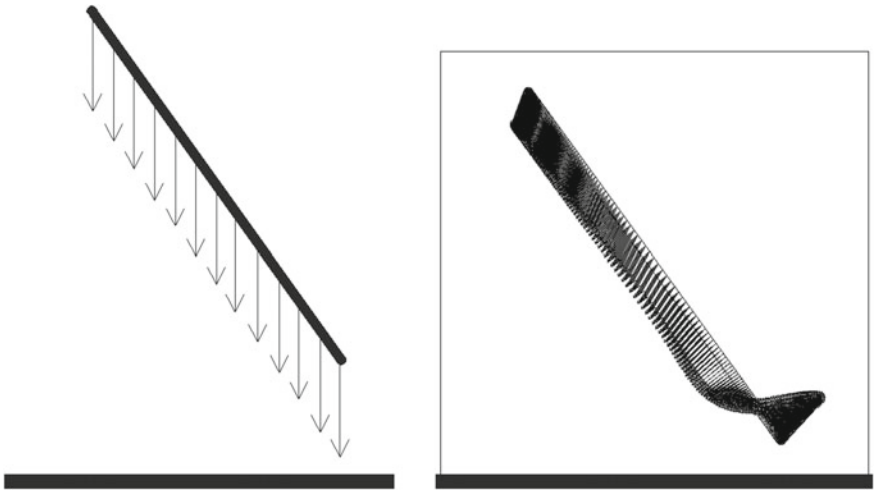

Fig. 7.1 A bar falls with a vertical velocity of -1 m / s on a rigid support with an angle $\theta = 54°$ with the horizontal. Its length is 0.6 m. Its width is 0.012 m. The two ends are rounded. The velocities after the first collisions are shown

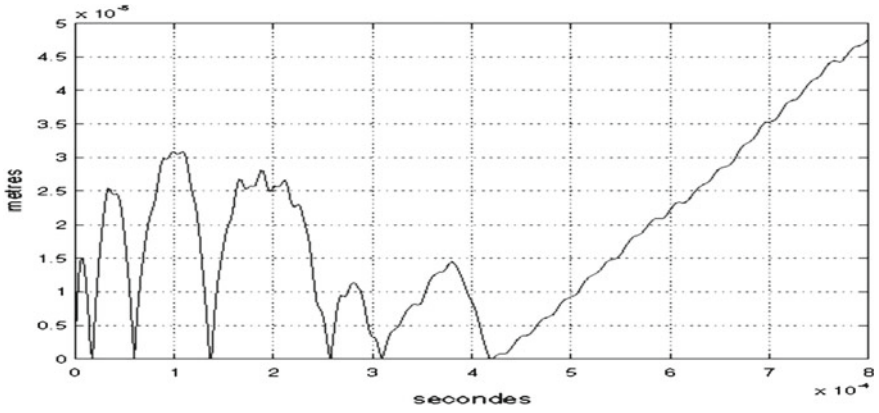

Fig. 7.2 The vertical position of a point of the lower part of the bar which collides with the rigid support. The bar vibrates after the first collision. It results microrebounds before the bar rises sufficiently above the rigid support [1]

part of the bar versus the time is shown in Fig. 7.2. Experiments have shown this behaviour, with a number of micro-rebounds of the same order [13].

7.6.3 Thermal Evolution When the Mechanical Equations Are Decoupled From the Thermal Equations

The equations to get the future temperatures and volume fractions are,

$$\begin{aligned}
&\rho_1[e_1] + \mathrm{div}(2\underline{T}_1\mathbf{Q}_{p1}) \\
&= \Sigma_1 : \mathsf{D}(\frac{\mathbf{U}_1^+ + \mathbf{U}_1^-}{2}) + B_{p1}\,[\beta_1] + \mathbf{H}_{p1}\cdot\mathbf{grad}\,[\beta_1] + \Sigma(T_1\mathcal{B}_1)\ , \\
&0 = \mathrm{div}\mathbf{H}_{p1} - B_{p1} + A_1,\ \text{in}\ \Omega_1\ , \\
&\rho_2[e_2] + \mathrm{div}(2\underline{T}_2\mathbf{Q}_{p2}) \\
&= \Sigma_2 : \mathsf{D}(\frac{\mathbf{U}_2^+ + \mathbf{U}_2^-}{2}) + B_{p2}\,[\beta_2] + \mathbf{H}_{p2}\cdot\mathbf{grad}\,[\beta_2] + \Sigma(T_2\mathcal{B}_2)\ , \\
&0 = \mathrm{div}\mathbf{H}_{p2} - B_{p2} + A_2,\ \text{in}\ \Omega_2\ ,
\end{aligned}$$

$$\begin{aligned}
[e_{s1}] &= \underline{T}_1 2\mathbf{Q}_{p1}\cdot\mathbf{N}_1 + \Sigma\left\{T_1(\mathcal{Q}_{p1} + \mathcal{B}_{s1})\right\}\ , \\
\mathbf{H}_{p1}\cdot\mathbf{N}_1 &= a_1,\ \text{on}\ \partial\Omega_1\backslash(\partial\Omega_1\cap\partial\Omega_2)\ ,
\end{aligned}$$

$$\begin{aligned}
[e_{s2}] &= \underline{T}_2 2\mathbf{Q}_{p2}\cdot\mathbf{N}_2 + \Sigma\left\{T_2(\mathcal{Q}_{p2} + \mathcal{B}_{s2})\right\}\ , \\
\mathbf{H}_{p2}\cdot\mathbf{N}_2 &= a_2,\ \text{on}\ \partial\Omega_2\backslash(\partial\Omega_1\cap\partial\Omega_2)\ ,
\end{aligned}$$

by using the Eqs. (7.22), (7.25), and (7.28) together with the constitutive law (7.42)

$$[e_{s1}] = \frac{\underline{T}_1}{\underline{T}_1 + \underline{T}_2}\mathbf{R}_p \cdot \mathbf{D}_s(\frac{\mathbf{U}^+ + \mathbf{U}^-}{2})$$
$$+\underline{T}_1 2\mathbf{Q}_{p1} \cdot \mathbf{N}_1 - \frac{2\underline{T}_1\underline{T}_2}{\underline{T}_1 + \underline{T}_2}(Q_{p2} - Q_{p1}) + \Sigma\{T_1\mathcal{B}_{s1}\}\ , \quad (7.56)$$
$$[e_{s2}] = \frac{\underline{T}_2}{\underline{T}_1 + \underline{T}_2}\left(\mathbf{R}_p \cdot \mathbf{D}_s(\frac{\mathbf{U}^+ + \mathbf{U}^-}{2})\right)$$
$$+\underline{T}_2 2\mathbf{Q}_{p2} \cdot \mathbf{N}_2 + \frac{2\underline{T}_1\underline{T}_2}{\underline{T}_1 + \underline{T}_2}(Q_{p2} - Q_{p1}) + \Sigma\{T_2\mathcal{B}_{s2}\},\ \text{on}\ \partial\Omega_1 \cap \partial\Omega_2\ , \quad (7.57)$$

and

$$\mathbf{H}_{p1} \cdot \mathbf{N}_1 = a_1,\ \mathbf{H}_{p2} \cdot \mathbf{N}_2 = a_2,\ \text{on}\ \partial\Omega_1 \cap \partial\Omega_2\ .$$

The equations are completed by relationships (7.15), (7.18), (7.23), (7.27) and, (7.29). The constitutive laws have already been chosen, (see formulas (7.42)). Let us recall those we need

$$-\mathbf{Q}_{p1} = \frac{k}{\underline{T}_1}\mathbf{grad}\underline{T}_1\ ,\ -\mathbf{Q}_{p2} = \frac{k}{\underline{T}_2}\mathbf{grad}\underline{T}_2\ ,$$
$$-(Q_{p2} - Q_{p1}) = \frac{\underline{T}_1 + \underline{T}_2}{\underline{T}_1\underline{T}_2}k^d_{ps}\delta\underline{T}\ ,$$
$$B_{p1} \in B^{fe}_{p1} + c\,[\beta_1] = -\frac{L_1}{T_0}(T_1^+ - T_0) + \partial I(\beta_1^+) + c\,[\beta_1]\ ,$$
$$\mathbf{H}_{p1} = \mathbf{H}^{fe}_{p1} + k_m\mathbf{grad}\,[\beta_1]\ ,$$
$$B_{p2} \in B^{fe}_{p2} + c\,[\beta_2] = -\frac{L_2}{T_0}(T_2^+ - T_0) + \partial I(\beta_2^+) + c\,[\beta_2]\ ,$$
$$\mathbf{H}_{p2} = \mathbf{H}^{fe}_{p2} + k_m\mathbf{grad}\,[\beta_2]\ ,$$

where the constants k and k^d_{ps} denote the different thermal conductivities and c and k_m are dissipative parameters. We have already chosen the volume free energies

$$\Psi(T, \beta) = -C_i T \ln T - \beta\frac{L_i}{T_0}(T - T_0) + \frac{k_i}{2}(\mathbf{grad}\beta)^2 + I(\beta)\ .$$

Since we assume the mechanical properties do not depend on the temperature, the surface free energies have a unique temperature dependent term which is chosen simple

$$\Psi_s(T) = -C_s T \ln T\ ,$$

where the C's are heat capacities.

We assume that the exterior heat impulses are null: $\Sigma(T_1\mathcal{B}_1) = \Sigma(T_2\mathcal{B}_2) = 0$, $\Sigma(T_1 Q_{p1}) = 0$ on $\partial\Omega_1\backslash(\partial\Omega_1 \cap \partial\Omega_2)$, $\Sigma(T_1\mathcal{B}_{s1}) = 0$ on $\partial\Omega_1$, $\Sigma(T_2 Q_{p2}) = 0$ on $\partial\Omega_2\backslash(\partial\Omega_1 \cap \partial\Omega_2)$, $\Sigma(T_2\mathcal{B}_{s2}) = 0$ on $\partial\Omega_2$ and that no external percussion work is provided $A_1 = A_2 = 0$, and $a_1 = a_2 = 0$.

Remark 7.7 It is also possible to assume that the exterior entropy impulses are given.

The energy balances (7.48), (7.49), (7.22), (7.54) and (7.56), (7.57), with the constitutive laws give the equations

$$C_1\,[T_1] + L_1\,[\beta_1] - 2k\Delta\underline{T}_1 = \Sigma_1 : \mathsf{D}(\frac{\mathbf{U}_1^+ + \mathbf{U}_1^-}{2}) + B_{p1}\,[\beta_1] + \mathbf{H}_{p1}\cdot\mathbf{grad}\,[\beta_1]\ , \tag{7.58}$$

$$c\,[\beta_1] - k_m\Delta\,[\beta_1] + \partial I(\beta_1^+) \ni \frac{L_1}{T_0}(T_1^+ - T_0)\ ,\ \text{in}\ \Omega_1\ , \tag{7.59}$$

$$C_2\,[T_2] + L_2\,[\beta_2] - 2k\Delta\underline{T}_2 = \Sigma_2 : \mathsf{D}(\frac{\mathbf{U}_2^+ + \mathbf{U}_2^-}{2}) + B_{p2}\,[\beta_2] + \mathbf{H}_{p2}\cdot\mathbf{grad}\,[\beta_2]\ , \tag{7.60}$$

$$c\,[\beta_2] - k_m\Delta\,[\beta_2] + \partial I(\beta_2^+) \ni \frac{L_2}{T_0}(T_2^+ - T_0)\ ,\ \text{in}\ \Omega_2\ , \tag{7.61}$$

where Δ denotes the laplacian operator,

$$C_{1s}\,[T_1] + 2k\frac{\partial\underline{T}_1}{\partial\mathbf{N}_1} = 0,\ k_m\frac{\partial\,[\beta_1]}{\partial\mathbf{N}_1} = 0\ ,\ \text{on}\ \partial\Omega_1\backslash(\partial\Omega_1\cap\partial\Omega_2)\ , \tag{7.62}$$

$$C_{2s}\,[T_2] + 2k\frac{\partial\underline{T}_2}{\partial\mathbf{N}_2} = 0,\ k_m\frac{\partial\,[\beta_2]}{\partial\mathbf{N}_2} = 0\ ,\ \text{on}\ \partial\Omega_2\backslash(\partial\Omega_1\cap\partial\Omega_2)\ , \tag{7.63}$$

these relationships are the boundary conditions on $\partial\Omega_1\backslash(\partial\Omega_1 \cap \partial\Omega_2)$ and $\partial\Omega_2\backslash(\partial\Omega_1 \cap \partial\Omega_2)$ of the Eqs. (7.58) and (7.60) in Ω_1 and Ω_2,

$$C_{1s}\,[T_1] + 2k\frac{\partial\underline{T}_1}{\partial\mathbf{N}_1} = \frac{\underline{T}_1}{\underline{T}_1 + \underline{T}_2}\left(\mathbf{R}_p\cdot\mathbf{D}_s(\frac{\mathbf{U}^+ + \mathbf{U}^-}{2})\right) + 2k_{ps}^d\delta\underline{T}\ , \tag{7.64}$$

$$C_{2s}\,[T_2] + 2k\frac{\partial\underline{T}_2}{\partial\mathbf{N}_2} = \frac{\underline{T}_2}{\underline{T}_1 + \underline{T}_2}\left(\mathbf{R}_p\cdot\mathbf{D}_s(\frac{\mathbf{U}^+ + \mathbf{U}^-}{2})\right) - 2k_{ps}^d\delta\underline{T}\ , \tag{7.65}$$

$$k_m\frac{\partial\,[\beta_1]}{\partial\mathbf{N}_1} = 0\ ,\ k_m\frac{\partial\,[\beta_2]}{\partial\mathbf{N}_2} = 0\ ,\ \text{on}\ \partial\Omega_1\cap\partial\Omega_2\ .$$

As already mentioned, relationships (7.64) and (7.65) together with (7.56) and (7.57) give the boundary conditions on $\partial\Omega_1 \cap \partial\Omega_2$ for the two partial differential equations (7.58) and (7.60) equations in Ω_1 and Ω_2 giving the future temperature T_1^+ and T_2^+. The equations giving the temperatures and the volume fractions are coupled due to the phase change latent heat.

7.6.4 The Temperature Variation in a Collision

Because collisions are dissipative, their thermal effect should be to warm the colliding solids. In this section, we investigate this problem. Let us assume that the temperatures before the collision are uniform (they do not depend on $\mathbf{x}$) in each solid and lower than the phase change temperature, i.e., $T_1^- < T_0$, $T_2^- < T_0$. We assume also that $\beta_1^- = \beta_2^- = 0$. The effect of k_{ps}^d is to equalize the temperature on the boundary thus we assume that $k_{ps}^d = 0$ in order to avoid this effect. We assume also that $\mathbf{H}_{p1} = \mathbf{H}_{p2} = 0$. By using the relationship $\underline{T} = T^- + [T]/2$, it results the equations,

$$\begin{aligned}
C_1[T_1] + L_1[\beta_1] - k\Delta[T_1] = \Sigma_1 : \mathsf{D}(\frac{\mathbf{U}_1^+ + \mathbf{U}_1^-}{2}) = Y_1 \ , \\
c[\beta_1] + \partial I(\beta_1^+) \ni \frac{L_1}{T_0}(T_1^+ - T_0) \ , \text{ in } \Omega_1 \ , \\
C_2[T_2] + L_2[\beta_2] - k\Delta[T_2] = \Sigma_2 : \mathsf{D}(\frac{\mathbf{U}_2^+ + \mathbf{U}_2^-}{2}) = Y_2 \ , \\
c[\beta_2] + \partial I(\beta_2^+) \ni \frac{L_2}{T_0}(T_2^+ - T_0) \ , \text{ in } \Omega_2 \ ,
\end{aligned} \tag{7.66}$$

because we have equations of motion $B_{p1} = 0$ and $B_{p2} = 0$,

$$\begin{aligned}
C_{1s}[T_1] + k\frac{\partial[T_1]}{\partial \mathbf{N}_1} = 0 = Y_{1s} \ , \text{ on } \partial\Omega_1 \backslash (\partial\Omega_1 \cap \partial\Omega_2) \ , \\
C_{2s}[T_2] + k\frac{\partial[T_2]}{\partial \mathbf{N}_2} = 0 = Y_{2s} \ , \text{ on } \partial\Omega_2 \backslash (\partial\Omega_1 \cap \partial\Omega_2) \ ,
\end{aligned}$$

and

$$\begin{aligned}
C_{1s}[T_1] + k\frac{\partial[T_1]}{\partial \mathbf{N}_1} = \frac{\underline{T}_1}{\underline{T}_1 + \underline{T}_2}\left(\mathbf{R}_p \cdot \mathbf{D}_s(\frac{\mathbf{U}^+ + \mathbf{U}^-}{2})\right) = Y_{1s} \ , \\
C_{2s}[T_2] + k\frac{\partial[T_2]}{\partial \mathbf{N}_2} = \frac{\underline{T}_2}{\underline{T}_1 + \underline{T}_2}\left(\mathbf{R}_p \cdot \mathbf{D}_s(\frac{\mathbf{U}^+ + \mathbf{U}^-}{2})\right) = Y_{2s} \ , \text{ on } \partial\Omega_1 \cap \partial\Omega_2 \ .
\end{aligned}$$

Let us define $X_1 = np([T_1])$ and $X_2 = np([T_2])$, where $np(A)$ is the negative part of A, $np(A) = \sup\{-A, 0\}$. The equation of motion for β_1 is

$$0 = B_{p1} \in B_{p1}^{fe} + \partial\Phi_1([\beta_1]) = -\frac{L_1}{T_0}(T_1^+ - T_0) + \partial I(\beta_1^+) + \partial\Phi_1([\beta_1])$$
$$= -\frac{L_1}{T_0}(T_1^+ - T_0) + \partial I([\beta_1]) + \partial\Phi_1([\beta_1]) \ ,$$

because $\beta_1^+ = [\beta_1]$. We get

$$\frac{L_1}{T_0}(T_1^+ - T_0)\,[\beta_1] \in (\partial I([\beta_1]) + \partial\Phi_1([\beta_1]))\,[\beta_1] \ ,$$

and

$$\frac{L_1}{T_0}(T_1^+ - T_0)\,[\beta_1] \geq 0 \ . \tag{7.67}$$

It results that if $[\beta_1] > 0$, $(T_1^+ - T_0) \geq 0$ and $(T_1^+ - T_1^-) \geq (T_1^+ - T_0) \geq 0$: then $X_1 = np([T_1]) = 0$. Thus we have proved that

$$L_1\,[\beta_1]\,X_1 = 0 \ , \tag{7.68}$$

because either $[\beta_1]$ or X_1 is zero. By multiplying Eqs. (7.62), (7.56), (7.58), by $X_1 = np([T_1])$ and Eqs. (7.57), (7.60), (7.63), by $X_2 = np([T_2])$, using relationship (7.68), and integrating over the Ω's and $\partial\Omega$'s

$$-\int_{\Omega_1} C_1(X_1)^2 d\Omega_1 - \int_{\Omega_1} k\,(\mathbf{grad}X_1)^2\,d\Omega_1 - \int_{\partial\Omega_1} C_{1s}(X_1)^2 d\Gamma_1$$
$$-\int_{\Omega_2} C_2(X_2)^2 d\Omega_2 - \int_{\Omega_2} (k\mathbf{grad}X_2)^2\,d\Omega_2 - \int_{\partial\Omega_2} C_{2s}(X_2)^2 d\Gamma_2$$
$$= \int_{\Omega_1} Y_1 X_1 d\Omega_1 + \int_{\partial\Omega_1} Y_{1s} X_1 d\Gamma_1 + \int_{\Omega_2} Y_2 X_2 d\Omega_2 + \int_{\partial\Omega_2} Y_{2s} X_2 d\Gamma_2 \ . \tag{7.69}$$

Due to the constitutive laws and properties of the subdifferentials, the right-hand sides Y's and Y_s's of the previous Eqs. (7.56)–(7.63) are non negative. Then the right-hand side of (7.69) is non negative. But the left-hand side is non positive. Thus both of them are zero and $X_1 = np([T_1])$ and $X_2 = np([T_2])$ are equal to zero. Thus $[T_1] \geq 0$ and $[T_2] \geq 0$.

As one expects, the temperatures increase when two solids collide. Phase change can occur. Relationship (7.67) shows that if it occurs at point $\mathbf{x}$, temperature $T_i^+(\mathbf{x})$ at that point is larger than the phase change temperature T_0.

References

1. Dimnet, E.: Collisions de solides déformables. Thèse de l'École nationale des Ponts et Chaussées, Paris (2000)
2. Dimnet, E., Frémond, M.: Instantaneous collisions of solids. In: ECCOMAS, Barcelone (2000)
3. Freddi, F., Frémond, M.: Collisions and fractures: a predictive theory. Eur. J. Mech. A/Solids **29**, 998–1007 (2010). doi:10.1016/j.euromechsol.2010.07.006
4. Frémond, M.: Méthodes variationnelles en calcul des structures. École nationale des Ponts et Chaussées, Paris (1982)
5. Frémond, M.: Internal constraints in mechanics. In: Pfeiffer, F.G. (ed.) Non-smooth Mechanics. Philosophical Transactions of the Royal Society, Mathematical, Physical and Engineering Sciences, A, **359** (1789), pp. 2309–2326, London (2001)
6. Frémond, M.: Non-smooth Thermomechanics. Springer, Berlin (2002)
7. Frémond, M.: Collisions. Edizioni del Dipartimento di Ingegneria Civile, Università di Roma "Tor Vergata" (2007). ISBN 978-88-6296-000-7
8. Frémond, M.: Phase change in mechanics. UMI-Springer Lecture Notes Series, vol. n13 (2011). ISBN 978-3-642-24608-1, http://www.springer.com/mathematics/book/978-3-642-24608-1, doi:10.1007/978-3-642-24609-8
9. Frémond, M., Gormaz, R., San Martin, J.: Collision of a solid with an uncompressible fluid. Theor. Comput. Fluid Dyn. **16**, 405–420 (2003)
10. Lions, J.L., Stampacchia, G.: Variational inequalities. Commun. Pure Appl. Math. **20**, 493–519 (1967)
11. Panagiotopoulos, P.D.: Inequality Problems in Mechanics and Applications. Birkhaüser Verlag, Basel (1985)
12. Rodrigues, J.F.: Obstacle Problems in Mathematical Physics. North Holland, New York (1987)
13. Stoianovici, D., Hurmuzlu, Y.: A critical study of the applicability of rigid-body collision theory. ASME, J. Appl. Mech. **63**, 307–316 (1996)

Chapter 8
Collisions of Rigid Solids and Fluids

Michel Frémond

8.1 Introduction

Consider an incompressible fluid in a closed vertical tube. Let us turn the tube rapidly upside down. Then the liquid falls and collides with the bottom of the tube: either it bounces or remains in contact with the bottom. Another interesting situation is a swimmer diving in a swimming pool. When he impacts the water, the diver can be horizontal and do a belly flop. In this situation a violent and painful collision occurs with the water, [1, 5, 6]. In mountain areas, for instance in Liguria, after a thunderstorm there may be debris flows colliding with buildings. Those buildings may be destroyed, [2–4, 13, 14].

In each of these problems a solid collides with a viscous incompressible fluid. The debris flow engineering problem is addressed in Chap. 9.

A general framework which deals with the collision of rigid bodies has been developed in the previous chapters. The basic ideas are to consider that the collisions are instantaneous and that the system made of the bodies is deformable because their relative position changes with respect to time.

In this approach, when there is a collision, interior generalized forces appear which are referred as interior percussions. These percussions are interior quantities, determined by constitutive laws depending on the relative velocities before and after the collision.

We apply the above described ideas, in order to obtain a macroscopic predictive theory of collisions of solids with viscous incompressible fluids.

The hypothesis of instantaneousness of collisions is compatible with the fluid incompressibility [15]. Further in addition to the percussion on the contact surfaces between the fluid and solids there are also percussion stresses inside the fluid when the collision occurs. At this time, the velocity field is a discontinuous function with respect to time. There exist a velocity field before and after the collision. We denote them respectively as $\mathbf{U}^-$ and $\mathbf{U}^+$.

The first and second laws of thermodynamics lead to the assumption of the percussion stress depending on the strain rate $\mathsf{D}(\mathbf{U}^+ + \mathbf{U}^-)$ where $D_{ij}(\mathbf{U}) = \frac{1}{2}(U_{i,j} + U_{j,i})$

M. Frémond, *Collisions Engineering: Theory and Applications*,
Springer Series in Solid and Structural Mechanics 6,
DOI 10.1007/978-3-662-52696-5_8

is the usual strain rate. In the same way the percussion contact force depends on the relative velocity $\mathbf{U} - \mathbf{U}_s$ of the fluid with respect to the solid ($\mathbf{U}_s$ denotes the solid velocity).

Choosing the simplest constitutive law, i.e., linear constitutive laws, results in a set of partial differential equations which gives the velocities $\mathbf{U}^+$ and $\mathbf{U}_s^+$ after the collision depending on the velocities $\mathbf{U}^-$ and $\mathbf{U}_s^-$ before the collision. This set of partial differential equations is coherent in term of both mechanical and mathematical point of view. Moreover the two examples which are investigated below, show that the theory takes into accounts the basic physical properties.

The chapter is organized as follows: first the equations of motions are derived from the principle of virtual work; then the constitutive laws are chosen in order to fulfill the second law of thermodynamics requirements. Examples are given: collision of a fluid with the bottom of a tube is described with a closed form solution. Then the diver problem in a swimming pool is investigated: an existence theorem is proved and numerical results are presented.

8.2 The Equation of Motion

We investigate the motion of a system made of a solid and a fluid in a time interval where we assume there is only one collision at time t. We denote by t_1 any time before t and denote by t_2 any time after t.

When a solid collides with water very large internal forces appear because of the incompatibility of the velocities of the solid and water: very large stresses inside and very large forces on the contact surface. In many circumstances the duration of the violent contact is very short compare to the duration of the smooth motion. For instance when skipping stones on the still water of a lake, the duration of the contact of the stone with the water is small compare to its time flight. As in the previous chapters, we decide as a schematization to consider that the collisions are instantaneous. Thus the velocities are discontinuous functions of the time: for the fluid, there is the velocity $\mathbf{U}^-(\mathbf{x}, t)$ before the collision at time t and the velocity $\mathbf{U}^+(\mathbf{x}, t)$ after the collision; for the solid, there is the velocity $\mathbf{U}_s^-(\mathbf{x}, t) = \mathbf{X}^-(t) + \Omega^-(t) \times (\mathbf{x} - \mathbf{x}_G(t))$ before the collision and the velocity $\mathbf{U}_s^+(\mathbf{x}, t) = \mathbf{X}^+(t) + \Omega^+(t) \times (\mathbf{x} - \mathbf{x}_G(t))$ after the collision. The velocity of the center of mass $\mathbf{x}_G(\tau)$ of the rigid body is $\mathbf{X}(\tau)$ and $\Omega(\tau)$ is its angular velocity. Because the collision is instantaneous, the very large internal forces are also concentrated in time: thus they become percussions.

8.2.1 The Principle of Virtual Work

It is usual to derive the equation of motion through the principle of virtual power, [7]. This principle can be used when all the quantities have densities with respect to the

Lebesgue measure. When it is not the case as in the present situation, the principle of virtual power can be advantageously replaced by the principle of virtual work.

Let us recall that there is a collision only at time t, thus the actual and virtual velocities are discontinuous with respect to time only time t with $t_1 < t < t_2$. The principle is:

the virtual work of the acceleration forces between the times t_1 and t_2 is equal to the sum of the virtual work of the interior forces between the times t_1 and t_2 and of the virtual work of the exterior forces between the times t_1 and t_2.

We will use this principle defining first the virtual velocities. As already said, the actual velocities can be discontinuous in the evolution of the fluid. Thus the virtual velocities are to be discontinuous functions of the time. In mathematical terms, it is wise to assume that the velocities are functions of bounded variation with respect to the time. With respect to the space, it is assumed that the velocities have the usual properties (for instance, they belong to convenient Sobolev spaces). The different virtual works are linear functions of the virtual velocities. They involve regular forces and stresses together with percussions and percussion stresses. The regular forces and stresses are quantities which have a density with respect to the Lebesgue measure. The percussions and percussion stresses can be thought as time concentrated quantities which define an atomic measure (for instance a Dirac measure) and intervene only at collisions times.

Let us consider the system made of the fluid and solids. For instance, the solids are the container of the fluid and a moving obstacle (Fig. 8.3). For the sake of simplicity, we suppose there is only one solid (for instance the container). The fluid occupies the domain $\Omega(t)$ and is in contact with the solid on the part $\Gamma_1(t)$ of its boundary $\partial\Omega(t)$. At an arbitrary time t, we consider the virtual velocities $(\mathbf{V}(\mathbf{x}, t), \mathbf{Y}(t), \boldsymbol{\omega}(t))$ defined on $\Omega(t)$. The velocity $\mathbf{Y}(t)$ is a virtual velocity of the center of mass of the rigid body and $\boldsymbol{\omega}(t)$ is a virtual angular velocity of the rigid body. It is denoted by $\mathbf{V}_s(\mathbf{x}, t) = \overrightarrow{Y}(t) + \boldsymbol{\omega}(t) \times (\mathbf{x} - \mathbf{x}_G(t))$, the virtual velocity at point $\mathbf{x}$ of the rigid body. The mass of the rigid body is M and its mass moment of inertia is I. The density of the fluid is ρ.

8.2.1.1 The Virtual Work of the Acceleration Forces

We choose the virtual work of the acceleration forces as

$$\mathcal{T}^{acc}(t_1, t_2, \mathbf{V}, \mathbf{Y}, \boldsymbol{\omega}) = \int_{\Omega(t)} \rho\,[\mathbf{U}(\mathbf{x}, t)] \cdot \frac{\mathbf{V}^+(\mathbf{x}, t) + \mathbf{V}^-(\mathbf{x}, t)}{2} dx \tag{8.1}$$

$$+ \int_{t_1}^{t_2} \int_{\Omega(\tau)} \rho \frac{d\mathbf{U}}{dt}(\mathbf{x}, \tau) \cdot \mathbf{V}(\mathbf{x}, \tau) dx d\tau \tag{8.2}$$

$$+M\,[\mathbf{X}(t)]\cdot\frac{\mathbf{Y}^{+}(t)+\mathbf{Y}^{-}(t)}{2}+M\int_{t_1}^{t_2}\frac{d\mathbf{X}}{dt}(\tau)\cdot\mathbf{Y}(\tau)d\tau \tag{8.3}$$

$$+I\,[\Omega(t)]\cdot\frac{\boldsymbol{\omega}^{+}(t)+\boldsymbol{\omega}^{-}(t)}{2}+\int_{t_1}^{t_2}\frac{dI\Omega}{dt}(\tau)\cdot\boldsymbol{\omega}(\tau)d\tau, \tag{8.4}$$

where $[A]=A^{+}-A^{-}$ is as usual the discontinuity of the quantity A

8.2.1.2 The Theorem of Kinetic Energy

Let us note that the actual work of acceleration forces is the variation of the kinetic energy

$$K(t)=\int_{\Omega(t)}\frac{\rho}{2}\mathbf{U}^{2}(t)dx+\frac{M}{2}\mathbf{X}^{2}(t)+\frac{I}{2}\Omega^{2}(t), \tag{8.5}$$

between times t_1 and t_2

$$K^{-}(t_2)-K^{+}(t_1)=\mathcal{T}^{acc}(t_1,t_2,\mathbf{U},\mathbf{X},\Omega). \tag{8.6}$$

If a collision occurs at times t_2, $K^{-}(t_2)$ is the kinetic energy before the collision and if a collision has occurred at time t_1, $K^{+}(t_1)$, is the kinetic energy after the collision.

8.2.1.3 The Virtual Work of the Interior Forces

The virtual work of the interior forces we choose, is a linear function of the virtual strain rate, $D_{ij}(\mathbf{V})=(1/2)(V_{i,j}+V_{j,i})$, and of the difference of the velocities on the contact surface, $\mathbf{V}-\mathbf{V}_s$. The densities with respect to the Lebesgue measure are the stress tensor σ and the interaction force $\mathbf{r}$ between the fluid and the solid. The densities with respect to the Dirac measure are the percussion stress tensor Σ and the interaction percussion $\mathbf{R}$ between the fluid and the solid. The percussion stress and the interaction percussion are generalized interior forces which appear when collisions occur. They are, as said earlier, usual interior forces concentrated in a very short period of time. The virtual work of the interior forces we choose, is

$$\mathcal{T}^{int}(t_1,t_2,\mathbf{V},\mathbf{Y},\boldsymbol{\omega})=-\int_{\Omega(t)}\Sigma(\mathbf{x},t):\frac{\mathsf{D}(\mathbf{V}^{+})(\mathbf{x},t)+\mathsf{D}(\mathbf{V}^{-})(\mathbf{x},t)}{2}dx \tag{8.7}$$

$$-\int_{\Gamma_1(t)}\mathbf{R}(\mathbf{x},t)\cdot\frac{\mathbf{V}^{+}(\mathbf{x},t')-\mathbf{V}_s^{+}(\mathbf{x},t)+\mathbf{V}^{-}(\mathbf{x},t)-\mathbf{V}_s^{-}(\mathbf{x},t)}{2}d\Gamma \tag{8.8}$$

$$-\int_{t_1}^{t_2}\int_{\Omega(\tau)}\sigma(\mathbf{x},\tau):\mathsf{D}(\mathbf{V})(\mathbf{x},\tau)dxd\tau \tag{8.9}$$

$$-\int_{t_1}^{t_2}\int_{\Gamma_1(\tau)}\mathbf{r}(\mathbf{x},\tau)\cdot(\mathbf{V}(\mathbf{x},\tau)-\mathbf{V}_s(\mathbf{x},\tau))d\Gamma d\tau. \tag{8.10}$$

The work of the interior forces has to satisfy the axiom of the interior forces, [7]:

the work of the interior forces is zero for any rigid system virtual velocities $\mathbf{V}(\mathbf{x}, t), \mathbf{Y}(t), \boldsymbol{\omega}(t)$.

The rigid system velocities are such that $\mathsf{D}(\mathbf{V}) = 0$ and $\mathbf{V} - \mathbf{V_s} = 0$ on the boundary Γ_1. Thus it is obvious that $\mathcal{T}^{int}(t_1, t_2, \mathbf{V}, \mathbf{Y}, \boldsymbol{\omega}) = 0$ for such a set of velocities $(\mathbf{V}, \mathbf{Y}, \boldsymbol{\omega})$.

8.2.1.4 The Virtual Work of the Exterior Forces

The virtual work of the exterior forces involves the possibility to apply both the classical forces and percussions. The chosen virtual work of the exterior forces is given by

$$\mathcal{T}^{ext}(t_1, t_2, \mathbf{V}, \mathbf{Y}, \boldsymbol{\omega}) = \int_{\partial\Omega(t)} \mathbf{G}^{ext}(\mathbf{x}, t) \cdot \frac{\mathbf{V}^+(\mathbf{x}, t) + \mathbf{V}^-(\mathbf{x}, t)}{2} d\Gamma \tag{8.11}$$

$$+\mathbf{H}^{ext}(t) \cdot \frac{\mathbf{V}_s^+(\mathbf{x}_H, t) + \mathbf{V}_s^-(\mathbf{x}_H, t)}{2} \tag{8.12}$$

$$+ \int_{t_1}^{t_2} \int_{\Omega(\tau)} \mathbf{f}^{ext}(\overrightarrow{x}, \tau) \cdot \mathbf{V}(\mathbf{x}, \tau) dx d\tau \tag{8.13}$$

$$+ \int_{t_1}^{t_2} \int_{\partial\Omega(\tau)} \mathbf{g}^{ext}(\mathbf{x}, \tau) \cdot \mathbf{V}(\mathbf{x}, \tau) d\Gamma d\tau \tag{8.14}$$

$$+ \int_{t_1}^{t_2} \mathbf{h}^{ext}(\tau) \cdot (\mathbf{Y}(\tau) + \boldsymbol{\omega}(\tau) \times (\mathbf{x}_h(\tau) - \mathbf{x}_G(\tau))) d\tau, \tag{8.15}$$

where $\mathbf{h}^{ext}(\tau)$ is a regular exterior force applied at the point $\mathbf{x}_h(\tau)$ of the rigid body; $\mathbf{H}^{ext}(t)$ is an exterior percussion applied at the point $\mathbf{x}_H$ of the rigid body; $\mathbf{f}^{ext}(\mathbf{x}, \tau)$ and $\mathbf{g}^{ext}(\mathbf{x}, \tau)$ are exterior regular volume and surface forces applied to the fluid; $\mathbf{G}^{ext}(\mathbf{x}, t')$ is an exterior surface percussion applied to the fluid.

Remark 8.1 As in Chap. 2, we say that there is a collision at time t if at least one of the four quantities $[\mathbf{U}(\mathbf{x}, t)]$, $\Sigma(\mathbf{x}, \mathsf{t})$, $\mathbf{H}^{ext}(t)$ and $\mathbf{G}^{ext}(\mathbf{x}, t)$ is non null. Within this point of view all the four quantities are defined at any time τ.

8.2.2 The Equations of Motion

They result from the principle of virtual work

$$\forall (t_1, t_2, \mathbf{V}, \mathbf{Y}, \boldsymbol{\omega}), \tag{8.16}$$

$$\mathcal{T}^{acc}(t_1, t_2, \mathbf{V}, \mathbf{Y}, \boldsymbol{\omega}) = \mathcal{T}^{int}(t_1, t_2, \mathbf{V}, \mathbf{Y}, \boldsymbol{\omega}) + \mathcal{T}^{ext}(t_1, t_2, \mathbf{V}, \mathbf{Y}, \boldsymbol{\omega}). \tag{8.17}$$

It is easy to get, *almost everywhere with respect to time*

$$\rho \frac{d\mathbf{U}}{dt} = \operatorname{div} \sigma + \mathbf{f}^{ext}, \ in \ \Omega(\tau), \tag{8.18}$$

$$\sigma \mathbf{N} = -\mathbf{r} + \mathbf{g}^{ext}, \ \in \ \Gamma_1(\tau), \tag{8.19}$$

$$\sigma \mathbf{N} = \mathbf{g}^{ext}, \ in \ \partial\Omega(\tau) \backslash \Gamma_1(\tau), \tag{8.20}$$

$$M \frac{d\mathbf{X}}{dt} = \int_{\Gamma_1(\tau)} \mathbf{R} d\Gamma + \mathbf{h}^{ext}, \tag{8.21}$$

$$\frac{d}{dt}(I\Omega) = \int_{\Gamma_1(\tau)} (\mathbf{x} - \mathbf{x}_G) \times \mathbf{r} d\Gamma + (\mathbf{x}_h - \mathbf{x}_G) \times \mathbf{h}^{ext}, \tag{8.22}$$

where the outwards normal vector to the fluid is $\mathbf{N}$ (Fig. 8.3). In case there are more than one solid, the boundary conditions and the last two equations are valid for each rigid body, i.e., the container and the obstacle (of course the mechanical characteristics, M, I, are different). These are the classical equations of motion when the fluid, and the solid evolve smoothly;

and following Remark 8.1 *at any time τ, for instance at time t when there is the collision*,

$$\rho \left[\mathbf{U}(\mathbf{x}, t)\right] = \operatorname{div} \Sigma(\mathbf{x}, t), \ \text{in } \Omega(t), \tag{8.23}$$

$$\Sigma(\mathbf{x}, t)\mathbf{N} = -\mathbf{R}(\mathbf{x}, t) + \mathbf{G}^{ext}(\mathbf{x}, t), \ \text{on } \Gamma_1(t), \tag{8.24}$$

$$\Sigma(\mathbf{x}, t)\mathbf{N} = \mathbf{G}^{ext}(\mathbf{x}, t), \ \text{on } \partial\Omega(t) \backslash \Gamma_1(t), \tag{8.25}$$

$$M[\mathbf{X}(t)] = \int_{\Gamma_1(t)} \mathbf{R}(\mathbf{x}, t) d\Gamma + \mathbf{H}^{ext}(t), \tag{8.26}$$

$$I[\Omega(t)] = \int_{\Gamma_1(t)} (\mathbf{x} - \mathbf{x}_G(t)) \times \mathbf{R}(\mathbf{x}, t) d\Gamma + (\mathbf{x}_H - \mathbf{x}_G(t)) \times \mathbf{H}^{ext}(t). \tag{8.27}$$

The boundary conditions and the last two equations are valid for any solid if more than one are in contact with the fluid.

Constitutive laws are needed for $(\sigma, \mathbf{r})$ and $(\Sigma, \mathbf{R})$ in order to solve the smooth and non smooth equations. They result from experiments and are restricted by a basic relation, namely the second principle of thermodynamics.

8.3 The Constitutive Laws

Because we intend to deal with incompressible fluids, we assume the temperature T to be constant and the internal energy and entropy to be also constant with respect to the time.

8.3.1 The Energy Balance

The energy balance is

$$K^-(t_2) - K^+(t_1) = \mathcal{T}^{ext}(t_1, t_{0,}t_2, \mathbf{U}, \mathbf{X}, \Omega) + T\,Q^{ext}(t_1, t_2), \tag{8.28}$$

where $K(t)$ is the kinetic energy and $T\,Q^{ext}(t_1, t_2)$ is the heat received from the exterior between times t_1 and t_2, $Q^{ext}(t_1, t_2)$ being the amount of entropy received. $\mathcal{T}^{ext}(t_1, t_2, t_2, \mathbf{U}, \mathbf{X}, \Omega)$ and $T\,Q^{ext}(t_1, t_2)$ are the mechanical and thermal exterior actions. The principle of virtual work with the actual velocities gives

$$K^-(t_2) - K^+(t_1) = \mathcal{T}^{int}(t_1, t_2, \mathbf{U}, \mathbf{X}, \Omega) + \mathcal{T}^{ext}(t_1, t_2, \mathbf{U}, \mathbf{X}, \Omega). \tag{8.29}$$

By subtracting the previous equations (8.28) and (8.29) it results

$$0 = -\mathcal{T}^{int}(t_1, t_2, \mathbf{U}, \mathbf{X}, \Omega) + T\,Q^{ext}(t_1, t_2). \tag{8.30}$$

8.3.2 The Second Law of Thermodynamics

The second law of thermodynamics is

$$0 \geq Q^{ext}(t_1, t_2). \tag{8.31}$$

This relation shows that a collision produces heat. The quantity of the heat produced is given by the energy balance.

The previous relations (8.30) and (8.31) give

$$\mathcal{T}^{int}(t_1, t_2, \mathbf{U}, \mathbf{X}, \Omega) \leq 0, \tag{8.32}$$

or

$$-\int_{\Omega(t)} \Sigma(\mathbf{x}, t) : \frac{\mathsf{D}(\mathbf{U}^+)(\mathbf{x}, t) + \mathsf{D}(\mathbf{U}^-)(\mathbf{x}, t)}{2} dx \tag{8.33}$$

$$-\int_{\Gamma_1(t)} \mathbf{R}(\mathbf{x}, t) \cdot \frac{\mathbf{U}^+(\mathbf{x}, t) - \mathbf{U}_s^+(\mathbf{x}, t) + \mathbf{U}^-(\mathbf{x}, t) - \mathbf{U}_s^-(\mathbf{x}, t)}{2} d\Gamma \tag{8.34}$$

$$-\int_{t_1}^{t_2} \int_{\Omega(\tau)} \sigma(\mathbf{x}, \tau) : \mathsf{D}(\mathbf{U})(\mathbf{x}, \tau) dx d\tau \tag{8.35}$$

$$-\int_{t_1}^{t_2} \int_{\Gamma_1(\tau)} \mathbf{r}(\mathbf{x}, \tau) \cdot (\mathbf{U}(\mathbf{x}, \tau) - \mathbf{U}_s(\mathbf{x}, \tau)) d\Gamma d\tau \leq 0, \tag{8.36}$$

in any actual evolution. Because these relationships are satisfied for any subdomain $\mathcal{D}$ of $\Omega(t)$ and any set of actual velocities $(\mathbf{U}, \mathbf{X}, \Omega)$, we get

$$\Sigma(\mathbf{x}, t) : \frac{\mathsf{D}(\mathbf{U}^+)(\mathbf{x}, t) + \mathsf{D}(\mathbf{U}^-)(\mathbf{x}, t)}{2} \geq 0, \text{ in } \Omega(t), \quad (8.37)$$

$$\mathbf{R}(\mathbf{x}, t) \cdot \frac{\mathbf{U}^+(\mathbf{x}, t) - \mathbf{U}_s^+(\mathbf{x}, t) + \mathbf{U}^-(\mathbf{x}, t) - \mathbf{U}_s^-(\mathbf{x}, t)}{2} \geq 0, \text{ on } \Gamma_1(t), \quad (8.38)$$

$$\sigma(\mathbf{x}, \tau) : \mathsf{D}(\mathbf{U})(\mathbf{x}, \tau) \geq 0, \text{ in } \Omega(\tau), \quad (8.39)$$

$$\mathbf{r}(\mathbf{x}, \tau) \cdot (\mathbf{U}(\mathbf{x}, \tau) - \mathbf{U}_s(\mathbf{x}, \tau)) \geq 0, \text{ on } \Gamma_1(\tau), \quad (8.40)$$

Relationships (8.40) are a guide to choose the constitutive laws. They are used in the following paragraph to choose the constitutive laws for $(\Sigma, \mathbf{R})$ and $(\sigma, \mathbf{r})$.

8.3.3 The Constitutive Laws for an Incompressible Fluid

The constitutive laws we choose have to satisfy relationships (8.40). For the smooth part, the constitutive laws are that of the incompressible viscous fluid together with the boundary conditions describing the unilateral interactions of the fluid with the solid, for instance its container

$$\sigma = 2\mu\mathsf{D}(\mathbf{U}) - p\mathsf{I}, \ \text{div}\mathbf{U} = 0, \quad (8.41)$$

where μ is the viscosity and p is the pressure, I being the identity tensor. It gives the regular Navier-Stokes equations. The surface interaction force is divided into a dissipative force $\mathbf{r}^d$, taking into account all the friction phenomenons, and a reaction force $\mathbf{r}^{reac}$, imposing the impenetrability

$$\mathbf{r} = \mathbf{r}^d + \mathbf{r}^{reac}. \quad (8.42)$$

For the dissipative force we take the simplest case: a linear function

$$\mathbf{r}^d = k(\mathbf{U} - \mathbf{U}_s), \ \text{with } k \geq 0, \quad (8.43)$$

where the physical parameter k accounts for the friction of the liquid on the solid. The case $k = \infty$ refers the case when the fluid remains in contact with its container, i.e., $\mathbf{U} = \mathbf{U}_s$. The case $k = 0$ describes the situation where there is no interaction between the fluid and the solid except their non impenetrability.

We choose the reaction force $\mathbf{r}^{reac}$ normal to the contact surface

$$\mathbf{r}^{reac} = r^{reac}\mathbf{N}, \ r^{reac} \in \partial I_-(U_n - U_{ns}), \quad (8.44)$$

where the outwards normal vector to the fluid is $\mathbf{N}$ (Fig. 8.3) and $U_n = \mathbf{U} \cdot \mathbf{N}$, $U_{ns} = \mathbf{U}_s \cdot \mathbf{N}$ are the normal velocities. The values of the impenetrability reaction r^{reac} belong to the subdifferential set ∂I_- of the indicator function I_- of the set of negative numbers R^-, defined by (see for example [11]):

$$\partial I_-(U_n - U_{ns}) = \begin{cases} \{0\}, & \text{if } U_n - U_{ns} < 0, \\ R^+, & \text{if } U_n - U_{ns} = 0, \\ \emptyset, & \text{if } U_n - U_{ns} > 0. \end{cases} \tag{8.45}$$

For the non smooth part, the inequality (8.36) and the expression of $\mathcal{T}^{int}$ suggest to assume $\boldsymbol{\Sigma}$ to depend on $\mathsf{D}(\mathbf{U}^+ + \mathbf{U}^-)$. This important assumption is very simple. It is possible to make more sophisticated assumptions, for instance that $\boldsymbol{\Sigma}$ depends separately on $\mathsf{D}(\mathbf{U}^+)$ and $\mathsf{D}(\mathbf{U}^-)$. It is to be seen with the examples that the previous simple assumption is sufficient to take account of the basic physical results. Thus we choose

$$\boldsymbol{\Sigma} = 2\gamma \mathsf{D}(\mathbf{U}^+ + \mathbf{U}^-) - P\mathsf{I}, \operatorname{div}(\mathbf{U}^+ + \mathbf{U}^-) = 0, \text{ with } \gamma \geq 0. \tag{8.46}$$

The incompressibility condition $\operatorname{div}(\mathbf{U}^+ + \mathbf{U}^-) = 0$ or $\operatorname{div}\mathbf{U}^+ = 0$ because $\operatorname{div}\mathbf{U}^- = 0$, results in the percussion pressure P, [5, 6, 9, 10].

The interaction percussion $\mathbf{R}$ between the solid and the fluid has to take into account their impenetrability. Thus the percussion is divided into a reaction $\mathbf{R}^{reac}$ to the impenetrability constraint and a dissipative percussion $\mathbf{R}^d$ which modelizes all the dissipative interactions between the fluid and the solid

$$\mathbf{R} = \mathbf{R}^d + \mathbf{R}^{reac}. \tag{8.47}$$

The inequality (8.36) and the expression of $\mathcal{T}^{int}$ suggest to assume $\mathbf{R}^d$ to depend on $(\mathbf{U}^+(\mathbf{x}, t) - \mathbf{U_s}^+(\mathbf{x}, t) + \mathbf{U}^-(\mathbf{x}, t) - \mathbf{U_s}^-(\mathbf{x}, t))$. Let us repeat that more sophisticated choices may be made but we consider the relation (8.36) as a guide and that the basic choice of a linear function for $\mathbf{R}^d$ to satisfy the inequality is simple but crucial. Thus we choose

$$\mathbf{R}^d(\mathbf{x}, t) = K(\mathbf{U}^+(\mathbf{x}, t) - \mathbf{U_s}^+(\mathbf{x}, t) + \mathbf{U}^-(\mathbf{x}, t) - \mathbf{U_s}^-(\mathbf{x}, t)), \text{ with } K \geq 0. \tag{8.48}$$

Of course the physical parameter K depends on the nature of the colliding solid and fluid.

We choose to have the impenetrability reaction to be active only when the risk of interpenetration is present, i.e., when the contact is persistent after the collision. Thus we choose the constitutive law

$$\mathbf{R}^{reac} = R^{reac}\mathbf{N}, \tag{8.49}$$

$$\text{with } R^{reac}(\mathbf{x}, t) \in \partial I_-(U_n^+(\mathbf{x}, t) - U_{ns}^+(\mathbf{x}, t)), \tag{8.50}$$

where ∂I_- is the subdifferential set of the indicator function I_- of the set of the negative numbers R^- (the set ∂I_- is defined in the formulas (8.45)). To prove that the inequality (8.36) is satisfied, one uses the fact that the physical parameters μ, γ, k and K are positive and the property of the impenetrability reaction given in the following lemma

Lemma 8.1 *The impenetrability reaction (8.50) satisfies,*

$$\mathbf{R}^{reac}(\mathbf{x},t)\cdot(\mathbf{U}^+(\mathbf{x},t)-\mathbf{U_s}^+(\mathbf{x},t)+\mathbf{U}^-(\mathbf{x},t)-\mathbf{U_s}^-(\mathbf{x},t))\geq 0. \tag{8.51}$$

Proof Let us recall that $U_n=\mathbf{U}\cdot\mathbf{N}$ and $U_{sn}=\mathbf{U_s}\cdot\mathbf{N}$ are the normal velocities. The relation (8.50) proves that the subdifferential set $\partial I(U_n^+(\mathbf{x},t)-U_{ns}^+(\mathbf{x},t))$ is not empty and thus that the impenetrability condition

$$U_n^+(\mathbf{x},t)-U_{ns}^+(\mathbf{x},t)\leq 0, \tag{8.52}$$

is satisfied. If $U_n^+(\mathbf{x},t)-U_{sn}^+(\mathbf{x},t)<0$ the properties of the subdifferential sets show that $R^{reac}=0$ and the relation (8.51) is satisfied. If $U_n^+(\mathbf{x},t)-U_{sn}^+(\mathbf{x},t)=0$, the properties of the subdifferential sets show that $R^{reac}\geq 0$. Because $U_n^-(\mathbf{x},t)-U_{sn}^-(\mathbf{x},t)\geq 0$, see the Fig. 8.3,

$$\mathbf{R}^{reac}(x,t)\cdot(\mathbf{U}^+(\mathbf{x},t)-\mathbf{U_s}^+(\mathbf{x},t)+\mathbf{U}^-(\mathbf{x},t)-\mathbf{U_s}^-(\mathbf{x},t)) \tag{8.53}$$

$$=R^{reac}(U_n^-(\mathbf{x},t)-U_{ns}^-(\mathbf{x},t))\geq 0. \tag{8.54}$$

Thus the relation (8.51) is satisfied.

Let us emphasizes that the impenetrability condition (8.50) has two meanings. The first one is to imply that $U_n^+-U_{sn}^+\leq 0$ and the second one is to give the value of the reaction R^{reac} which is 0 when contact is not maintained after the collision and which is positive when contact is maintained after the collision. Now, a direct consequence of the lemma and of the constitutive laws is that inequalities (8.40) are satisfied:

Theorem 8.1 *In any actual evolution, inequalities (8.40) are satisfied.*

At this point the predictive theory is achieved. It is to be checked if it is consistent in terms of mathematics, numerics and if it has the ability to account for the more obvious experimental results. Let us again repeat that we have decided to choose the simplest constitutive laws which satisfy the basic requirements of mechanics. The collision constitutive laws are characterized only by two parameters γ which takes into account the volume phenomenons occurring in a collision and K which describes the surface interaction between the surface of the solid and the fluid. We are convinced that this is the minimal number of informations which are needed to predict what occur after a collision.

8.4 An Incompressible Fluid in a Tube

Consider a fluid in a tube and turn the tube upside down rapidly. The fluid falls and collides with the bottom of the tube (Fig. 8.1). We intend to describe this collision.

We assume the velocity of the tube is zero before and after the collision and that the velocity of the fluid before the collision is vertical and homogeneous: $\mathbf{U}^- = (0, 0, U^-)$, where U^- is constant with $U^- \leq 0$. The equations of motion of the fluid in the collision are

$$\rho\,[\mathbf{U}] = \mathrm{div}\Sigma, \tag{8.55}$$

$$\mathrm{div}\mathbf{U}^+ = 0, \tag{8.56}$$

in the volume. The boundary condition on the bottom and the vertical sides are

$$\Sigma\mathbf{N} = -\mathbf{R}^d - P^{reac}\mathbf{N}, \tag{8.57}$$

The boundary condition on the top of the fluid is

$$\Sigma\mathbf{N} = 0. \tag{8.58}$$

The constitutive law are given by

$$\Sigma = 2\gamma \mathsf{D}(\mathbf{U}^+ + \mathbf{U}^-) - P\mathsf{I},$$
$$\mathbf{R}^d = K(\mathbf{U}^+ + \mathbf{U}^-),\ \ P^{reac} \in \partial I_-(U_n^+).$$

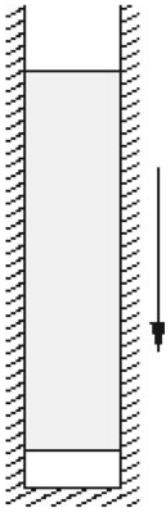

Fig. 8.1 The bottom of the tube and the falling liquid just before the collision

They are the equations which relate $\mathbf{U}^+$, the unknown velocity after the collision, to $\mathbf{U}^-$, the velocity before the collision. In order to find a closed form solution we look for the velocity $\mathbf{U}^+$ vertical. It results from (8.56) that the vertical velocity is constant

$$\mathbf{U}^+ = (0, 0, U^+), \text{ where } U^+ \text{is constant.} \tag{8.59}$$

The Eq. (8.55) give

$$\rho\mathbf{U}^+ - 2\gamma\Delta\mathbf{U}^+ + \nabla P = \rho\mathbf{U}^- + 2\gamma\Delta\mathbf{U}^-, \tag{8.60}$$

which reduces to

$$\rho\mathbf{U}^+ + \nabla P = \rho\mathbf{U}^-. \tag{8.61}$$

This equation gives the percussion pressure

$$P(x, y, z) = P_0 - \rho(U^+ - U^-)z, \tag{8.62}$$

where P_0 is a constant. The boundary condition on the top (8.58) gives

$$P_0 = \rho(U^+ - U^-)L, \tag{8.63}$$

where L is the height of the fluid column. The boundary condition on the bottom (8.57) gives

$$-P_0\mathbf{N} = -K(\mathbf{U}^+ + \mathbf{U}^-) - P^{reac}\mathbf{N}, \tag{8.64}$$

and replacing P_0 from (8.63) we obtain

$$\rho(U^+ - U^-)L = -K\left(U^+ + U^-\right) + P^{reac}, \tag{8.65}$$

which is the equation giving U^+, because P^{reac} depends on U^+. This dependance is $P^{reac} \in \partial I_-(U_n^+) = \partial I_-(-U^+) = -\partial I_+(U^+)$, where ∂I_+ is the subdifferential set of the indicator function of the positive numbers R^+. It gives the following equation

$$(\rho L - K)U^- \in (K + \rho L)U^+ + \partial I_+(U^+). \tag{8.66}$$

The multivoque function $f(x) = (K + \rho L)x + \partial I_+(x)$, is a maximal monotone operator, as we can see in Fig. 8.2, then for any given U^- there exist a unique U^+ solution of (8.66): if $K > \rho L$, that is, if there is a small amount of fluid, the solution is

$$U^+ = -\frac{K - \rho L}{K + \rho L}U^-, \text{ with } P^{reac} = 0. \tag{8.67}$$

Otherwise, if there is a large amount of fluid, $K \leq \rho L$, the solution is

$$U^+ = 0, \text{ with } P^{reac} = (K - \rho L)U^- \geq 0. \tag{8.68}$$

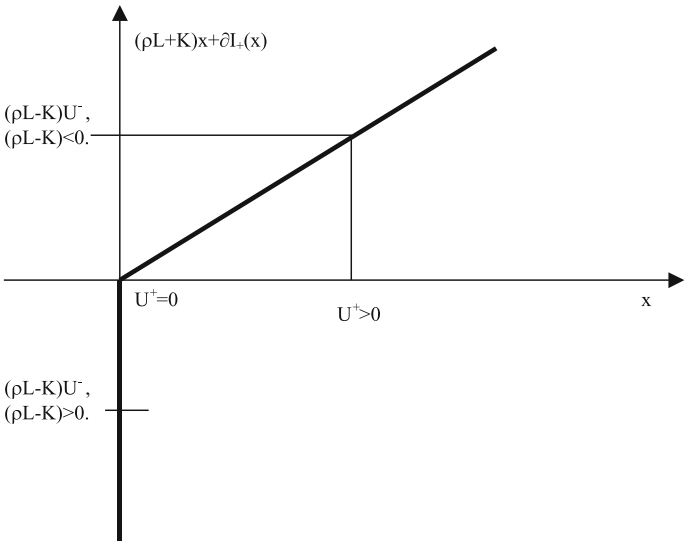

Fig. 8.2 The graph $f(x) = (K + \rho L)x + \partial I_+(x)$ is monotone and maximal. The equation $f(x) = (\rho L - K)U^-$ has one and only one solution. When there is a large quantity of fluid, $\rho L - K > 0$, the fluid does not bounce on the bottom of the tube. When there is only a droplet, $\rho L - K < 0$, it bounces

We conclude that a droplet of fluid bounces on the bottom of the tube but a large quantity of fluid does not bounce.

8.5 The Diver Problem

For the sake of simplicity a 2D problem is investigated. It is assumed that the swimming pool is a fixed rectangle. The horizontal swimmer Γ_1 dives at the middle of the swimming pool (Fig. 8.3). We assume that the diver is symmetric, flat (Fig. 8.3) and its thickness is zero. Its velocities when hitting the water are

$$\mathbf{X}^- = (0, X^-), \tag{8.69}$$

$$\Omega^- = \mathbf{0}. \tag{8.70}$$

It is assumed that no external load is applied. It result from the symmetries that the solution

$$\mathbf{U}^+(x, y) = \left(U_1^+(x, y), U_2^+(x, y)\right) \tag{8.71}$$

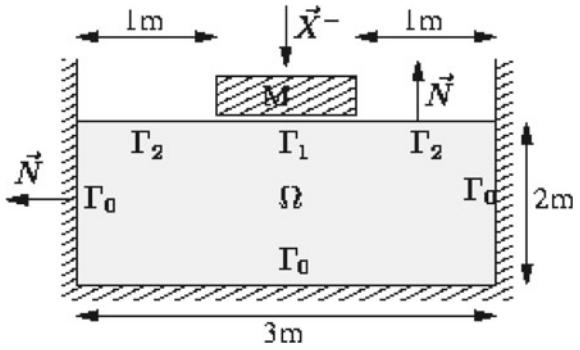

Fig. 8.3 The diver and the swimming pool. The normal velocity of the diver before the collision is negative, $U_n^- - U_{ns}^- = -X^- \leq 0$

is such that $\mathbf{U}^+(-x, y) = \left(-U_1^+(x, y), U_2^+(x, y)\right)$ and that $\mathbf{X}^+ = (0, X^+)$ and $\Omega^+ = \mathbf{0}$. All the points of the rigid body have the same vertical velocity, which is the velocity of the middle of Γ_1.

8.5.1 The Equations

Let Ω be the swimming pool, an open subset in $\mathbb{R}^2$ with piecewise $\mathcal{C}^2$ boundary with outwards normal vector $\mathbf{N}$, (Fig. 8.3). This domain contains a viscous homogeneous incompressible fluid. We suppose that at time t the velocity field is known and equal to $\mathbf{U}^-(\mathbf{x}, t) = 0$. At this time t, the diver schematized by a rigid body, collides the part Γ_1 of the boundary $\partial\Omega$. We suppose that the remaining boundary $\partial\Omega \backslash \Gamma_1$ is decomposed into two additional disjoint parts: a rigid boundary Γ_0 and a free boundary Γ_2. We are interested in finding the velocities $\mathbf{U}^+(\mathbf{x}, t)$ and $\mathbf{X}^+(t)$ after the collision. The equations follow from the equations of motion

$$\rho \mathbf{U}^+ = \text{div}\Sigma, \tag{8.72}$$

$$M[\mathbf{X}(t)] = \int_{\Gamma_1} \mathbf{R}_1(\mathbf{x}, t) d\Gamma, \tag{8.73}$$

$$\Sigma\mathbf{N} = -\mathbf{R}_0(\mathbf{x}, t), \text{ on } \Gamma_0, \tag{8.74}$$

$$\Sigma\mathbf{N} = -\mathbf{R}_1(\mathbf{x}, t), \text{ on } \Gamma_1, \tag{8.75}$$

$$\Sigma n\mathbf{N} = 0 \text{ on } \Gamma_2, \tag{8.76}$$

and the constitutive laws

$$\Sigma = 2\gamma \mathsf{D}(\mathbf{U}^+) - P\mathsf{I}, \tag{8.77}$$

$$\mathbf{R}_0 = K_0\mathbf{U}^+ + R_0^{reac}\mathbf{N},\ R_0^{reac} \in \partial I_-(U_n^+), \tag{8.78}$$

$$\mathbf{R}_1 = K_1(\mathbf{U}^+ - \mathbf{X}^+ - \mathbf{X}^-) + R_1^{reac}\mathbf{N},\ R_1^{reac} \in \partial I_-(U_n^+ - X^+), \tag{8.79}$$

where $U_n^+ - X^+$ is the normal velocity on Γ_1 and U_n^+ is the normal velocity on Γ_0. Both normal velocities are negative due to the impenetrability condition.

8.5.2 The Variational Formulation

The set of partial differential equations (8.72)–(8.79) gives the velocities $(\mathbf{U}^+, \mathbf{X}^+)$ after the collision depending on the velocities $(\mathbf{U}^-, \mathbf{X}^-)$ before the collision.

In this subsection we show that the equations fit in the variational inequalities theory and that they have a unique solution.

We begin by defining the functional spaces framework. For the fluid velocity field we define the space

$$V = \left\{\mathbf{W} \in (H^1(\Omega))^2 : \mathrm{div}\mathbf{W} = 0\right\}, \tag{8.80}$$

where $H^1(\Omega)$ is the usual Sobolev space. For the coupled system of fluid-rigid body we define the following convex cone for the cinematically admissible velocities

$$C = \{(\mathbf{W}, Y) \in V \times \mathbb{R} : \mathbf{W}\cdot\mathbf{N} \le 0 \text{ on } \Gamma_0, \mathbf{W}\cdot\mathbf{N} - Y\mathbf{N} \le 0 \text{ on } \Gamma_1\}. \tag{8.81}$$

Let us consider $(\mathbf{W}, Y) \in C$, multiplying (8.72) by the function $\mathbf{W} - \mathbf{U}^+$ and (8.73) by the function $Y - X^+$, we prove that any classical solution must satisfy the equation

$$\int_\Omega \rho\mathbf{U}^+\cdot(\mathbf{W} - \mathbf{U}^+)dx + M(X^+ - X^-)(Y - X^+) \tag{8.82}$$

$$+ \int_\Omega 2\gamma\mathsf{D}(\mathbf{U}^+) : \mathsf{D}(\mathbf{W} - \mathbf{U}^+)dx + \int_{\Gamma_0} K_0\mathbf{U}^+\cdot(\mathbf{W} - \mathbf{U}^+)d\Gamma \tag{8.83}$$

$$+ \int_{\Gamma_1} K_1(\mathbf{U}^+ - X^+\mathbf{N} - X^-\mathbf{N})\cdot(\mathbf{W} - Y\mathbf{N} - (\mathbf{U}^+ - X^+\mathbf{N}))d\Gamma \tag{8.84}$$

$$= \int_{\Gamma_0} -R_0^{reac}(W_n - U_n^+)d\Gamma - \int_{\Gamma_1} R_1^{reac}\{W_n - Y - (U_n^+ - X^+)\}d\Gamma. \tag{8.85}$$

Due to the properties of the subdifferential sets, we have

$$\forall(\mathbf{W}, Y) \in C,\ R_0^{reac}(W_n - U_n^+) \le 0,\ R_1^{reac}\{W_n - Y - (U_n^+ - X^+)\} \le 0. \tag{8.86}$$

It follows

$$(\mathbf{U}^+, X^+) \in C, \ \forall (\mathbf{W}, Y) \in C, \tag{8.87}$$

$$\int_\Omega \rho \mathbf{U}^+ \cdot (\mathbf{W} - \mathbf{U}^+) dx + M(X^+ - X^-)(Y - X^+) \tag{8.88}$$

$$+ \int_\Omega 2\gamma \mathsf{D}(\mathbf{U}^+) : \mathsf{D}(\mathbf{W} - \mathbf{U}^+) dx + \int_{\Gamma_0} K_0 \mathbf{U}^+ \cdot (\mathbf{W} - \mathbf{U}^+) d\Gamma \tag{8.89}$$

$$+ \int_{\Gamma_1} K_1 (\mathbf{U}^+ - X^+ \mathbf{N} - X^- \mathbf{N}) \cdot (\mathbf{W} - Y\mathbf{N} - (\mathbf{U}^+ - X^+ \mathbf{N})) d\Gamma \geq 0. \tag{8.90}$$

Conversely, it can be proved that a solution of the variational inequality (8.90), if it is smooth enough, satisfies the equation of motion (8.72)–(8.76) together with the constitutive laws (8.79).

8.5.2.1 An Existence Theorem

Let us define some notations

$$a(\mathbf{V}, \mathbf{W}) = \int_\Omega \rho \mathbf{V} \cdot \mathbf{W} dx + \int_\Omega 2\gamma \mathsf{D}(\mathbf{V}) : D(\mathbf{W}) dx + \int_{\Gamma_0} K_0 \mathbf{V} \cdot \mathbf{W} d\Gamma, \tag{8.91}$$

$$b(Y, Z) = MYZ, \tag{8.92}$$

$$c(\mathbf{V}, \mathbf{W}) = \int_{\Gamma_1} K_1 \mathbf{V} \cdot \mathbf{W} d\Gamma, \tag{8.93}$$

$$L(Y) = M(X^-)Y, \tag{8.94}$$

$$L_1(\mathbf{W}) = \int_{\Gamma_1} K_1 (X^- \mathbf{N}) \cdot \mathbf{W} d\Gamma. \tag{8.95}$$

The Eq. (8.90) can be rewritten

$$(\mathbf{U}^+, X^+) \in C, \ \forall (\mathbf{W}, Y) \in C, \tag{8.96}$$

$$a(\mathbf{U}^+, \mathbf{W} - \mathbf{U}^+) + b(X^+, Y - X^+) + c(\mathbf{U}^+ - X^+ \mathbf{N}, \mathbf{W} - Y\mathbf{N}) \geq \tag{8.97}$$

$$L(Y - X^+) + L_1(\mathbf{W} - \mathbf{U}^+) - L_1(Y\mathbf{N} - X^+ \mathbf{N}). \tag{8.98}$$

In this form, it is a variational inequality. It can be proved that this variational inequality (8.98) or (8.90) has an unique solution:

Theorem 8.2 *The variational inequality (8.98) has an unique solution.*

Proof The bilinear form

$$A((\mathbf{W}, Y), (\mathbf{V}, Z)) = a(\mathbf{W}, \mathbf{V}) + b(Y, Z) + c(\mathbf{W}, \mathbf{V}), \tag{8.99}$$

is symmetric, continuous and coercive on $V \times R$. The linear form

$$B(((\mathbf{W}, Y)) = L(Y) + L_1(\mathbf{W}) - L_1(Y\mathbf{N}), \tag{8.100}$$

is continuous on the same space. The set C is a non-empty closed convex subset of $V \times R$. It follows from the Lions-Stampacchia [8, 12, 15], theorem that the variational inequality (8.98) equivalent to

$$(\mathbf{U}^+, X^+) \in C, \ \forall (\mathbf{W}, Y) \in C, \tag{8.101}$$

$$A((\mathbf{W}, Y) - (\mathbf{U}^+, X^+), (\mathbf{U}^+, X^+)) \geq B((\mathbf{W}, Y) - (\mathbf{U}^+, X^+)), \tag{8.102}$$

has a unique solution

8.5.3 Numerical Results

Let us consider the example of a diver in a swimming pool. Knowing the situation before the collision, we compute the velocities of diver and water after the collision. These velocities are the initial velocities to describe the smooth evolution after the collision described by Eq. (8.22) and constitutive laws (8.41)–(8.44).

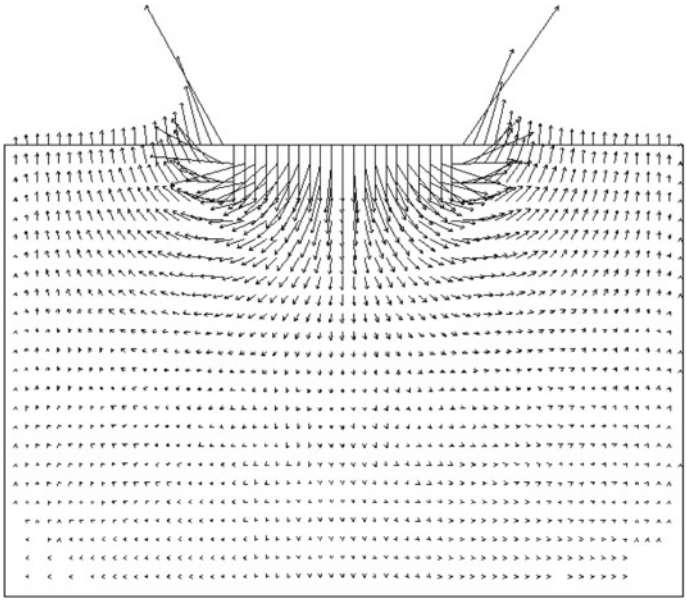

Fig. 8.4 The velocity of the water which splashes up on the two sides of the diver. The length of the arrows are proportional to the velocities

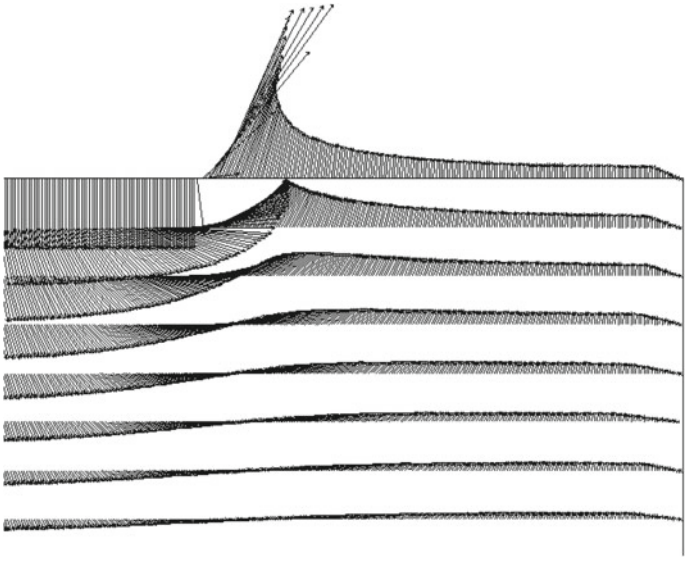

Fig. 8.5 The velocity of the water at different depths

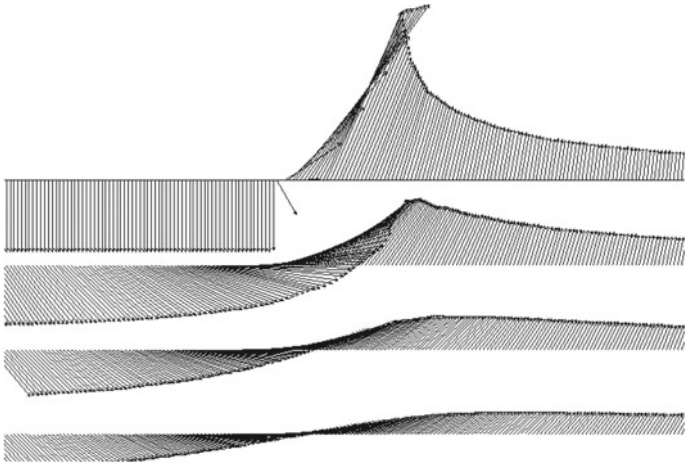

Fig. 8.6 Details of the velocity of the water at different depths

The diver has the mass $M = 100\,\text{Kg}$ and falls vertically from a height of 1 m with vertical velocity $U^- = \sqrt{2g} = 4.47\,\text{m/s}$. The density of the water is $\rho = 1000\,\text{Kg/m}^3$. The parameter defining the collision constitutive laws are

$$K_0 = K_1 = 1\ \text{N/m}^2,\ \gamma = 0.25\ \text{N/m}. \tag{8.103}$$

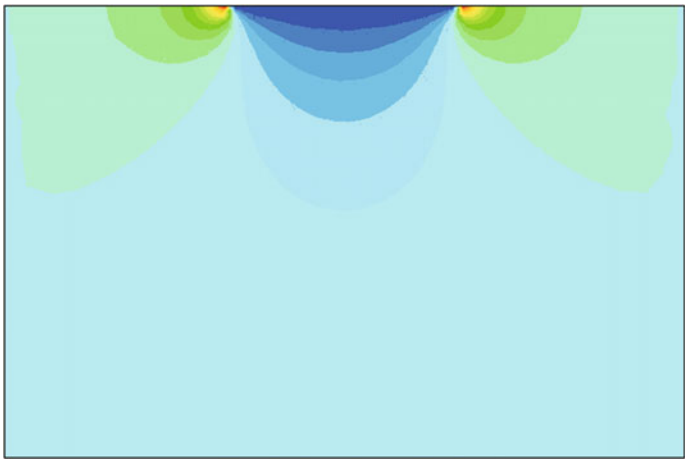

Fig. 8.7 The intensity of the vertical velocity. *Red* is upwards velocity. *Blue* is downwards velocity. *Dark blue* is large downwards velocities, *light blue* is low downwards velocity

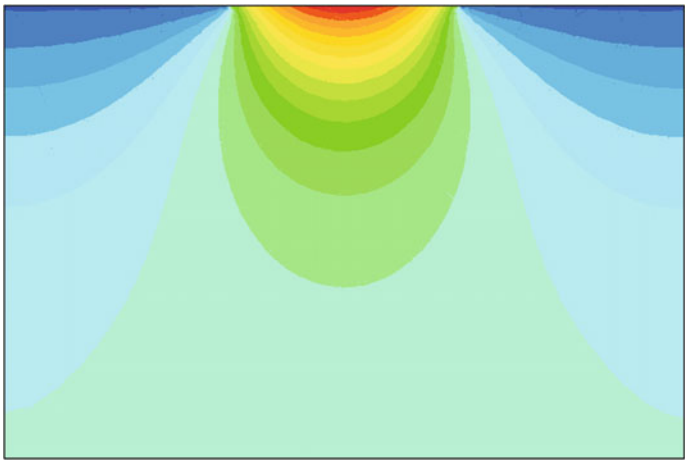

Fig. 8.8 The pressure in the water. *Red* is a high pressure and *blue* a low pressure

The equations may be solved by the classical numerical methods for variational inequalities, for instance the Uzawa method. In the present situation it is better to take advantage of the fact that the solution is unique: the equations are solved with the assumption that the contact is maintained on the parts Γ_0 and Γ_1 and it is checked that the reaction computed with the boundary conditions are negative (in case they are positive somewhere the solution is such that the contact is not maintained everywhere). The water splashes up on the two sides of the diver as shown on the Fig. 8.4. The velocity of the diver after the collision is the velocity of the water (-0.75 ms^{-1}), in agreement with every day experiments!

Details are shown on the following Figs. 8.5 and 8.6: the velocity is drawn at different depth of the pool. The intensity of the vertical velocity is shown on Fig. 8.7. The maximum horizontal velocity is 1.96 m/s. The maximum vertical velocity is 1.95 m/s and the minimum is -0.75 m/s.

Remark 8.2 The percussion pressure is shown on the Fig. 8.8. The average percussion stress $\mathbf{\Sigma N}$ under the diver is -373 $\mathrm{Nm^2 s^{-1}}$ and the average percussion pressure is 371 $\mathrm{Nm^2 s^{-1}}$.

8.6 Skipping Stones

When skipping stones on the still water of a lake, consider a flat stone colliding the water with a non null horizontal velocity, a vertical velocity and a null angular velocity,

$$\mathbf{X}^- = (Z^-, X^-), \tag{8.104}$$

$$\boldsymbol{\omega}^- = \mathbf{0}. \tag{8.105}$$

The theory applies to compute the velocity after collision. The rigid solid represents the stone. Figure 8.9 shows what occurs when the horizontal velocity is

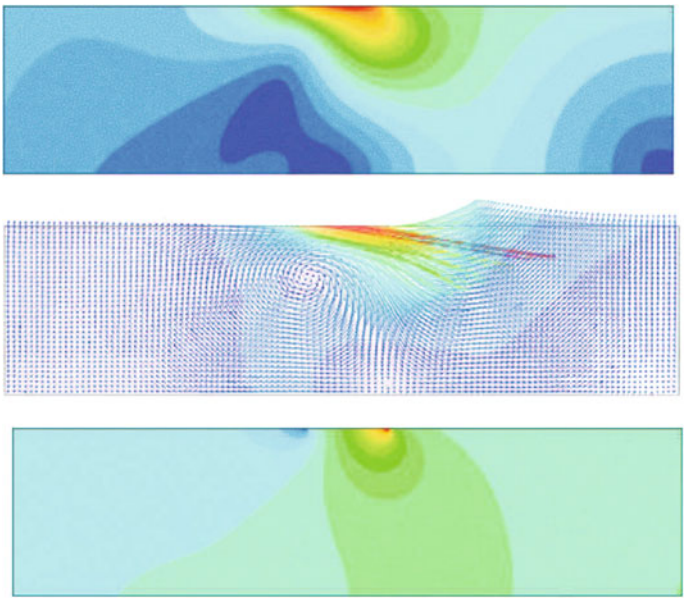

Fig. 8.9 The stone arrives with a large horizontal velocity $\mathbf{X}^- = (5 \text{ m/s}, -1 \text{ m/s})$, with null angular velocity $\omega^- = 0$. It rebounds on the water and rotates. Velocities after collision are $\mathbf{X}^+ = (2,46 \text{ m/s}, \ 0,09 \text{ m/s})$ and $\omega^+ = -0,49$ rad/s. From *top* to *bottom*, are shown the fluid velocity modulus, the fluid velocity and the percussion pressure in the fluid

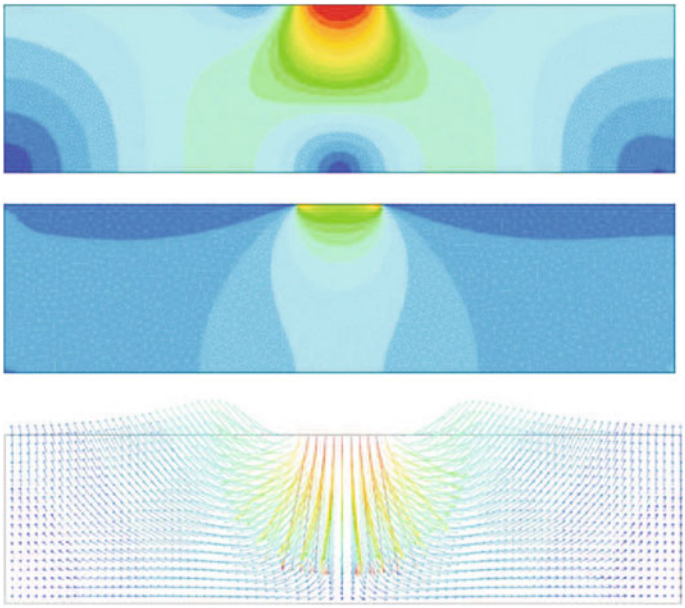

Fig. 8.10 The stone falls vertically with velocities $\mathbf{X}^- = (0, -5\ \text{m/s})$, with null angular velocity, $\omega^- = 0$. It does not rebound. The velocities of the solid and of surface of the water after collision, $\mathbf{X}^+ = (0, -0.07\ \text{m/s})$ and $\omega^+ = 0$, are equal. From top to bottom, are shown, the fluid velocity modulus, the percussion pressure and the fluid velocity

large compared to the vertical velocity. The stone rebounds and rotates whereas it neither rebounds nor rotates if it falls vertically, Fig. 8.10. These results are due to Eric Dimnet and Raul Gormaz [1]. Constitutive law giving surface percussions $\mathbf{R}_0$ and $\mathbf{R}_1$ have normal, K_N and tangential, K_T coefficients. For instance,

$$\mathbf{R}_0 = K_{0T}\mathbf{U}_T^+ + K_{0N}U_N^+ N + R_0^{reac}\mathbf{N},$$

where $\mathbf{U}_T$ and U_N are the tangential and vertical velocities. Values of the parameters are

$$K_{0N} = K_{1N} = 1\ \text{Kg/m}^2,\ K_{0T} = K_{1T} = 0.25\ \text{Kg/m}^2, \tag{8.106}$$

$$\gamma = 1.8\ \text{Kg/m}^2,\ M = 0.5\ \text{Kg},\ \rho = 1000\ \text{Kg/m}^3. \tag{8.107}$$

8.7 Conclusions

The theory of collisions of fluids and solids outlined in this chapter is consistent from the mechanical point of view. It has good mathematical formulations to which usual

numerical methods apply. The examples given in Sects. 8.4, 8.5 and 8.6 show that the basic physical properties are taken into account.

Let us emphasize that the basic idea which is to take into account the interior forces when a collision occurs that capture and sum up the very sophisticated physical phenomenons which intervene during the short time of the collision. The interior forces are defined by duality i.e., by their work. In this setting the choice of the work of the interior forces in collisions is very crucial as well as the choice of the average strain rate $\mathsf{D}(\mathbf{U}^+ + \mathbf{U}^-)$ to define the percussion stress.

References

1. Dimnet, E., Frémond, M., Gormaz, R., San Martin, J.A.: Collisions involving solids and fluids. In: Frémond, M., Maceri, F. (eds.) Novel Approaches in Civil Engineering. Springer, Berlin (2003)
2. Faella, C., Nigro, E.: Dynamic impact of the debris flows on the constructions during the hydrogeological disaster in Campania-1998: failure mechanical models and evaluation of the impact velocity. In: Picarelli, L. (ed.) Fast Slope Movements Prediction and Prevention for Risk Mitigation, 1. Pàtron, Bologna (2003)
3. Federico, F., Cesali, C.: The role of micro-mechanical parameters in the runout length of high-speed granular masses. In: Modeling and Numerical Simulations, International Symposium on Geomechanics From Micro to Macro (IS Cambridge 2014), September, 1–3, Cambridge, UK (2014)
4. Federico, F., Cesali, C.: An energy-based approach to predict debris flow mobility and analyze empirical relationships. Can. Geotech. J **52**(12), 2113–2133 (2015). doi:10.1139/cgj-2015-0107
5. Frémond, M.: Collisions, Edizioni del Dipartimento di Ingegneria Civile, Università di Roma "Tor Vergata" (2007). ISBN 978-88-6296-000-7
6. Frémond, M., Gormaz, R., San Martin, J.: Collision of a solid with an uncompressible fluid. Theor. Comput. Fluid Dyn. **16**, 405–420 (2003)
7. Germain, P.: Mécanique des milieux continus. Masson, Paris (1973)
8. Lions, J.L., Stampacchia, G.: Variational inequalities. Comm. Pure Appli. Math. **20**, 493–519 (1967)
9. Moreau, J.J.: Sur la naissance de la cavitation dans une conduite. C. R. Acad. Sci., Paris, **259**(0), 3948–3950 (1965)
10. Moreau, J.J.: Principes extrémaux pour le problème de la naissance de la cavitation. J. de Mécanique **5**, 439–470 (1966)
11. Moreau, J.J.: Fonctionnelles convexes, Edizioni del Dipartimento di Ingegneria Civile, Università di Roma "Tor Vergata", 2003, ISBN 978-88-6296-001-4 and Séminaire sur les équations aux dérivées partielles. Collège de France, Paris (1966)
12. Panagiotopoulos, P.D.: Inequality Problems in Mechanics and Applications. Birkhaüser, Basel (1985)
13. Prochaska, A.B., Santi, M.P., Higgins, J.D., Cannon, S.H.: A study of methods to estimate debris flow velocity. Landslides (2008). doi:10.1007/s10346-008-0137-0
14. Revellino, P., Hungr, O., Guadagno, F.M., Evans, S.G.: Velocity and runout simulation of destructive debris flows and debris avalanches in pyroclastic deposits, Campania region, Italy. Environ. Geol. **45**, 295–311 (2004)
15. Thompson, W.: On vortex motion. Trans. R. Soc. Edinb. **25**(1), 217–260 (1868)
16. Rodrigues, J.F.: Obstacle problems in mathematical physics, North Holland (1987)

Chapter 9
Debris Flows and Collisions of Fluids and Deformable Solids

Francesco Federico and Michel Frémond

9.1 The Solid Liquid Collision

In previous chapters, we have investigated collisions of solids. But solids and fluids can also collide, [3–5, 27, 37]: a sea wave may collide a harbour breakwater, [6, 55]. A swimmer can suffer a belly flop when diving in a swimming pool. A boat with a flat hull may fall violently in a rough sea, [8, 35, 44]. The basic laws of mechanics apply to predict these motions. A detailed presentation is given in [13, 29, 30].

In this chapter we investigate debris flows colliding civil engineering structures, [46, 47]. These collisions can be very destructive due to the velocity of the flow, up to 20 m/s, [48], and its high density, [14, 21, 22, 49]. We study a schematic situation; a wall is impacted by a debris flow. The results of the predictive theory allow to quantify some protective measures as protection by a soft layer fasten to the structures.

9.1.1 The Debris Flows

Debris flows may occur when strong rains on hill or mountain slopes cause extensive erosion, [1, 42, 43, 45]. Debris flows are accelerated downhill by gravity and follow steep mountain channels, [20, 39]. The front of a debris-flow surge often contains a high content of coarse material such as stones and logs, [16]. Trailing behind the high-friction flow front is a lower-friction liquefied flow body that contains a higher percentage of granular material. Due to high friction properties, the front tends to be rather steep even perpendicular to the slope. We investigate a schematic situation. Let us consider a fluid colliding a solid, for instance a debris flow colliding a wall, [36], (see Fig. 9.1). The front of the debris flow is perpendicular to the slope and collides the wall at time t. The duration of the collision, the time required for the fluid to adapt to the kinematic incompatibility due to the presence of the wall is, very short compared to the duration of the flow before the contact with the wall and very short compared to the subsequent evolution of the flow and wall, [10, 17, 19, 23, 24]. This duration is the time for the velocity of the water and of the wall to become

M. Frémond, *Collisions Engineering: Theory and Applications*,
Springer Series in Solid and Structural Mechanics 6,
DOI 10.1007/978-3-662-52696-5_9

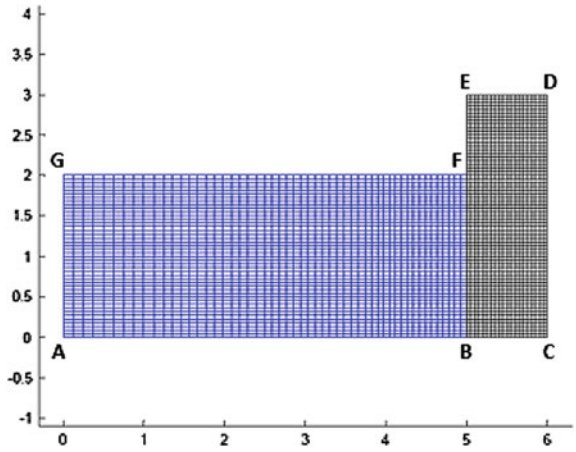

Fig. 9.1 The debris flow and the wall on the right. The mesh of the domains

equal. Thus we assume this phenomenon is instantaneous and assume that velocities are discontinuous at collision time t. The fluid is in rectangle GFBA denoted Ω_f. It collides the wall occupying rectangle BFEDC denoted Ω_s on contact or collision surface BF denoted Γ. The fluid and the solid are on the soil or bedrock ABC which is immobile. Some mechanical properties may be given to the contact wall-soil on part BC denoted Γ_s. For the sake of simplicity, we assume the contact soil-fluid contact velocity is not influenced by the collision and assume the velocity of the fluid to be null there (we choose a null velocity because the base of the front is in contact with the wall slightly before the bulk of the front). The distance of part AG to collision surface BF is large enough for the collision effect to be negligible on surface AG where we assume we know the velocity which is not affected by the collision. The air on part GFEDC has no effect on the collision, [6].

9.1.2 The Principle of Virtual Work

The kinematic quantities are the velocity of the fluid $\mathbf{U}_f$ and the velocity of the wall, $\mathbf{U}_s$. For each velocity, there is the velocity before the collision

$$\mathbf{U}^-(x,t) = \lim_{\Delta t \to 0, \Delta t > 0} \mathbf{U}^-(x, t - \Delta t), \tag{9.1}$$

and the velocity after the collision

$$\mathbf{U}^+(x,t) = \lim_{\Delta t \to 0, \Delta t > 0} \mathbf{U}^+(x, t + \Delta t). \tag{9.2}$$

Because collision time t is fixed we delete it in the sequel.

In this situation, the principle of virtual work means that the exterior work provided to the system produces an evolution of the velocities, the work of which is the work of the acceleration percussions, and an evolution of the velocities of deformation, the work of which is the work of the interior percussions.

The virtual work of the acceleration percussions is

$$\int_{\Omega_f} \rho_f(\mathbf{U}_f^+(x) - \mathbf{U}_f^-(x)) \cdot \frac{\mathbf{V}_f^+(x) + \mathbf{V}_f^-(x)}{2} dx + \int_{\Omega_s} \rho_s(\mathbf{U}_s^+(x) - \mathbf{U}_s^-(x)) \cdot \frac{\mathbf{V}_s^+(x) + \mathbf{V}_s^-(x)}{2} dx, \tag{9.3}$$

where the $\mathbf{V}^+$ and $\mathbf{V}^-$ are virtual velocities.

The work of the interior percussions is

$$-\int_{\Omega_f} \Sigma_f(x) : \mathsf{D}(\frac{\mathbf{V}_f^+(x) + \mathbf{V}_f^-(x)}{2}) dx - \int_{\Omega_s} \Sigma_s(x) : \mathsf{D}(\frac{\mathbf{V}_s^+(x) + \mathbf{V}_s^-(x)}{2}) dx \tag{9.4}$$

$$-\int_{\Gamma} \mathbf{R}(x) \cdot \frac{\mathbf{V}_f^+(x) - \mathbf{V}_s^+(x) + \mathbf{V}_f^-(x) - \mathbf{V}_s^-(x)}{2} d\Gamma \tag{9.5}$$

$$-\int_{\Gamma_s} \mathbf{R}_s(x) \cdot \frac{\mathbf{V}_s^+(x) - \mathbf{V}_s^-(x)}{2} d\Gamma, \tag{9.6}$$

where the Σ_f and Σ_s is the percussion stresses in the fluid and the solid, $\mathbf{R}$ is the percussion on the collision surface Γ_s and $\mathbf{R}_s$ the percussion on the soil-solid contact surface. We assume the velocity of the soil remains constant in the collision. Quantity

$$\mathsf{D}(\mathbf{V})_{ij} = \frac{1}{2}(V_{i,j} + V_{j,i}) \tag{9.7}$$

is the usual strain rate.

The work of the exterior action is due to the action of the air and the soil on the parts $\partial\Omega_f \backslash \Gamma$ and $\partial\Omega_s \backslash (\Gamma \cup \Gamma_s)$ of the boundary of the system

$$\int_{\partial\Omega_f \backslash \Gamma} \mathbf{P}_f(x) \cdot \frac{\mathbf{V}_f^+(x) + \mathbf{V}_f^-(x)}{2} d\Gamma + \int_{\partial\Omega_s \backslash (\Gamma \cup \Gamma_s)} \mathbf{P}_s(x) \cdot \frac{\mathbf{V}_s^+(x) + \mathbf{V}_s^-(x)}{2} d\Gamma. \tag{9.8}$$

Percussion $\mathbf{P}_f$ is the action of the soil on the fluid, the action of the external part of the fluid on surface AG and the action of the air on part GF, which is assumed a null percussion. Percussion $\mathbf{P}_s$ is the action of the soil on the solid and the action of the air on part FEDC which is also assumed a null percussion. Those percussion are reactions given by the equations of motion in case the velocities are given on this part. They may be given by a constitutive law if needed. We give such a constitutive law in Sect. 9.6 in part BC for the contact soil-wall.

9.1.3 The Equations of Motion

The principle of virtual work gives the equations of motion

$$\rho_f(\mathbf{U}_f^+ - \mathbf{U}_f^-) = \mathrm{div}\boldsymbol{\Sigma}_f,\ in\ \Omega_f,\ \rho_s(\mathbf{U}_s^+ - \mathbf{U}_s^-) = \mathrm{div}\boldsymbol{\Sigma}_s,\ in\ \Omega_s, \tag{9.9}$$

$$\boldsymbol{\Sigma}_f\mathbf{N} = -\mathbf{R},\ \boldsymbol{\Sigma}_s\mathbf{N} = \mathbf{R},\ on\ \Gamma,\ \boldsymbol{\Sigma}_s\mathbf{N}_s = -\mathbf{R}_s,\ on\ \Gamma_s, \tag{9.10}$$

$$\boldsymbol{\Sigma}_f\mathbf{N}_f = \mathbf{P}_f,\ on\ \partial\Omega_f\backslash\Gamma,\ \boldsymbol{\Sigma}_s\mathbf{N}_s = \mathbf{P}_s,\ on\ \partial\Omega_s\backslash(\Gamma\cup\Gamma_s), \tag{9.11}$$

where $\mathbf{N}_f$ is the outward normal vector to the debris flow domain, $\mathbf{N}_s$ is the outward normal vector to the wall domain and $\mathbf{N} = \mathbf{N}_f = -\mathbf{N}_s$ is the normal vector to the debris flow domain on collision surface Γ.

Remark 9.1 The main reason for virtual velocities $(\mathbf{V}^+ + \mathbf{V}^-)/2$ to intervene in the theory is that this choice gives that the actual power of the acceleration forces is the variation of the kinetic energy. This result is important for the theorem of the kinetic energy which is useful when deriving the constitutive laws, see Chap. 2 and [29].

9.1.4 The Laws of Thermodynamics and Constitutive Laws

There are four interior percussions which have to satisfy the laws of thermodynamics, see [29] and Chaps. 7, 8. If we do not take into account the thermal phenomenons, the laws of thermodynamics imply that the following inequalities are to be satisfied

$$\begin{gathered}\boldsymbol{\Sigma}_f : \mathsf{D}(\frac{\mathbf{U}_f^+ + \mathbf{U}_f^-}{2}) \geq 0,\ \boldsymbol{\Sigma}_s : \mathsf{D}(\frac{\mathbf{U}_s^+ + \mathbf{U}_s^-}{2}) \geq 0,\\ \mathbf{R}\cdot\frac{\mathbf{U}_f^+ - \mathbf{U}_s^+ + \mathbf{U}_f^- - \mathbf{U}_s^-}{2} \geq 0.\ \mathbf{R}_s\cdot\frac{\mathbf{U}_s^+ + \mathbf{U}_s^-}{2} \geq 0.\end{gathered} \tag{9.12}$$

The constitutive laws which sum up all the sophisticated and fast phenomenons occurring during the collision relate the interior percussions stresses $\boldsymbol{\Sigma}_f$, $\boldsymbol{\Sigma}_s$ and percussions $\mathbf{R}$, $\mathbf{R}_s$ on collision surface and soil-solid contact surface to strain rates

$$\mathsf{D}(\frac{\mathbf{U}_f^+ + \mathbf{U}_f^-}{2}),\ \mathsf{D}(\frac{\mathbf{U}_s^+ + \mathbf{U}_s^-}{2}), \tag{9.13}$$

and gap velocities

$$\frac{\mathbf{U}_f^+ - \mathbf{U}_s^+ + \mathbf{U}_f^- - \mathbf{U}_s^-}{2},\ \frac{\mathbf{U}_s^+ + \mathbf{U}_s^-}{2}. \tag{9.14}$$

They have to take into account the impenetrability of debris flow and wall and impenetrability of soil and solid, and possibly the incompressibility of the debris flow.

To insure inequalities (9.12) are satisfied, we define them with pseudo-potentials of dissipation

$$\Phi_f(\mathsf{D}(\frac{\mathbf{U}_f^+ + \mathbf{U}_f^-}{2})),\ \Phi_s(\mathsf{D}(\frac{\mathbf{U}_s^+ + \mathbf{U}_s^-}{2})), \tag{9.15}$$

$$\Phi_\Gamma(\frac{\mathbf{U}_f^+ - \mathbf{U}_s^+ + \mathbf{U}_f^- - \mathbf{U}_s^-}{2}, \frac{\mathbf{U}_f^- - \mathbf{U}_s^-}{2}), \Phi_\Gamma(\frac{\mathbf{U}_s^+ + \mathbf{U}_s^-}{2}, \frac{\mathbf{U}_s^-}{2}), \tag{9.16}$$

with

$$\Phi_f(\mathsf{D}) = 2k_f\mathsf{D}^2 + I_0(tr\mathsf{D}),\ \Phi_s(\mathsf{D}) = \hat{k}_s\,(tr\mathsf{D})^2 + 2k_s\mathsf{D}:\mathsf{D}), \tag{9.17}$$

where I_0 is the indicator function of the origin of $\mathbb{R}$ and

$$\Phi_\Gamma(\mathbf{X},\mathbf{Y}) = 2k\mathbf{X}^2 + I_-\left((\mathbf{X}-\mathbf{Y})\cdot\mathbf{N}\right)\mathbf{N}\ or\ \Phi_\Gamma(\mathbf{X}) = k\mathbf{X}_T^2 + I_0\left((\mathbf{X}-\mathbf{Y})\cdot\mathbf{N}\right)\mathbf{N}, \tag{9.18}$$

where $\mathbf{X}_T$ is the tangential component of vector $\mathbf{X}$ on collision surface Γ

$$\Phi_{\Gamma_s}(\mathbf{X},\mathbf{Y}) = 2k_{\Gamma_s}\mathbf{X}^2 + I_-\left((\mathbf{X}-\mathbf{Y})\cdot\mathbf{N}\right)\mathbf{N}\ or\ \Phi_{\Gamma_s}(\mathbf{X},\mathbf{Y}) = I_0(\mathbf{X}-\mathbf{Y}), \tag{9.19}$$

where I_0 is the indicator function of the origin of $\mathbb{R}^3$. The constitutive laws are

- for the percussion stress in the debris flow

$$\Sigma_f \in \partial\Phi_f(\mathsf{D}(\frac{\mathbf{U}_f^+ + \mathbf{U}_f^-}{2})) = 2k_f\mathsf{D}(\mathbf{U}_f^+ + \mathbf{U}_f^-) - P\mathbf{1}, \tag{9.20}$$

$$P \in \partial I_0(\mathrm{div}(\mathbf{U}_f^+ + \mathbf{U}_f^-)) = \partial I_0(\mathrm{div}(\mathbf{U}_f^+) = \mathbb{R}, \tag{9.21}$$

  where P is the percussion pressure resulting from the incompressibility of the debris flow, $\mathrm{div}(\mathbf{U}_f^+ + \mathbf{U}_f^-) = \mathrm{div}\mathbf{U}_f^+ = 0$, because the flow is incompressible before the collision $\mathrm{div}\mathbf{U}_f^- = 0$. Viscosity parameter quantifies the spacial influence of a perturbation in the debris flow. When it is small the phenomenons are local. When it is large the phenomenons intervene in the whole fluid which becomes rigid;
- for the percussion stress in the solid

$$\Sigma_s = \partial\Phi_s(\mathsf{D}(\frac{\mathbf{U}_s^+ + \mathbf{U}_s^-}{2})) \tag{9.22}$$

$$= \hat{k}_s\mathrm{div}(\mathbf{U}_s^+ + \mathbf{U}_s^-)\mathbf{1} + 2k_s\mathsf{D}(\mathbf{U}_s^+ + \mathbf{U}_s^-). \tag{9.23}$$

  Viscosity parameters $\hat{k}_s$ and k_s quantify the spatial influence of a perturbation in the solid. When they become large the solid behaves like a rigid solid;

- for the percussion collision surface reaction $\mathbf{R}$, there are two choices for the constitutive law. In the first choice, the contact is unilateral: the flow can bounce after collision, i.e., a gap may appear between the solid and the flow. Moreover there is a friction on the solid surface, with friction coefficient k

$$\mathbf{R} \in \partial \Phi_{\Gamma} \left(\frac{\mathbf{U}_f^+ - \mathbf{U}_s^+ + \mathbf{U}_f^- - \mathbf{U}_s^-}{2} \right), \tag{9.24}$$

giving

$$\mathbf{R} = k \left(\mathbf{U}_f^+ - \mathbf{U}_s^+ + \mathbf{U}_f^- - \mathbf{U}_s^- \right) + R^{reac}\mathbf{N}, \; R^{reac} \in \partial I_- \left(\left(\mathbf{U}_f^+ - \mathbf{U}_s^+ \right) \cdot \mathbf{N} \right). \tag{9.25}$$

In the second choice, contact is maintained on the contact surface, i.e., the normal velocities of solid and flow are equal after collision; There remains a tangential friction with coefficient k

$$\mathbf{R} \in \partial \Phi_{\Gamma} \left(\frac{\mathbf{U}_f^+ - \mathbf{U}_s^+ + \mathbf{U}_f^- - \mathbf{U}_s^-}{2} \right), \tag{9.26}$$

giving

$$\mathbf{R} = k \left(\mathbf{U}_f^+ - \mathbf{U}_s^+ + \mathbf{U}_f^- - \mathbf{U}_s^- \right)_T + R^{reac}\mathbf{N}, \; R^{reac} \in \partial I_0 \left(\left(\mathbf{U}_f^+ - \mathbf{U}_s^+ \right) \cdot \mathbf{N} \right) = \mathbb{R}, \tag{9.27}$$

- for the soil-solid percussion reaction on the soil solid contact surface. We have chosen two possible behaviors. With the first one the solid may separate from the soil due to the collision. Of course, interpenetration is impossible. When viscosity parameter k_{Γ_s} is large it is difficult to have separation, when it is small the separation is more easy

$$\mathbf{R}_s \in \partial \Phi_{\Gamma_s} \left(\frac{\mathbf{U}_s^+ + \mathbf{U}_s^-}{2} \right), \tag{9.28}$$

giving

$$\mathbf{R}_s = k_{\Gamma_s} \left(\mathbf{U}_s^+ + \mathbf{U}_s^- \right) + R_s^{reac}\mathbf{N}, \; R_s^{reac} \in \partial I_- \left(\mathbf{U}_s^+ \cdot \mathbf{N}_s \right), \tag{9.29}$$

The second possible behaviour corresponds to viscosity parameter k_{Γ_s} infinite. Separation does not occur whatever the percussion. Velocity of the solid remains equal to the velocity of the soil.

$$\mathbf{R}_s \in \partial \Phi_{\Gamma_s} \left(\frac{\mathbf{U}_s^+ + \mathbf{U}_s^-}{2} \right), \tag{9.30}$$

giving

$$\mathbf{R}_s = \mathbf{R}_s^{reac},\ \mathbf{R}_s^{reac} \in \partial I_0\left(\mathbf{U}_s^+\right) = \mathbb{R}^3. \tag{9.31}$$

The constitutive laws are simple: they are linear besides the reactions to the internal constraints. Of course they may be upgraded to fit with experimental results. For instance, the contact of the wall with the soil may be described by relationship (9.29) assuming an unilateral contact together with friction.

These constitutive laws are used in the sequel and their effects are investigated.

9.2 An Example

We investigate the debris flow shown on Fig. 9.1 with length of flow 5 m; height of flow 2 m; thickness of wall 1 m; height of wall 3 m.

9.2.1 The Equations of the Predictive Theory

They result from the equations of motion and constitutive laws. They are

- in the fluid domain Ω_f

$$\rho_f(\mathbf{U}_f^+ - \mathbf{U}_f^-) = 2k_f\Delta(\mathbf{U}_f^+ + \mathbf{U}_f^-) - \mathbf{grad}P,\ \mathrm{div}(\mathbf{U}_f^+ + \mathbf{U}_f^-) = 0,\ in\ \Omega_f, \tag{9.32}$$

with boundary conditions

$$\begin{aligned} \mathbf{U}_f^+ &= 0,\ on\ AB, \\ \Sigma_f\mathbf{N}_f = \mathbf{P}_f &= 0,\ on\ FG; \\ \mathbf{U}_f^+ &= \mathbf{U}_f^-,\ on\ GA. \end{aligned}$$

Velocity $\mathbf{U}_f^-$ is given in Ω_f;

- on the collision surface Γ or BF, for the constitutive law, we make the first choice (9.25)

$$\Sigma_f\mathbf{N} = \Sigma_s\mathbf{N} = -\mathbf{R}, \tag{9.33}$$

$$\mathbf{R} = k\left(\mathbf{U}_f^+ - \mathbf{U}_s^+ + \mathbf{U}_f^- - \mathbf{U}_s^-\right) + R^{reac}\mathbf{N}, \tag{9.34}$$

$$R^{reac} \in \partial I_-\left(\left(\mathbf{U}_f^+ - \mathbf{U}_s^+\right)\cdot\mathbf{N}\right). \tag{9.35}$$

The stress is continuous on collision surface and the flow may rebound on the wall. Let us recall $\mathbf{N} = \mathbf{N}_f$ is the outward normal vector to the fluid domain. The

horizontal velocity is continuous in case the contact is maintained after collision. This is the case if the normal reaction stress is a pressure. Tangential velocity is not continuous. The tangential stress being due to friction between the flow and the wall;

- in the wall

$$\rho_s(\mathbf{U}_s^+) = (\hat{k}_s + k_s)\mathbf{grad}(\mathrm{div}(\mathbf{U}_s^+)) + k_s \Delta \mathbf{U}_s^+, \ in\ \Omega_s, \tag{9.36}$$

with velocity $\mathbf{U}_s^- = 0$. The boundary conditions are

$$\boldsymbol{\Sigma}_s \mathbf{N}_s = \mathbf{P}_s = 0, \ on\ \partial\Omega_s \backslash (\Gamma \cup \Gamma_s)\ or\ FEDC, \tag{9.37}$$

$$\mathbf{U}_s^+ = 0, \ on\ \Gamma_s. \tag{9.38}$$

In this example, we have chosen the wall to be fixed to a rigid immobile bedrock.

Remark 9.2 The slope of the soil does not play a role in the collision equations because gravity is not an external percussion. It is an external force which has a density with respect to the time Lebesgue measure.

9.2.2 The Numerical Approximation

The equations given in the previous section may be solved with variational formulations and their related numerical methods, [28]. The numerical solution of the predictive theory is computed with a FEM code developed in MATLAB environment. According to the chosen geometry, the mesh created is composed by rectangular elements and the interpolation functions are linear. For the dimension two problem of the example, the mesh is shown in Fig. 9.1.

9.3 Properties of the Physical Parameters

The predictive theory depends on few parameters: ρ_f (density of fluid), ρ_s (density of solid), k_f (percussion viscosity of fluid), k_s and $\hat{k}_s$ (percussion viscosities of the solid). In this investigation, the geometry of the structure is fixed once for all. The given schematic velocity before the impact is shown in Fig. 9.2.

In Fig. 9.2 the given velocity is not computed with the equation of fluid mechanics. But it is realistic and has some destructive potential with a 2 m/s maximum horizontal velocity. Note that very destructive velocities may be up to 20 m/s, [31, 48].

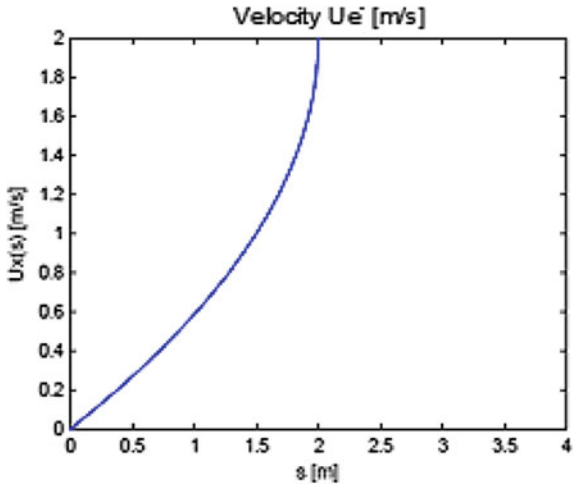

Fig. 9.2 The horizontal velocity before collision U_f^- [m/s], versus the vertical position. The vertical velocity before collision is null

9.3.1 The Basic Case

In order to investigate the effects of the different physical parameter, we choose a basic set of parameters defining the basic case

- $\rho_e = 1000$ kg/m^3;
- $\rho_s = 2500$ kg/m^3;
- $k_f = 1$ Pa $\cdot$ s^2;
- k_s and $\hat{k}_s \approx 100$ Pa $\cdot$ s^2;
- $k = 0$ Pa/m $\cdot$ s^2 (no friction between fluid and solid);
- $k_{\Gamma s} = \infty$ Pa/m $\cdot$ s^2 ("rigid" behavior of soil foundation).

The flow is a water flow. The wall is made of concrete. The percussion water viscosity is of the order of the water kinematic viscosity. The percussion viscosities of the solid are chosen in such a way they are not too small (the wall is not too weak) and not too large (the wall is not too rigid). Finally, the friction between fluid and solid is null neglecting this phenomenon for the sake of simplicity. For the same reason, quantity $k_{\Gamma s}$ is infinite assuming the soil to be a rigid bedrock with perfect wall adherence ($\mathbf{U} = 0$ at the base of the wall assuming a lubrificating layer).

Velocities after collision are shown on Fig. 9.3, the horizontal velocity and on Fig. 9.4, the vertical velocity.

The flow is stopped by the wall which gets a small velocity due to the collision. The flow jumps along the wall with a rather large vertical velocity.

Norm of percussion stress tensor is shown on Fig. 9.5. Note that it is large on collision surface.

On the collision surface, vertical and horizontal velocities versus the vertical position are shown on Fig. 9.6. Horizontal velocity of the wall and of the water are small. But the vertical velocity of the water is large. The horizontal motion of the water is slowed down by the collision whereas its vertical motion becomes

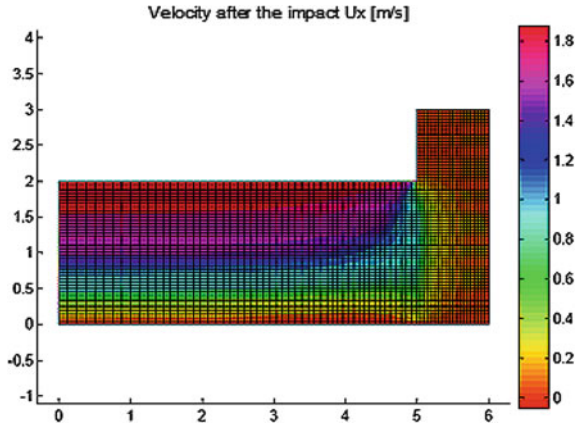

Fig. 9.3 The horizontal velocity after the impact U_x [m/s]

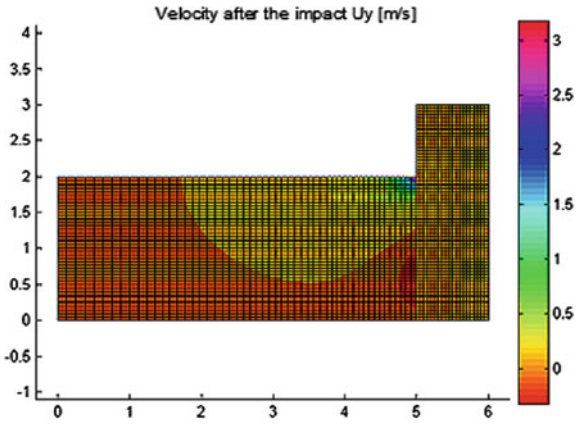

Fig. 9.4 The vertical velocity after the impact U_y [m/s]

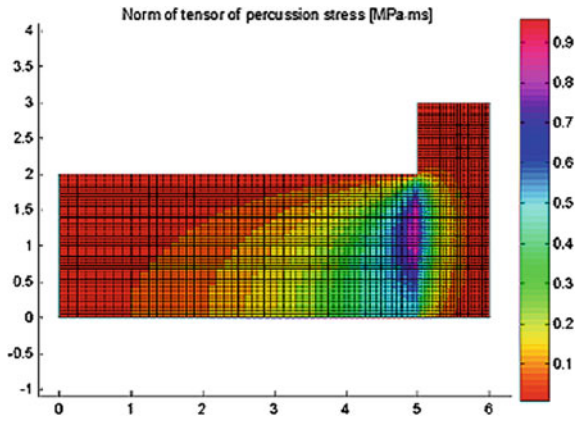

Fig. 9.5 Norm of percussion stress tensor in [MPa · ms]

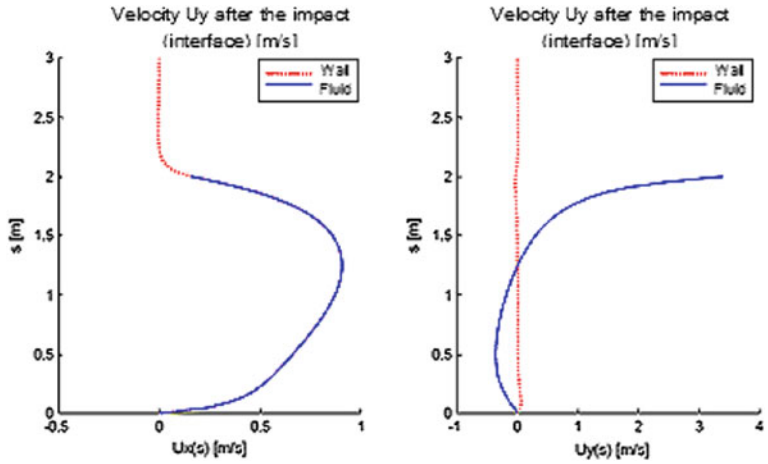

Fig. 9.6 Profiles of velocities U_x and U_y after the impact in the interface [m/s]

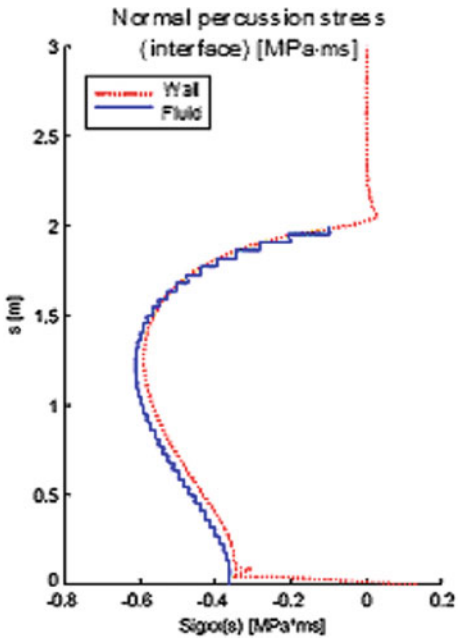

Fig. 9.7 Profile of normal percussion stress in the interface [MPa · ms]

large mainly at the surface of the flow. Note that within the flow there is a slightly negative vertical velocity producing a recirculation of fluid. Vertical velocity of the wall remains almost null (Fig. 9.6).

On the collision surface, the fluid does not rebound

$$\left(\mathbf{U}_f^+ - \mathbf{U}_s^+\right) \cdot \mathbf{N} = 0, \tag{9.39}$$

and the normal reaction percussion stress

$$-R^{reac}\mathbf{N}.\mathbf{N} \leq 0, \tag{9.40}$$

is negative. It is a pressure which satisfies

$$\mathbf{\Sigma}_f\mathbf{N} = -R^{reac}\mathbf{N},\ R^{reac} \in \partial I_{-}\left(\left(\mathbf{U}_f^{+} - \mathbf{U}_s^{+}\right)\cdot\mathbf{N}\right). \tag{9.41}$$

9.3.2 The Effect of the Density of the Debris Flow ρ_f

We investigate the effect of the debris flow density. Three values: $\rho_f = 1500\,\text{kg/m}^3$; $\rho_f = 2500\,\text{kg/m}^3$; $\rho_f = 4500\,\text{kg/m}^3$ have been chosen. The velocities are shown in Figs. 9.8 and 9.9. The norm of tensor of percussion stress are shown in Fig. 9.10. Velocities and stresses, in the interface, are shown on Figs. 9.11 and 9.12.

The horizontal velocity in the fluid after the impact on the fluid-wall interface increases with the density. For example the maximum of velocity increases from 0.8 m/s to 1.5 m/s. Otherwise, the vertical velocity U_y after the impact decreases when ρ_f increases. Intensity of the percussion stress increases from 0.9 MPa · ms ($\rho_f = 1000\,\text{kg/m}^3$) to 1.4 Mpa · ms ($\rho_f = 4500\,\text{kg/m}^3$). This behaviour is supported by experiments, [2, 11, 12, 32, 34, 41, 50–53].

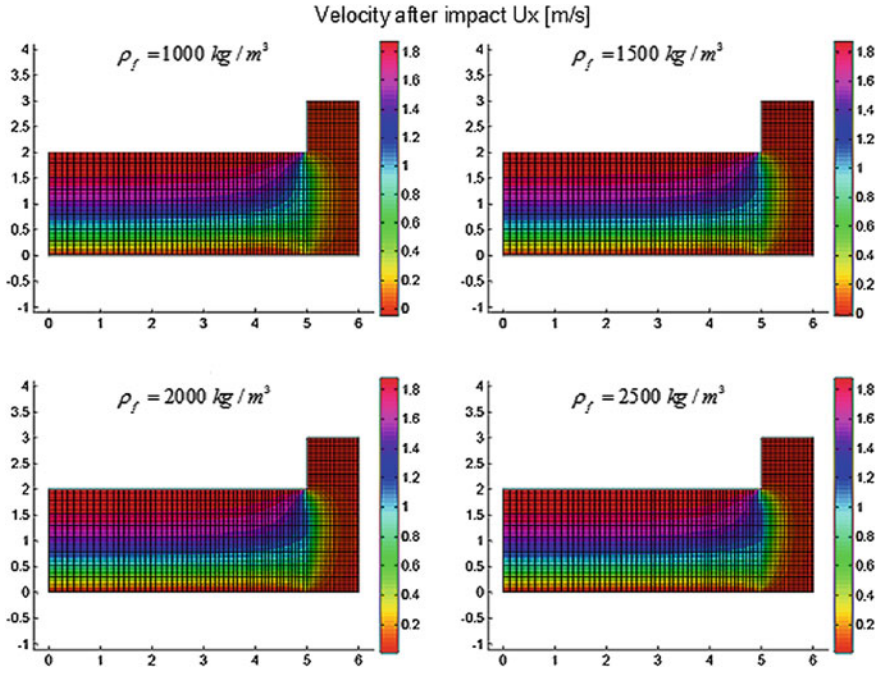

Fig. 9.8 Comparison of the velocity Ux after the impact due to the variation of ρ_f [m/s]

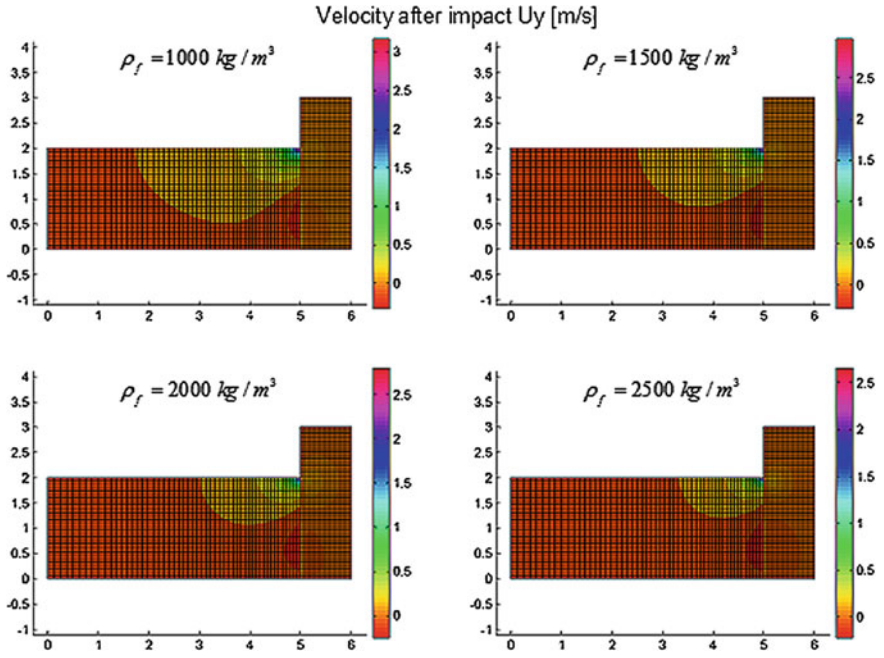

Fig. 9.9 Comparison of the velocity Uy after the impact due to the variation of ρ_f [m/s]

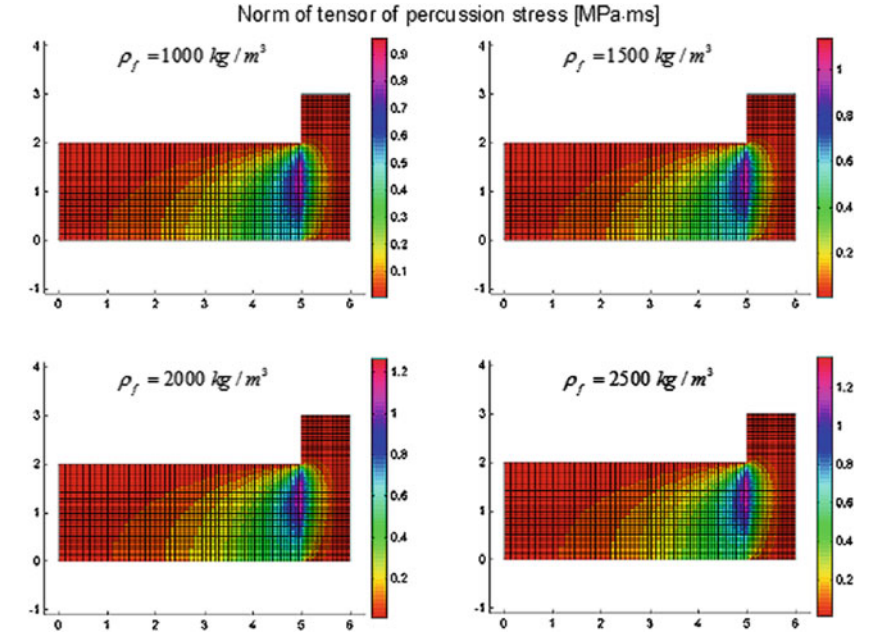

Fig. 9.10 Comparison of the norm of percussion stress due to the variation of ρ_f [MPa · ms]

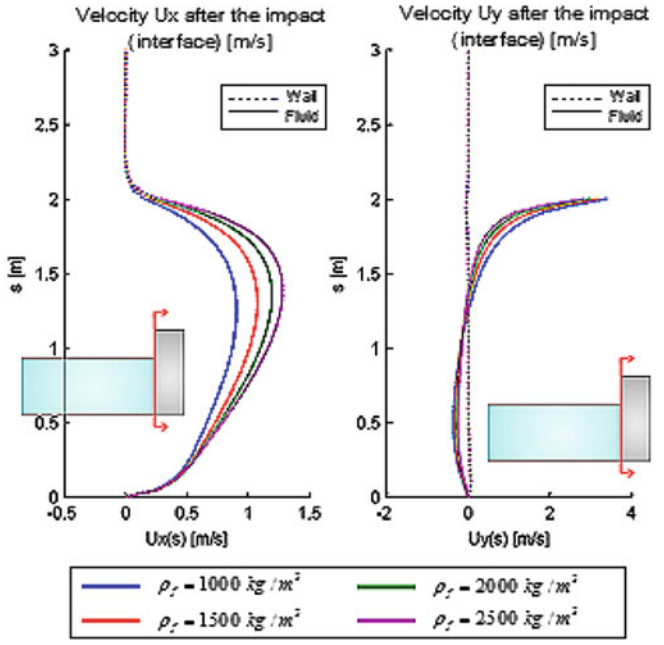

Fig. 9.11 Comparison of the velocity after the impact due to the variation of ρ_f in the interface [m/s]

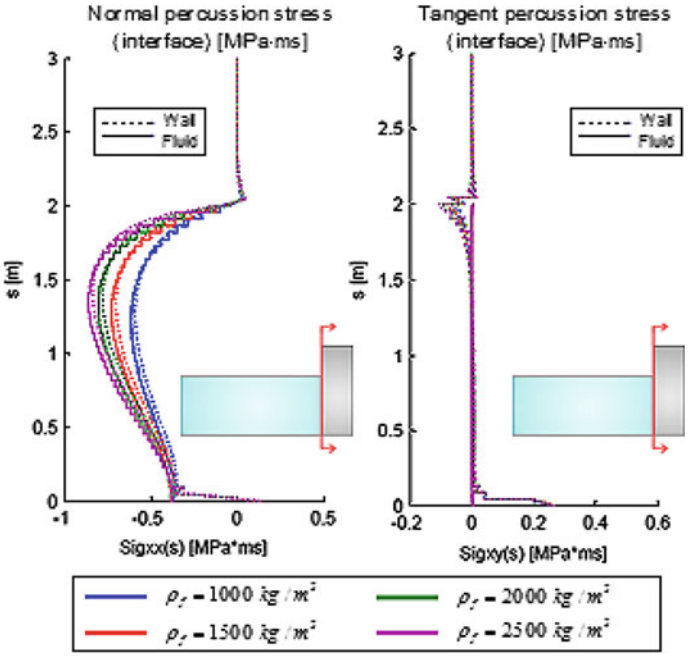

Fig. 9.12 Comparison of the normal percussion stress due to the variation of ρ_e in the interface [MPa · ms]

9.3.3 The Effect of Percussion Viscosity k_f of the Debris Flow

We investigate the effect of the percussion viscosity of the flow (Figs. 9.13, 9.14, 9.15, 9.16, 9.17 and 9.18). It is a dissipative parameter that quantifies the spatial influence of the collision in the fluid. If it is small, collision on the wall has an effect only in the neighbourhood of the wall. If it is large, the effect of the collision has an effect in the whole fluid.

We consider three cases: $k_f = 0.01$ Pa $\cdot$ s^2; $k_f = 0.1$ Pa $\cdot$ s^2; $k_f = 5$ Pa $\cdot$ s^2.

Parameter k_f has almost no effect on the horizontal velocity U_x after the impact and on the normal percussion stress on the contact surface.

In Figs. 9.18, it is clearly identified the spatial effect of viscosity parameter k_f: the larger k_f, the larger the domain of influence. This is a practical way to estimate parameter k_f.

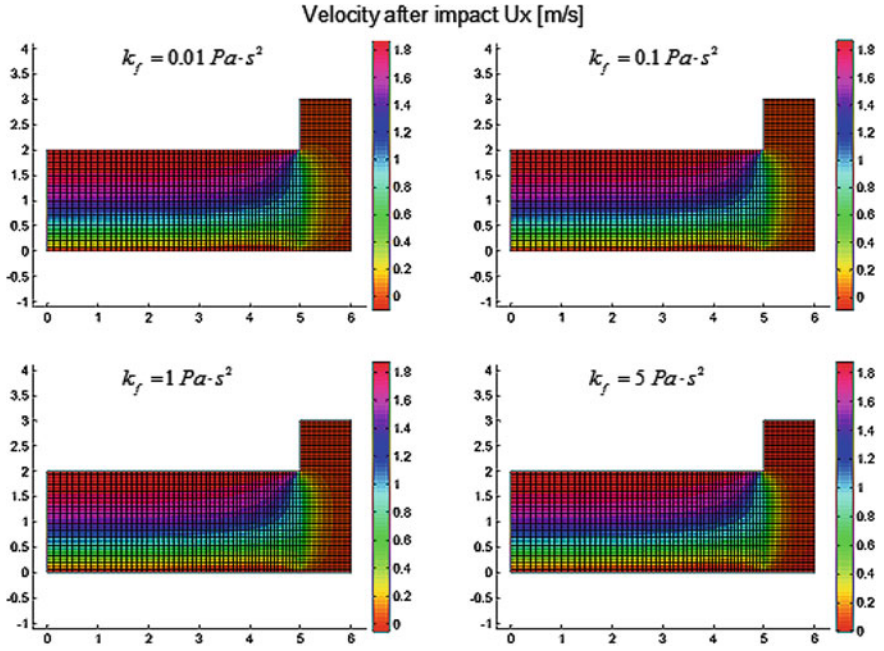

Fig. 9.13 Comparison of the velocity U_x after the impact due to the variation of k_f [m/s]

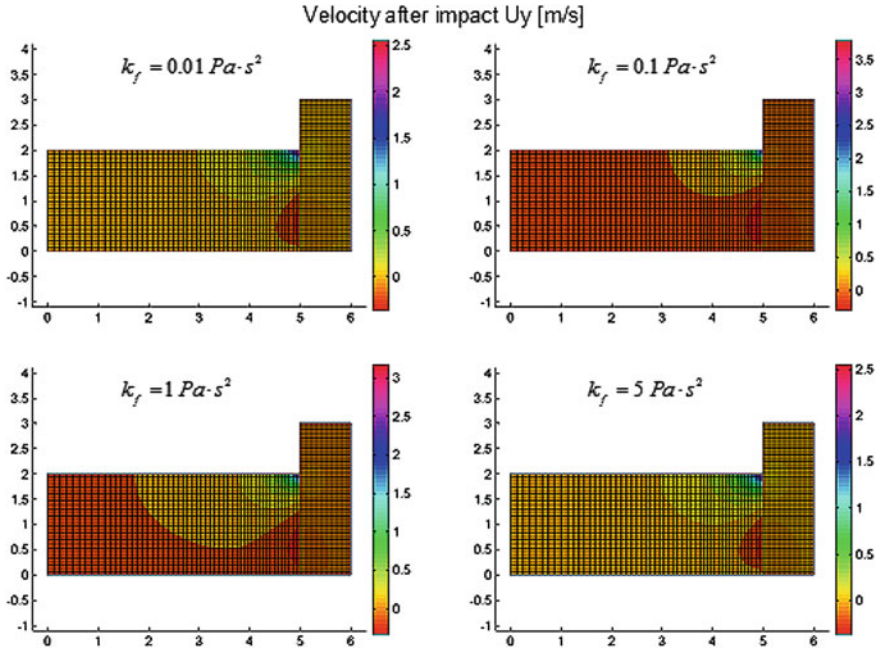

Fig. 9.14 Comparison of the velocity U_x after the impact due to the variation of k_f [m/s]

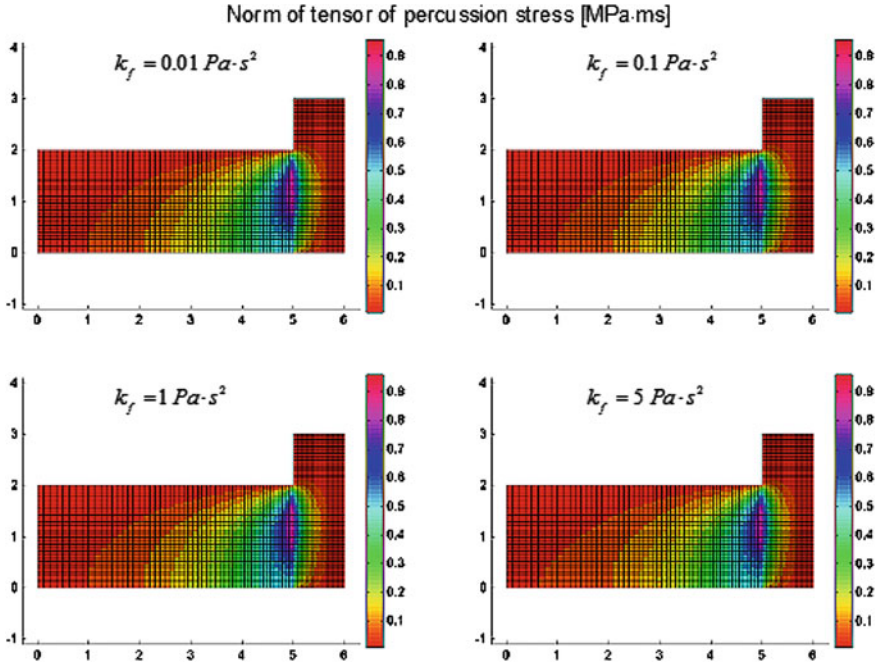

Fig. 9.15 Comparison of the norm of percussion stress due to the variation of k_f [MPa · ms]

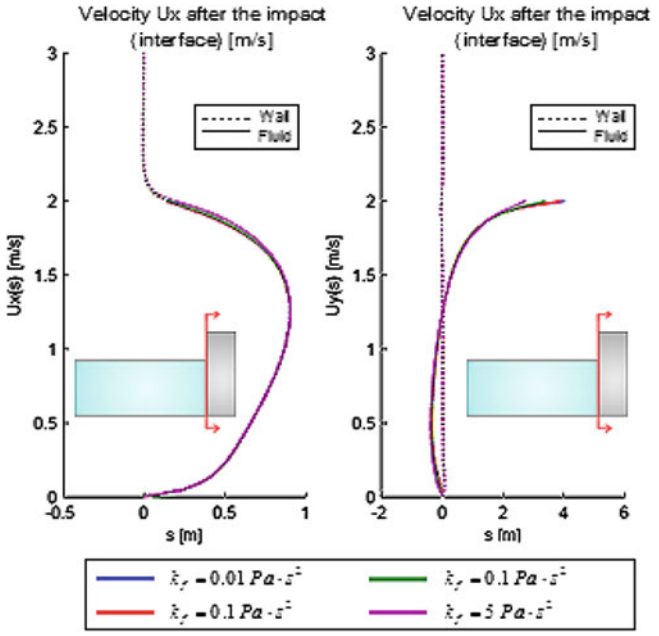

Fig. 9.16 Comparison of the velocity after the impact due to the variation of k_f in the interface [m/s]

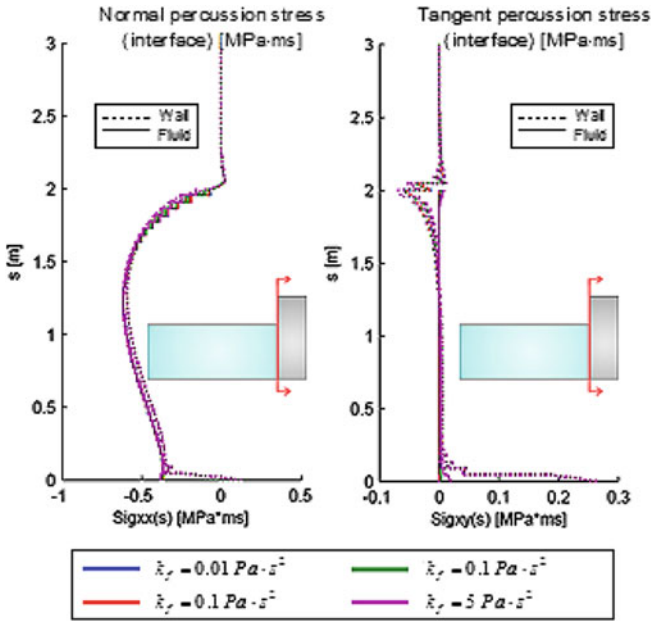

Fig. 9.17 Comparison of the normal and tangent percussion stress due to the variation of k_f in the interface [MPa · ms]

9.3.4 The Effect of Percussion Viscosities k_s and $\hat{k}_s$ of the Wall

Parameters k_s and $\hat{k}_s$ are dissipative parameters (Figs. 9.18, 9.19, 9.20, 9.21, 9.22 and 9.23). When they are large the wall is rigid. When they are low, the wall is deformable and its effect on the flow is less important.

We consider again three cases: $(k_s, \hat{k}_s) \approx 1$ Pa $\cdot$ s^2; $(k_s, \hat{k}_s) \approx 1000$ Pa $\cdot$ s^2; (k_s and $\hat{k}_s$) $\approx 10^6$ Pa $\cdot$ s^2.

On the contact surface the results are: when the parameters k_s and $\hat{k}_s$ increase, horizontal velocity U_x after the impact decreases from 1.8 m/s $(k_s, \hat{k}_s) \approx 1$ Pa $\cdot$ s^2 for a weak wall, to 0 m/s $(k_s, \hat{k}_s) \approx 10^6$ Pa $\cdot$ s^2 for a rigid wall. Further, velocity U_y increases from 1 m/s $(k_s, \hat{k}_s) \approx 1$ Pa $\cdot$ s^2, weak wall, to 5 m/s $(k_s, \hat{k}_s) \approx 10^6$ Pa $\cdot$ s^2, rigid wall. When k_s and $\hat{k}_s$ increase the wall becomes more rigid: velocity U_x after the impact becomes zero and the vertical jump velocity of the fluid increases.

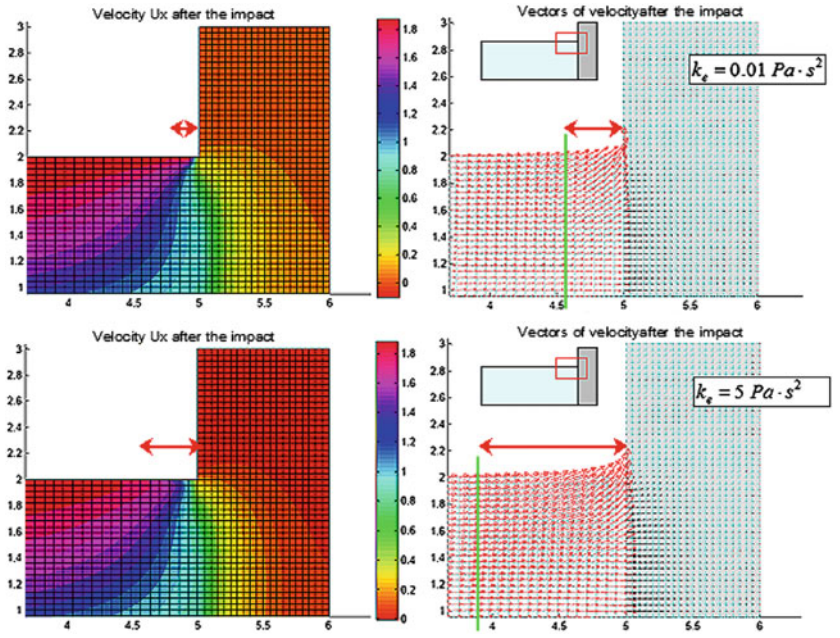

Fig. 9.18 The collision influence length

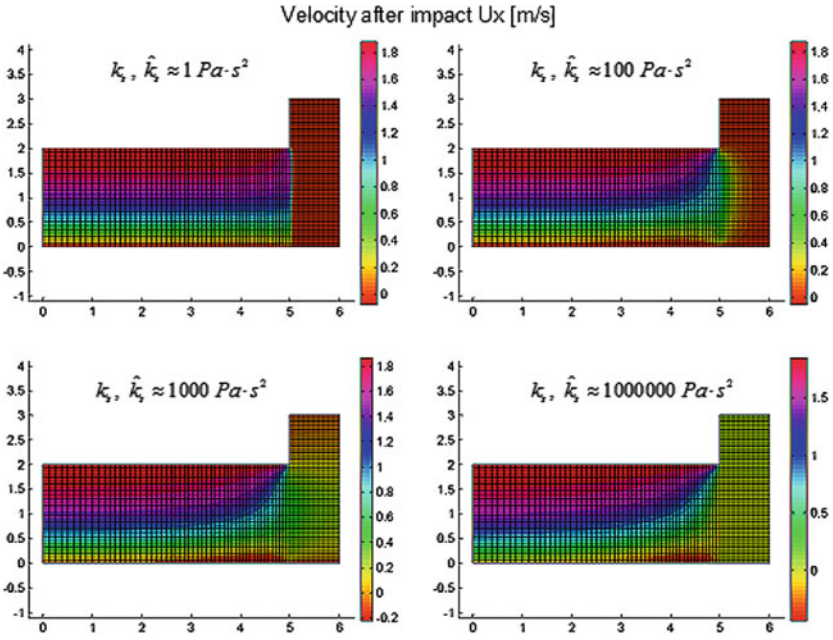

Fig. 9.19 Comparison of the velocity U_x after the impact due to the variation of k_s and $\hat{k}_s$ [m/s]

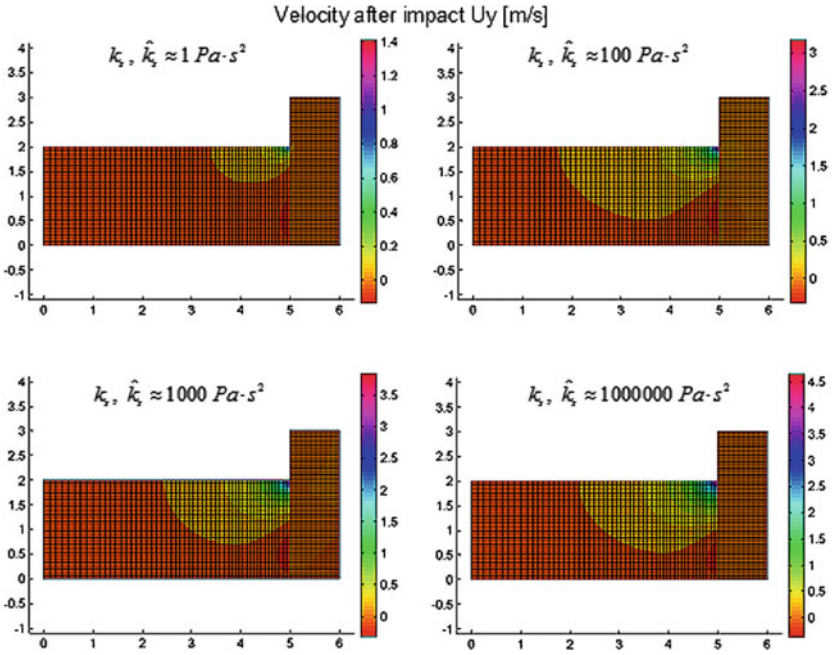

Fig. 9.20 Comparison of the velocity U_y after the impact due to the variation of k_s and $\hat{k}_s$ [m/s]

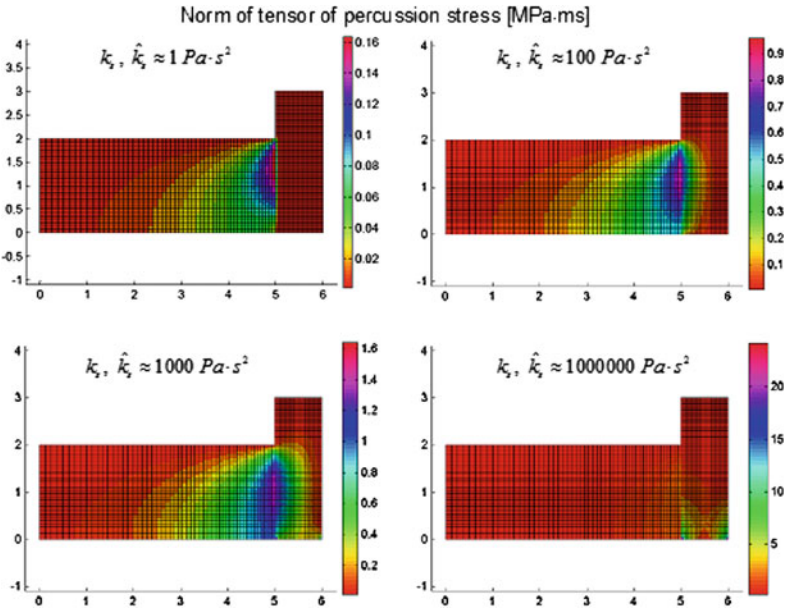

Fig. 9.21 Comparison of the norm of percussion stress due to the variation of k_s and $\hat{k}_s$ [MPa · ms]

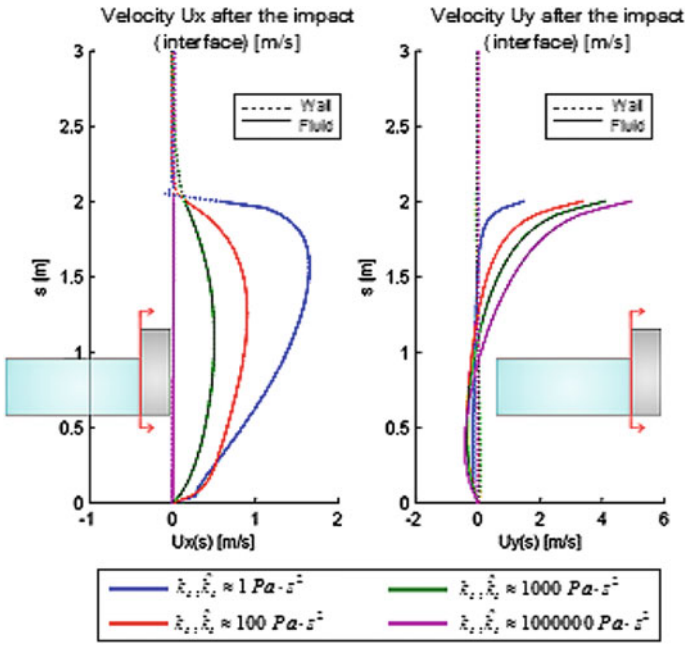

Fig. 9.22 Comparison of the velocity after the impact due to the variation of k_s and $\hat{k}_s$ in the interface [m/s]

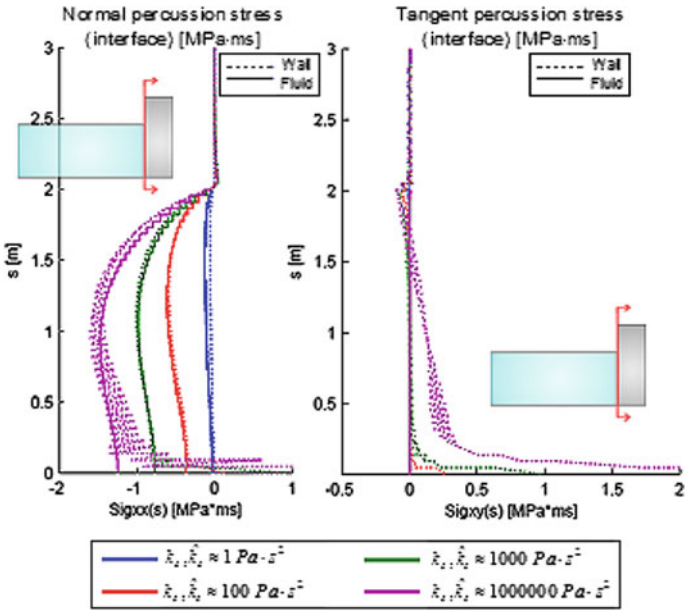

Fig. 9.23 Comparison of the velocity after the impact due to the variation of k_s and $\hat{k}_s$ in the interface [MPa · ms]

9.3.5 *The Effect of the Friction of the Debris Flow with the Wall*

Quantity k quantifies the friction between fluid and wall on the interface. If it is null, there is no friction as in the basic case. In the other hand, if this parameter is very large, there is perfect adherence of the fluid to the wall. In this case, the vertical velocity is null. Figure 9.24 illustrates these properties, with four values of the friction coefficient: $k = 0$ Pa/m · s^2, $k = 10$ Pa/m · s^2, $k = 1000$ Pa/m · s^2 and $k = 10^7$ Pa/m · s^2.

9.4 Smooth Predictive Theory Versus Non Smooth Predictive Theory

The collision problem is usually investigated assuming the mechanical quantities evolve smoothly but very rapidly, [15, 17–19, 25, 26]. It results the collision has a duration $\bar{t}$. The best quantity to represent the results of the smooth predictive theory is the impulsive force developed on the interface during the impact, [16]. This impulsive

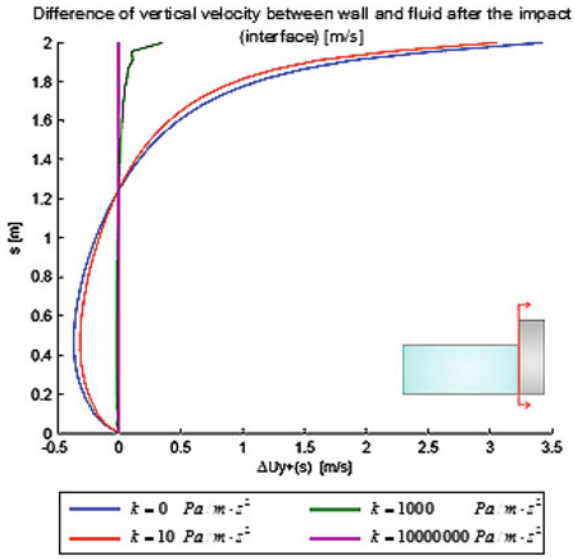

Fig. 9.24 Comparison of the difference of velocity due to the variation of k in the interface [m/s]

force, P_s applied to the impacted interface, is the integral with respect to time of the normal resultant force $F(t)$ applied to the interface during the collision

$$P_s = \int_0^{\bar{t}} F(t)dt/B. \tag{9.42}$$

This quantity is normalized by the horizontal length B of the debris flow for the purpose of comparison with the present computations which are in dimension two. In the non smooth theory, the actually new parameters are the viscosity percussion parameters. The practical role of parameters k_s and $\hat{k}_s$ is to be compared with the practical role of elastic modulus E of the wall constitutive law. We remark that these parameters k_s and $\hat{k}_s$ are not only related to the elastic behavior but they resume all the elastic and dissipative phenomena inside the materials during the impact. In a first investigation, we may verify that k_s and $\hat{k}_s$ are related to modulus E assuming the smooth predictive theory involves only elastic phenomena. To compare the traditional point of view with the non smooth results, we assume quantity P_s which is a percussion is equal to the integral on the interface Γ_s of the normal percussion stress $\boldsymbol{\Sigma}_f\mathbf{N}\cdot\mathbf{N} = \boldsymbol{\Sigma}_s\mathbf{N}\cdot\mathbf{N}$

$$P_{ns} = \int_{\Gamma_s} \boldsymbol{\Sigma}_f\mathbf{N}\cdot\mathbf{N}d\Gamma. \tag{9.43}$$

With relationship

$$P_s = P_{ns}, \tag{9.44}$$

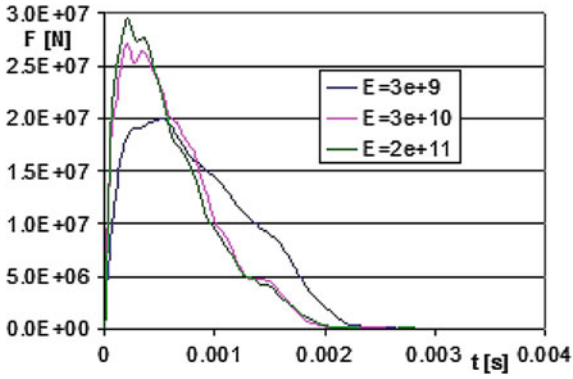

Fig. 9.25 Impact force developed in the interface fluid-wall

we may identify parameters of one theory assuming parameters of the other theory are known. For instance, let us identify the dissipative parameters of the wall, viscosity parameters $\hat{k}_s$ and k_s. Let us recall they quantify the spatial influence of a collision in the solid. When they become large the wall behaves like a rigid solid. Thus we may assume they depend mainly on the modulus E of the wall elastic constitutive law. The structure and flow parameters we use for a comparaison are: height of debris flow 1 m ; length of debris flow 3 m; thickness of wall 0.8 m; height of wall 1.5 m; density of fluid 1000 kg/m^3; density of wall 2500 kg/m^3; percussion viscosity of fluid 1 Pa $\cdot$ s^2; no friction fluid-wall and rigid soil foundation. The velocity before the impact is constant and equal to 15 m/s, a very destructive velocity.

In Fig. 9.25, are shown the normal resultant force applied to the wall versus time for three moduli E.

The impulsive force for two reference values of Young's modulus are

$$\begin{aligned} P_s &\approx 8.5\,\text{MPa/m} \cdot \text{ms} \text{ for } E = 2 \cdot 10^{11}\,\text{N/m}^2, \\ P_s &\approx 7.5\,\text{MPa/m} \cdot \text{ms} \text{ for } E = 2 \cdot 10^{09}\,\text{N/m}^2. \end{aligned} \tag{9.45}$$

For k_s and $\hat{k}_s$, the normal stress is shown on Fig. 9.26 and we get using relationship (9.44)

$$\begin{aligned} P_{ns} &\approx 8\,\text{MPa/m} \cdot \text{ms} \quad \text{for } k_s, \hat{k}_s \approx 10^9\,\text{Pa} \cdot \text{s}^2, \\ P_{ns} &\approx 7.5\,\text{MPa/m} \cdot \text{ms} \text{ for } k_s, \hat{k}_s \approx 10^4\,\text{Pa} \cdot \text{s}^2. \end{aligned} \tag{9.46}$$

This example and other computations show that it is possible to relate parameters k_s and $\hat{k}_s$ to familiar parameters as the modulus. But in case sophisticated non linear phenomena occur during collisions, for instance damage, plasticity, viscosity,… this simple identification is no longer valid. But parameters k_s and $\hat{k}_s$ keep their meaning, they sum up the collision phenomenon, and may be used in predictive theories. To relate them to the parameters of the smooth constitutive law is a delicate task. Experiments are also useful, [7, 9, 54]. Both predictive theories are useful and able to predict the evolutions.

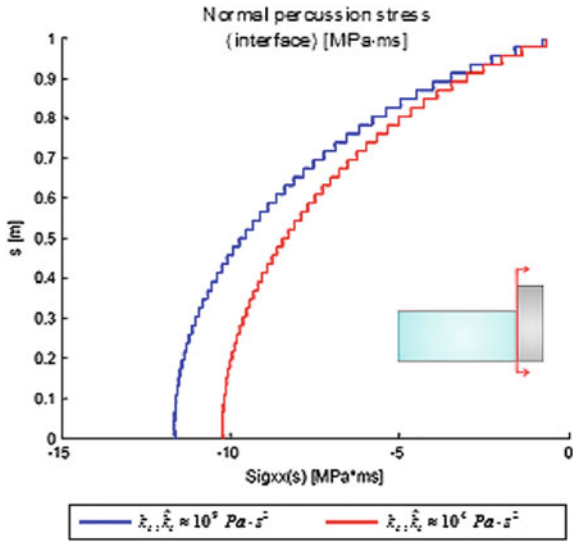

Fig. 9.26 Normal percussion stress in the interface for the cases k_s, $\hat{k}_s \approx 10^4$ Pa $\cdot$ s^2 and k_s, $\hat{k}_s \approx 10^9$ Pa $\cdot$ s^2

In conclusion, it is important to remark the difference between the approach in these models. In the smooth predictive theory the time is an important quantity. An immediate problem arises: what is the duration $\bar{t}$ of the collision? The determination of the collision duration is related to a lot of parameters: behavior of the wall, behavior of debris flow, position of the impact points,… In general this estimation is very difficult either with an analytical solution or with some experiment. The smooth evolution assumption gives more opportunities but it requires to know perfectly the wall constitutive law which has often to be non linear because of the large accelerations and a careful numerical treatment due the dynamical aspect.

On the other hand, non smooth predictive theory does not involve time and has simple constitutive laws which sum up the sophisticated constitutive laws involved in time depending evolutions. We have shown that the parameters of the new constitutive laws may be related to the classical mechanical parameters. It results equations easy to solve. Let us emphasizes that the non smooth predictive theory focuses only on the collision.

9.5 The Coupled Influence of the Debris Flow Density and Height

We investigate the coupled effect of the debris flow height h_f and of its density, ρ_f. We plot the resultant normal percussion on the wall versus these two physical quantities. We fix

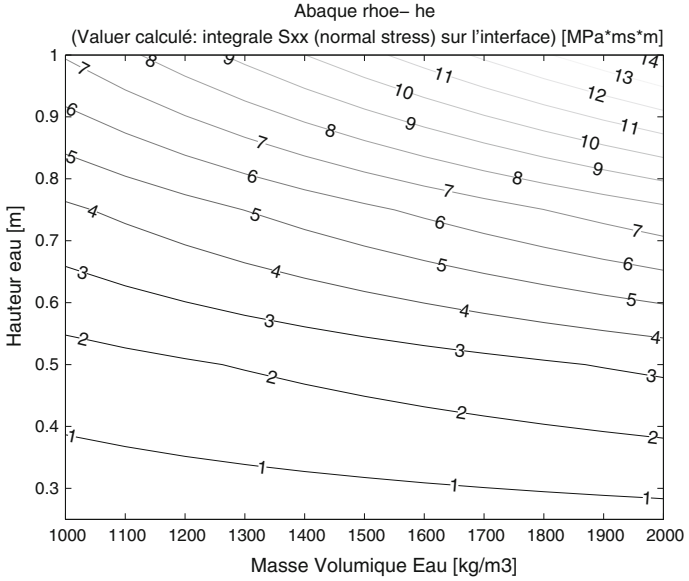

Fig. 9.27 Abaque of the resultant normal percussion versus ρ_e-h_e

$$\begin{array}{l} L_s = 1\,\mathrm{m} \quad \rho_s = 2500\,\mathrm{kg/m^3} \\ h_s = 1.5\,\mathrm{m} \;\; \hat{k}_s, k_s \approx 10^9\,\mathrm{Pa}\cdot\mathrm{s}^2 \\ L_f = 10\,\mathrm{m} \; \hat{k}_f, k_f \approx 10^9\,\mathrm{Pa}\cdot\mathrm{s}^2 \end{array} \tag{9.47}$$

Height h_f of the debris flow varies between 0.2 and 2/3 of the wall height, $h_s = 1.5\,\mathrm{m}$. Density ρ_f varies between 1000 kg/m^3 and 2000 kg/m^3.

The results on Fig. 9.27, show that the effect of the height of the debris flow increases with its density. This is in agreement with observations, [17, 18].

9.6 The Effect of the Soil Deformation

In Sects. 9.3.4 and 9.3.5, we have seen that the dissipative properties of the wall are important. From this point of view, it has to be noted that the wall is not perfectly fixed on the ground and the deformation of the soil could be accounted for. We improve the boundary conditions on contact surface with the soil

$$\left(\mathbf{U}_s^+\right)_T = 0, \tag{9.48}$$

$$\left(\Sigma_s \mathbf{N}\right)_N + k_{soil}\left(\mathbf{U}_s^+ + \mathbf{U}_s^-\right)_N = 0, \;\text{ on } \Gamma_s, \tag{9.49}$$

where the indices T and N refer to the tangential or horizontal direction and to the normal or vertical direction. The horizontal velocity remains null but the vertical velocity is depends on the normal percussion. Parameter k_{soil} is the soil percussion reaction modulus. More sophisticate contact laws, for instance unilateral contact laws, may be introduced.

9.7 An Application. The Protection of a Wall by a Damping Sand Layer

A concrete wall with thickness 0.8 m and height 1 m, is impacted by a debris flow with height 1 m. We investigate the effect of the replacement of a layer of concrete by a damping layer, for instance sand, see Fig. 9.28. The velocity of the impacting flow is shown on Fig. 9.29, [40]. It is a flow with an important destructive potential.

The mechanical parameters are

- $\rho = 1500$ kg/m, debris flow, mixture of soil and water;
- $\rho = 1800$ kg/m3, sand;
- $\rho = 2500$ kg/m3, concrete;
- k_f Pa $\cdot$ s^2, debris flow percussion viscosity;;
- $k_s = 100$ Pa $\cdot$ s^2, $\hat{k}_s = 100$ Pa $\cdot$ s^2, sand percussion viscosity;
- $k_s = 10^5$, $\hat{k}_s = 10^5$ Pa $\cdot$ s^2, concrete percussion viscosity.

The contact debris flow-wall is assumed without friction.

The horizontal velocities in the walls versus vertical position y at different abscissa x (the red lines in the walls) are shown on Fig. 9.30. The vertical velocities in the walls versus vertical position y at different abscissae x (the red lines in the walls) are shown on Fig. 9.31. The percussion stress Σ_{xx} in the walls versus vertical position y at different abscissae x (the red lines in the walls) are shown on Fig. 9.32 The effect of

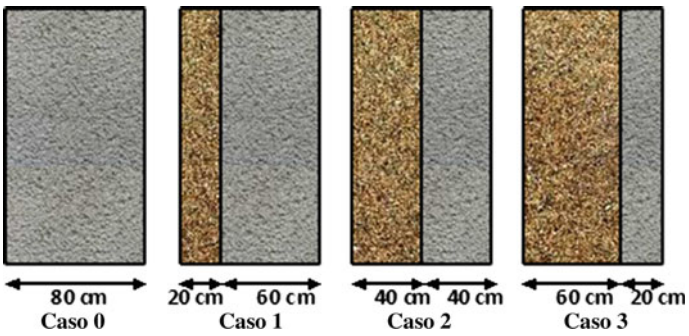

Fig. 9.28 A wall is split into a concrete part on the *right* and a damping sand part on the *left*

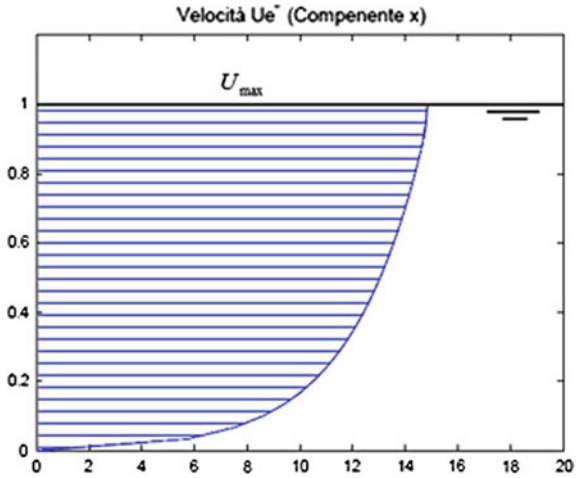

Fig. 9.29 The velocity of the destructive impacting flow

the sand, the damping layer, is to decrease the stress Σ_{xx} then to increase the bearing capacity of the layered wall. This is a practical way to protect structures which can be impacted by debris flows, [7, 9, 33, 38, 54].

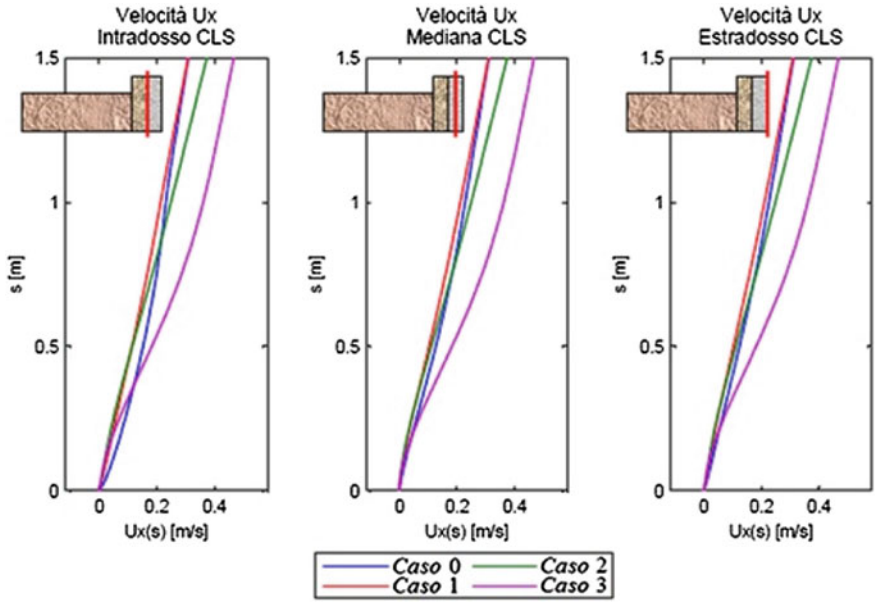

Fig. 9.30 The horizontal velocities in the walls versus the vertical position at different absicssae (the *red lines* in the walls)

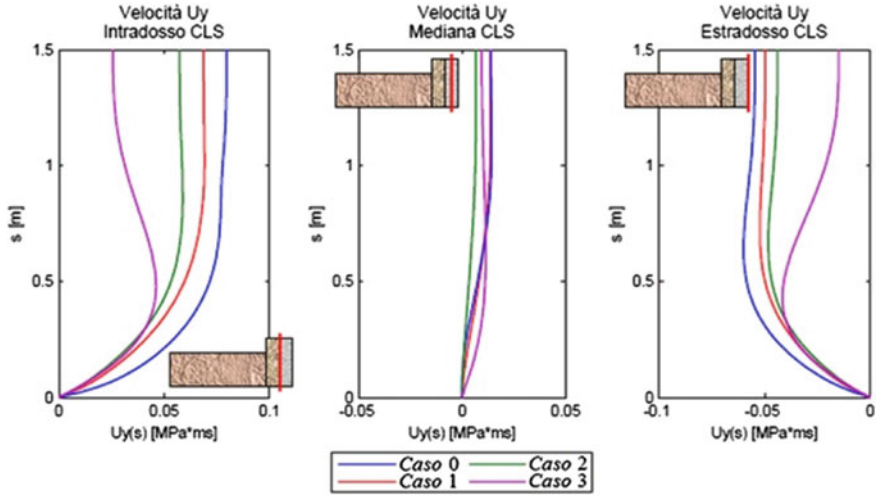

Fig. 9.31 The vertical velocities in the walls versus the vertical position at different abscissae (the *red lines* in the walls)

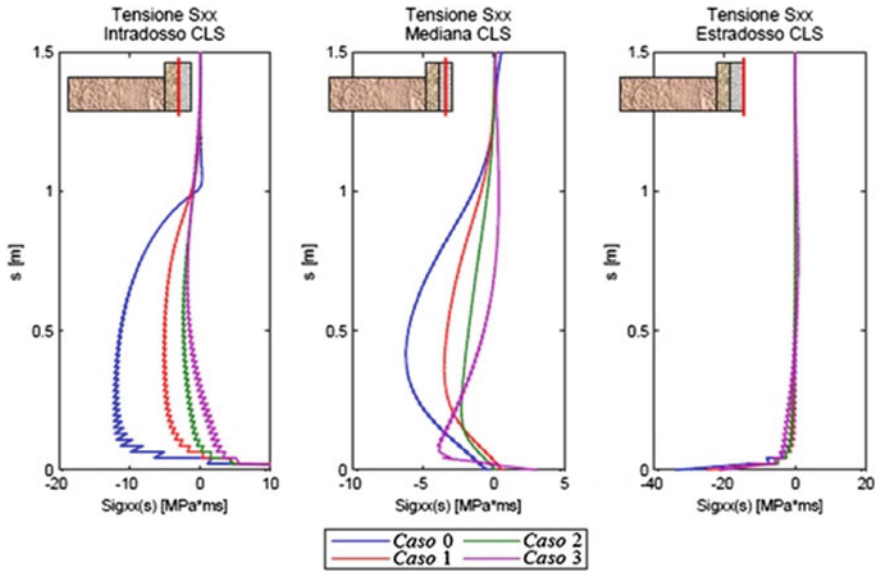

Fig. 9.32 The percussion stress Σ_{xx} versus the vertical position at different abscissae (the *red lines* in the walls). This stress is weaker in a wall with a damping sand part

Acknowledgments The computation of this chapter are due to Dr. Alberto Frau. The Authors express him their sincere gratitude for his helpful collaboration.

References

1. Amoruso, A.: Analisi dell'impatto di colate detritiche ad alta velocitá contro strutture. Ph.D. thesis in Ingegneria delle Strutture e Geotecnica, Università di Roma "Tor Vergata" (2010)
2. Armanini, A.: On the dynamic impact of debris flows. In: Armanini, A., Michiue, M. (eds.) Recent Developments on Debris Flow, pp. 208–226. Springer, Berlin (1997)
3. Armanini, A., Scotton, P.: On the dynamic impact of a debris flow on structures. In: Proceedings of XXV Congress IAHR, Tokyo, Tech. Sess. B, III, pp. 203-210 (1993)
4. Armanini, A., Larcher, M., Odorizzi, M.: Dynamic impact of steep waves against a vertical wall. In: First European Congress of the IAHR. Edinburgh, 4–6 May 2010
5. Armanini, A., Larcher, M., Odorizzi, M.: Dynamic impact of a debris flow front against a vertical wall. In: 5th International Conference on Debris-flow Hazard Mitigation, Roma, Casa Editrice Universitá La Sapienza, 2011, pp. 1041-1049, Proceedings of DFHM, Padova, 14–17 June 2011
6. Bredmose, H., Peregrine, D.H., Porter, A., Bullock G.N.: Wave impact and aerated water. In: Proceedings of the 18th International Workshop on water waves and floating bodies, École centrale de Nantes (2003)
7. Bugnion, L., Mcardell, B.W., Bartelt, P., Wendeler, C.: Measurements of hillslope debris flow impact pressure on obstacles. Landslides **9**(2), 179–187 (2012)
8. Bullock, G., Obhrai, C., Müller, G., Wolters, G., Peregrine, D.H., Bredmose, H.: Characteristics and design implications of breaking wave impacts. In: Proceedings of 29th International Conference on Coastal Eng., ASCE, Lisbon (2004)
9. Canelli, L., Ferrero, A.M., Migliazza, M., Segalini, A.: Debris flow risk mitigation by the means of rigid and flexible barriers - experimental tests and impact analysis. Nat. Hazards Earth Syst. Sci. **12**, 1693–1699 (2012)
10. Cooker, M.J.: Liquid impact, kinetic energy loss and compressibility: Lagrangian, Eulerian and acoustic viewpoints. J. of Engng. Math. **44**(259), 276 (2002)
11. Daido, A.: Impact force of mud debris flows on structures. XXV IAHR Congress, Technical Session B. **3**, 211–213 (1993)
12. Davies, T.: Dynamically similar small-scale debris flow models, In Univ. of Trento I, Ed., International Workshop on floods and inundations related to large earth movements, IAHS Publ (1994)
13. Dimnet, E., Frémond, M., Gormaz, R., San Martin, J.A.: Collisions involving solids and fluids. In: Frémond, M., Maceri, F. (eds.) Novel Approaches in Civil Engineering. Springer, Berlin (2003)
14. Faella, C., Nigro, E.: Dynamic impact of the debris flows on the constructions during the hydrogeological disaster in Campania-1998: failure mechanical models and evaluation of the impact velocity. In: Picarelli, L. (ed.) Fast slope movements prediction and prevention for risk mitigation, 1. Pàtron, Bologna (2003)
15. Federico, F., Amoruso, A.: Numerical analysis of the dynamic impact of debris flows on structures. In: ISEC-03, 3rd International "Structural Engineering and Construction Conference" September, 2005, Shunan, Japan (2005)
16. Federico, F., Amoruso, A.: Impact of avalanche boulders on structures. In: Third International Conference on Structural Engineering, Mechanics and Computation (SEMC 2006) 2006
17. Federico, F., Amoruso, A.: Simulation of mechanical effects due to the impact of fluid-like debris flows on structures. Ital. J. Eng. Geol. Environ. **04**, 5–24 (2008)
18. Federico, F., Amoruso, A.: Impact between fluids and solids. Comparison between analytical and FEA results. Int. J. Impact Eng. **36**(1), 154–164 (2009)

19. Federico, F., Amoruso, A.: Analytical and numerical solutions of the dynamic impact force of fluidized debris flows onto structures. In: NUMGE 2010, 7th European Conference on Numerical Methods in Geotechnical Engineering, June 2–4, 2010, Trondheim, Norway (2010)
20. Federico, F., Cesali, C.: Modeling of runout length of high-speed granular masses. In: International Conference Vajont 1963–2013 (Padua-Italy, 8-10 October 2013). "Italian Journal of Engineering Geology and Environment" - IJEGE (Publishing House Sapienza Universitá Editrice), IJEGE Book Series (2013)
21. Federico, F., Cesali, C.: The role of micro-mechanical parameters in the runout length of high-speed granular masses. In: Modeling and numerical simulations, International Symposium on Geomechanics From Micro to Macro (IS Cambridge 2014), September, 1–3. Cambridge, UK (2014)
22. Federico, F., Cesali, C.: An energy-based approach to predict debris flow mobility and analyze empirical relationships. Can. Geotech. J. **52**(12), 2113–2133 (2015). doi:10.1139/cgj-2015-0107
23. Federico, F., Musso, A., Amoruso, A.: Theoretical analyses of the impact force by debris flows on structures. In: Proceedings International International Workshop, Living with landslides: effects on structures and urban settlements. Strategies for risk reduction, pp. 165–175, 27–28 Oct 2003, Anacapri (2003)
24. Federico, F., Musso, A., Amoruso, A.: Mechanical effects of impact forces by debris flows on containment structures. Colloquium Lagrangianum, Montpellier, France (2003)
25. Federico, F., Musso, A., Amoruso, A.: Analisi dell'impatto di colate detritiche ad alta velocitá su strutture di contenimento. In: Workshop "Modelli matematici per la simulazione di catastrofi idrogeologiche", Rende (CS), 30, 31 March 2004
26. Federico, F., Musso, A., Amoruso, A.: Impact of a fluid-like debris flow on reinforced concrete pillars. In: Numerical simulations and back-analyses of a failure case, 11 ICF - International Conference on Fractures - Post Symposium on "Damage and Repair of Historical and Monumental Building", Venice, 29 March 2005
27. Field, J.E.: Liquid impact and cavitation erosion processes. In: Briscoe, B.J., Adams, M.J. (eds.) Tribology in Particulate Technology, pp. 416–438. Adam Hilger, Bristol and Philadelphia (1987). Chap. 4.8
28. Frémond, M.: Méthodes variationnelles en calcul des structures. École nationale des Ponts et Chaussées, Paris (1982)
29. Frémond, M.: Collisions, Edizioni del Dipartimento di Ingegneria Civile, Università di Roma "Tor Vergata" (2007). ISBN 978-88-6296-000-7
30. Frémond, M., Gormaz, R., San Martin, J.: Collision of a solid with an uncompressible fluid. Theor. Comput. Fluid Dyn. **16**, 405–420 (2003)
31. Guo, S., Xu, P., Zheng, Z., Gao, Y.: Estimation of flow velocity for a debris flow via the two-phase fluid model. Nonlinear Process. Geophys. **22**, 109–116 (2015) www.nonlin-processes-geophys.net/22/109/2015/. doi:10.5194/npg-22-109-2015
32. Hübl, J., Suda, J., Proske, D., Kaitna, R., Scheidl, C.: Debris flow impact estimation. In: Popovska C., Jovanovski M. (eds.) 11th International Symposium on Water Management and Hydraulic Engineering, University Ss. Cyril and Methodius, Faculty of Civil Engineering, Skopje, Macedonia, pp. 137–148 (2009)
33. Hungr, O., Morgan, G.C., Kellerhals, R.: Quantitative analysis of debris torrent hazards for design of remedial measures. Can. Geotech. J. **21**, 663–667 (1984)
34. Ishikawa, N., Inoue, R., Hayashi, K., Hasegawa, Y., Mizuyama, T.: Experimental approach on measurement of impulsive fluid force using debris flow model. In: Conference Proceedings Interpraevent 2008, pp. 192–193. Dornbirn, Austria (2008)
35. Korobkin, A.: Elastic response of catamaran wet deck to liquid impact. Ocean Eng. **25**, 687–714 (1998)
36. Kosinska, A.: Interaction of debris with a solid obstacle: numerical analysis. J. Hazard. Mater. **177**, 602–612 (2010)
37. Lesser, M.: Thirty years of liquid impact research: a tutorial review. Wear, n.186–187, 28–34 (1995)

38. Lo, D.O.K., Ho, K.K.S., Pun, W.K., Pang, R.P.L.: Design of barriers for natural terrain landslides. GeoEng 2000, Melbourne, Australia, Conference proceedings (2000)
39. Lorenzini, G., Mazza, N.: Debris Flow: Phenomenology and Rheological Modelling, Chap. 6.7, A debris-flow classification based on dimensional analysis, WIT Press (2004)
40. Marchi, E., Rubatta, A.: Meccanica dei Fluidi. Utet, Torino (1981). ISBN 88-02-03659-4
41. Moriguchi, S., Borja, R.I., Yashima, A., Sawada, K.: Estimating the impact force generated by granular flow on a rigid obstruction. Acta Geotechnica. **4**, 57–71 (2009)
42. Musso, A., Olivares, L.: Flowslides in pyroclastic soils: transition from "static liquefaction" to "fluidization". Invited paper. In: Picarelli L. (ed.) Proceedings of International Workshop on Occurrence and mechanisms of flow-like landslides in natural slopes and earthfills. Sorrento, May 2003, pp. 117–128 (2003)
43. Musso, A., Federico, F., Troiano, A.: A mechanism of pore pressure accumulation in rapidly sliding submerged porous blocks. Comput. Geotech. **31**, 209–226 (2004). Issn 0266-352x
44. Obhrai, C., Bullock, G., Wolters, G., Müller, G., Peregrine, D.H., Bredmose, H.: Violent wave impacts on vertical and inclined walls: large scale model tests. In: Proceedings of 29th International Conference Coastal Engineering, ASCE, Lisbon (2004)
45. Olivares, L., Picarelli, L.: Shallow flowslides triggered by intense rainfalls on natural slopes covered by loose unsaturated pyroclastic soils. Gotechnique **53**(2), 283–288 (2003)
46. Peregrine, D.H.: Water-wave impact on walls. Annu. Rev. Fluid Mech. **35**(23), 43 (2003)
47. Peregrine, D.H., Bredmose, H., Bullock, G., Obhrai, C., Müller, G. Wolters, G.: Violent water wave impact on a wall. In: Proceedings of the 29th International Conference on Coastal Engineering. ASCE, Lisbon (2004)
48. Prochaska, A.B., Santi, M.P., Higgins, J.D., Cannon, S.H.: A study of methods to estimate debris flow velocity. Landslides (2008). doi:10.1007/s10346-008-0137-0
49. Revellino, P., Hungr, O., Guadagno, F.M., Evans, S.G.: Velocity and runout simulation of destructive debris flows and debris avalanches in pyroclastic deposits, Campania region, Italy. Environ. Geol. **45**, 295–311 (2004)
50. Scheidl, C., Chiari, M., Mullegger, M., Proske, D.: Estimation of debris-flow impact forces using a small scale modelling approach. In: 12th Congress Interpraevent 2012, Grenoble, Extended Abstracts (2012) www.interpraevent.at
51. Scheidl, C., Chiari, M., Mullegger, M., Proske, D.: Analysing Debris-flow impact models based on a small scale modelling approach. Surv. Geophys. **34**, 121–140 (2013). (Chap. 3.1 - Scaling Consideration) doi:10.1007/s10712-012-9199-6
52. Scotton, P., Deganutti, A.M.: Phreatic line and dynamic impact in laboratory debris flow experiments. In: Debris-Flow Hazards Mitigation, ASCE, New York (1997)
53. Tiberghien, D., Laigle, D., Naaim, M., Thibert, E., Ousset, F.: Experimental investigation of interaction between mudflow and obstacle. In: Chen C.I., Major J.J. (eds.) Debris-Flow Hazards Mitigation. Mechanics, Prediction, and Assessment. Rotterdam, Millpress. Chengdu, China: 281–292 (2007)
54. Vagnon, F., Ferrero, A.M., Segalini, A.: Studi teorici sperimentali per la valutazione di spinte su ostacoli determinate da fenomeni di flusso. IARG 2015, Cagliari (2015)
55. Walkden, M.J., Wood, D.J., Bruce, T., Peregrine, D.H.: Impulsive seaward loads induced by wave overtopping on caisson breakwaters. Coast. Eng. **42**, 257–276 (2001)

Chapter 10
Shape Memory Alloys and Collisions

Michel Frémond and Michele Marino

10.1 Introduction

We have investigated the collisions of solids in Chap. 7 producing both discontinuities of velocities and discontinuities of temperatures at collision time t. In this chapter we consider the solid is made of shape memory alloys. It occupies domain Ω with boundary $\partial\Omega$. There is a vast literature on shape memory alloys. We mention some of the papers on modelling, mechanics and mathematics, knowing that we are not exhaustive, [1–23, 25–54]. The predictive theory of shape memory alloys, [20, 21, 28, 38–40] introduces besides the macroscopic velocities, velocities at the microscopic level which are responsible for the phase changes between the martensites and austenite phases. We have chosen to represent at the macroscopic level, the velocities at the microscopic level by the velocities

$$\frac{d\beta_i}{dt},$$

of the volumes fractions β_i of the different phases, β_3 for the austenite phase and β_1, β_2 for the martensite phases, assuming there are two of them.

We keep the assumption of the previous chapters: collisions are instantaneous. We denote with subscript $^-$, quantities before collision and subscript $^+$, quantities after collisions. For example, we denote

$$\mathbf{U} = (\mathbf{U}^+, \mathbf{U}^-),$$

the actual velocities, $\mathbf{U}^-$ being the actual velocity before the collision and $\mathbf{U}^+$ being the actual velocity after. As in the previous chapters, we denote $[X] = X^+ - X^+$, the discontinuity of quantity X

M. Frémond, *Collisions Engineering: Theory and Applications*,
Springer Series in Solid and Structural Mechanics 6,
DOI 10.1007/978-3-662-52696-5_10

In collisions, there are rapid variations of the velocities at the microscopic level resulting in rapid phase evolution or rapid variations of the volumes fractions β_i, which are represented by discontinuities [24, 25, 27, 38].

$$[\beta_i] = \beta_i^+ - \beta_i^- .$$

The collisions being dissipative phenomena, they produce burst of heat which intervene in the thermal evolution. They result in temperature discontinuities and they may produce phase changes. Moreover voids may also appear, [29]. Thus the volume fractions discontinuities and the temperature discontinuities are coupled as they are in smooth evolutions, [22]. Transient and fast but smooth phenomena in shape memory alloys are investigated in [13, 16]. The last paper contains experimental results.

10.1.1 The State Quantities

They are

$$E = (\varepsilon(\mathbf{u}), \beta_i, \mathbf{grad}\beta_i, T) ,$$

In a collision, the small displacement $\mathbf{u}$ does not change, thus the small deformation, $\varepsilon(\mathbf{u})$, remains constant. But as already seen, the phase volume fractions and the temperature T do vary in collisions. We have the state quantities before collision, E^-, and E^+ after.

10.1.2 Quantities Which Describe the Evolution

The quantities which describe the evolution are the evolution of the velocity of deformation already chosen in Chap. 7

$$\mathsf{D}(\frac{\mathbf{U}^+ + \mathbf{U}^-}{2}), \tag{10.1}$$

where D is the usual deformation operator, and the gradient of the average temperature already introduced in Chap. 7, together with the variation of the volume fractions and their gradients. The average temperature is

$$\underline{T} = \frac{T^+ + T^-}{2},$$

where T^+ and T^- are the temperatures after and before collision. Its gradient is involved in the description of heat diffusion occurring in collisions, as shown in Chap. 7. Thus the quantities which describe the evolution, δE is

$$\delta E = (\mathsf{D}(\frac{\mathbf{U}^+ + \mathbf{U}^-}{2}), [\beta_i], \mathbf{grad}\,[\beta_i], \mathbf{grad}\underline{T}).$$

The discontinuity $[\beta_i]$ is the non smooth part of the velocity $d\beta_i/dt$.

10.2 The Principle of Virtual Work and the Equations of Motion

The virtual work of the internal forces, the internal percussion forces, is

$$\mathcal{T}_{int}(\mathbf{V}, \gamma) \quad (10.2)$$
$$= -\int_\Omega \Sigma : \mathsf{D}(\frac{\mathbf{V}^+ + \mathbf{V}^-}{2}) d\Omega - \sum_{i=1}^{3} \int_\Omega B_i^p \left[\gamma_i\right] + \mathbf{H}_i^p \cdot \mathbf{grad}\left[\gamma_i\right] d\Omega,$$

where $\mathbf{V} = (\mathbf{V}^+, \mathbf{V}^-), \gamma_i = (\gamma_i^+, \gamma_i^-)$ are virtual velocities: $\mathbf{V}^-, \gamma_i^-$ are the velocities before the collision and $\mathbf{V}^+, \gamma_i^+$ are the velocities after.

It appears percussion stresses Σ and percussion work B_p and work flux vector $\mathbf{H}_p$. The virtual work of the acceleration forces is

$$\mathcal{T}_{acc}(\mathbf{V}, \gamma) = \int_\Omega \rho\,[\mathbf{U}] \cdot \frac{\mathbf{V}^+ + \mathbf{V}^-}{2} d\Omega.$$

The actual work of the acceleration forces

$$\mathcal{T}_{acc}(\mathbf{U}, \gamma) = \int_\Omega \rho\,[\mathbf{U}] \cdot \frac{\mathbf{U}^+ + \mathbf{U}^-}{2} d\Omega = \int_\Omega \rho \frac{(\mathbf{U}^+)^2}{2} d\Omega - \int_\Omega \rho \frac{(\mathbf{U}^-)^2}{2} d\Omega, \quad (10.3)$$

is equal to the variation of the kinetic energy. This relationship is an element of the theorem of kinetic energy. The virtual work of the external forces is

$$\mathcal{T}_{ext}(\mathbf{V}, \gamma) \quad (10.4)$$
$$= \int_\Omega \mathbf{F}^p \cdot \frac{\mathbf{V}^+ + \mathbf{V}^-}{2} d\Omega + \int_{\partial\Omega} \mathbf{G}^p \cdot \frac{\mathbf{V}^+ + \mathbf{V}^-}{2} d\Gamma$$
$$+ \int_\Omega A_i^p \left[\gamma_i\right] d\Omega_1 + \int_{\partial\Omega} a_i^p \left[\gamma_i\right] d\Gamma.$$

We assume that the surface external percussions $\mathbf{G}^p$ are applied to the whole boundary of the solid. The $\mathbf{F}^p$ are the volume external percussions. The A_p and a_p are the volume and surface percussion work provided by possible external actions. The equations of motion result from the principle of virtual work

$$\forall \mathbf{V}, \forall \gamma,\ \mathcal{T}_{acc}(\mathbf{V}, \gamma) = \mathcal{T}_{int}(\mathbf{V}, \gamma) + \mathcal{T}_{ext}(\mathbf{V}, \gamma).$$

Different choices of the virtual velocities $\mathbf{V}$ and γ give

$$\rho\,[\mathbf{U}] = \text{ div } \boldsymbol{\Sigma} + \mathbf{F}^p, \ \text{ in } \ \Omega, \tag{10.5}$$

$$-B_i^p + \text{div } \mathbf{H}_i^p + A_i^p = 0, \ \text{ in } \ \Omega, \tag{10.6}$$

and

$$\boldsymbol{\Sigma}\mathbf{N} = \mathbf{G}^p, \ \mathbf{H}_i^p \cdot \mathbf{N} = a_i^p, \ \text{ on } \ \partial\Omega. \tag{10.7}$$

10.3 The Mass Balance

It is

$$[\rho(\beta_1 + \beta_2 + \beta_3)] = 0,$$

or

$$[(\beta_1 + \beta_2 + \beta_3)] = 0, \tag{10.8}$$

assuming the density ρ is constant and the same for each phase. In case the densities are not the same, the voids volume fraction

$$\beta_{voids} = 1 - (\beta_1 + \beta_2 + \beta_3),$$

evolves in the collision, [29, 51].

Remark 10.1 The mass balance in a smooth evolution

$$\frac{d}{dt}\int_{\mathcal{D}} \rho(\beta_1 + \beta_2 + \beta_3)d\Omega = -\int_{\partial\mathcal{D}} \mathbf{m}\cdot\mathbf{N}d\Gamma,$$

where $\mathbf{m}$ is the external mass flux vector, becomes in a non smooth evolution

$$\int_{\mathcal{D}} [\rho(\beta_1 + \beta_2 + \beta_3)]\, d\Omega = -\int_{\partial\mathcal{D}} \mathbf{M}\cdot\mathbf{N}d\Gamma,$$

where $\mathbf{M}$ is the external mass impulse vector. In smooth motion we have $\mathbf{m} = 0$. We get the non smooth mass balance

$$[\rho(\beta_1 + \beta_2 + \beta_3)] + \text{div } \mathbf{M} = 0.$$

It describes the possible mass diffusion in the collision. The mass impulse may be split into

$$\mathbf{M} = \mathbf{M}^+ + \mathbf{M}^-.$$

We may assume that

$$\mathbf{M}^+ = \frac{\rho k}{2}\mathbf{U}^+,\ \mathbf{M}^- = \frac{\rho k}{2}\mathbf{U}^-,$$

giving

$$[\beta_1 + \beta_2 + \beta_3] + k\text{div}\ \frac{\mathbf{U}^+ + \mathbf{U}^-}{2} = 0,$$

assuming the densities of the phases are identical and constant. The mass balance is a relationship involving quantities describing the evolution. Note that this relationship relates the variation of the voids volume fraction, $\beta_{voids} = 1 - \beta_1 + \beta_2 + \beta_3$, to the average variation of volume

$$[\beta_{voids}] = k\text{div}\ \frac{\mathbf{U}^+ + \mathbf{U}^-}{2}.$$

We may also assume that

$$\mathbf{M} = -k\mathbf{grad}\,[\beta_1 + \beta_2 + \beta_3]\,,$$

giving

$$[\beta_1 + \beta_2 + \beta_3] - k\Delta\,[\beta_1 + \beta_2 + \beta_3] = 0.$$

This equation makes the voids to decrease where they are numerous and to increase where there are few of them. Let us note that this mass impulse sophisticates the motion and energy balance equation. Thus for the time being we keep the basic mass balance equation (10.8).

10.4 The Laws of Thermodynamics

The first and second laws of thermodynamics intervene in the derivation of the constitutive laws. We recall them to get the new mechanical and thermal collision constitutive laws.

10.4.1 The First Law

It is

$$[\mathcal{E}] + [\mathcal{K}] = \mathcal{T}_{ext}(\mathbf{U}, \beta) + \mathcal{C}, \tag{10.9}$$

where

$$\mathcal{E} = \int_{\Omega} e d\Omega,$$

is the internal energy, $\mathcal{K}$ is the kinetic energy, and $\mathcal{C}$ is the thermal impulse received by the solid. With the principle of virtual work where the velocities are the actual velocities, i.e., with the theorem of kinetic energy, (10.3), the first law gives

$$[\mathcal{E}] = -\mathcal{T}_{int} + \mathcal{C}.$$

The temperature may be discontinuous, [22, 24]: we have already defined T^- the temperature before the collision and T^+ the temperature after the collision and

$$\underline{T} = \frac{T^+ + T^-}{2}.$$

We assume that the external impulse heat is received either at temperature T^- or at temperature T^+

$$\mathcal{C} = \int_{\partial\Omega} -\left(T^+\mathbf{Q}_p^+ + T^-\mathbf{Q}_p^-\right)\cdot\mathbf{N}d\Gamma + \int_{\Omega} T^+\mathcal{B}^+ + T^-\mathcal{B}^- d\Omega,$$

where $\mathbf{Q}_p$ is the impulsive entropy flux vector and $\mathcal{B}$ the impulsive entropy source. Relationship (10.9) being true for any subdomain of Ω, we get the energy balance law

$$\begin{aligned}[e] = \Sigma : \mathsf{D}(\frac{\mathbf{U}^+ + \mathbf{U}^-}{2}) + B_i^p\,[\beta_i] + \mathbf{H}_i^p\cdot\mathbf{grad}\,[\beta_i] \\ -\mathrm{div}(T^+\mathbf{Q}_p^+ + T^-\mathbf{Q}_p^-) + T^+\mathcal{B}^+ + T^-\mathcal{B}^-.\end{aligned} \tag{10.10}$$

By using the Helmholtz relationship, $e = \Psi + Ts$, we have

$$[e] = [\Psi] + \underline{s}\,[T] + \underline{T}\,[s] \tag{10.11}$$

$$= \Sigma : \mathsf{D}(\frac{\mathbf{U}^+ + \mathbf{U}^-}{2}) + B_i^p\,[\beta_i] + \mathbf{H}_i^p\cdot\mathbf{grad}\,[\beta_i] \tag{10.12}$$

$$-\mathrm{div}\left(\underline{T}\Sigma\left(\mathbf{Q}_p\right) + [T]\,\Delta\left(\mathbf{Q}_p\right)\right) + \underline{T}\Sigma\left(\mathcal{B}\right) + [T]\,\Delta\left(\mathcal{B}\right), \tag{10.13}$$

where a sum

$$T^+\mathcal{B}^+ + T^-\mathcal{B}^- = \Sigma(T\mathcal{B}),$$

is split in an other sum

$$\Sigma(T\mathcal{B}) = \underline{T}\Sigma\left(\mathcal{B}\right) + [T]\,\Delta\left(\mathcal{B}\right),$$

with

$$\Sigma(\mathcal{B}) = \mathcal{B}^+ + \mathcal{B}^- \; and, \; \Delta(\mathcal{B}) = \frac{\mathcal{B}^+ - \mathcal{B}^-}{2}.$$

Remark 10.2 To avoid too many notation, we use letter Σ with two meanings: the percussion stress Σ which appears in the equation of motion and the sum $\Sigma(\mathcal{B}) = \mathcal{B}^+ + \mathcal{B}^-$. They appear in different contex and the sum $\Sigma(\mathcal{B})$ has always an argument.

10.4.2 The Second Law

It is

$$[\mathcal{S}] = \int_\Omega [s]\, d\Omega \geq -\int_\Gamma \left(\mathbf{Q}_p^+ + \mathbf{Q}_p^-\right) \cdot \mathbf{N} d\Gamma + \int_\Omega \mathcal{B}^+ + \mathcal{B}^- d\Omega,$$

which gives

$$[s] \geq -\text{div}\, \Sigma\left(\mathbf{Q}_p\right) + \Sigma(\mathcal{B}). \tag{10.14}$$

Combining relationships (10.13) and (10.14), we get

$$[\Psi] + \underline{s}\,[T] + \text{div}\, \left([T]\, \Delta(\mathbf{Q}_p)\right) - [T]\, \Delta(\mathcal{B}) \tag{10.15}$$

$$\leq \Sigma : \mathsf{D}(\frac{\mathbf{U}^+ + \mathbf{U}^-}{2}) + B_i^p\, [\beta_i] + \mathbf{H}_i^p \cdot \mathbf{grad}\, [\beta_i] - \mathbf{grad}\underline{T} \cdot \Sigma(\mathbf{Q}_p). \tag{10.16}$$

Let us note that the right hand side is a scalar product between internal forces and related evolution quantities whereas the left hand side is not a scalar product. Let us try to relate $[\Psi]$ to a scalar product. We have

$$[\Psi] = \Psi(T^+, \beta_i^+, \mathbf{grad}\beta_i^+) - \Psi(T^-, \beta_i^-, \mathbf{grad}\beta_i^-) \tag{10.17}$$

$$= \Psi(T^+, \beta^+, \mathbf{grad}\beta^+) - \Psi(T^+, \beta_i^-, \mathbf{grad}\beta_i^-) \tag{10.18}$$

$$+ \Psi(T^+, \beta_i^-, \mathbf{grad}\beta_i^-) - \Psi(T^-, \beta_i^-, \mathbf{grad}\beta_i^-). \tag{10.19}$$

Because the free energy is a concave function of temperature T, we have

$$\Psi(T^+, \beta_i^-, \mathbf{grad}\beta_i^-) - \Psi(T^-, \beta_i^-, \mathbf{grad}\beta_i^-) \leq -s^{fe}\,[T], \tag{10.20}$$

with

$$-s^{fe} \in \hat{\partial}\Psi_T(T^-, \beta_i^-, \mathbf{grad}\beta_i^-), \tag{10.21}$$

where $\hat{\partial}\Psi_T$ is the set of the uppergradients of the concave function

$$T \to \Psi_T(T, \beta_i^-, \mathbf{grad}\beta_i^-) = \Psi(T, \beta_i^-, \mathbf{grad}\beta_i^-). \tag{10.22}$$

We assume Ψ is a convex function of $(\boldsymbol{\beta}, \mathbf{grad}\ \boldsymbol{\beta})$. Thus we have

$$\Psi(T^+, \beta_i^+, \mathbf{grad}\beta_i^+) - \Psi(T^+, \beta_i^-, \mathbf{grad}\beta_i^-) \leq B_i^{fe}[\beta_i] + \mathbf{H}_i^{fe} \cdot \mathbf{grad}[\beta_i], \tag{10.23}$$

with

$$\left(B_i^{fe}, \mathbf{H}_i^{fe}\right) \in \partial\Psi_{\beta,\mathbf{grad}\beta}(T^+, \beta_i^+, \mathbf{grad}\beta_i^+), \tag{10.24}$$

where $\partial\Psi_{\beta,\mathbf{grad}\beta}$ is the subdifferential set of convex function Ψ of $(\boldsymbol{\beta}, \mathbf{grad}\ \boldsymbol{\beta})$. The internal forces $\left(B_i^{fe}, \mathbf{H}_i^{fe}\right)$ depend on the future state $(T^+, \beta_i^+, \mathbf{grad}\ \beta_i^+)$, in agreement with our idea that the constitutive laws sum up what occurs during the collision. It results

$$[\Psi] + \underline{s}[T] + \text{div}\ [T]\,\Delta(\mathbf{Q}_p) - [T]\,\Delta(\mathcal{B}) \tag{10.25}$$

$$\leq B_i^{fe}[\beta_i] + \mathbf{H}_i^{fe} \cdot \mathbf{grad}[\beta_i] - s^{fe}[T] + \bar{s}[T] + \text{div}\ [T]\,\Delta(\mathbf{Q}_p) \tag{10.26}$$

$$= B_i^{fe}[\beta_i] + \mathbf{H}_i^{fe} \cdot \mathbf{grad}[\beta_i] + (-s^{fe} + \bar{s} + \text{div}\ \Delta(\mathbf{Q}_p))[T] + \Delta(\mathbf{Q}_p) \cdot \mathbf{grad}[T]. \tag{10.27}$$

As usual, we assume no dissipation with respect to $[T]$ [22, 24, 25] and have

$$\begin{aligned} \Delta(\mathbf{Q}_p) &= 0, \\ -s^{fe} + \bar{s} + \text{div}\ \Delta(\mathbf{Q}_p) - \Delta(\mathcal{B}) &= 0. \end{aligned} \tag{10.28}$$

Thus

$$\Delta(\mathcal{B}) + S = 0, \tag{10.29}$$

with $S = s^{fe} - \bar{s}$. This relationship splits either the received heat impulse, $T^+\mathcal{B}^+ + T^-\mathcal{B}^-$, or the received entropy impulse, $\mathcal{B}^+ + \mathcal{B}^-$, between the two temperatures, T^+ and T^-. Let us note that this relationship depends on the future state via the average entropy $\bar{s}$.

We may choose a pseudo-potential of dissipation

$$\Phi(\Delta E^{\pm}, E) = \Phi(\mathsf{D}(\frac{\mathbf{U}^+ + \mathbf{U}^-}{2}), [\beta_i], \mathbf{grad}[\beta_i], \mathbf{grad}\underline{T}, E), \tag{10.30}$$

and constitutive laws

$$\left(\Sigma, (B_i^p - B_i^{fe}), (\mathbf{H}_i^p - \mathbf{H}_i^{fe}), -2\mathbf{Q}_p\right) \tag{10.31}$$

$$\in \partial\Phi(\mathsf{D}(\frac{\mathbf{U}^+ + \mathbf{U}^-}{2}), [\beta_i], \mathbf{grad}\,[\beta_i], \mathbf{grad}\underline{T}, \underline{T}). \tag{10.32}$$

it results from this choice that the internal forces satisfy inequality

$$0 \leq \Sigma : \mathsf{D}(\frac{\mathbf{U}^+ + \mathbf{U}^-}{2}) + (B_i^p - B_i^{fe})\,[\beta_i] + (\mathbf{H}_i^p - \mathbf{H}_i^{fe}) \cdot \mathbf{grad}\,[\beta_i] - 2\mathbf{grad}\underline{T} \cdot \mathbf{Q}_p, \tag{10.33}$$

and the second law is satisfied.

Theorem 10.1 *If constitutive laws (10.24), (10.29) and (10.32) are satisfied, then the second law is satisfied.*

Proof If relationship (10.32) is satisfied, inequality (10.33) is satisfied. Then it is easy to prove that the inequality (10.16) which is equivalent to the second law is satisfied.

Remark 10.3 The discontinuity $[\Psi]$ may be split in a different manner

$$[\Psi] = \Psi(T^+, \beta_i^+, \mathbf{grad}\beta_i^+) - \Psi(T^-, \beta_i^-, \mathbf{grad}\beta_i^-) \tag{10.34}$$

$$= \Psi(T^+, \beta_i^+, \mathbf{grad}\beta_i^+) - \Psi(T^-, \beta_i^+, \mathbf{grad}\beta_i^+) \tag{10.35}$$

$$+\Psi(T^-, \beta_i^+, \mathbf{grad}\beta_i^+) - \Psi(T^-, \beta_i^-, \mathbf{grad}\beta_i^-). \tag{10.36}$$

We get

$$\Psi(T^+, \beta_i^+, \mathbf{grad}\beta_i^+) - \Psi(T^-, \beta_i^+, \mathbf{grad}\beta_i^+) \leq -\hat{s}^{fe}\,[T], \tag{10.37}$$

$$-\hat{s}^{fe} \in \hat{\partial}\Psi_T(T^-, \beta_i^+, \mathbf{grad}\beta_i^+). \tag{10.38}$$

If Ψ it is a convex function of $(\beta, \mathbf{grad}\ \beta)$

$$\Psi(T^-, \beta_i^+, \mathbf{grad}\beta_i^+) - \Psi(T^-, \beta_i^-, \mathbf{grad}\beta_i^-)) \leq \hat{B}^{fe}\,[\beta] + \hat{H}^{fe} \cdot \mathbf{grad}\,[\beta] \tag{10.39}$$

$$\left(\hat{B}^{fe}, \hat{H}^{fe}\right) \in \partial\Psi_{\beta, \mathbf{grad}\beta}(T^-, \beta_i^-, \mathbf{grad}\beta_i^-). \tag{10.40}$$

The internal forces $\left(\hat{B}^{fe}, \hat{H}^{fe}\right)$ depend entirely on the past state $(T^-, \beta_i^-, \mathbf{grad}\beta_i^-)$. Because we think that the constitutive laws sum up what occurs during the collision, it is mandatory that the internal forces depend on the future state $(T^+, \beta_i^+, \mathbf{grad}\ \beta_i^+)$. Thus this splitting of the free energy does not seem as good as the one we have chosen.

10.5 The Free Energy

A shape memory alloy is considered as a mixture of the martensite and austenite phases with volume fractions β_i. The volumic free energy of the mixture we choose is

$$\Psi = \Psi(E) = \sum_{i=1}^{3} \beta_i \Psi_i(E) + h(E), \tag{10.41}$$

where the Ψ_i's are the volume free energies of the i phases and h is a free energy describing interactions between the different phases. We have assumed that internal constraints are physical properties, hence, we decide to choose properly the two functions describing the material, i.e., the free energy Ψ and the pseudo-potential of dissipation Φ, in order to take these constraints into account. Since, the pseudo-potential describes the kinematic properties (i.e., properties which depend on the velocities) and the free energy describes the state properties, obviously the internal constraints

$$0 \leq \beta_i \leq 1, \tag{10.42}$$

and

$$\beta_1 + \beta_2 + \beta_3 \leq 1, \tag{10.43}$$

because voids may appear, are to be taken into account with the free energy Ψ.

For this purpose, we assume the Ψ_i's are defined over the whole linear space spanned by β_i and the free energy is defined by

$$\Psi(E) = \beta_1 \Psi_1(E) + \beta_2 \Psi_2(E) + \beta_3 \Psi_3(E) + h(E)\,. \tag{10.44}$$

We choose the very simple interaction free energy

$$h(E) = I_C(\boldsymbol{\beta}) + \frac{k}{2} \left|\mathbf{grad}\boldsymbol{\beta}\right|^2, \tag{10.45}$$

where I_C is the indicator function of the convex set

$$C = \{(\gamma_1, \gamma_2, \gamma_3) \in \Re^3;\, 0 \leq \gamma_i \leq 1;\, \gamma_1 + \gamma_2 + \gamma_3 \leq 1\}\,. \tag{10.46}$$

Moreover, and by $(k/2)\left|\mathbf{grad}\boldsymbol{\beta}\right|^2$ we mean the product of two tensors $\mathbf{grad}\boldsymbol{\beta}$ multiplied by the *interfacial energy* coefficient $(k/2) > 0$. The terms $I_C(\boldsymbol{\beta}) + (k/2)\left|\mathbf{grad}\boldsymbol{\beta}\right|^2$ may be seen as a *mixture or interaction free-energy*.

The only effect of $I_C(\boldsymbol{\beta})$ is to guarantee that the proportions β_1, β_2 and β_3 take admissible physical values, i.e., they satisfy constraints (10.42) and (10.43) (see also 10.46). The interaction free energy term $I_C(\boldsymbol{\beta})$ is equal to zero when the mixture is physically possible ($\boldsymbol{\beta} \in C$) and to $+\infty$ when the mixture is physically impossible ($\boldsymbol{\beta} \notin C$).

Let us note even if the free energy of the voids phase is 0, the voids phase has physical properties due to the interaction free energy term $(k/2)\,|\mathbf{grad}\boldsymbol{\beta}|^2$ which depends on the gradient of $\boldsymbol{\beta}$. It is known that this gradient is related to the interfaces properties: $\mathbf{grad}\beta_1$, $\mathbf{grad}\beta_2$ describes properties of the voids-martensites interfaces and $\mathbf{grad}\beta_3$ describes properties of the voids-austenite interface. In this setting, the voids have a role in the phase change and make it different from a phase change without voids. The model is simple and schematic but it may be upgraded by introducing sophisticated interaction free energy depending on $\boldsymbol{\beta}$ and on $\mathbf{grad}\boldsymbol{\beta}$.

For the sake of simplicity, we choose the volume free energies, [20, 28]

$$\Psi_1(E) = \frac{1}{2}\varepsilon(\mathbf{u}) : K : \varepsilon(\mathbf{u}) - \tau(T)1 : \varepsilon(\mathbf{u}) - CT\log T, \tag{10.47}$$

$$\Psi_2(E) = \frac{1}{2}\varepsilon(\mathbf{u}) : K : \varepsilon(\mathbf{u}) + \tau(T)\mathbf{1} : \varepsilon(\mathbf{u}) - CT\log T, \tag{10.48}$$

$$\Psi_3(E) = \frac{1}{2}\varepsilon(\mathbf{u}) : K : \varepsilon(\mathbf{u}) - \frac{l_a}{T_0}(T - T_0) - CT\log T, \tag{10.49}$$

where K is the volume elastic tensor and C the volume heat capacities of the phases and the quantity l_a is the latent heat martensite-austenite volume phase change at temperature T_0.

Concerning the stress $\tau(T)\mathbf{1}$, we assume the schematic simple expression

$$\tau(T) = (T - T_c)\overline{\tau},\ \textit{for}\ T \le T_c,\ \tau(T) = 0,\ \textit{for}\ T \ge T_c, \tag{10.50}$$

with $\overline{\tau} \le 0$ and assume the temperature T_c is greater than T_0. With those assumptions, it results

$$\Psi(E) = \frac{\beta_1 + \beta_2 + \beta_3}{2}\{\varepsilon(\mathbf{u}) : K : \varepsilon(\mathbf{u})\} \tag{10.51}$$

$$-(\beta_1 - \beta_2)\tau(T)\mathbf{I} : \varepsilon(\mathbf{u}) - \beta_3\frac{l_a}{T_0}(T - T_0) \tag{10.52}$$

$$-(\beta_1 + \beta_2 + \beta_3)CT\log T + \frac{k}{2}\,|\mathbf{grad}\boldsymbol{\beta}|^2 + I_C(\boldsymbol{\beta})\,. \tag{10.53}$$

Remark 10.4 Depending on the sign of $\mathbf{I} : \varepsilon(\mathbf{u}) = \operatorname{div}\mathbf{u}$, free energy Ψ is either a concave or a convex function of temperature T. As explain in [25], (see Remark 5.3 page 72), it is easy to overcome this difficulty to have in any case Ψ a concave function of T. Experiments show that rigidity matrix K depends on T. With this result, it is easy to have Ψ a concave function of T, as shown in [25]. In this chapter, we keep the schematic expression for Ψ and we note that we will assume the solid is not deformed when colliding, i.e., $\operatorname{div}\mathbf{u} = 0$. In this situation, the schematic free energy is a concave function of T.

10.6 The Pseudo-potential of Dissipation

From experiments, it is known that the behaviour of shape memory alloys depends on time, i.e., the behaviour is dissipative. We define a pseudo-potential of dissipation with

$$\Phi((\mathsf{D}(\frac{\mathbf{U}^+ + \mathbf{U}^-}{2}), [\beta_i], \mathbf{grad}\,[\beta_i], \mathbf{grad}\underline{T}, \underline{T})) \tag{10.54}$$

$$= k_v \left(D(\frac{\mathbf{U}^+ + \mathbf{U}^-}{2})\right)^2 + \frac{c}{2}([\beta_i])^2 + \frac{\upsilon}{2}(\mathbf{grad}\,[\beta_i])^2 + \frac{\lambda}{2\underline{T}}\left(\mathbf{grad}\underline{T}\right)^2 \tag{10.55}$$

$$+ I_0([\beta_1 + \beta_2 + \beta_3]), \tag{10.56}$$

where $\lambda \geq 0$ represents the thermal conductivity in collisions and $k_v > 0$, $c \geq 0$, $\upsilon \geq 0$ stand for collisions viscosities related to macroscopic and microscopic dissipative phenomena.

The pseudo-potential takes into account the mass balance relationship, I_0 is the indicator function of the origin of $\Re$.

10.7 The Constitutive Laws

They are given by relationships (10.28), (10.29) and (10.24)

$$\left(B_i^{fe}, \mathbf{H}_i^{fe}\right) \in \partial\Psi_{\beta,\mathbf{grad}\beta}(T^+, \beta_i^+, \mathbf{grad}\beta_i^+), \tag{10.57}$$

giving

$$\mathbf{B}^{fe} = \left| \begin{array}{l} \frac{1}{2}\varepsilon(\mathbf{u}) : K : \varepsilon(\mathbf{u}) - \tau(T^+)\mathbf{1} : \varepsilon(\mathbf{u}) - CT^+ \log T^+ \\ \frac{1}{2}\varepsilon(\mathbf{u}) : K : \varepsilon(\mathbf{u}) + \tau(T^+)\mathbf{1} : \varepsilon(\mathbf{u}) - CT^+ \log T^+ \\ \frac{1}{2}\varepsilon(\mathbf{u}) : K : \varepsilon(\mathbf{u}) - \frac{l_u}{T_0}(T^+ - T_0) - CT^+ \log T^+ \end{array} \right| + \mathbf{B}_{reac}^{fe}, \tag{10.58}$$

$$\mathbf{B}_{reac}^{fe} \in \partial I_C(\boldsymbol{\beta}^+), \tag{10.59}$$

$$\mathbf{H}_i^{fe} = k\mathbf{grad}\beta_i^+, \tag{10.60}$$

and by relationship (10.32)

$$\Sigma = k_v \mathsf{D}(\mathbf{U}^+ + \mathbf{U}^-), \tag{10.61}$$

$$B_i^p - B_i^{fe} = c\,[\beta_i] - P, \tag{10.62}$$

$$-P \in \partial I_0([\beta_1 + \beta_2 + \beta_3]), \tag{10.63}$$

$$\mathbf{H}_i^p - \mathbf{H}_i^{fe} = \upsilon\mathbf{grad}\,[\beta_i], \tag{10.64}$$

$$-2\mathbf{Q}_p = \frac{\lambda}{\underline{T}}\mathbf{grad}\underline{T}, \tag{10.65}$$

where P is the percussion reaction pressure due to the mass balance, and

$$e = (\beta_1 + \beta_2 + \beta_3)CT + l_a\beta_3 + \frac{1}{2}\varepsilon(\mathbf{u}) : K : \varepsilon(\mathbf{u}) + \frac{k}{2}\,|\mathbf{grad}\boldsymbol{\beta}|^2 \quad (10.66)$$

$$-(\beta_1 - \beta_2)(\tau(T) - T\partial\tau(T))\mathbf{I} : \varepsilon(\mathbf{u}). \quad (10.67)$$

The internal energy within the small perturbation assumption is

$$e = (\beta_1 + \beta_2 + \beta_3)CT + l_a\beta_3. \quad (10.68)$$

10.8 The Equations in a Collision

They result from the energy balance, the equations of motion and the constitutive laws.

10.8.1 The Energy Balance

We assume adiabatic evolution

$$T^+\mathcal{B}^+ + T^-\mathcal{B}^- = 0, \quad (10.69)$$

and have

$$[e] = \Sigma : \mathsf{D}(\frac{\mathbf{U}^+ + \mathbf{U}^-}{2}) + B_i^p\,[\beta_i] + \mathbf{H}_i^p \cdot \mathbf{grad}\,[\beta_i] \quad (10.70)$$

$$-\text{div}\,(T^+\mathbf{Q}_p^+ + T^-\mathbf{Q}_p^-) + T^+\mathcal{B}^+ + T^-\mathcal{B}^-. \quad (10.71)$$

$$\Delta(\mathbf{Q}_p) = 0, \quad (10.72)$$

$$\Delta(\mathcal{B}) + S = 0, \quad (10.73)$$

$$s^{fe} - \bar{s} = S. \quad (10.74)$$

It results

$$[e] + \text{div}\,(2\underline{T}\mathbf{Q}_p) = \Sigma : \mathsf{D}(\frac{\mathbf{U}^+ + \mathbf{U}^-}{2}) + B_i^p\,[\beta_i] + \mathbf{H}_i^p \cdot \mathbf{grad}\,[\beta_i]\,. \quad (10.75)$$

Note that the reactions, for instance $\mathbf{B}^{fe}_{reac}$, work, with work

$$\mathbf{B}^{fe}_{reac}[\boldsymbol{\beta}] \geq 0. \tag{10.76}$$

This a property of collisions already seen in the previous chapters, for instance in Chap. 2, Sects. 2.7.2.1 and 2.8.1.1: the reactions to perfect constraints work whereas they do not work in smooth evolutions.

10.8.2 The Equations of Motion

$$\rho[\mathbf{U}] = \text{div}\,\boldsymbol{\Sigma} + \mathbf{F}^p, \text{ in } \Omega, \tag{10.77}$$
$$-B^p_i + \text{div}\,\mathbf{H}^p_i + A^p_i = 0, \text{ in } \Omega, \tag{10.78}$$

and

$$\boldsymbol{\Sigma}\mathbf{N} = \mathbf{G}^p, \ \mathbf{H}^p_i \cdot \mathbf{N} = a^p_i, \text{ on } \partial\Omega. \tag{10.79}$$

10.8.3 The Mass Balance

As already said, we assume neither voids nor interpenetration in the evolution, and have

$$[\beta_1 + \beta_2 + \beta_3] = 0. \tag{10.80}$$

10.8.4 The Constitutive Laws

For the sake of simplicity, we assume the material is undeformed $\varepsilon(\mathbf{u}) = 0$ at collision time. Thus we have

$$\mathbf{B}^{fe} = \left| \begin{array}{c} -CT^+ \log T^+ \\ -CT^+ \log T^+ \\ -\frac{l_a}{T_0}(T^+ - T_0) - CT^+ \log T^+ \end{array} \right| + \mathbf{B}^{fe}_{reac}, \tag{10.81}$$

$$\mathbf{B}^{fe}_{reac} \in \partial I_C(\boldsymbol{\beta}^+), \tag{10.82}$$

$$\mathbf{H}^{fe}_i = k\mathbf{grad}\beta^+_i, \tag{10.83}$$

and by relationship (10.32)

$$\begin{aligned} \Sigma &= k_v \mathsf{D}(\mathbf{U}^+ + \mathbf{U}^-), \\ B_i^p - B_i^{fe} &= c\,[\beta_i] - P, \\ -P &\in \partial I_0([\beta_1 + \beta_2 + \beta_3]), \\ \mathbf{H}_i^p - \mathbf{H}_i^{fe} &= \upsilon \mathbf{grad}\,[\beta_i]\,, \\ -2\mathbf{Q}_p &= \frac{\lambda}{\underline{T}} \mathbf{grad} \underline{T}. \end{aligned} \tag{10.84}$$

There are 4 equations for the 4 unknowns $\mathbf{U}^+$, $\boldsymbol{\beta}^+$, P and T^+, the equations of motion for $\mathbf{U}^+$ and $\boldsymbol{\beta}^+$, the mass balance for the pressure P and the energy balance for the temperature T^+.

10.8.5 The Evolution Equations

We assume no external percussions $\mathbf{F}^p$ and A_i^p, a_i^p but there is an external surface percussion $\mathbf{G}^p$, for instance an hammer stroke on part Γ_1 of the boundary, the solid being fixed to a support on part Γ_0, with Γ_0, Γ_1 a partition of boundary $\delta\Omega$.

10.8.5.1 The Mechanical Equations

The equations for P, $\mathbf{U}^+$ and $\boldsymbol{\beta}^+$ are

$$-P \in \partial I_0([\beta_1 + \beta_2 + \beta_3]),$$

$$\rho \mathbf{U}^+ - k_v \Delta \mathbf{U}^+ = 0, \text{ in } \Omega, \tag{10.85}$$

$$\begin{aligned} c\,[\boldsymbol{\beta}] - \upsilon \Delta\,[\boldsymbol{\beta}] - k\Delta\boldsymbol{\beta}^+ + \mathbf{B}_{reac}^{fe} + \\ + \begin{vmatrix} -P - CT^+ \log T^+ \\ -P - CT^+ \log T^+ \\ -\frac{l_a}{T_0}(T^+ - T_0) - P - CT^+ \log T^+ \end{vmatrix} = 0, \text{ in } \Omega, \end{aligned} \tag{10.86}$$

$$\mathbf{B}_{reac}^{fe} \in \partial I_C(\boldsymbol{\beta}^+).$$

The boundary conditions are

$$\begin{aligned} \Sigma\mathbf{N} = \mathbf{G}^p,\ \mathbf{H}_i^p \cdot \mathbf{N} = 0, \text{ on } \Gamma_1, \\ \mathbf{U}^+ = \mathbf{U}^- = 0,\ \mathbf{H}_i^p \cdot \mathbf{N} = 0, \text{ on } \Gamma_0. \end{aligned} \tag{10.87}$$

where percussion $\mathbf{G}^p$ is the given hammer percussion on part Γ_1. The solid is fixed on an immobile support on part Γ_0. Quantities β^- and $\mathbf{U}^-$ before collision are known.

10.8.5.2 The Thermal Equation

The equation for T^+ is using the mass balance

$$(\beta_1^- + \beta_2^- + \beta_3^-)C\,[T] + l_a\,[\beta_3] + \frac{k}{2}\left[|\mathbf{grad}\boldsymbol{\beta}|^2\right] - \lambda\Delta\underline{T} =$$
$$= \Sigma : \mathsf{D}(\frac{\mathbf{U}^+ + \mathbf{U}^-}{2}) + B_i^p\,[\beta_i] + \mathbf{H}_i^p \cdot \mathbf{grad}\,[\beta_i]\,, \quad \text{in } \Omega, \tag{10.88}$$

with boundary condition

$$\frac{\partial \underline{T}}{\partial N} = 0, \tag{10.89}$$

assuming no external heat impulse on part Γ_1 of the boundary and $\underline{T}$ or T^+ is given on part Γ_0. Note that another boundary condition may be

$$\lambda\frac{\partial \underline{T}}{\partial N} + k(\underline{T} - T^{ext}) = 0,$$

assuming the surface heat impulse is proportional to the temperature difference with the exterior. Temperature T^- before collision is known.

Quantity

$$B_i^p\,[\beta_i] + \mathbf{H}_i^p \cdot \mathbf{grad}\,[\beta_i] - \frac{k}{2}\left[|\mathbf{grad}\boldsymbol{\beta}|^2\right] \geq 0, \tag{10.90}$$

is the dissipated work due to the microscopic motions producing the phase change. It is negligible compared to the dissipated work

$$\mathcal{T} = \Sigma : D(\frac{\mathbf{U}^+ + \mathbf{U}^-}{2}) = 2k_v\left(D(\frac{\mathbf{U}^+ + \mathbf{U}^-}{2})\right)^2, \tag{10.91}$$

due to the macroscopic motion. Thus the thermal equation becomes

$$(\beta_1^- + \beta_2^- + \beta_3^-)C\,[T] + l_a\,[\beta_3] - \lambda\Delta\underline{T} =$$
$$= \Sigma : D(\frac{\mathbf{U}^+ + \mathbf{U}^-}{2}) = 2k_v\left(D(\frac{\mathbf{U}^+ + \mathbf{U}^-}{2})\right)^2 = \mathcal{T}, \text{ in } \Omega, \tag{10.92}$$

10.9 Mathematics

It is possible to prove that the set of partial differential equations when neglecting the dissipative work due to phase changes, has solutions in a convenient variational framework, [30]. This results insures the coherency of the theory and of its numerical approximations by classical numerical methods. Before the presentation of numerical results, let us investigate the mechanical properties with closed form solutions.

10.10 Closed Form Examples

We assume the macroscopic velocity after collision is known. Thus we know the dissipated work

$$\mathcal{T} = \Sigma : \mathsf{D}(\frac{\mathbf{U}^+ + \mathbf{U}^-}{2}) = 2k_v \left(\mathsf{D}(\frac{\mathbf{U}^+ + \mathbf{U}^-}{2})\right)^2, \tag{10.93}$$

neglecting the dissipated work due to phase changes.

The last assumption is that the volume fractions and temperatures are homogeneous, i.e., their values do not depends on space variable x. The equations become non linear algebraic equations

$$c\,[\boldsymbol{\beta}] + \partial I_C(\boldsymbol{\beta}^+) + \begin{vmatrix} -P - CT^+ \log T^+ \\ -P - CT^+ \log T^+ \\ -\frac{l_a}{T_0}(T^+ - T_0) - P - CT^+ \log T^+ \end{vmatrix} = 0, \tag{10.94}$$

$$(\beta_1^- + \beta_2^- + \beta_3^-)C\,[T] + l_a\,[\beta_3] = \mathcal{T}, \tag{10.95}$$

$$[\beta_1 + \beta_2 + \beta_3] = 0. \tag{10.96}$$

We may prove that system (10.96) has one and only one solution depending on the quantities before collision.

10.10.1 Example 1. The Non Dissipative Case, $c = 0$

We let

$$-P - CT^+ \log T^+ = -\hat{P}.$$

The equations become

$$\partial I_C(\boldsymbol{\beta}^+) = \begin{vmatrix} \hat{P} \\ \hat{P} \\ \frac{l_a}{T_0}(T^+ - T_0) + \hat{P} \end{vmatrix} = 0, \tag{10.97}$$

$$(\beta_1^- + \beta_2^- + \beta_3^-)C\,[T] + l_a\,[\beta_3] = \mathcal{T}, \tag{10.98}$$

$$[\beta_1 + \beta_2 + \beta_3] = 0. \tag{10.99}$$

The solution depends on the intensity of the hammer stroke which is quantified by the dissipated work $\mathcal{T}$.

10.10.1.1 Temperature T^- is Low and Hammer Stroke is Weak

We choose

$$\beta_1^- = \beta_2^- = \frac{1}{2},\ \beta_3^- = 0, \qquad T^- < T_0, \tag{10.100}$$

which is an equilibrium state at low temperature.

Due to the hammer stroke, temperature increases and

$$T^+ = \frac{\mathcal{T}}{C} + T^- > T^-, \tag{10.101}$$

$$\beta_1^+ = \beta_2^+ = \frac{1}{2},\ \beta_3^+ = 0, \tag{10.102}$$

is the solution as long as $T^+ \leq T_0$, i.e.,

$$T^+ = \frac{\mathcal{T}}{C} + T^- \leq T_0, \tag{10.103}$$

or

$$\mathcal{T} \leq C\left(T_0 - T^-\right). \tag{10.104}$$

There is no phase change. There is only an increase of temperature due to the dissipative character of collisions.

10.10.1.2 Temperature T^- is Low and Hammer Stroke is Medium

With the same state before collision, we have

$$T^+ = T_0, \tag{10.105}$$

$$\beta_3^+ = \frac{\mathcal{T} - C\left(T_0 - T^-\right)}{l_a},$$

$$\beta_1^+ + \beta_2^+ + \beta_3^+ = 1,\ \beta_1^+ = \beta_2^+.$$

It is the solution as long as

$$0 \leq \beta_3^+ = \frac{\mathcal{T} - C\left(T_0 - T^-\right)}{l_a} \leq 1,$$

or

$$C\left(T_0 - T^-\right) \leq \mathcal{T} \leq C\left(T_0 - T^-\right) + l_a.$$

There is a phase change; Austenite appears but some martensites remain. The temperature increases up to the martensite-austenite phase change temperature T_0.

10.10.1.3 Temperature T^- is Low and Hammer Stroke is Large

With the same state before collision, we have

$$\begin{aligned} T^+ &= \frac{\mathcal{T}-l_a}{C} + T^- \geq T_0, \\ \beta_1^+ &= \beta_2^+ = 0,\ \beta_3^+ = 1, \end{aligned}$$

is solution for

$$\mathcal{T} \geq C\left(T_0 - T^-\right) + l_a. \tag{10.106}$$

There is a complete phase change. No martensite remains and temperature is larger than the austenite-martensite phase change temperature. Note that to have a mixture of the three phases, the temperature has to be the phase change temperature T_0.

10.10.1.4 Temperature T^- is Large

We choose initial state

$$\begin{aligned} \beta_1^- = \beta_2^- = 0,\ \beta_3^- = 1, \\ T^- > T_0, \end{aligned} \tag{10.107}$$

which is an equilibrium state at large temperature. Temperature increases and

$$\begin{aligned} T^+ &= \frac{\mathcal{T}}{C} + T^- > T^-, \\ \beta_1^+ &= \beta_2^+ = 0,\ \beta_3^+ = 1. \end{aligned} \tag{10.108}$$

There is no phase change because austenite is already present at large temperature. The effect of the collision is only to increase the temperature.

10.10.1.5 Comments

The effect of the hammer stroke is to increase the temperature and in some cases, to have phase change. If martensites are present they are transformed into austenite if the stroke is large enough, i.e., if the dissipated work is large enough. The evolution which follows begins at large temperature with non null velocity $\mathbf{U}^+$. In case the solid

is in contact with cold air, cooling occurs and there is dissipation consuming kinetic energy and avoiding too large deformations of the solid. This property could be used in engineering. A collision produces phase change in a solid and its deformation. When cooling the solid recovers progressively its initial shape and its alloy initial composition. The dissipated work has been given to the exterior of the solid by the cooling process. The collision does not result in a permanent deformation. See the numerical examples in Sect. 10.11.

10.10.2 Example 2. The Non Dissipative Case $c = 0$ and Voids

We assume there are voids before collision and for the sake of simplicity, the temperature before collision is the martensite-austenite phase change temperature, T_0. We choose initial state

$$\beta_1^- = \beta_2^- = \frac{1}{4},\ \beta_3^- = 0, \qquad T^- = T_0, \tag{10.109}$$

which is an equilibrium state when there are voids.

10.10.2.1 Weak Hammer Stoke

The solution is

$$\beta_1^- = \beta_2^- = \frac{1}{4} - \frac{\beta_3^+}{2},\ \beta_3^+ = \frac{\mathcal{T}}{l_a}, \qquad T^+ = T_0, \tag{10.110}$$

for

$$\frac{1}{4} - \frac{\beta_3^+}{2} \geq 0,$$

or

$$\mathcal{T} \leq \frac{l_a}{2}.$$

An amount of martensites is transformed into austenite. The temperature does not change. It remains equal to the phase change temperature.

10.10.2.2 Large Hammer Stoke

The solution is

$$\beta_1^+ = \beta_2^+ = 0,\ \beta_3^+ = \frac{1}{2}, \qquad (10.111)$$
$$T^+ = T_0 + \frac{1}{C}(\mathcal{T} - \frac{l_a}{2}),$$

for

$$\mathcal{T} \geq \frac{l_a}{2}.$$

The whole martensites are transformed into austenite and the temperature increases.

10.10.2.3 Comments

Once again, the effect is to transform the martensites into austenite and to increase the temperature when the stroke is large.

With the mass balance we have chosen, the voids volume fraction remains constant. As said in Remark 10.1, it is possible to have a more sophisticated mass balance equation allowing evolution of the voids volume fraction.

10.10.3 Example 3. The Dissipative Case, $c > 0$

We investigate the situation where a mixture of the three phases can coexist after the collision

$$0 < \beta_i^+ < 1.$$

The equations are

$$c\,[\boldsymbol{\beta}] + \partial I_C(\boldsymbol{\beta}^+) + \begin{vmatrix} -P - CT^+ \log T^+ \\ -P - CT^+ \log T^+ \\ -\frac{l_a}{T_0}(T^+ - T_0) - P - CT^+ \log T^+ \end{vmatrix} = 0, \qquad (10.112)$$
$$(\beta_1^- + \beta_2^- + \beta_3^-)C\,[T] + l_a\,[\beta_3] = \mathcal{T},$$
$$[\beta_1 + \beta_2 + \beta_3] = 0,$$

with

$$\partial I_C(\boldsymbol{\beta}^+) = \begin{bmatrix} D \\ D \\ D \end{bmatrix} \text{ with } D \in \Re.$$

We choose initial state

$$\beta_1^- = \beta_2^- = \frac{1}{2},\ \beta_3^- = 0.$$

We get from the first equation

$$\beta_1^+ = \beta_2^+,\ c(\beta_3^+ - (\beta_1^+ - \frac{1}{2})) = \frac{l_a}{T_0}(T^+ - T_0).$$

With the last equation, we have

$$c(\beta_3^+ - (\frac{1}{2} - \frac{\beta_3^+}{2}) + \frac{1}{2}) = \frac{l_a}{T_0}(T^+ - T_0).$$

It results

$$\beta_3^+ = \frac{2l_a}{3cT_0}(T^+ - T_0).$$

Note that we retrieve that if there is not dissipation, the temperature has to be equal to the phase change temperature. From the second equation, we get

$$C(T^+ - T^-) + \frac{2l_a^2}{3cT_0}(T^+ - T_0) = \mathcal{T},$$

giving

$$(C + \frac{2l_a^2}{3cT_0})T^+ = \mathcal{T} + CT^- + \frac{2l_a^2}{3c}.$$

Function $\mathcal{T} \to T^+$ is increasing. This is the solution as long as

$$0 \leq \beta_3^+ \leq 1,$$

or

$$0 \leq T^+ - T_0 \leq \frac{2l_a}{3cT_0}.$$

To satisfy these conditions, the dissipated work $\mathcal{T}$ has to verify

$$0 \leq \mathcal{T} + C(T^- - T_0) \leq \frac{3cCT_0 + 2l_a^2}{2l_a}.$$

In case there is dissipation, $c > 0$, the three phases may coexist at temperatures different from T_0 whereas the temperature has to be equal to T_0 in case there is not dissipation, $c = 0$. Of course, depending on the temperature before collision, the dissipated work $\mathcal{T}$ has to be not too small and not too large. The complete phase change occurs for a dissipated work large enough.

10.11 Numerical Examples

Numerical results obtained from the proposed predictive theory are here presented in order to prove its soundness in describing the phenomena occurring during a collision with a structure made of shape memory alloys (SMAs), as well as for better elucidating the physical meaning of model parameters.

The state after the collision is obtained by solving Eqs. (10.85), (10.86) and (10.92). It is worth pointing out that the post-collision velocity is obtained from Eq. (10.85) independently from the solutions of the phase-evolution, Eq. (10.86), and of the thermal problem, Eq. (10.92). On the contrary, the latter two equations are coupled and are solved through an iterative numerical scheme.

By introducing the orthonormal basis $(\mathbf{i}, \mathbf{j})$, we present numerical results for a 1D rod and a 2D solid which are made up of shape memory alloys and are submitted to external percussions, [38]. A finite-element discretization is employed with quadratic Lagrange basis functions and mesh element size (triangles in the 2D case) equal about to one cent of the structure maximum size. In agreement with the theoretical framework previously described, the collision is assumed to be adiabatic. Moreover, null non-mechanical phase-change sources are considered (that is, $A_i^p = a_i^p = 0$).

If not differently specified, model parameters are chosen referring to a Ni-Ti alloy: $\rho = 6500$ kg/m^3, $l_a = 80$ MJ/(m^3), $C = 5.4$ MJ/(m^3 K), $\lambda = 18$ Ws/(Km), [41]. As initial conditions (constant in the region occupied by the structure) before the collision (occurring at time $t = 0$), the structures in both examples are assumed to be at rest ($\mathbf{U}^- = \mathbf{0}$) and at uniform low temperature $T^- = 0.9T_o$, where $T_o = 332.75$ K is the transformation temperature from martensite to austenite. Accordingly, the alloy is assumed to be made up of an uniform mixture of the two martensites $\beta_1^- = \beta_2^- = 0.5$ with null austenite volume fraction $\beta_3^- = 0$.

10.11.1 A Percussion Is Applied to a Rod: 1D Application

Consider a SMA rod modeled as a 1D domain of length $L_o = 10$ m along the $\mathbf{i}-$direction, parametrized in $x \in [0, L_o]$. The structure is fixed at $x = 0$ and the percussion stress $\mathbf{G}^p = -G^p\mathbf{i}$ with $G^p = 20$ MPa $\cdot$ s is applied at $x = L_o$. Figure 10.1 shows the post-collision velocity, temperature and phase composition fields obtained from the predictive theory: the percussion stress determines a post-collision velocity of the structure, namely a discontinuity of the velocity at collision time; the velocity discontinuity is associated with dissipative phenomena that determine the heating of the structure (through the term $\mathcal{T}$ in Eq. (10.92)) which is, in turn, coupled with the phase change from martensite to austenite.

Moreover, parametric analyses on the values of parameters governing the collision response (that is, k_v, c, and $\upsilon = k$) have been conducted in order to elucidate their physical meaning.

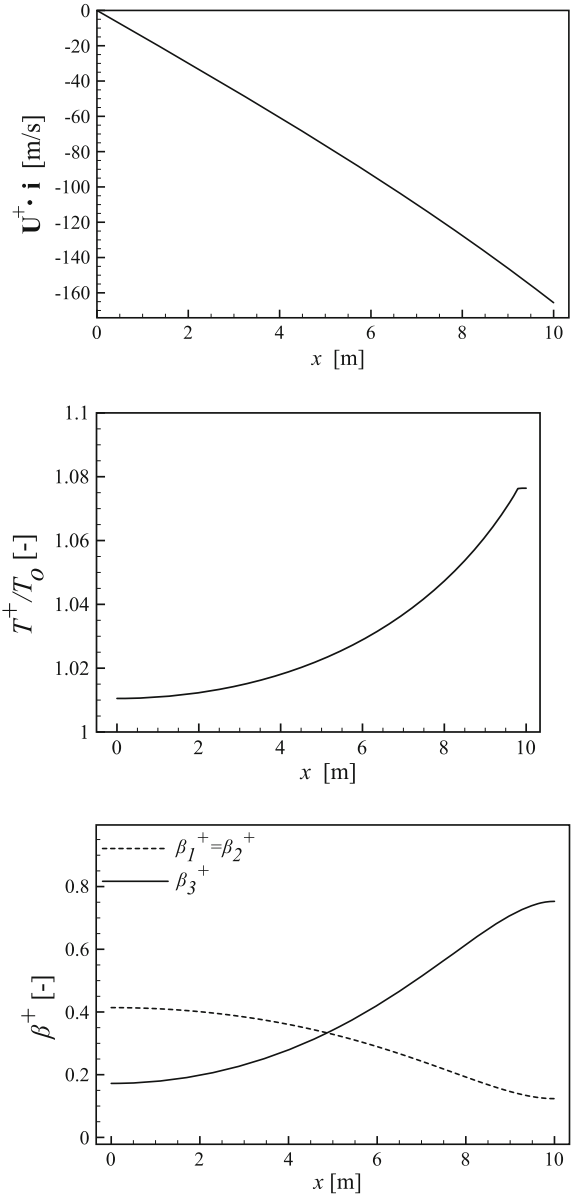

Fig. 10.1 A percussion is applied to a rod: post-collision velocity $\mathbf{U}^+ \cdot \mathbf{i}$, normalized temperature T^+/T_o and martensite/austenite volume fractions $\beta_1^+ = \beta_2^+$, β_3^+ (from *top* to *bottom*) versus x. Parameters: $k_v = 1$ MPa · s, $c = 0.05\, l_a$, $\upsilon = k = 5$ MPa

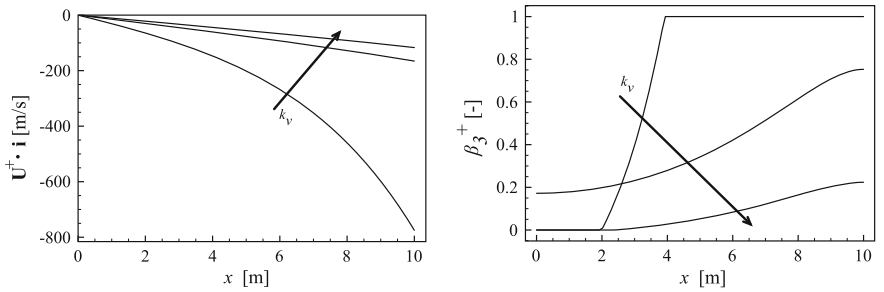

Fig. 10.2 A percussion is applied to a rod: sensitivity of collision model. Post-collision velocity $\mathbf{U}^+ \cdot \mathbf{i}$ (*left*) and austenite volume fraction β_3^+ (*right*) versus x for $k_v = 0.1$ MPa · s, $k_v = 1$ MPa · s and $k_v = 1.5$ MPa · s. Other parameters: $c = 0.05\, l_a$ and $\upsilon = k = 5$ MPa

Addressing the parameters involved in the mechanical problem, Fig. 10.2 highlights that parameter k_v is inversely proportional with the post-collision velocity. Analysing the after-collision phase composition, two opposite mechanisms occur on dissipation $\mathcal{T}$ when reducing k_v: in fact, the term $|\mathsf{D}((\mathbf{U}^+ + \mathbf{U}^-)/2)|$ increases but k_v decreases. As a result of these opposite mechanisms, phase change is highly non-uniform with austenitic phase close to the percussion.

In order to show the sensitivity of the model to phase transformation viscosity c, the spatial gradients of phase volume fractions and temperature are assumed to vanish (that is, $k,\ \upsilon,\ \lambda \to +\infty$) reducing the 1D model to a 0D one. Results are shown in Fig. 10.3 in terms of post-collision temperature and phases volume fraction as a function of dissipated work $\mathcal{T}$. It clearly appears that the model predicts no phase change when $\mathcal{T}$ is such that $T^+ \leq T_o$, while austenite appears when $T^+ > T_o$. The value of $\mathcal{T}$ corresponding to a complete phase transformation (that is, $\beta_3^+ = 1$) is directly proportional to viscosity c. Furthermore, it clearly arises that, when a partial phase change (that is, $0 < \beta_3^+ < 1$) is addressed, the post-collision temperature is constant and equal to $T^+ \approx T_o$ for small values of c.

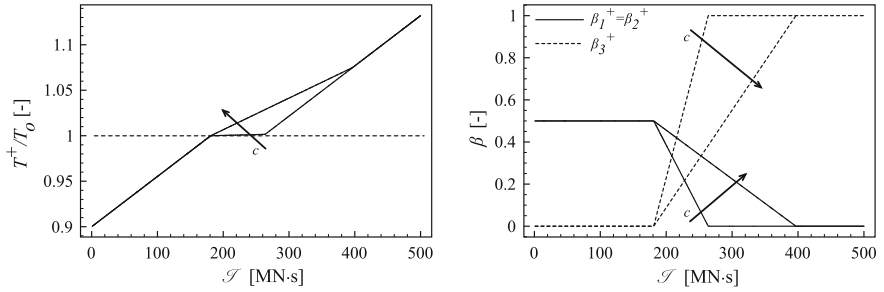

Fig. 10.3 A percussion is applied to a rod: sensitivity of collision model. Post-collision normalized temperature T^+/T_o (*left*) and martensite/austenite volume fractions $\beta_1^+ = \beta_2^+$, β_3^+ (*right*) versus dissipated work $\mathcal{T}$ for $c = 10^{-3} l_a$ and $c = 5 \cdot 10^{-2} l_a$. Results are obtained in the 0D case (that is, $k,\ \upsilon,\ \lambda \to +\infty$)

10.11.2 A Surface Percussion Is Applied to a Solid: 2D Application

Application to a 2D square solid structure ($L_o = 1$ m wide) is addressed in Fig. 10.4. The percussion stress is applied on the central portion ($L_o/3$ wide) of the top boundary and it is inclined with respect to the boundary normal ($\|\mathbf{G}^p\| = 20$ GPa $\cdot$ s and $\alpha = 60°$) as in figure.

The post-collision temperature T^+, the velocity field $\mathbf{U}^+$ and phase composition β_1^+, β_2^+, and β_3^+ are shown confirming the soundness of the proposed approach: the percussion stress induces a significant discontinuity in the velocity field, the temperature increases where the dissipative phenomena are more relevant and austenite appears where the dissipation is more important. The graphs shown in the figure highlight that the model allows to compute the non-uniform post-collision fields in the domain. Interestingly, temperature increases in the collision region but also near the fixed boundary where the gradient of the post-collision velocity field assumes relevant values and where a percussion reaction originates. Phase transformation clearly follows the same behavior.

10.11.3 Evolution Following the Collision: Configuration and Alloy Composition Depending on Time

In order to highlight the peculiarities of shape memory alloys, as well as possible engineering applications, the evolution after the collision (starting from the post-collision state previously computed) is also obtained and shown.

The post-collision temperature T^+, the velocity field $\mathbf{U}^+$ and phase composition β_1^+, β_2^+, and β_3^+, computed by means of the proposed predictive theory, are the initial conditions for the smooth problem describing the post-collision evolution of the structure. Reference is made to both the 1D and 2D applications previously addressed. By assuming no voids and a Young's modulus equal to 47 GPa (equal for martensite and austenitic phase), the SMA constitutive model presented in [25, 29], and enriched in [38–40], is employed. The model accounts for the typical shape-memory (i.e., thermal induced transformations) and pseudoelastic (i.e., stress-induced transformations) effects of such materials. The evolution problem is numerically solved by means of an incremental algorithm based on an explicit Euler time discretization (namely, an updated-Lagrangian formulation). Analogously to the collision problem, a finite-element discretization with quadratic Lagrange basis functions is employed with mesh element size about one cent of the structure maximum size. Convective heat transfer is prescribed on the boundary with convection coefficient equal to 100 W/(m^{2}K).

Addressing the 1D application in Sect. 10.11.1, the displacement of rod's end at $x = L_o$ is plotted in Fig. 10.5 and compared with the one obtained when a linearly-elastic material is addressed. Despite of a slightly larger maximum displacement

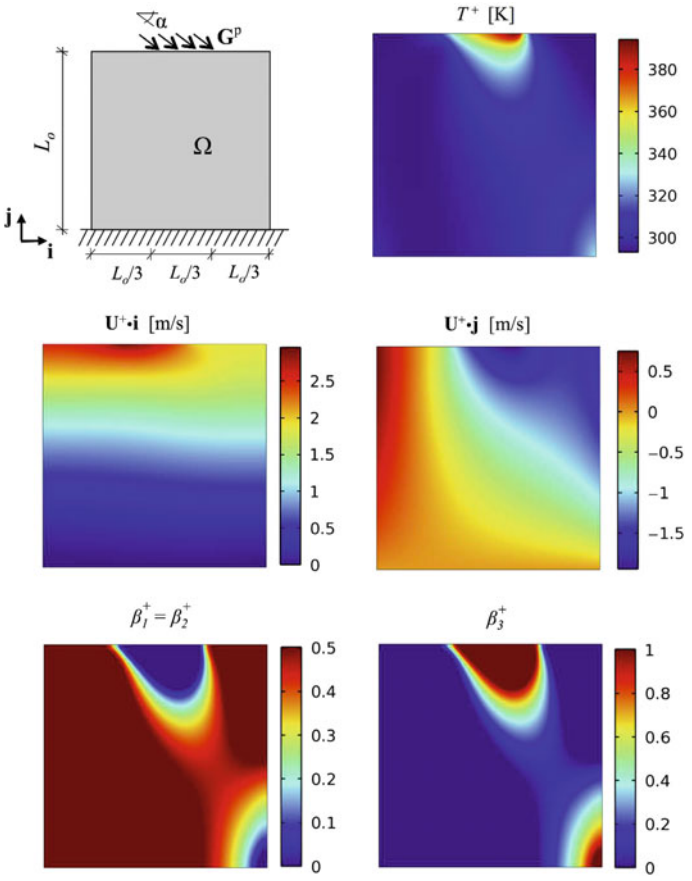

Fig. 10.4 A percussion is applied to a 2D solid: post-collision velocity $\mathbf{U}^+$, temperature T^+, and martensites/austenite volume fractions β_1^+, β_2^+, and β_3^+. Parameters: $k_v = 1$ MPa · s, $c = 5 \cdot 10^{-2} l_a$, and $k = \upsilon = 0.5$ MPa

due to the pseudoelastic behavior of the alloy, a significant damping effect appears. The post-collision velocity induces in fact a significant deformation of the rod in its post-collision evolution. The occurrence of the dissipation mechanisms related to stress-induced phase change induces the damping of the displacement which is not present in the linearly elastic case. This outcome is in quantitative agreement with results obtained in [16]. These considerations are indeed confirmed in Fig. 10.5 where the evolution of the average values of β_1, β_2 and β_3 in the rod are also shown. In fact, a discontinuity of alloy composition occurs at collision time ($\beta_1^- = \beta_2^- = 0.5$, and $\beta_3^- = 0$), and then the austenite progressively transforms into the martensites due to stress-induced transformations.

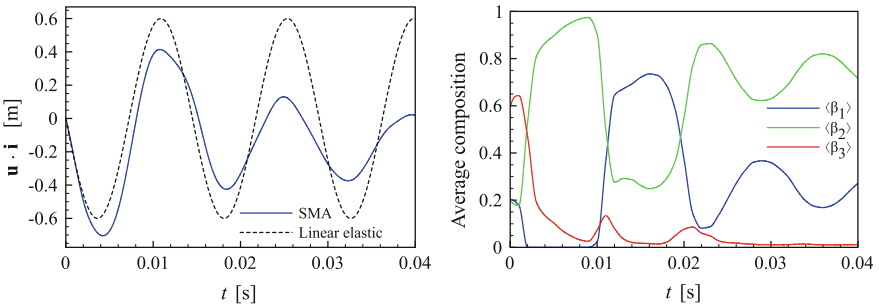

Fig. 10.5 A percussion is applied to a rod: post-collision smooth evolution. Displacement $\mathbf{u}\cdot\mathbf{i}$ of the right end $x = L_o$ (*left*) and average martensites/austenite volume fractions $\langle\beta_1^+\rangle$, $\langle\beta_2^+\rangle$, $\langle\beta_3^+\rangle$ with $\langle\beta_i\rangle = (\int_0^{L_o}\beta_i dx)/L_o$ (*right*) versus time t. Parameters: $k_v = 0.8$ MPa · s, $c = 0.05\,l_a$, $\upsilon = k = 5$ MPa, $G^p = 20$ MPa · s

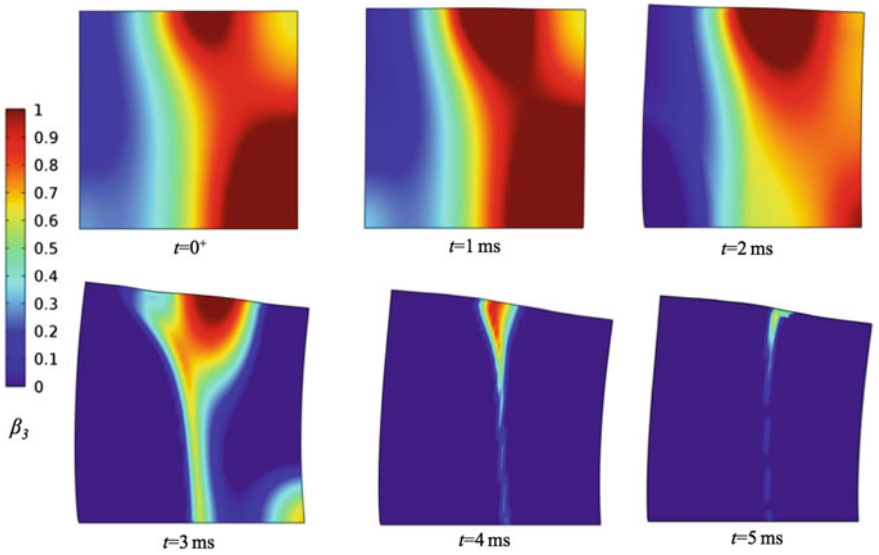

Fig. 10.6 A percussion is applied to a 2D solid: post-collision smooth evolution. Austenite volume fraction β_3 in the domain versus time t. Parameters: $k_v = 1$ MPa · s, $c = 5\cdot 10^{-2} l_a$, and $k = \upsilon = 0.5$ MPa, $\|\mathbf{G}^p\| = 35$ MPa · s, $\alpha = 60°$

Similar outcomes are obtained when the 2D case is addressed (see Fig. 10.6). The application is identical to the one described in Sect. 10.11.2 with an higher percussion stress (namely, $\|\mathbf{G}^p\| = 35$ MPa · s instead of $\|\mathbf{G}^p\| = 20$ MPa · s). Accordingly, the post-collision austenite volume fraction (at $t = 0^+$) is higher than the one previously obtained. Figure 10.6 highlights that collision-induced and stress-induced transformation mechanisms strongly couple and, therefore, affect the mechanical response of the overall structure. The solid globally rotates and the austenite progressively

disappears (namely, its volume fraction goes back to its null initial value) due to stress-induced phase change. Accordingly, the martensites appear, associated with material pseudoelastic response.

10.12 Experimental Results and Other Modeling Approaches

There are few experimental results on the collision of structures made up of shape memory alloys [48, 52]. Predictive theories for their analyses are developed introducing a finite time duration of the collision, leading to numerical challenges associated with fast transient analyses [13, 16]. These challenges are here overcome thanks to the assumption that the collision is instantaneous. In agreement with the proposed theory, experiments and other modeling approaches show that collisions produce an increase of the austenite phase, together with an increase of temperature.

References

1. Achenbach, M.: A model for an alloy with shape memory. Int. J. Plast. **5**, 371–395 (1989)
2. Auricchio, F., Petrini, L.: A three-dimensional model describing stress-temperature induced solid phase transformations. Part I: solution algorithm and boundary value problems. Int. J. Num. Methods Eng. **61**, 807–836 (2004)
3. Auricchio, F., Petrini, L.: A three-dimensional model describing stress-temperature induced solid phase transformations. Part II: thermomechanical coupling and hybrid composite applications. Int. J. Num. Methods Eng. **61**, 716–737 (2004)
4. Balandraud, X., Ernst, E., Soós, E.: Phénomènes rhéologiques dans les alliages à mémoire de forme, C. R. Acad. Sci, Paris, II, **327**(1), 33–39 1999
5. Ball, J.M., James, R.D.: Theory for the microstructure of martensite and applications. In: Wayman, C.M., Perkings, J. (eds.) Proceedings of the International Conference on Martensitic Transformations. Monterey (1992)
6. Berriet, C., Lexcellent, C., Raniecki, B., Chrysochoos, A.: Pseudoelastic behaviour analysis by infrared thermography and resistivity measurements of polycristalline shape memory alloys, ICOMAT 92, Monterey (1992)
7. Berveiller, M., Patoor, E. (eds.): Technologie des alliages à mémoire de forme. Hermès, Paris (1994)
8. Berveiller, M., Patoor, E.: Micromechanical modelling of the thermomechanical behaviour of shape memory alloys. In: Berveiller, M., Fischer, F. (eds.) Mechanics of Solids with Phase Change. Springer, Vienna (1997)
9. Bonetti, E.: Global solvability of a dissipative Frémond model for shape memory alloys. Part I: mathematical formulation and uniqueness. Q. Appl. Math. **61**, 759–781 (2003)
10. Bonetti, E.: Global solvability of a dissipative Frémond model for shape memory alloys. Part II: existence. Q. Appl. Math. **62**, 53–76 (2004)
11. Bonetti, E., Frémond, M.: A phase transition model with the entropy balance. Math. Methods Appl. Sci. **26**, 539–556 (2003)
12. Bonetti, E., Frémond, M., Lexcellent, C.: Modelling shape memory alloys. J. de Phys. IV Fr. **115**, 383–390 (2004)

13. Chen, Y.C., Lagoudas, D.: Impact induced transformation in shape memory alloys. J. Mech. Phys. Solids **48**, 275–300 (2000)
14. Chrysochoos, A., Pham, H., Maisonneuve, O.: Une analyse expérimentale du comportement d'un alliage à mémoire de forme de type Cu-Zn-Al, C. R. Acad. Sci., Paris **316**(II) 1031–1036 (1993)
15. Chrysochoos, A., Löbel, M., Maisonneuve, O.: Couplages thermomécaniques du comportement pseudoélastique d'alliages Cu-Zn-Al et Ni-Ti, C. R. Acad. Sci., Paris, **320**(IIb), 217–223 (1994)
16. Collet, M., Ouisse, M., Foltete, E., Lexcellent, C.: Isothermal and anisothermal implementations of 2D shape memory alloy modeling for transient impact response calculation. Smart Mater. Struc. **18**(12), 125019 (2009). doi:10.1088/0964-1726/18/12/125019
17. Colli, P., Sprekels, J.: Global solution to the full one-dimensional Frémond model for shape memory alloys. Math. Methods. Appl. Sci. **18**, 371–385 (1995)
18. Colli, P., Frémond, M., Visintin, A.: Thermomechanical evolution of shape memory alloys. Q. Appli. Math. XLVIII **1**, 31–47 (1990)
19. Falk, F.: Landau theory and martensitic phase transition, J. de Phys.; Colloque C4, Supplément au no 12, 43 (1982)
20. Frémond, M.: Matériaux à mémoire de forme, C. R. Acad. Sci., Paris, 304. II **7**, 239–244 (1987)
21. Frémond, M.: L'éducation des matériaux à mémoire de forme. Rev. Eur. des éléments finis **7**(8), 35–46 (1998)
22. Frémond, M.: Phase change with temperature discontinuities. Gakuto Int. Ser. Math. Sci. Appl. **14**, 125–134 (2000)
23. Frémond, M.: Non-smooth Thermomechanics. Springer, Berlin (2002)
24. Frémond, M.: Collisions, Edizioni del Dipartimento di Ingegneria Civile, Università di Roma "Tor Vergata" (2007). ISBN 978-88-6296-000-7
25. Frémond, M.: Phase Change in Mechanics. UMI-Springer Lecture Notes Series, vol. 13 (2011). doi:10.1007/978-3-642-24609-8. http://www.springer.com/mathematics/book/978-3-642-24608-1, ISBN 978-3-642-24608-1
26. Frémond, M., Maceri, F. (eds.): Novel Approaches in Civil Engineering. Springer, Berlin (2003)
27. Frémond, M., Marino, M.: Shape memory alloys and collisions. In: International Congress of Theoretical and Applied Mechanics, Session SM09 Mechanics of phase transformations, Beijing (2012)
28. Frémond, M., Myasaki, S.: Shape Memory Alloys. CISM, Courses and Lectures Notes, vol. 351. Springer, Vienna (1996)
29. Frémond, M., Rocca, E.: A model for shape memory alloys with the possibility of voids. Discret. Contin. Dyn. Syst., Ser. A, **27** 4, (2009). http://aimsciences.org/journals/displayPapers1.jsp?pubID=357
30. Frémond, M., Marino, M., Rocca, E.: Collisions of solids made of shape memory alloys (2015, to appear)
31. Guénin, G.: Alliages à mémoire de forme, Techniques de l'Ingénieur, M 530, Paris (1986)
32. Lebon coordonnateur, F.: Modélisation des alliages à mémoire de forme, Rev. Eur. des éléments finis **7**, 8 (1998)
33. Leclercq, S.: De la modélisation thermomécanique et de l'utilisation des alliages à mémoire de forme. Thèse de l'Université de Franche-Comté, Besançon (1995)
34. Leclercq, S., Lexcellent, C.: General macroscopic description of the thermomechanical behaviour of shape memory alloys. J. Mech. Phys. Solids. **44**, 953–981 (1996)
35. Lexcellent, C., Licht, C.: Some remarks on the modelling of the thermomechanical behaviour of shape memory alloys. J. de Phys., Colloque C4, 1, 35–39 (1991)
36. Löbel, M.: Caractérisation thermomécanique d'alliages à mémoire de forme de type NiTi et CuZnAl. Domaine de transition et cinétique de changement de phase, Thèse de l'Université des Sciences et des Techniques du Languedoc, Montpellier (1994)
37. Marfia, S., Sacco, E., Reddy, J.N.: Superelastic and shape memory effects in laminated shape-memory-alloy beams. Am. Inst. Aeronaut. Astronaut. **41**(1), 100–109 (2003)

38. Marino, M.: Pseudopotentials and thermomechanical response of materials and structures: a convex analysis approach. Ph.D. Thesis. Department of Civil Engineering and Computer Science, University of Rome "Tor Vergata" (2013)
39. Marino, M.: Shape memory alloys at high temperature: an ideal model for their pseudo-plastic response. In: Bruno, D., Olivito, R.S. (eds.) Problemi Attuali e Prospettive nell'Ingegneria delle Structture, pp. 181–192. Luigi Pellegrini Editore, Cosenza, Italy (2014)
40. Marino, M.: An ideal model for stress-induced martensitic transformations in shape-memory alloys. Fract. Struct. Integr. **29**, 96–110 (2014). doi: 10.3221/IGF-ESIS.29.10
41. Messner, C., Werner, E.A.: Temperature distribution due to localised martensitic transformation in SMA tensile test specimens. Comput. Mater. Sci. **26**, 95–101 (2003)
42. Mielke, A., Roubíček, T.: A rate-independent model for inelastic behavior of shape-memory alloys. Multiscale Model. Simul. **1**, 571–597 (2003)
43. Morin, C., Moumni, Z., Zaki, W.: Influence of heat transfer on the thermomechanical behavior of shape memory alloys. Int. Rev. Mech. Eng. **5**, 329–339 (2011)
44. Nguyen Quoc Son: On standard dissipative gradient models. Ann. Solid Struct. Mech. **1, 2**, 79–86 (2010). doi:10.1007/s12356-010-0006-0
45. Nguyen Quoc Son, Moumni, Z.: Sur une modélisation du changement de phases solides, C. R. Acad. Sci., Paris, II, 321, 3, 87–92 (1995)
46. Niezgodka, M., Sprekels, J.: Convergent numerical approximation of the thermomechanical phase transitions in shape memory alloys. Numer. Math. **58**, 759–778 (1991)
47. Pham, H.: Analyse thermomécanique d'un alliage à mémoire de forme de type Cu-Zn-Al. Thèse de l'Université des Sciences et des Techniques du Languedoc, Montpellier (1994)
48. Raghavan, J., Bartkiewicz, T., Boyko, S., Kupriyanov, M., Rajapakse, N., Yu, B.: Damping, tensile, and impact properties of superelastic shape memory alloy (SMA) fiber-reinforced polymer composites. Compos. Part B: Eng. **41**, 214–222 (2010)
49. Rajagopal, K.R., Roubíček, T.: On the effect of dissipation in shape-memory alloys. Nonlinear Anal.: Real World Appl. **4**, 581–597 (2003)
50. Raniecki, B., Lexcellent, C., Tanaka, K.: Thermodynamics models of pseudoelastic behaviour of shape memory alloys. Arch. Mech. **44**(3), 261–284 (1992)
51. Rodríguez, P.P., Ibarra, A., Iza-Mendia, A., Recarte, V., Pérez-Landazábal, J.I., San Juan, J., Nó, M.L.: Influence of thermomechanical processing on the microstructure of Cu-based shape memory alloys produced by powder metallurgy. Mater. Sci. Eng. A **378**, 263–268 (2004)
52. Tsoi, K.A., Stalmans, R., Schrooten, J., Wevers, M., Mai, Y.-W.: Impact damage behaviour of shape memory alloy composites. Mater. Sci. Eng.: A **342**, 207–215 (2003)
53. Wörsching, G.: Numerical simulation of the Frémond model for shape memory alloys. In: Kenmochi, N., Niesgodka, M., Strzelecki, P. (eds.) Gatuko Int. series: Math. Sci. and Appl. Non-linear analysis and Appl., vol. 7, pp. 425–433. Tokyo (1995)
54. Zhang, Y., Zhu, J., Moumni, Z., Van Herpen, A., Zhang, W.: Energy-based fatigue model for shape memory alloys including thermomechanical coupling. Smart Mater. Struct. **25** (2016). doi:10.1088/0964-1726/25/3/035042

Chapter 11
Conclusion

The theory for collisions we have built and illustrated has only one mandatory assumption: the duration of the collision is short compare to the whole duration of the motion. As shown by the examples, this subjective assumption is less restrictive than it may look at first glance.

Because the predictive theory is founded on the very basis of mechanics, it is reliable and flexible. The innovative concept is that a system made of two solids is deformable because their relative position changes. The definition of the velocities of deformation of the system introduced in the classical developments of mechanics:

- principle of the virtual work giving the equations of motion;
- constitutive laws derived with the laws of thermodynamics and observation;

allows a large range of applications.

The scope of the applications is even larger than it could be expected: social sciences and mechanics are united to predict the motion of crowds with application to transport management and evacuation of theaters management.

The classical problem which is to predict the motion of crowds of solids, i.e., the motion of granular materials, has been explored with the motion of three balls. The results show how sophisticated and versatile are the challenging results due to interactions at a distance.

This collision theory may also help to design protections of civil engineering structures collided by debris flows.

Thermal effects are inseparably linked to mechanical effects in collisions which are always dissipative. Experiments exhibiting temperature jumps up to 7 °C and the shape memory alloy example show how important this aspect of collisions can be.

Multiple openings may be foreseen for further applications in different domains, for instance in bio-mechanics.

M. Frémond, *Collisions Engineering: Theory and Applications*,
Springer Series in Solid and Structural Mechanics 6,
DOI 10.1007/978-3-662-52696-5_11

Appendix A
Some Elements of Convex Analysis

A.1 Convex Sets

Let C be a set of linear space V. This set is convex if

Definition A.1 $\forall x \in C, \forall y \in C,\ \forall \theta \in]0, 1[$, point $\theta x + (1-\theta)y \in C$.

Segment $[0, 1]$ of space $V = \mathbb{R}$ is convex. The interior of a circle is a convex set of $V = \mathbb{R}^2$. On the contrary the exterior of a circle is not convex.

Convex sets are useful in mechanics to describe numerous and various properties. For instance, the possible positions of a soccer ball above the football field is a convex set: it is

$$C = \{\mathbf{x} = (x_i),\ i = 1, 3\,|x_i \in \mathbb{R},\ x_3 \geq 0\}\,.$$

A.2 Convex Functions

Let $\overline{\mathbb{R}} = \mathbb{R} \cup \{+\infty\}$ where the regular addition is completed by the rules

$$\forall a \in \mathbb{R}\ ,\ a + (+\infty) = +\infty,$$
$$+\infty + (+\infty) = +\infty.$$

Multiplication by positive numbers is completed by

$$\forall a \in \mathbb{R}\ ,\ a > 0,\ a \times (+\infty) = +\infty.$$

In this context, it is forbidden to multiply either by 0 or by negative numbers.

Let f an application from linear space V into $\overline{\mathbb{R}}$. This function is convex if

M. Frémond, *Collisions Engineering: Theory and Applications*,
Springer Series in Solid and Structural Mechanics 6,
DOI 10.1007/978-3-662-52696-5

Definition A.2 $\forall x \in V, \forall y \in V, \ \forall \theta \in]0, 1[,$

$$f(\theta x + (1-\theta)y) \leq \theta f(x) + (1-\theta) f(y).$$

Remark A.1 Function f is actually multiplied by positive numbers because $\theta \in]0, 1[$.

A.2.1 Examples of Convex Functions

It is easy to prove that functions f_p where $V = \mathbb{R}$

$$x \in \mathbb{R} \rightarrow f_p(x) = \frac{1}{p} |x|^p \,, \quad with\, p \in \mathbb{R} \,,\ p \geq 1,$$

are convex.

Let function I from $V = \mathbb{R}$ into $\overline{\mathbb{R}}$ is defined by

$$I(x) = 0, \ if \ x \in [0, 1] \,,$$
$$I(x) = +\infty, \ if \ x \notin [0, 1] \,.$$

This function is convex. It is called the indicator function of segment [0, 1] (Fig. A.2). More generally, we denote indicator function of set $C \subset V$, function I_C defined by

$$I_C(x) = 0 \,, \ if \ x \in C,$$
$$I_C(x) = +\infty \,, \ if \ x \notin C.$$

It is easy to connect the convex function and convex set notions. It is shown that

Theorem A.1 *A convex $C \subset V$ is convex if and only if its indicator function I_C is convex.*

Indicator functions may seem a little bit strange. In the sequel it is to be seen in the examples that they are productive tools in mechanics for dealing with internal constraints relating mechanical quantities. Three other indicator functions are useful for $V = \mathbb{R}$. They are the indicator functions I_+, I_- and I_0 of the sets of the non negative and non positive numbers and of the origin:

$$I_+(x) = 0 \,, \ if \ x \geq 0,$$
$$I_+(x) = +\infty \,, \ if \ x < 0,$$

$$I_-(x) = 0 \,, \ if \ x \leq 0,$$
$$I_-(x) = +\infty \,, \ if \ x > 0,$$

and

$$I_0(0) = 0,$$
$$I_0(x) = +\infty, \quad if \;\; x \neq 0.$$

The positive part function, $\mathrm{pp}(x),\ x \in \mathbb{R}$, is defined by

$$\mathrm{pp}(x) = \sup\{x, 0\} = \begin{cases} x, \ \text{if } x \geq 0, \\ 0, \ \text{if } x \leq 0, \end{cases} \tag{A.1}$$

and the negative part function, $\mathrm{np}(x),\ x \in \mathbb{R}$,

$$\mathrm{np}(x) = \begin{cases} 0, \ \text{if } x \geq 0, \\ -x, \ \text{if } x \leq 0, \end{cases} \tag{A.2}$$

are convex functions as well as their difference the absolute value function, $abs(x) = |x|$,

$$|x| = abs(x) = pp(x) + np(x). \tag{A.3}$$

A.3 Linear Spaces in Duality

Definition A.3 Two linear spaces V and $V^*$are in duality if there exist a bilinear form $\langle \cdot, \cdot \rangle$ defined on $V \times V^*$ such that

for any $x \in V$, $x \neq 0$, *there exists* $y^* \in V^*$, *such that* $\langle x, y^* \rangle \neq 0$;
for any $y^* \in V^*$, $y^* \neq 0$, *there exists* $x \in V$, *such that* $\langle x, y^* \rangle \neq 0$.

A.3.1 Examples of Linear Spaces in Duality

Spaces
$V = \mathbb{R}$, $V^* = \mathbb{R}$ are in duality with the bilinear form which is the usual product

$$\langle x, y \rangle = x \cdot y; \tag{A.4}$$

$V = \mathbb{R}^n$, $V^* = \mathbb{R}^n$ are in duality with the bilinear form which is the usual scalar product

$$\langle x, y \rangle = \mathbf{x} \cdot \mathbf{y} = \sum_{i=1}^{i=n} x_i y_i, \tag{A.5}$$

where $\mathbf{x} = (x_i)$ and $\mathbf{y} = (y_i)$ are vectors of $\mathbb{R}^n$, the coordinates of which are x_i and y_i;

$V = S$, $V^* = S$ where S is the linear space of symmetric matrices 3×3, are in duality with the bilinear form

$$\mathsf{e} \in V,\ \mathsf{s} \in V^*,\ \langle \mathsf{e}, \mathsf{s} \rangle = \mathsf{e} : \mathsf{s} = \sum_{i,j=1}^{i,j=3} e_{i,j} s_{i,j}$$
$$= e_{i,j} s_{i,j} = e_{11}s_{11} + e_{22}s_{22} + e_{33}s_{33} + 2e_{12}s_{12} + 2e_{13}s_{13} + 2e_{23}s_{23}, \qquad \text{(A.6)}$$

where we use the Einstein summation rule. Be careful, linear spaces $V = S$ and $V^* = S$ are also in duality with the bilinear form

$$\langle\langle \mathsf{e}, \mathsf{s} \rangle\rangle = e_{11}s_{11} + e_{22}s_{22} + e_{33}s_{33} + e_{12}s_{12} + e_{13}s_{13} + e_{23}s_{23},$$

which is different from the preceding one. Let us give two more examples. Linear space of the velocities $\mathbf{U}$ in a domain Ω of $\mathbb{R}^3$

$$V = \left\{ \mathbf{U}(\mathbf{x}) \,\middle|\, \mathbf{U} \in L^2(\Omega) \right\},$$

is in duality with the linear space of the forces $\mathbf{f}$ applied to the points of the domain

$$V^* = \left\{ \mathbf{f}(\mathbf{x}) \,\middle|\, \mathbf{f} \in L^2(\Omega) \right\},$$

with bilinear form

$$\langle \mathbf{U}, \mathbf{f} \rangle = \int_\Omega \mathbf{U}(\mathbf{x}) \cdot \mathbf{f}(\mathbf{x}) d\Omega,$$

which is the power of the force applied to the domain. The linear space of the strain rates

$$V = \left\{ \mathsf{D} = \left(D_{ij}(\mathbf{x})\right) \,\middle|\, D_{ij} = D_{ji},\ D_{ij} \in L^2(\Omega) \right\},$$

is in duality with the stresses linear space

$$V^* = \left\{ \sigma = \left(\sigma_{ij}(\mathbf{x})\right) \,\middle|\, \sigma_{ij} = \sigma_{ji},\ \sigma_{ij} \in L^2(\Omega) \right\},$$

with bilinear form

$$\langle \mathsf{D}, \sigma \rangle = \int_\Omega \sigma(\mathbf{x}) : \mathsf{D}(\mathbf{x}) d\Omega = \int_\Omega \sigma_{ij}(\mathbf{x}) D_{ij}(\mathbf{x}) d\Omega,$$

which is the power of the stresses. This bilinear form is used in the definition of the work of the interior forces, see Chaps. 7 and 8.

A.4 Subgradients and Subdifferential Set of Convex Functions

Convex function f_p given above, is differentiable for $p > 1$ but it is not for $p = 1$ where it is equal to the absolute value function $x \to |x|$, which has no derivative at the origin. In the same way, indicator function I is not differentiable because its value is $+\infty$ at some points and it has no derivative at points $x = 0$ and $x = 1$. Let us recall that for smooth convex functions of one variable, the derivative is an increasing function and this property yields

$$\left(\frac{df}{dx}(y) - \frac{df}{dx}(z)\right)(y - z) \geq 0. \tag{A.7}$$

Thus it seems that we have to loose all the calculus properties related to derivatives. Fortunately, this is not the case. Indeed, it is possible to define generalized derivatives and keep a large amount of properties related to derivatives. Consider function f shown in Fig. A.1. It is convex but it is not differentiable because it has no derivative at point A. At a point where the function has a derivative, the curve is everywhere above the tangent. At point A, there exist several lines which have this properly.

The slopes of these lines are the subgradients which generalize the derivative:

Definition A.4 Let convex function f defined on V in duality with V^*. A subgradient of f at point $x \in V$ is an element $x^* \in V^*$ which satisfies

$$\forall z \in V \ , \ \langle z - x, x^* \rangle + f(x) \leq f(z). \tag{A.8}$$

The set of the x^* which satisfy (A.8) is the subdifferential set f at point x, denoted $\partial f(x)$.

Remark A.2 The subgradient depends on f but depends also on the bilinear form $\langle \cdot, \cdot \rangle$.

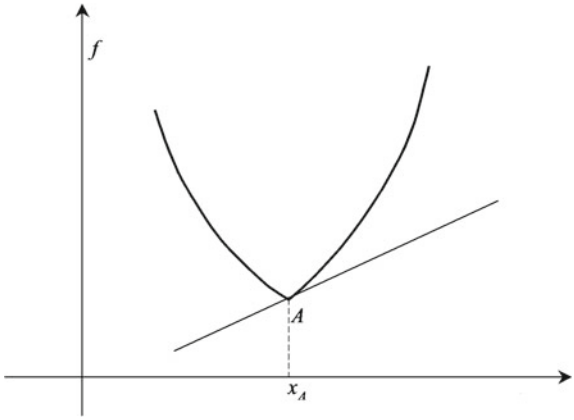

Fig. A.1 Convex function f has not a derivative at point A. It has generalized derivatives: the slopes of the lines which pass at point A and are under the curve representing function f. These slopes are the sub-gradients which constitute the subdifferential set

A.4.1 Two Properties of the Subdifferential Set

The subdifferential set keeps usual properties of the derivative: a function is not differentiable where its value is $+\infty$ and a differentiable convex function satisfies relationship (A.7). For a convex function first property becomes:

Theorem A.2 *Let convex function $f \neq +\infty$. If this function is subdifferentiable at point x, i.e., if $\partial f(x) \neq \emptyset$, then it is finite at that point: $f(x) < +\infty$.*

Proof Let us assume f is subdifferentiable at point x: let $y^* \in \partial f(x)$. Let us reason ab absurdo and assume that f is not finite at that point: $f(x) = +\infty$. Let us write relationship (A.8) at a point z where $f(z) < +\infty$. Such a point exists because $f \neq +\infty$. Then we have

$$+\infty = \langle z - x, y^* \rangle + f(x) \leq f(z).$$

We deduce that $+\infty = f(z)$. Which is contradictory with the assumption. Let us note that if the only point z where $f(z) < +\infty$ is x itself, then $f(x) < +\infty$ for f not to be identical to $+\infty$. □

This theorem applies in numerous constitutive laws where we have the relationship $B \in \partial I(\beta)$: because $\partial I(\beta)$ is not empty, we have $I(\beta) < +\infty$ which implies that $I(\beta) = 0$ and $0 \leq \beta \leq 1$, see Fig. A.2. Thus relationship $B \in \partial I(\beta)$ implies that quantity β which may be a phase volume fraction is actually in between 0 and 1.

Now let us prove that relationship (A.7) is satisfied in some sense by the subdifferential set :

Theorem A.3 *Let f a function convex. We have*

$$\forall y^* \in \partial f(y),\ \forall z^* \in \partial f(z),\ \langle y - z, y^* - z^* \rangle \geq 0.$$

Proof It is sufficient to write relationship (A.8) at points x and y. □

Remark A.3 It is said that the subdifferentiation operator is a monotone operator.

A.4.2 Examples of Subdifferential Sets

Let us begin by the subdifferential set of indicator function I of interval $[0, 1]$. It is easy to see that the subdifferential set is (Figs. A.2 and A.3)

$$\partial I(0) = \mathbb{R}^- \ ;\ \partial I(1) = \mathbb{R}^+ \ ;\ \text{if } x \in]0, 1[\ ,\ \partial I(x) = \{0\}\ ;$$
$$\text{if } x \notin [0, 1]\ ,\ \partial I(x) = \emptyset.$$

The subdifferential of indicator function I_+ is also easily computed. It is shown in Fig. A.3.

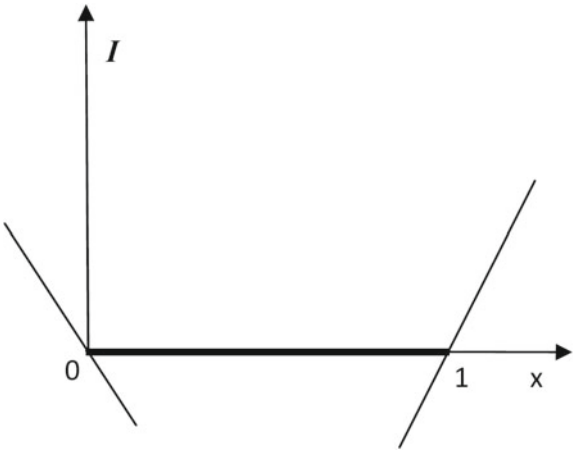

Fig. A.2 Indicator function of segment [0, 1]. Its value $I(x)$ is 0, if $0 \leq x \leq 1$, and $+\infty$, if either $x < 0$ or $x > 1$. The subgradients at points 0 and 1 are the slopes of the lines which are under the curve representing the function and in contact with the curve at points 0 or 1

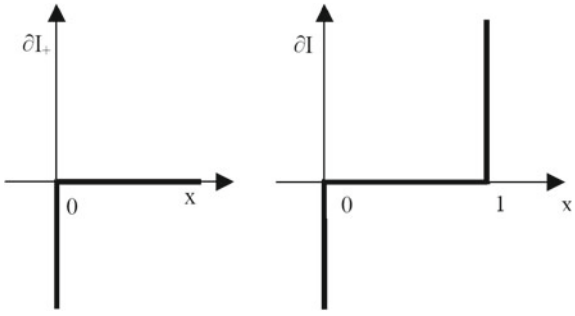

Fig. A.3 On the *left*, subdifferential set ∂I_+ of indicator function of the set of the positive numbers $\mathbb{R}^+$: $\partial I_+(0) = \mathbb{R}^-$, $\partial I_+(x) = \{0\}$ for $x > 0$ and $\partial I_+(x) = \emptyset$ for $x < 0$. On the *right*, subdifferential set ∂I of indicator function I of segment [0, 1]

The subdifferential set of the positive part function, $\text{pp}(x),\ x \in \mathbb{R}$ is

$$\partial \text{pp}(x) = H(x) = \begin{cases} \{0\} \text{ if } x < 0, \\ [0,1] \text{ if } x = 0, \\ \{1\},\ \text{if } x > 0. \end{cases} \tag{A.9}$$

It is the Heaviside graph.

The subdifferential set of the absolute value function is

$$\partial \text{abs}(x) = sgn(x) = \begin{cases} \{-1\} \text{ if } x < 0, \\ [-1,1] \text{ if } x = 0, \\ \{1\},\ \text{if } x > 0. \end{cases} \tag{A.10}$$

It is the sign graph. Let us consider triangle K with vertices O, A and B. It is a convex set of $\mathbb{R}^2$ (Fig. A.4). Let I_K be its indicator function. Let us compute its subdifferential set when the bilinear form is the usual scalar product (A.5) of $\mathbb{R}^2$. Then a subgradient

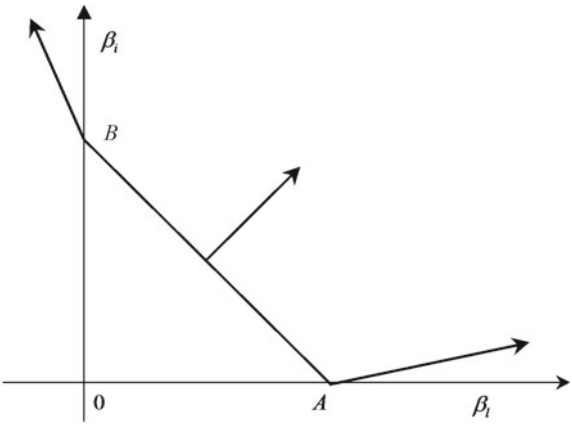

Fig. A.4 Vector $\mathbf{B} \in \partial I_C(\boldsymbol{\beta})$ is normal to triangle K. Vectors $\mathbf{B}$ at vertices A and B and on side AB of triangle K

of indicator function I_K at point $\mathbf{x}$ is a vector $\mathbf{B}$ which satisfies (A.8)

$$\forall \mathbf{y} \in \mathbb{R}^2 \ , \ I_K(\mathbf{y}) \geq I_K(\mathbf{x}) + (\mathbf{y} - \mathbf{x}) \cdot \mathbf{B}.$$

We deduce that

if $\mathbf{x} \notin K$, there exists no vector $\mathbf{B}$ which satisfies the previous relationship (apply Theorem A.2);

if $\mathbf{x} \in K$, the previous relationship gives,

$$\forall \mathbf{y} \in K \ , \ 0 \geq (\mathbf{y} - \mathbf{x}) \cdot \mathbf{B}.$$

This relationship proves that vector $\mathbf{B}$ is normal to convex set K (Fig. A.4).

A.5 Dual Functions

Let spaces V and V^* in duality with bilinear form $\langle ., . \rangle$. Let f a convex function of V into $\overline{\mathbb{R}} = \mathbb{R} \cup \{+\infty\}$, the dual function f^* of f is a function of V^* into $\overline{\mathbb{R}}$ defined by

$$f^*(y^*) = sup \left\{ \langle x, y^* \rangle - f(x) \, | x \in V \right\}.$$

It is possible to prove

Theorem A.4 *Dual function f^* is convex. If function f is subdifferentiable at point x, the properties*

$$y^* \in \partial f(x) \ , \ x \in \partial f^*(y^*) \ , \ and \, f(x) + f^*(y^*) = < x, y^* > , \qquad (A.11)$$

are equivalent.

As for an example, let us compute dual function of the indicator function I of segment $[0, 1]$ with $V^* = \mathbb{R}$ and the bilinear form being the usual multiplication $\langle x, y\rangle = xy$. Dual function is defined by

$$I^*(y) = \sup\{xy - I(x)\,|x \in V = \mathbb{R}\} = \sup\{xy\,|x \in [0, 1]\}.$$

It is called the support function of segment $[0, 1]$. It easy to get

$$I^*(y) = y, \quad if\ y \geq 0\ , \text{and}\ \ I^*(y) = 0\ ,\ if\ y \leq 0.$$

Function I^* is the positive part function already defined

$$pp(y) = \sup\{y, 0\}\,.$$

A.5.1 The Internal Energy and the Free Energy

The state quantities of a material are $E = (T, \chi)$. It is known the internal energy e is a function of entropy s and of the state quantities χ. But it does not depend on temperature T and it is a convex function of s, see [3, 4], for example. Its dual function $e^*(T, \chi)$ with respect to s depends on the whole state quantities $E = (T, \chi)$, [3]. Thus it depends on the temperature and is defined by

$$e^*(y, \chi) = \sup\{xy - e(x, \chi)\,|x \in V = \mathbb{R}\},$$

Dual function $e^*(T, \chi)$ defines the free energy

$$\Psi(s, \chi) = -e^*(s, \chi),$$

which is the opposite of a convex function of T. Thus it is a concave function of T, see the definition below. It results also the equivalent relationships

$$T \in \partial e(s, \chi)\ ,\ s \in -\partial\Psi(T, \chi)\ ,\ \text{and}\ e(s, \chi) = sT + \Psi(T, \chi),$$

where the subdifferential sets are with respect to s and T, χ being a parameter. Note that

$$\forall x\ , \forall y\ ,\ e(y, \chi) - \Psi(x, \chi) \geq xy.$$

A.6 Concave Functions

A function f is concave if its opposite $-f$ is convex. For concave function, upper-gradient, instead of subgradient, are defined. They satisfy

$$\forall z \in V,\ \left\langle z - x, x^* \right\rangle + f(x) \geq f(z).$$

We denote $\hat{\partial} f(x)$, upperdifferential set, the set of the uppergradient at point x. It is easy to prove that

$$\hat{\partial} f(x) = -\partial(-f)(x).$$

A.6.1 Example of Concave Functions

The free energy $\Psi(T, \varepsilon, \beta, \text{grad}\,\beta)$ is a concave function of temperature T, because it is the dual function of the opposite of internal energy $e(s, \varepsilon, \beta, \text{grad}\,\beta)$ which is a convex function of entropy s, [3]. It results the heat capacity

$$-\frac{\partial^2 \Psi}{\partial T^2},$$

is non negative.

Remark A.4 If the internal constraint

$$T \geq 0,$$

is taken into account by

$$\Psi(T, \chi) = \Psi(T, \chi) - I_+(T),$$

the free energy $\Psi(T, \chi)$ is still a concave function of T, [2].

Precise presentation of convex analysis with applications is given either in books by Jean Jacques Moreau, [5] and by Ivar Ekeland and Roger Temam, [1] or by Bernard Nayroles, [6].

References

1. Ekeland, I., Temam, R.: Convex Analysis and Variational Problems. North Holland, Amsterdam (1976)
2. Frémond, M.: Non-Smooth Thermomechanics. Springer, Berlin (2002)
3. Germain, P.: Mécanique des milieux continus. Masson, Paris (1973)
4. Kling, R.: Thermodynamique générale et applications. Editions Technip, Paris (1967)
5. Moreau, J.J.: Fonctionnelles convexes, Edizioni del Dipartimento di Ingegneria Civile, Università di Roma "Tor Vergata", 2003, ISBN 978-88-6296-001-4 and Séminaire sur les équations aux dérivées partielles. Collège de France, Paris (1966)
6. Nayroles, B.: Point de vue algébrique. Convexité et intégrandes convexes en mécanique des solides, C.I.M.E., Bressanone, Ed. Cremonese (1973)